COMPUTER-AIDED CHEMICAL SPECIATION IN METAL-BASED DRUG DESIGN

THEMBELANI EDMUND NOMKOKO

A Thesis Submitted to the Department of Chemistry, Faculty of Science, University of Cape Town, Rondebosch, Cape Town, in fulfilment of the requirements for the degree of Doctor of Philosophy.

30th September 2002

"Politics is for the present but the equation is for the future"

Albert Einstein - 1930

DECLARATION

I, *Thembelani Edmund Nomkoko*, sincerely and solemnly declare that **COMPUTER-AIDED CHEMICAL SPECIATION IN METAL-BASED DRUG DESIGN** - is my own, unaided work, and that all sources I have used or quoted have been indicated and acknowledged by means of complete references. This thesis is being submitted for the degree DOCTOR OF PHILOSOPHY, to the Department of Chemistry, Faculty of Science, at the University of Cape Town, Rondebosch, Cape Town and has not been submitted before for any degree or examination at any other University.

T. E. Nomkoko,

Signed by candidate

Signature Removed

30th September 2002

Supervisor's Name and Signature: *Prof. G.E. Jackson,*

DEDICATION

I dedicate this work to my late brother, Mandla John Nomkoko, my mother, Nomthandazo Primrose, my younger brother, Sabelo Christopher and my two younger sisters, Vuyiseka Vivian and Nolusindiso Monica.

ACKNOWLEDGEMENTS

I wish to express my sincere and warmest thanks to, and I am also pleased to acknowledge the help and continued encouragements I have received from my supervisor, Prof. G.E. Jackson during the course of this work.

I also wish to thank the following, for their help in the progress of this work,

- the members of staff of the Chemistry Department (UCT) for their direct and indirect support and encouragement,
- Professor R. Hunter for his guidance on synthetic work and Dr S. Bourne for acquisition and solving of the crystal structure,
- Drs A. Hunter and R.A. Hendrikse, E. Dyani (Radiation Oncology Department), J. Boniaszczuk (Nuclear Medicine Department), J. Visser (Animal Unit) and my colleagues, T. Jackson, S. Odisitse, and D. Jappie for their technical assistance in the animal experiments,
- Dr W.K.A. Louw and Mr Jan Rijn Zeevart of the South African Nuclear Energy Corporation (Ltd) at Pretoria for preparing and supplying me with $^{64}CuCl_2$,
- the National Research Foundation (NRF) and the Council of the University of Cape Town for financial support,
- Professor B.S. Nakani of the Department of Chemistry at the University of Transkei for introducing me to Chemical Speciation and Modelling studies and finally,
- my family and friends for their love and support.

Abstract

Formation constants of Cu^{2+}, Ni^{2+}, Zn^{2+}, Ca^{2+} and Gd^{3+} with the polyamine(amide) ligands N,N'-bis(2-hydroxyiminopropionyl) propane-1,3-diamine (L^2) and (1,15)-bis(N,N-dimethyl)-5,11-dioxo-8-(N-benzyl)-1,4,8,12,15-pentaazapentadecane (L^3) as well as those of Gd^{3+} with 3,3,9,9-tetramethyl-4,8-diazaundecane-2,10-dione dioxime (L^1) were investigated by glass electrode potentiometry at 25^0C and an ionic strength (I) of 0.15 *mol* dm^{-3}.

There is a substantial variation in the reported equilibrium constants which follow the order $Gd^{3+} \approx Ca^{2+} < Ni^{2+} < Cu^{2+} > Zn^{2+}$. The indication from these constants is that Ni^{2+} and Cu^{2+} sit in a square-planar N_4 arrangement of the L^2 donor atoms in the $[ML^2H_{-1}]$ and $[ML^2H_{-2}]$ species. In contrast, the corresponding $[ML^3H_{-1}]$ and $[ML^3H_{-2}]$ complexes have Cu^{2+} in a distorted octahedral environment. Ni^{2+} does not seem to form the $[ML^3H_{-1}]$, instead the neutral $[ML^3H_{-2}]$ is produced which precipitates out of solution.

The pronounced variation in the stability constants of Ni^{2+} and Cu^{2+} when compared with Zn^{2+}, Ca^{2+} and Gd^{3+} are largely due to the inability of the latter metal ions to deprotonate the amide nitrogen donor atoms. Although Gd^{3+} forms stable [ML], $[MLH_{-1}]$ and $[MLH_{-2}]$ complexes with L^1, the mixed-hydroxo $[MLH_{-3}]$ species precipitates out of solution.

Ligand selectivities of 9-11 orders of magnitude have been observed in favour of $[CuLH_{-1}]$, over analogous complexes of its *in vivo* competitors, Zn^{2+} and Ca^{2+}. Plasma mobilising index (p.m.i.) calculations further indicate that indeed L^1 and L^2 are able to mobilise Cu^{2+} *in vivo* at concentrations as low as 10^{-6} and 10^{-3} *mol* dm^{-3} respectively. In contrast, at these ligand concentrations the Zn^{2+} and Ca^{2+} p.m.i's are less than 0.01. L^3 is devoid of any mobilising ability. The selectivity and mobilising ability is $L^1 > L^2 > L^3$. This is an important result in the development of copper anti-inflammatory drugs for rheumatoid arthritis. Exogenously administered L^1 and L^2 ligands are predicted to be able to increase the l.m.w. copper fraction without altering the equilibria of *in vivo* Zn^{2+} and Ca^{2+}.

UV-Vis spectrophotometric studies confirmed the square planar MN_4 type of coordination for $[MLH_{-1}]$ and $[MLH_{-2}]$ complexes of Cu^{2+} and Ni^{2+} with L^2. L^3, on the other hand, is proposed to form tetragonally distorted octahedral $[MLH_{-1}]$ and $[MLH_{-2}]$ with Cu^{2+}. These studies indicate that in both species the two amide nitrogens, the central and one of the terminal amines are coordinated. Furthermore, in $[CuL^3H_{-1}]^+$, the second terminal amine is protonated and the formation of the neutral $[CuL^3H_{-2}]^0$, is due to the deprotonation of this group. Unfortunately, it has not been possible to predict the structure of the potentiometrically determined $[NiL^3H_{-2}]^0$ species due to precipitation.

The cationic $[NiL^1H_{-1}]^+$ species was crystallised as a perchlorate salt with a molecular formula $C_{13}H_{27}ClN_4NiO_6$, M_r=429.55 *g/mol*. The crystal system is orthorhombic with space group-Pbca (#61) and unit cell dimensions a=13.3960(10), b=12.3490(10), c=21.9330(10). The crystal and computer simulated structures of $[NiL^1H_{-1}]^+$ and those of the corresponding Cu^{2+} and Zn^{2+} species also show a square-planar geometry.

As a measure of dermal absorption of the Cu^{2+} complexes, octanol/water partition coefficients were determined. The results indicate that 2-6% of all the $[CuLH_{-1}]$ complexes should permeate the skin when applied percutaneously. However, their IC_{50} values are 3-4 orders of magnitude higher than those of the native Cu-Zn SOD enzyme. Hence, these compounds are poor mimics of this enzyme.

Biodistribution studies using ^{64}Cu-labeled $[CuLH_{-1}]$ species injected intravenously on mice revealed a rapid clearance of these complexes from the blood circulatory system. In fact, only less than 1% of the total injected activity was left in the blood 1hr postinjection. The liver recorded significant uptake of Cu-64 throughout the 24hr investigation period. There was also an appreciable uptake of these complexes by the heart, lung and muscle. In contrast, the $^{64}Cu[CuL^2H_{-1}]$ species is excreted exclusively by the renal system.

Overall, these results are encouraging enough to merit further evaluation of the $[CuLH_{-1}]$ complexes of L^1 and L^2 in chemotherapy and diagnosis.

Figure 1.1: Structures and abbreviations of some important ligand systems mentioned in this thesis.

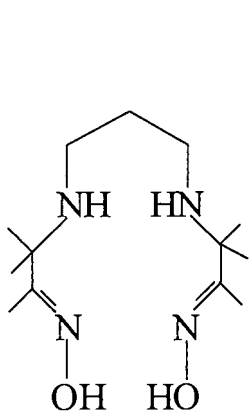

L^1 (PrAO)

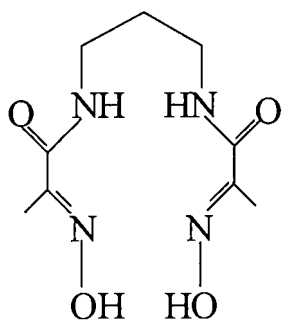

L^2 (H_2pap)

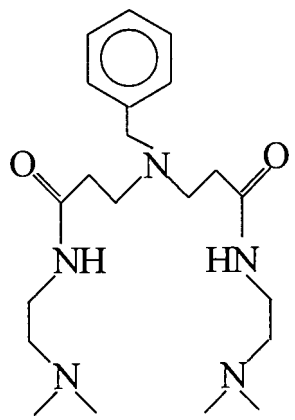

L^3 (BIDPAP)

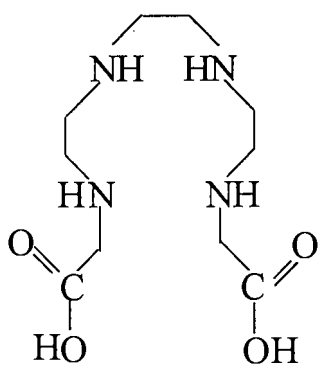

L^a (H_2ttda)

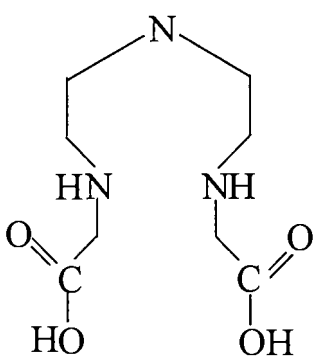

L^b (H_2dtda)

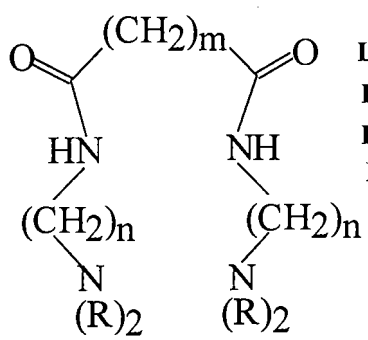

	m	n	R
L^{c1}	0	2	Me
L^{c2}	1	2	Me
L^{c3}	0	3	Me
L^{c4}	0	2	Et

L^c derivatives

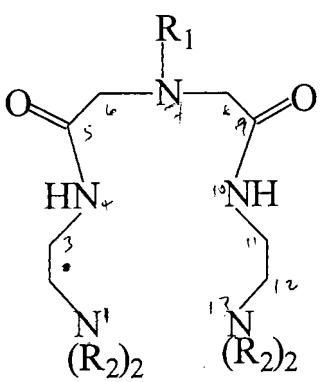

L^d derivatives

L^{d1} (IDA), R_1=H, R_2=CH_3

L^{d2} (BID), R_1=$CH_2C_6H_5$, R_2=CH_3

L^{d3} (EDA), R_1=$(CH_2)_2C_6H_5$ R_2=H

L^{d4} (DME), R_1=$(CH_2)_2C_6H_5$ R_2=CH_3

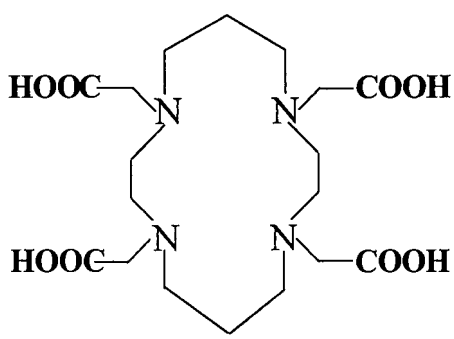

L^e (TETA)

Figure 1.1 continues: Structures and abbreviations of some important ligand systems mentioned in this thesis

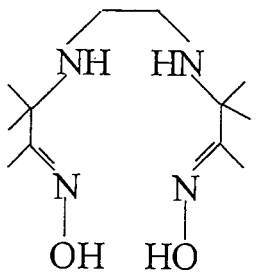

L^f (EnAO)

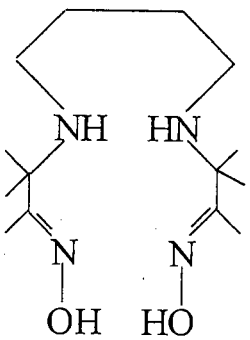

L^g (BuAO)

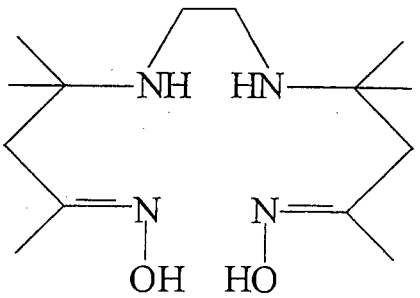

L^h (H_2tmdddo)

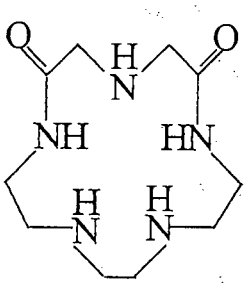

L^i

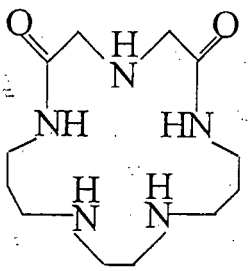

L^j

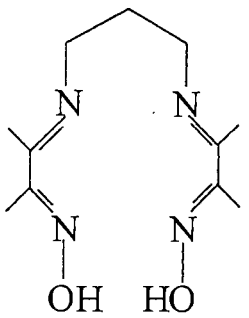

L^k (PreH)

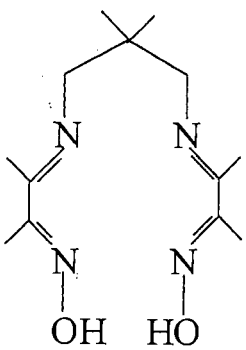

L^l (Me_2PreH)

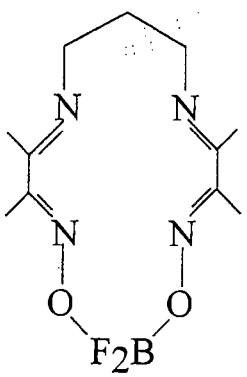

L^m (Cyclops)

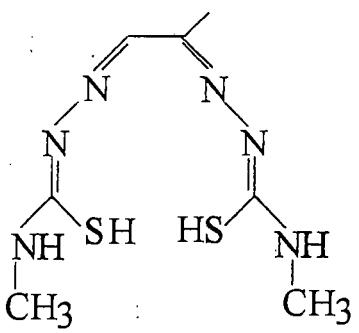

L^n (PTSM)

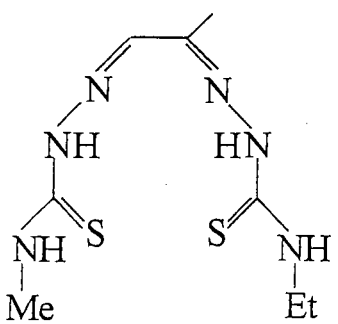

L^o (Et-PTSM)

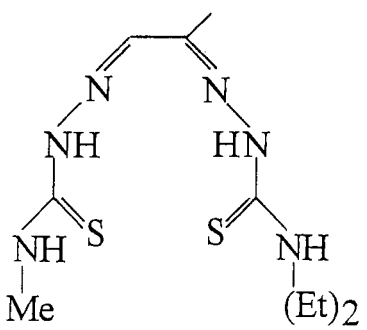

L^p ((Et) 2-PTSM)

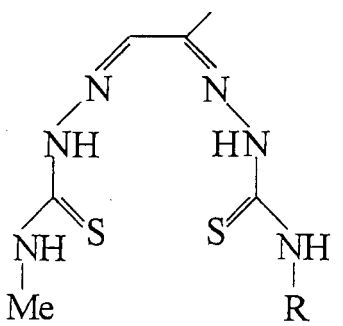

L^q (R=Cyclo-N(CH 2)5)

L^r (R=Cyclo-N(CH 2)6)

LIST OF ABBREVIATIONS

L^1 (PrAO)	- 3,3,9,9-tetramethyl-4,8-diazaundecane-2,10-dione dioxime
L^2 (H_2pap)	- N,N'-bis(2-hydroxyiminopropionyl) propane-1,3-diamine
L^3 (BIDPAP)	- (1,15)-bis(N,N-dimethyl)-5-11-dioxo-8-(N-benzyl)-1,4,8,12,15-pentaazapentadecane
L^4 (Me_2PrAO)	- 3,3,6,6,9,9-hexamethyl-4,8-diazaundecane-2,10-dione dioxime
L^5 (Me_2H_2pap)	- 2,2-dimethyl-N,N'-bis(2-hydroxyiminopropionyl) propane-1,3-diamine
L^{5a} (Hpap)	- N-(2-hydroxyiminopropionyl) N'-(2-hydroxyiminopropiaza) propane-1,3-diamine
L^{5b} (Me_2Hpap)	- 2,2-dimethyl-N-(2-hydroxyiminopropionyl) N'-(2-hydroxyiminopropiaza) propane-1,3-diamine
L^6 (BMPAP)	- (1,14)-bis(N,N-dimethyl)-5-oxo-8-benzyl-1,4,8,11,14-pentaazatetradecane
L^{6a} (BIDPA)	- (1,14)-bis(N,N-dimethyl)-5,10-dioxo-8-benzyl-1,4,8,11,14-pentaazatetradecane
L^a (H_2ttda)	- 3,5,9,12-tetraazatetradecanedioic acid
L^b (H_2dtda)	- 3,6,9-triaazaundecanedioic acid
L^c (BDE)	- N,N'-bis[(2-(dimethylamino)ethyl) ethane diamide]
L^d (BID)	- (1,13)-bis(N,N-dimethyl)-5,9-dioxo-7-benzyl-1,4,7,10,13-pentaazatridecane
L^e (TETA)	- 1,4,8,11-tetraazacyclotetradecane−1,4,8,11-tetraacetic acid
L^f (EnAO)	- 3,3,8,8-tetramethyl-4,7-diazadecane-2,9-dione dioxime
L^g (BuAO)	- 3,3,10,10-tetramethyl-4,9-diazadecane-2,11-dione dioxime
L^h (H_2tmdddo)	- 4,4,9,9-tetramethyl-5,8-diazadodecane-2,11-dione dioxime
L^i	- 2.6-dioxo-1,4,7,10,13-pentaazacyclopentadecane
L^j	- 2.6-dioxo-1,4,7,11,14-pentaazacycloheptadecane
L^k (PreH)	- 2,10-dioximo-3,9-dimethyl-4,8-diazaundeca-3,8-diene
L^l (Me_2PreH)	- 2,10-dioximo-3,6,6,9-tetramethyl-4,8-diazaundeca-3,8-diene
L^m (Cyclops)	- 1,1-difluoro-4,5,11,12-tetramethyl-1-bora-3,6,10,11-tetraaza-2,14-dioxocyclotetradeca-3,5,10,12-tetraene
L^n (PTSM)	- Pyruvaldehyde bis(N^4-methylthiosemicarbazone)

L^o (EtPTSM) - Pyruvaldehyde -1-N^4-ethylthiosemicarbazone-2-N^4-methylthiosemicarbazone

L^p ($(Et)_2$PTSM) - Pyruvaldehyde -1-N^4,N^4-diethylthiosemicarbazone-2-N^4-methylthiosemicarbazone

L^q (Cyclo-$N(CH_2)_5$PTSM) - Pyruvaldehyde -1-piperidylthiosemicarbazone-2-N^4-methylthiosemicarbazone

L^r (Cyclo-$N(CH_2)_6$PTSM) - Pyruvaldehyde -1-hexamethyleneiminyl-thiosemicarbazone-2-N^4-methylthiosemicarbazone

Cyclam - 1,4,8,11-tetraazacyclotetradecane

TMC - 1,4,8,11-tetramethyl-1,4,8,11-tetraazacyclotetradecane

A_{obs}^{λ} - Absorbance observed at wavelength λ

ATP - Adenosine triphosphate

Autm - Aurothiomaleate

Auts - Aurothiosulphate

ε^{λ} - Calculated molar absorptivity at wavelength λ

DMARDs - Disease-modifying anti-rheumatic drugs

D-Pen - D-Penicillamine

ECCLES - Computer program for Evaluation of Constituent Concentrations in Large Equilibrium Systems

E - Electrode potential

E^0 - Electrode response intercept

s - Electrode response slope

ESTA - Equilibrium Simulation for Titration Analysis

I - Ionic strength given in *mol* dm^{-3}

% ID - Percentage injected dose

IC_{50} - Concentration of the drug required to reduce diformazan formation by 50%

r_{ij} - Correlation coefficient between parameters i and j

P.m.i. - Plasma mobilising index

pH = (-log H^+) - A measure of acidity or alkalinity

Pgp - P-glycoproteins

R_H - Hamiltonian R-factor

R_{lim} - Hamiltonian R-limit

l.m.w.	- Low-molecular-weight
MRI	- Magnetic resonance imaging
NBT	- Nitrobluetraazolinium
NSAIDs	- Non-steroidal anti-inflammatory drugs
RA	- Rheumatoid Arthritis
$\log\beta_{pqr}$	- Logarithm of the overall stability constant
σ_{pqr}	- denotes standard deviation in log β_{pqr} for species pqr
SAARDs	- Slow-acting anti-inflammatory drug
SOD	- Superoxide Dismutase
SF	- Synovial fluid
SM	- Synovial membrane
U_{obj}	- Objective function
OBJE	- Task to calculate the objective function
Z-bar	- Complex formation function
ZBAR	- Task to calculate the complex formation function
Q-bar	- Deprotonation function
QBAR	- Task to calculate the deprotonation function
SPEC	- Task to calculate the speciation as a function of the pH
Log $K_{oct/aq}$	- Logarithm of the partition coefficient determined in an octanol/water mixture

TABLE OF CONTENTS

CHAPTER 4 - EXPERIMENTAL AND ANALYTICAL METHODS

LIST OF FIGURES

LIST OF TABLES

CHAPTER 1

Introduction

An overview of rheumatoid arthritis, its diagnosis and present therapy

1.1 Origin of Rheumatoid Arthritis

A fundamental unit of life, the living cell, throughout its entire life, is faced with the challenge of being able to survive the physiological imbalances occuring within and/or outside of it. If its cellular organization is destroyed through these processes, the cellular function is likewise altered. Although some vital functions such as enzymatic activities may persist, the cell becomes disorganized and dies. Rheumatoid arthritis, in particular, is believed to be a multi-factorial disease[1-13] induced by such imbalances occuring in articular regions.

The designation "rheumatoid arthritis" (RA) implies that the disease is an inflammatory process of auto-immune nature characterised by an invasive synovial hyperplasia, which leads to polyarticular destruction.[1-13] It afflicts about 5% of the western world's population of which women are afflicted more than men, with a ratio of 2-3:1. Although there is no cure, it may, however, be controlled with immuno-suppressive drugs or the symptoms treated with anti-inflammatory drugs.[1,6]

Although the etiology of RA remains unknown, and its pathophysiology poorly understood, recent results show that rheumatoid synovial cells have a transformed phenotype.[6-8] Immunohistological examination of the synovial membrane (SM) shows it to have all the hallmarks of a T-cell driven lesion: an accumulation of predominantly CD4 T-cells belonging to the memory phenotype, activated macrophages and synoviocytes or specialised synovial fibroblasts and lysosomal enzymes.

The stimulatory interactions between these cell types lead to the release of a number of inflammatory cytokines and pharmacological mediators, which contribute to the development of synovitis, resorption of bone and cartilage that lead ultimately to fibrous and even osseous ankylosis.[3,4,6-8]

In addition to these cells, there is a vast amount of information suggesting the existence of tissue degrading enzymes, including metalloproteinases (MMPs) and serine proteinases. MMPs are members of a unique family of at least twenty proteolytic, structurally related enzymes that contain a zinc ion at their active sites.

These enzymes can degrade collagen, elastin and other macromolecules of the extracellular matrix.[10,11]

Accumulating evidence indicates that oxygen free radicals such as the super-oxide anion ($^{\cdot}O_2^-$) and hydroxyl radical ($^{\cdot}OH^-$) derived from activated macrophages and granulocytes infiltrating arthritic joints are involved in the pathogenesis of RA.[12] Nitric oxide, (NO), another free radical, is derived mainly from endothelial cells, but may also be produced by marcophages, neutrophils, synovial cells and chondrocytes. Although NO is recognised as a physiologic regulator of blood-pressure, its combination with $^{\cdot}O_2^-$, produces tissue destructive species particularly the peroxynitrite anion ($ONOO^-$).[13]

Exposure to these radicals leads to depolymerisation of hyaluronic acid, peroxidation of lipid, destruction of cartilage matrix, damage to DNA and induction of inflammatory cytokines and thereby destruction of joint structure.[12,13] All these factors point to the multi-factorial nature of RA.

There is a need and desire to monitor and restore the proper functioning of the physiological processes using non-natural systems. Chemotherapy becomes the obvious choice at this stage of disease progression. Complicating such efforts is the recognition that it is often not a single sequence that is ideally targeted but rather an ensemble of physiological imbalances. This has resulted in the widespread use of combination therapy of two or more drugs directed at different imbalances. However, the side effects of combination therapy have been found to be additive. In spite of these challenges, the most interesting contributions to the past and recent year's literature[1,6] on RA focus on the treatment of this difficult and disabling disease.

1.2 Therapy for rheumatoid arthritis

Ideally, a treatment should be highly efficacious and totally devoid of side effects, affordable and acceptable to the patient. Traditionally,[14] copper rich diets such as crayfish and peanuts were administered as a way of treating RA. Also, wearing of copper jewellery such as the famous copper bangle was also accepted as a standard

treatment. This traditional way of treatment[14] has been slowly replaced by more scientific therapeuticals.[15-21]

A new approach in treatment of RA is to commence with non-steroidal anti-inflammatory drugs (NSAIDs) and then move more rapidly to the slow acting anti-inflammatory drugs (SAARDs) followed by immunosuppressive drugs.[15-21] In order to achieve sufficient suppression of rheumatoid inflammation, combination therapy of multiple SAARDs has been tried. The combination therapy has been found to be more effective and may as such have advantages over treatment with a single SAARD.[18-20] The effectiveness of combination therapy has recently been questioned by Quinn et al.[15] and such assertion should be treated with caution. The reason for that probably originates on the additive nature of its side effects.

1.2.1 NSAIDs

NSAIDs are characterised by an absence of steroid moiety in their structure as the name indicates. They are frequently used as "first-line" agents in the treatment of minor to severe inflammation.[18-20] In addition to their anti-inflammatory activities, they also possess analgesic properties hence they remain the most frequently prescribed therapeuticals for RA.

Although these drugs are generally well tolerated, they are associated with a wide spectrum of potential clinical toxicities.[18-20] The most common side effect of NSAIDs is gastrointestinal tract irritation (GTI).[15-20] Salicylates are not recommended for pregnant women, while imdomethacin and diflusinal induce premature closure of ductus arteriosus.[17-20] This might give rise to pulmonary hypertension in susceptible neonates. Because of this, it is not appropriate to use these drugs during both pregnancy and lactation periods.[17-20]

Aspirin is the most difficult of the NSAIDs to use effectively. It has more side effects and the most complex dosing schedule. It has also more dangerous side effects if overdoses are taken and the complications tend to be dose related.

Pharmacodynamic investigations suggest that inhibition of prostaglandin (PG) synthesis in the synovial compartment is the dominant mechanism of action for most salicylates, if not all NSAIDs.[18,19] Because NSAIDs suppress PG synthesis, gastric acid production is increased whereas the production of gastric mucus and bicarbonate is decreased. The rate of cellular proliferation of the gastric mucosa is also decreased thus impairing the normal protective mechanisms of the stomach. This results in gastric irritation and the exacerbation of peptic ulcers. If gastrointestinal bleeding recurs, it is worsened, because NSAIDs decrease platelet adhesiveness and increase acid production in the stomach.[17-20]

PG inhibition is believed to mediate the anti-inflammatory effect of the drugs.[18,19] The mediator of their analgesic effect is not yet understood. Other NSAIDs like azapropazone would more likely operate by inhibiting lysosomal enzyme release and superoxide anion and interleukin-1 (IL-1) production than by inhibiting PG synthesis.[18,19]

1.2.2 DMARDs

DMARDs is a term for a group of medications with diverse mechanisms of action. They are also called "second-line" anti-rheumatic drugs, a term derived from their position in relation to the pyramid approach of medication.[15-21] Included in this broad category of drugs are slow-acting anti-rheumatic drugs (SAARDs) and remission-inducing drugs, the former requiring saturation of tissues (4 to 6 months) before a therapeutic benefit can be achieved. These types of drugs and their life threatening effects are discussed thoroughly in a number of rheumatology texts[16-21] and only a brief account will be given here.

Anti-malarial drugs such as chloroquine and hydroxychloroquine are prescribed for patients with inflammatory arthritis including progressive, erosive RA and juvenile chronic arthritis. They are usually well tolerated despite the cutaneous side effects such as rash and changes in pigmentation as well as cramps, abdominal distention, nausea and diarrhea.[16-20]

Gold therapy is considered by some rheumatologists to be the best drug available to modify the cause of the disease and is indicated in the treatment of progressive, erosive RA.

Sodium aurothiomaleate (Autm or Myochrysine) and aurothiosulphate (Auts or Solganal) are two parenterial forms of gold available for RA.[17-20] Both Autm and Auts are highly water soluble, containing gold bound to the thiolate groups of thiomaleate and thiosulphate ligands respectively. Autm is oligomeric containing about 8 subunits while Auts is monomeric and both complexes inhibit the oxidative burst of polymorphonuclear leukocytes (PMN) by about 30% at concentrations above 5 μM.

Auranofin (Ridaura), an oral preparation,[17-20] is monomeric with tetraacetylthioglucose and triethylphosphine ligands binding gold. It is thought to have less severe renal and hematopoetic toxicities than parenteral gold, but may be less effective than the intramuscular injected preparations. While the chemical structure of auranofin is known in much more detail than Autm and Auts, there is considerable uncertainty about the replacement of the ligands *in vivo*.

Although gold compounds are considered the backbone of therapy for progressive RA, considerable concern must be exercised during their administration because of potential toxicity. Mild toxicities include stomatitis, pruritis and local rash. More serious toxicities include bone marrow suppression, thrombocytopenia, leukopenia and aplastic anaemia.[18,19]

D-Penicillamine (D-Pen), a thiol and a product of metabolism of penicillin is a slow acting drug used to treat active RA and juvenile chronic arthritis.[18-20] Pharmacokinetic studies have provided some support for associations between biotransformation at the S-H group of D-Pen and its toxicity and efficacy.

Although it has been reported to be as effective as gold salts, it is, however, more toxic than other slow-acting and cytotoxic drugs. Side effects of D-Pen such as bone marrow suppression and nephropathy are comparable to those of gold whereas

the risk of thrombocytopenia from it is higher. Some of the side effects subside upon withdrawal of the drug.[18-20]

Sulfasalazine is quite effective for RA treatment. Toxicities include gastrointestinal intolerance and musculocutaneous toxicity. Apart from skin reactions, which can occur, more serious and potentially fatal conditions such as haemolytic anaemia, aplastic anaemia and leukopenia have been reported.[18-20]

Leflunomide, an isoxazole derivative is another DMARD currently in third stage of clinical trials. Kalden and co-workers[23,24] and Cohen et al.[25] have recently conducted long term treatments studies of arthritic patients with leflunomide. These studies provided firm evidence of its high efficacy in these patients compared with sulfasalazine and methotrexate.

It is believed to exhibit its mode of action through a number of mechanisms. These include selective inhibition of dihydro-orotate dehydrogenase, a key enzyme in the *de novo* synthesis of pyrimidine and subsequent inhibition of RNA and DNA synthesis. Activated T-lymphocytes which are involved in the pathogenesis of RA are believed to synthesise pyrimidine by the same *de novo* pathway. Recent investigation indicates that leflunomide also inhibits reactive oxygen radicals, matrix metalloproteinases, polymorpholeukocyte chemotaxis and the migration of these cells into the synovial cavity.[25]

1.2.3 Glucocorticoids in RA

Glucocorticoids are used in the treatment of RA for their anti-inflammatory and immunosuppressive effects.[26,27] The mechanisms by which these drugs produce such effects are exceedingly complex. Steroids are believed to inhibit phospholipase A_2, which releases arachidonic acid from cell membranes. This is the first step in the production of inflammatory prostaglandins and leukotrienes.[15-20]

They are administered as oral and parenteral preparations. The latter are given intra-articularly or at peri-articular sites of local inflammation, and are effective at relieving pain and swelling.[15-20,26,27]

For prednisone and cortisone, hydroxylation to prednisolone and cortisol, respectively, at the C_{11} site is necessary for activity. In patients with faulty hydroxylation systems, active drugs such as prednisolone or methylprednisolone are preferred or patients will appear unresponsive to these medications.[18,19,26]

Although they can produce dramatic results in acutely ill patients, the side effects from these drugs can be equally dramatic. The side effects vary directly with increasing doses of the drug and duration of use. Suppression of the pituitary-adrenal axis for about one week can occur in patients taking 50 *mg* of prednisone daily for only 5 days. They can cause gastritis, ulceration and severe myopathy.

1.2.4 Some new and novel therapies for RA

The best long-term hope for patients suffering from RA is the development of new therapies based on targets defined by concepts developed from the understanding of its pathogenesis.[16,28,29] Recent reports indicate that immunopathological features of RA synovial membrane and tissue reflect clinical disease activity; that is an accumulation of predominantly CD4 T-cells.[1-3,16,28,29]

It is the stimulatory interactions between these cell types that lead to the release of a number of inflammatory cytokines and pharmacological mediators. The new therapies should be directed against these defined targets. These include immunotherapy which makes use of immunologically specific agents, such as monoclonal antibodies and antigenic peptides, directed against the cell types. 'Tolerance-inducing' immunotherapy is aimed at bringing about an end to the auto-immune process by inducing tolerance, e.g. anti-CD4 antibody therapy.[17-20]

The 'anti-inflammatory' immunotherapy is directed against specific mediators in the inflammatory cascade such as inflammatory cytokines, which are released during rheumatoid synovitis. An example of the latter immunotherapy is antibody therapy directed against TNF or adhesion molecules and it does not induce tolerance.[17-20]

Immunomodulation on the other hand utilises simple drugs, which either enhance desirable or suppress undesirable features of the immune response such as the those of metalloproteinases. Corticosteroids, the cytotoxics, cyclosporin A, methotrexate and levamisole are presently available drugs of this type.[17-20,28] Some of the new therapies[17-21,29] under investigation in the treatment of this refractory disease are discussed fully in the references cited therein.

1.3 RA and its diagnosis

Chemotherapy and its usefulness rest more on the proper diagnosis of the disease in question. Remarkable progress has been made in the development of diagnostic techniques based on immunoassays and MRI. MRI is now widely used to quantitatively assess the morphologic properties of the synovial joint, inflammatory soft tissue and cartilage and bone changes during the early[30,31] and late[32-36] stages in RA. It has also been demonstrated to aid in the selection of site for biospy, monitor the response of the tissue to therapy as well as give guidance prior to surgery.[30-36]

MRI exploits the differences in relaxation of water protons in tissues translating them into three-dimensional anatomical information. In general, excellent soft-tissue contrast is obtained without the use of contrast agents, but the difficulty in separating certain lesions from adjacent oedema and the monitoring of tissue function has led to the search for new contrast enhancement agents.[37,38]

MRI uses non-radioactive Gd^{3+}, Fe^{2+} and Mn^{2+} complexes as contrast agents. The majority of these agents are based on gadolinium(III) and are used to increase image contrast between normal and diseased tissues. Gd^{3+}, in particular, is ideally suited to this as it contains seven unpaired electrons and hence has a high relaxivity.[37]

1.3.1 Gd(III) based contrast agents in MRI

Presently, the dimeglumine salt of Gd-DTPA (MAGNEVIST™, gadopentetate), Gd-[DTPA-BMA](OMNISCAN™, gadodiamide), Gd-DOTA (DOTAREM™, gadoterate) and Gd-[HP-DO3A] (ProHance™, gadoteridol), just to mention a few, are in routine use in most clinical laboratories.[37,38] DTPA-BMA is a derivative of DTPA where two carboxylates have been substituted by two amide

moieties and both are linear poly(amino/amido) polycarboxylates. The latter three contrast agents are based on tetraazacyclododecane.[37,38]

The choice of using these poly(aminocarboxylate) type ligands lies on their ideal properties of high water solubility, enhanced chemical stability and low toxicity *in vivo*. Because the majority of these ligands are octa-chelating in nature, the nineth co-ordination site of the metal ion is usually occupied by a single water molecule. The presence of this co-ordinated water molecule, which interacts with the bulk of solvent molecules increases the complex's relaxivity by an inner-sphere mechanism.

In spite of the favourable properties exhibited by these ligands and resulting chelates, there are still factors that need to be fine-tuned and these require correlating aspects of the co-ordination chemistry of the complexes with *in vivo* behaviour. Although there are few absolute rules for such correlation, pertinent factors worthy of consideration include the thermodynamic stability, stereochemistry, charge and lipophilicity of the metal complex. In addition, the target organ or tissue to be imaged seems to dictate the desired characteristics of the agent.

Although thermodynamic stability of non-radioactive metal complexes can help predict *in vitro* stability, it is often not indicative of *in vivo* stability. Although these agents are routinely used in MRI scans, the toxic effect of uncomplexed Gd^{3+} and free pro-ligand arising from dissociation of the metal complex *in vivo* is still one of the major concerns in MRI.[37,38]

Such toxicity is associated with the accumulation of $Gd(PO_4)$ in the lysosomes of hepatocytes and macrophages in the spleen, bone marrow and lungs.[37,38] In addition, it has been noted that another more important factor is the thermodynamic selectivity of the ligand towards Gd^{3+} over endogenously available metal ions such as Ca^{2+}, Zn^{2+} and Cu^{2+}. In particular, it has been observed that transmetallation with Zn^{2+} is highly predictive of acute toxicity.[37,38]

It has long been recognised that lipophilic complexes generally have higher uptake in the liver or in fatty tissues and are able to cross the blood-brain barrier just like neutral species. It has also been observed that many positively charged ions

accumulate in the heart while negatively charged compounds tend to clear through the kidneys.

Neutral contrast agents are preferred to ionic species because they have a lower osmolality and hence greatly reduced physiological complications. Contrast agents with an osmolality close to that of blood and the extracellular fluid (290 mmol kg^{-1}) are more desirable. The conversion of two carboxylates in gadopentetate to two methylamides in gadodiamide has resulted in a decrease in osmolality from 1940 mmol kg^{-1} to 789 mmol kg^{-1} as well as the charge reduction from -2 to 0.[37,38]

It should be mentioned that these contrast agents are extracellular agents with non-specific bio-localization. Another challenge in this field is therefore the design of ligands and hence complexes which are able to target specific tissues and organs in the body.[37,38] Stereochemistry is important when targeting complexes to specific receptors.

1.4 Conclusion

The presently available NSAIDs and DMARDs are rather unsatisfactory, being poorly effective and having considerable and sometimes, severe and life-threatening side effects. This may be due to lack of specificity in action of these drugs. Gold compounds are considered the backbone of therapy for progressive RA. However, because of inadequate gold elimination they can have quite severe side effects.

Although glucocorticoids can produce dramatic results in acutely ill-patients, the side effects from these drugs can be equally dramatic. As a result of disease chronicity in the majority of RA patients, many may develop steroid dependency. The side effects vary directly with increasing doses of the drug and duration of use.

Thus, the search for less expensive, more effective and safer therapies for this disease and/or the inflammation associated with it, is an urgent task to which considerable effort is being devoted. Elucidation of the key factors involved in the perpetuation of chronic inflammation in RA is essential to the design of effective therapeutic interventions.

Despite remarkable progress in the development of MRI contrast agents for disease diagnosis, there is still a need in the design and synthesis of new agents with high relaxivity and hence excellent tissue contrast. These should show high stability *in vivo* to circumvent the toxic effect of uncomplexed Gd^{3+} and free pro-ligand arising from dissociation of the complex, which is still one of the major concerns in MRI.[37,38] In addition the design of tissue and/or organ specific contrast agents is one of challenges facing co-ordination chemists.

With the above-mentioned conclusion in mind, the thesis is centred on the solution chemistry of Cu^{2+}, Ni^{2+}, Zn^{2+}, Ca^{2+} and Gd^{3+} with three polyamine(amide) ligands, 3,3,9,9-tetramethyl-6,7-diazaundecane-2,10-dione dioxime (L^1), N, N'-bis(2-hydroxyiminopropionyl) propane-1,3-diamine (L^2), and 1,15-bis(N,N-dimethyl)-5,11-dioxo-8-(N-benzyl)-1,4,8,12,15-pentaazapentadecane (L^3) for possible use of copper and gadolinium complexes as anti-inflammatory in RA and as contrast agents in MRI respectively. However, to better obtain information from the solution chemistry of these ligands with the metal ions, a thorough investigation of the current trends in drug design is necessary which is the focus of chapter 2.

References

1. *Mechanisms and Models in Rheumatoid Arthritis*, 1995, 25, 67-71, [Editors: B. Henderson, J.C.W. Edwards and E.R. Pettipher].
2. E.C. Huskinson and F.D. Hart, *Joint Disease: All the arthropathies*, 1973, 93.
3. R.W. Kinne, E. P.-Kinne and F. Emmrich, *Biochim. Biophys. Acta*, 1997, **360**, 109.
4. D.A. Fox, *Arthritis Rheum*, 1997, **40**, 598.
5. *Yearbook of Rheumatology* (1995), 1-81, [Editors: J.S. Sergent, E. Carwile Le Roy, R.F. Meenam, R.S. Panush and M. Reichlin].
6. *Colloquia Geigy, Rheumatoid Arthritis - Pathogenetic Mechanisms and Consequences in Therapeutics*, 1971, 1-36, 511-665, [Editors: W. Muller, H.G. Harwerth and K. Fehr].
7. C.C. R.-Schuijt, W.J.E. van Esch, C. van Kooten, N.P.M. Ezendam, E.W.N. Levarht, F.C. Breedveld and C.L. Verweij, *Arthritis Rheum.*, 2001, **44**, 2029.
8. B.B. Bohm, T. Aigner, C.P. Blobel, J.R. Kalden and H. Burkhardt, *Arthritis Rheum.*, 2001, **44**, 2046.
9. J. Smolen and G. Steiner, *Arthritis Rheum.* 2001, **44**, 2218.
10. M. Whittaker, C.D. Floyd, P. Brown and A.J.H. Gearing, *Chem. Rev.* 1999, **99**, 2735.
11. G. Cunnane, O. FitzGerald, C. Beeton, T.E. Cawston and B. Bresnihan, *Arthritis Rheum.*, 2001, **44**, 2263.
12. J.M. McCord, *Science*, 1974, **185**, 529.
13. M. Stefanovic-Racic, J. Stadler, C.H. Evans, *Arthritis Rheum.*, 1993, **36**, 1036.
14. J.R.J Sorenson, *In Metal ions in biological systems, Inorganic drugs in deficiency and disease*, 1982, **14**, 104, [Editor: H. Sigel], Marcel Dekker, Inc. New York.
15. J. Garcia and R.D. Altman, *Semin Arthritis Rheum.*, 1997, **27,** 1.
16. M.A. Quinn, P.G. Conaghan and P. Emery, *Rheumatology*, 2001, **40**, 1211.
17. L.C. Corman, C.L. Bell, N.L. Edwards and C.E. Harmon, *Rheumatology for the House Officer*, 1990, 289, 294.
18. M.H. Weisman and M.E. Weinblatt, *Treatment of the Rheumatic Diseases, Companion to the Textbook of Rheumatology*, 1995, 31.

19. D.J. McCarthy, *Arthritis and Allied Conditions, A Textbook of Rheumatology*, 11th Ed., 1989, 507, 622. M616.722 ART

20. J.J. Canoso, *Rheumatology in Primary Care*, 1997, 59. M616.723 CAN

21. J.R. O'Dell, K.W. Blakely, J.A. Mallek, P. James-Eckhoff, R.D. Leff, S.J. Wees, K.M. Sems, A.M. Fernandez, W.R. Palmer, L.W. Klassen, G.A. Paulsen, C.E. Haire and G.F. Moore, *Arthritis Rheum.*, 2001, **44**, 2235.

22. *Rheumatoid Arthritis, Recent Research Advances*, 1992, 365, [Editors: J.S. Smolen, J.R. Kalden and R.N. Maini].

23. J.R. Kalden, D.L. Scott, J.S. Smolen, M. Schattenkirchner, B. Rozman, B.D. Williams, T.K. Kvien, P. Jones, R.B. Williams, C. Oed and R. Rosenburg. *J. Rheumatol.*, 2001, **28**, 1983.

24. D.L. Scott, J.S. Smolen, J.R. Kalden, L.B.A. van de Putte, A. Larsen, T.K. Kvien, M. Schattenkirchner, P. Nash, C. Oed, I. L.-Friedrich, *Ann. Rheum. Dis.*, 2001, **60**, 913.

25. S. Cohen, G.W. Cannon, M. Schiff, A. Weaver, R. Fox, N. Olsen, D. Furst, J.S.L. Moreland, J. Caldwell, J. Kaine and V. Strand, *Arthritis Rheum.*, 2001, **44**, 1984.

26. D.L. Conn, *Arthritis Care Res.* 2001, **45**, 462.

27. K.G. Saag, *Arthritis Care Res.* 2001, **45**, 468.

28. M. Cutolo, A. Sulli, C. Pizzorni, B. Seriolo and R.H. Straub, *Ann. Rheum. Dis.* 2001, **60**, 729.

29. A. VanderBorght, P. Geusens, J. Raus and P. Stinissen, *Semin Arthritis Rheum.* 2001, **31**, 160.

30. B. Ostendorf, R. Peters, P. Dann, A. Becker, F. Wedekind, J. Friemann, K.-P. Schulitz, U. Modder and M. Scheider, *Arthritis Rheum.*, 2001, **44,** 2492.

31. H. Lindegaard, J. Vallo, K. H.-Petersen, P. Junker, M. Ostergaard, *Ann. Rheum. Dis.*, 2001, **60**, 770.

32. A.Savnik, H. Malmskov, H.S. Thomsen, L.B. Graff, H. Nielsen, B. D.-Samsoe, J. Boesen and H. Bliddal, *J. Rheumatol.*, 2001, **28**, 2193.

33. M. Szkudlarek, M. C.-Payen, C. Strandberg, M. Klarlund, T. Klausen, and M. Ostergaard, *Arthritis Rheum.*, 2001, **44**, 2018.

34. P. Olivier, D. Loenil, A. Watrin, F.Walter, S. Etienne, P. Netter, P. Gillet, and A. Blum, *Arthritis Rheum.*, 2001, **44,** 2295.

35. R. Burgkart, C. Glaser, A. H.-Durr, K.H. Englmeier, M. Reiser and F. Eckstein, *Arthritis Rheum.*, 2001, **44,** 2077.

36. D. McGonagle, C. Pease, H. M.-Ortega, P. O'Connor, W. Gibbon and P. Emery, *J. Rheumatol.*, 2001, **28**, 1837.

37. P. Caravan, J.J. Ellison, T.J. McMurry, and R.B. Lauffer, *Chem. Rev.* 1999, **99**, 2293.

38. V. Comblin, D. Gilsoul, M. Hermann, V. Humblet, V. Jacques, M. Mesbahi, C. Sauvage, J.F. Desreux, *Coord. Chem. Rev.* 1999, **185**, 451.

CHAPTER 2

Background to this study

Metal complexes in biomedical analyses - Recent advances in chemotherapy and diagnosis

2.1 Metal complexes in chemotherapy and diagnosis

The use of metal complexes in chemotherapy and/or diagnostic medical imaging has grown impressively in recent years as the result of an advanced understanding of biological structure and function. However, metal complexes that will ultimately prove successful in chemotherapy and as contrast agents in MRI must meet numerous criteria including high efficacy and an overall image enhancement, low toxicity *in vivo*, tissue and organ specificity and rapid clearance by the biological system.

2.2 Copper and RA - Present approach

The traditional approach[1] of treating RA with copper was relatively effective, but has been slowly replaced by more scientific therapeuticals. However, these therapeuticals commonly used for treatment of RA have adverse side effects. In addition, in spite of accumulating evidence indicating the involvement of reactive oxygen free radicals on the pathogenesis of RA, there are few agents which have been specifically designed and directed at the modulation of the ill-effects of these radicals. Leflunomide is an exception as it has been observed to inhibit these oxygen radicals as one of its many functions.[2]

Many articles,[3-5] indicating that copper complexes can be effective in the alleviation of inflammation associated with the disease, have appeared in the literature. One common fact from these articles is that the ligands alone are not effective, but when complexed to copper they become more effective. Furthermore, it has been reported that some of the anti-inflammatory agents discussed in the preceding chapter are also more active when complexed to copper.[3-5]

Recently, studies conducted by Berthon *et al.*[6,7] using computer-aided speciation, indicated that the common assumption that copper-NSAIDs complexes represent active forms of NSAIDs is of little significance for salicylate.[6,7] This is because the ternary Cu(II)-His-Sal complex does not exceed 0.1% at drug plasma therapeutic levels and, in addition, is electrically charged. Salicylate is believed to reduce the inflammation by scavenging hydroxyl ($^{\cdot}OH$) radicals.

The extra anti-inflammatory activity of administered copper-salicylate is due probably to the increase in Cu(II)-His complexes induced by administration of exogenous copper. On the other hand, anthranilate, which represents the inactive form is believed to mobilise copper in a pH dependent manner only in the inflammed site, i.e., as the pH decreases the more the inflammation and the more copper is bound to anthranilate. It is thus proposed that anthranilate may be regarded as a potential ·OH-inactivating ligand (OIL).

Some recent investigations have also shown that other copper(II) complexes have a high superoxide dismutase (SOD) mimetic activity when superoxide anion radicals are generated by the xanthine-xanthine oxidase system.[8,9] It is believed that copper is responsible for all these activities.

2.2.1 Possible modes of action of copper(II) complexes

Although several possibilities exist, the mechanism of action by which copper exhibits its anti-inflammatory activity is not yet understood. Sorenson has discussed extensively, several modes whereby copper may exhibit its anti-inflammatory activity.[1] These include the modulation of several enzymatic, histaminic systems, T-lymphocyte responses and prostaglandin syntheses, as well as stabilization of human gamma globulin and lysosomal membrane, and induction of lysyl oxidase and superoxide dismutase. The latter three activities deserve special elaboration as there is ample evidence indicating the involvement of copper in these processes.

2.2.1.1 Stabilisation of Lysosomal membrane

In addition to superoxide anions and several amines, the synovial fluid also contains lysosomal enzymes, which are destructive towards cartilage.[1] Copper is reported to decrease the permeability of human synovial lysosomes, thus decreasing the release of free lysosomal enzymes into the synovial fluid.[1]

2.2.1.2 Induction of Lysyl Oxidase

Lysyl oxidase is a copper dependent enzyme responsible for repair of damaged tissues as a result of inflammation.[1,10] The process requires cross-linking and extracellular maturation of the connective tissue components, collagen and elastin. It has been demonstrated that copper(II) sulphate does induce lysyl oxidase activity in copper deficient chickens.[10]

2.2.1.3 Induction of Superoxide Dismutase activity and Superoxide Dismutase - Mimetic Activity

The cells of all aerobic organisms which have been tested, are found to contain an active metallo-enzyme known as copper-zinc superoxide dismutase (hereafter, $Cu^{(II)}_2Zn^{(II)}_2$ SOD).[11-15] This enzyme contains two identical polypeptide sub-units, each of which contains one copper and one zinc atoms bridged by the imidazolate group of a histidyl residue. It catalyses the dismutation of the superoxide anion to molecular oxygen and hydrogen peroxide.[11-15]

The process involves stepwise and cyclic reduction and oxidation of Cu^{2+} to Cu^{+} and vice-versa by the superoxide anion radical ($\cdot O_2^-$).[11-15] The imidazolate group is believed to dissociate from the Cu^{+} ion and is immediately protonated. Other reports have indicated that it remains covalently bonded to Cu^{+}. Although this mechanism of $\cdot O_2^-$ quenching might seem appealing, there are other mechanisms which cannot be ruled out.[16,17]

There is firm evidence indicating that charged residues at the entrance of the catalytic cavity produce an overall electrostatic field, which increases the rate of approach of the $\cdot O_2^-$ ion toward Cu^{2+} to levels above the normal diffusion limit.[18-20] Arg-143 which is much closer to the copper ion probably assists the substrate in entering the cavity. Such a role was proposed on the basis of chemical modification experiments[18-20] and recently demonstrated through site directed mutagenesis.[21,22]

Recent investigations[23,24] have provided evidence that there is a pool of metal-deficient Cu-Zn SOD inside living cells like human lymphoblasts and undifferentiated K562 cells. In addition, the activity of native SOD in synovial fluid of arthritic patients is significantly reduced when compared to patients with non-inflammatory arthropathy. Induction of the metal-deficient Cu-Zn SOD depends on its exposure to Cu^{2+} and Zn^{2+} ions.[23,24] It should be added that Zn^{2+} in Cu-Zn SOD appears to be important in structure but not essential in the catalytic mechanism of the enzyme.[18-22]

In contrast, the synovial fluid of arthritic patients contains catalase, which decomposes hydrogen peroxide to oxygen and water.[23] The two enzyme systems furnish disposal routes for superoxide and peroxide anions and it turns out that this protection is a pre-requisite for the adaptation of living cells to the utilisation of oxygen.

Because of the efficient and uniqueness of the catalytic activity of Cu_2-Zn_2 SOD, it would be more useful to employ synthesised SOD as human therapeutics. Recombinant SOD proteins have been used in animal models of collagen induced arthritis (CIA) and in clinical trials, but the effectiveness is hampered by the relative short-half lives of proteins in the circulation.[25] In addition to their immunogenicity, high cost and ready clearance by the kidney, SODs are impermeable to membranes due to their high molecular weight and hence are unable to enter cells and the synovial cavity, in particular.[25]

These limitations have led many investigators to search for stable, non-toxic, low molecular weight complexes of copper(II) that have SOD mimetic activity (also called synzymes or synthetic enzymes), which could be substituted for SOD in clinical applications, with the desirable qualities of being low cost, reasonably permeable to cell and non-immunogenic.[25] Ligands in these l.m.w. copper complexes would offer the possibility of being vehicles of copper, delivering it to the site of inflammation where the enzyme is inactivated. They may also act as intermediates, allowing insertion of metal ions into appropriate proteins and enzymes.

Recently, a large number of l.m.w. copper(II) complexes have been synthesised, characterised and have been found to exhibit high SOD mimetic activities when superoxide radicals are generated by the xanthine-xanthine oxidase system.[8,9]

This SOD mimetic behaviour may suggest a much simpler mechanism that does not involve an enzyme. The extraordinarily efficient catalytic activity observed in both the enzyme and its mimetics has recently been accounted for by both the electrochemical potential of the pair Cu^{2+}/Cu^{+}, which is intermediate between potentials of the pairs O_2/O_2^{-} (E = -0.16V) and O_2^{-}/O_2^{2-} (E = 0.89V).[22] In fact, it is believed that any redox pair with a potential intermediate between the above two values can act as a catalyst for the dismutation reaction.[22]

Recently, SOD-mimetic copper complexes have been observed to down regulate nitric oxide synthase enzyme activity and hence decrease the synthesis of NO.[26] This observation should serve as an impetus in designing more l.m.w. complexes which have modulatory functions on the cascade of ill-processes responsible for the pathogenesis of RA. Since the biological anti-oxidant systems can be consumed during oxidative stress at levels that can exceed their production, these synzymes can serve as human therapeutics to counteract the deleterious effects of these oxidising substances.

2.2.2 Potential copper(II)-complexes as anti-inflammatory drugs in rheumatoid arthritis

In attempts to search for more effective and safer therapies, Jackson et al.[27] used computer simulation in an attempt to study the complexing conditions occurring *in vivo* and to assess Sorenson's biological activity data for copper chelate antiarthritic agents. In the simulation of oral treatment, COMPLOT models involving the equilibria between drug and protons and metal ions were used. These models approximate administration on an empty stomach and are based on the assumption that the presence of dietary and digestive components can be omitted since (i) the drugs exist in relatively high concentrations, and (ii) the gastro-intestinal contents are likely to have a constant influence upon the series of agents under consideration.

For subcutaneous administration of charged and neutral copper complexes, attempts were made to correlate COMPLOT simulation studies of concentration of these complexes with Sorenson's biological response data. Unfortunately, no correlations were found. The reason was that the complexes were administered as suspensions, which were insoluble and solubility and rates of dissolution could not be incorporated into the model calculations. However, oral administration at pH 2 indicated a direct correlation between anti-ulcer activity and the concentration of neutral complexes.

The blood plasma simulation studies using the ECCLES program,[27] revealed that all the administered copper complexes, with the exception of carboxyisoquinoline, release their copper to serum albumin. There were, however, ligands which encouraged a redistribution of the remaining copper amongst the l.m.w. ligand complexes present.

In general, the therapeutic activity is enhanced by administering exogenous copper, thereby increasing the total labile copper concentration in the anti-rheumatic process. However, it is also more difficult to move transition metal ions through a series of biofluid compartments without binding to proteins. The equilibrium competition for copper ion of administered ligand with the endogenous labile protein containing copper ion seems a more promising way of effecting this increase.

From their studies, Jackson et al.[27] eventually reported a list of desirable properties for future design of rheumatoid arthritic agents and these properties included among others the following:

- Powerful copper complexing properties as reflected by a high plasma mobilising index (p.m.i.).
- A multidentate ligand containing predominantly nitrogen donor atoms, which would confer a high degree of selectivity towards copper in order to minimise competition with zinc and calcium. These latter metal ions are present in plasma in "large" concentrations.
- The ligand must possess at least one dissociable proton and must not be easily metabolised.

Jackson and Kelly[28] used computer simulation (ECCLES program) in order to identify those features of a ligand, which would make it an ideal vehicle for the delivery of copper to the anti-rheumatic process. The simulation studies indicated that an ideal ligand would be a linear dicarboxylate, diphenolate or dialkyl phosphate substituted polyamine. These substituted polyamines would lose two protons on co-ordination to copper to form neutral complexes.

These results led to the synthesis of H_2ttda (L^a) and H_2dtda (L^b) (Figure1.1) and investigation of their complexation equilibria with copper,[29] zinc and calcium[30] as potential competitors of copper. The potentiometric results revealed that Cu^{2+} formed more stable complexes than Zn^{2+} and Ca^{2+} whereas the p.m.i.'s indicated that these two ligands were potential mobilisers of copper(II) *in vivo*. Dtda in addition, also caused some redistribution of zinc(II). Animal screens, however, showed that the copper-ttda complex was rapidly excreted into the urine. The complex remains intact in the blood stream and is too polar to effectively pass out of the blood into the tissue.

Recently, a number of diamine diamide (L^c derivatives)[31] and triamine-diamide[32] (L^d derivatives - Figure 1.1) ligands have been investigated potentiometrically, the latter containing a central amine with benzyl- or phenylethyl- substituents. The presence of the central amine was initially thought to provide a fifth strong coordination donor atom for copper(II) resulting in an enhanced thermodymamic stability of the complexes. The benzyl- and phenylethyl- groups at this central amine were envisaged to increase the lipophilicity of these complex species. In spite of these morphological alterations on these ligands, it was observed that the resulting copper(II) complexes are more likely to dissociate in plasma. This is due to their low formation constants and hence low mobilising indices. Low octanol/water partition coefficients of these copper complexes indicated that they are likely to be of little utility as topical agents in RA chemotherapy.

In an attempt to change the tissue distribution of these copper(II) complexes, tetramethyldiazadione dioxime ligands; PrAO (L^1), EnAO (L^f) and BuAO (L^g) (Figure 1.1) in which dione dioximes replaced the secondary amines and dicarboxylates of ttda

were considered.[33] In addition, solution equilibria of Zn^{2+} and Ca^{2+} with L^1 were also investigated.[34]

Potentiometric results showed the order of stability of the 11-1 copper(II) complex species dominant at pH 7.4 to be $L^1 > L^f > L^g$. The Zn^{2+} formation constant with L^1 for the same species was observed to be 11 orders of magnitude lower than that of copper while Ca^{2+} was found not to form any complex species with the ligand.

Blood-plasma computer simulation studies revealed that increased low-molar-mass copper(II) caused by L^1 was nearly the same as that caused by ttda. The blood-plasma mobilising indices of both ligands were some orders of magnitude greater than L^f and L^g. At a ligand concentration of 1.0×10^{-6} mol dm^{-3} the Zn^{2+} p.m.i. is less than 0.01 while that of Cu^{2+} is approximately equal to 1. Overall, these results indicated that the ligand L^1 is able to mobilise Cu^{2+} *in vivo* with little or no interference on Zn^{2+} and Ca^{2+} equilibria.

As a measure of the lipophilicity of the $[Cu(L^1)H_{-1}]^+$ complex, octanol/water partition coefficients were determined.[34] At pH 5.5-6.5 and 7.4, the pH range for the skin and plasma respectively, this species has a log $P_{oct/water}$ value of -1.01. This complex is reasonably lipophilic to predict that approximately 6% of it is likely to permeate both the skin and biomembranes when applied percutaneously and/or injected.[34] It is also predicted that the $[Cu(L^1)H_{-1}]^+$ complex should not decompose *in vivo*[33] in the same way as was found for $[Cu(ttda)H_{-2}]$.[30] The presence of methyl groups in $[Cu(L^1)H_{-1}]^+$ are believed to contribute significantly to the lipophilic nature of the complex in comparison with $[Cu(ttda)H_{-2}]$ and, it may therefore undergo slower urinary excretion.

2.3 Recent advances in the design of gadolinium(III) based contrast agents in MRI

Proper disease diagnosis plays a pivotal role in the design of chemotherapy and its usefulness for the disease in question. The use of contrast enhancement agents in MRI have revolutionised the technique by being able to highlight lesions that might otherwise be missed or overlooked on normal magnetic resonance images.[35]

Gd^{3+} is ideally suited to the design and use of contrast agents in MRI since it contains seven unpaired electrons, and hence high magnetic moment and relaxivity. On the other hand, polyaminocarboxylate chelating agents are used primarily to enhance thermodynamic stability. An added advantage offered by these polyaminocarboxylates is their high water solubility, which is ideal for *in vivo* applications. The octa-chelating nature of these ligands allows a single water molecule to interact with the bulk of solvent molecules, thereby increasing the relaxivity of the chelates by an inner sphere mechanism.[35,36]

The different ways in which the relaxivity of a given contrast agent may be modulated can be appreciated by a consideration of the equations defining the water relaxation rate, R_1. The paramagnetic contribution (eq. 2.1) to the overall relaxation rate is made up of outer-sphere, second-sphere and inner-sphere terms, of which the latter is usually the most significant.[35,36]

$$R_{1p} = R_{1p}^{os} + R_{1p}^{ss} + R_{1p}^{is} \qquad \text{---2.1}$$

$$\text{where } R_{1p}^{is} = (cq/55.6)\,[(T_{1m} + \tau_m)^{-1}] \qquad \text{---2.2}$$

The inner-sphere contribution is a function of four variables (eq. 2.2), i.e., the concentration of the complex, c; the number of directly bound water molecules, q; the exchange lifetime of the coordinated H_2O molecule, τ_m; and the longitudinal water proton relaxation time, T_{1m}. T_{1m} also depends on τ_r, the rotational correlation time.

Optimization of these molecular parameters determining the relaxivity of Gd^{3+} chelates is an ongoing objective, of relevance to the development of new, more effective MRI contrast agents.

The c and q variables can be modulated to a little extent since increasing the number of bound water molecules leads to a decreased *in vivo* stability of the complex and hence increased concentration and toxicity of hydrated Gd^{3+}. Image contrast enhancements are desirable at low concentrations of the complexes due to the toxic

nature of Gd^{3+}(aq), as well as the complications resulting from osmolality differences between the contrast agent and body fluids.

The relaxivity of low molecular weight Gd^{3+}-containing contrast agents is mainly limited by their fast rotational motion. Since the relaxivity of sphere-shaped molecules increases approximately linearly with molecular weight, new-generation MRI contrast agents will probably be complexes attached to, or incorporated in macromolecules.

Caravan,[35] Comblin[36] and Reichert et al.[37] have recently reviewed major efforts directed at the incorporation of gadolinium chelates in these large structures such as polymers, dendrimers, proteins, and micelles. In fact, the rotational correlational times of Gd^{3+} agents conjugated to β-cyclodextrins,[38] dendrimers,[39] and micelles[40] for example, have been found to be long enough for the water exchange to influence, or even limit, the overall proton relaxivity at imaging fields.

To date, the commercially approved Gd^{3+} compounds and those at several stages of clinical trials are extracellular agents with non-specific biodistribution and have relaxivities in the range 1-50 $mM^{-1}s^{-1}$. It is hoped that this new generation of contrast agents under development will also enable targeting of macromolecules associated with specific tissues or disease states thereby localizing the agent to the site of interest. At the high concentrations of contrast agents normally used in MRI scans, imaging of receptors is virtually impossible since they can be easily saturated. Higher relaxivities of the order of 100-200 $mM^{-1}s^{-1}$ will allow one to obtain MRI images with less contrast agent and could allow imaging of receptors as well.[35,36]

2.4 Structure and properties of skin and biomembranes in relation to dermal absorption and drug transport

The skin through the horny layer (or the stratum corneum (SC))[41-45] and lipid bilayers of biomembranes,[46-51] act as selective permeability barriers controlling the amount and nature of the substances that pass across them. The rigidity of the SC and

hence its ability to act as a barrier to drug translocation is due to the high levels of ceramides, glycosilceramides and cholesterol it contains.[44]

The initial process of drug's translocation across the skin involves partitioning of the penetrant into the surface lipids and lamellar domains of the SC.[44] This process is followed by diffusion through the epidermis and dermis before gaining access to the systematic circulation through the cutaneous microvasculature.[44] The ability of drugs to cross these biological barriers strongly affects their pharmacokinetic behaviour and capability to access the targets of interest such as the inflammatory sites and tumours.

The synovial joint of arthritic patients is regarded as a peripheral compartment of distribution and the target organ of NSAIDs, DMARDs and glucocorticoid therapy mentioned in the preceding chapter and the envisaged copper(II)-based anti-inflammatory drugs required for the induction of copper-zinc SOD. Their concentration in this synovial fluid is, therefore, an important determinant of clinical response.

These processes are depicted by the hypothetical model indicating the movement of drug from the epidermal surface through a series of body compartments before reaching the synovial fluid as given below.

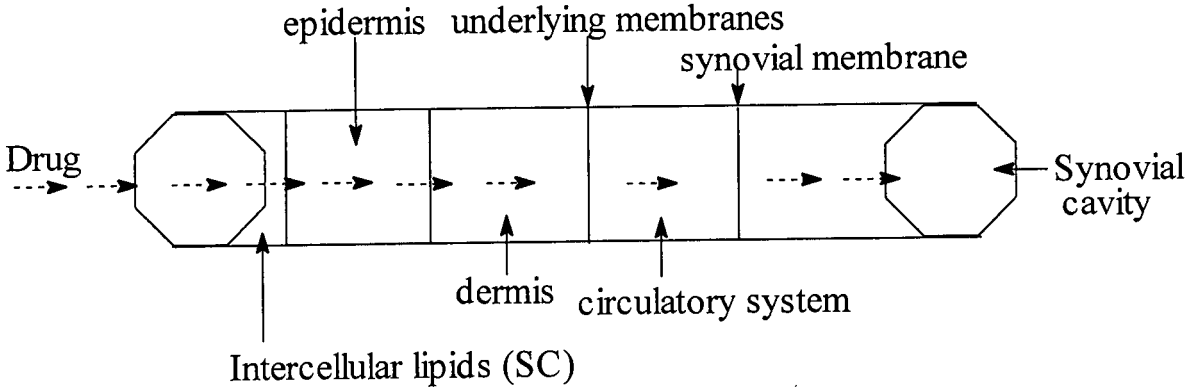

This joint is separated from the blood compartment by the synovial membrane, which can be likened to a double barrier consisting of the capillary endothelium and synovial tissue interstitium. Just like in percutaneous absorption, the trans-synovial transport of drugs is a process of limited diffusion. It is governed by the drugs' chemical

and physical properties such as the molecular weight, lipophilicity, protein binding and the joint space characteristics, for example, disease state and protein concentration.[48]

Since the pH of the skin[41,44] ranges between 5.5-6.5 while that of the blood-plasma[46-51] is 7.4, neutral species are desirable in this pH range for a larger concentration of the drug to reach the target site, the synovial cavity. Low molecular agents ($M_r \leq 600$ g/mol) are ideally suited for passive diffusion since available evidence indicates that the primary penetration pathway is through the intercellular lipids and passage openings termed pores.[44]

It has long been observed that percutaneous absorption as an initial permeation process, is enhanced in the diseased skin because the barrier zone (stratum corneum and to some extent the stratum granulosum) is defective.[44,45] Furthermore, because the synovial membrane in particular is damaged in acute RA, permeation rate across it increases resulting in higher concentrations of chemotherapeutic agents reaching the target site.

There should be a balance between the lipophilic and hydrophilic nature of the drug in question. This is because although its lipophilicity enhances the initial partitioning into the epidermal intercelluar lipids, the inner viable underlying hydrophilic dermis can hinder the penetration of very hydrophobic agents.[44] Hence, it remains bound in lipid bilayer.

Drug translocation across the skin and membranes also depends on the membrane fluidity[45-50] as demonstrated in rat canalicular membrane vesicles.[46,47] In fact, epidermal lipids such as phospholipids, which contain unsaturated fatty acids make the membrane more permeable to drugs.

There is ample evidence indicating the presence of drug transporters in biomembranes, which facilitate drug translocation.[45-50] The nature and functioning of these transporters are poorly understood but an important process may involve drug partitioning followed by its interaction with the transporter within the lipid phase.[46-50]

Much research work has been directed at the development of vehicles to enhance percutaneous absorption of metal ion containing chemotherapeutic agents.[44] This is as a result of low observed permeation rates observed for these often charged hydrophilic compounds compared to normal organic compounds. This is actually one of the reasons why metal-based therapies have been of little interest to medicinal chemists and the pharmaceutical industries.[52]

Oil/water and dimethyl sulphoxide/water mixures have been extensively used as vehicles. These vehicles should exhibit reduced affinity for the drug to promote absorption. The use of water as a component of a vehicle mixture stems from its ability to increase membrane permeability to topically applied agents.

Lichtenstein and Margalit[52] have recently studied the thermodynamics and kinetics of drug encapsulation in liposome to improve delivery. Morganti et al.[44] give an extensive review of the structure of skin in relation to drug transport and the latest research advancements in drug targeting.

Presently, the reference parameter for the prediction of passive diffusion of drugs through biological barriers is the measure of their lipophilicity, expressed as the logarithm of the partition coefficient between 1-octanol and an aqueous phase.[54]

Besides being widely used to predict the lipophilicity of drugs, octanol/water partition coefficient investigations have been recognised in Quantitative Structure-Activity Relationship (QSAR) studies[54-56] to effectively correlate with various biological phenomena. These phenomena include the prediction of binding of solutes to biological molecules such as serum albumin and several purified enzymes.[54] Such studies are, as a result, essential in the initial screening process of drug bio-availability.

2.5 Conclusion

Metal complexes that will ultimately prove successful in chemotherapy must meet numerous criteria, including high efficacy *in vivo*, low metal toxicity, tissue and organ

specificity, rapid clearance by the biological system, and an overall image enhancement when applied to contrast agents in MRI.

One real challenge pertaining to the design of functional metal ion diagnostic and/or therapeutic agents, lies among other features, in the need for a precise control of ligand coordination abilities.

Relying upon these metal complexes for chemotherapy and diagnostic tools, researchers are striving to develop new non-natural ligand systems that simultaneously offer biomimicry, biostability, biocompatibility and bioactivity. Successful research in this area will be able to produce therapeutic agents and biomimetic agents that will be useful and safe for *in vivo* applications. In an attempt to make significant strides in this direction the aims and objectives of this study were set out as briefly discussed below.

2.6 Aims and objectives of this study were:

- To synthesise and characterise three poly amine/amide/dioxime ligands, L^1 (PrAO), L^2 (H_2pap) and L^3 (BIDPAP), Figure 1.1.
- To determine the formation constants of Gd^{3+} with L^1 and those of Cu^{2+}, Ni^{2+}, Zn^{2+}, Ca^{2+} and Gd^{3+} with L^2 and L^3 using glass-electrode potentiometry at 25^0C and an ionic strength of 0.15 *mol* dm^{-3} NaCl. The interest is centered on the possible use of Cu^{2+} and Gd^{3+} complexes in chemotherapy and as contrast agents in MRI respectively, while simultaneously gaining more insight on the potency of Zn^{2+} and Ca^{2+} as *in vivo* competitors. The Ni^{2+} solution equilibria are investigated for comparison since the metal normally forms stable complexes with ligands which coordinate strongly to copper.
- To calculate p.m.i.'s based on the formation constants determined since a high selectivity of the ligand for a particular metal ion and its ability to mobilise it *in vivo* is usually reflected by a high p.m.i..
- To elucidate the structures of the various copper(II) and nickel(II) species present in solution, using spectroscopic techniques.

- To measure the octanol/water partition coefficient of the copper(II) complexes of L^2 and L^3 as an indication of their lipophilicity.
- To investigate the SOD mimetic activity of the copper(II) complexes and lastly,
- To perform biodistribution experiments of radio-labeled ^{64}Cu-L complexes on mice as animal screens in order to get an insight on their *in vivo* behaviour and stability.

2.7 Thesis structure

- Chapter 1 is an introduction where the focus is centered on the origin of RA, its diagnosis using MRI and its present therapy.
- Chapter 2 focuses on recent developments in copper chemotherapy in RA and contrast agents in MRI.
- A literature review of the experimental techniques and design is the theme of chapter 3 while chapter 4 details the experimental procedures and analytical methods to achieve the objectives of this study.
- The results are given in chapter 5 together with the discussion whereas chapter 6 outlines the major conclusions drawn from this study.

References

1. J.R.J Sorenson, *In Metal ions in biological systems, Inorganic drugs if deficiency and disease*, 1982, **14**, 104, [Editor: H. Sigel], Marcel Dekker, Inc. New York.
2. D.L. Scott, J.S. Smolen, J.R. Kalden, L.B.A. van de Putte, A. Larsen, T.K. Kvien, M. Schattenkirchner, P. Nash, C. Oed, I. Loew-Friedrich, *Ann. Rheum. Dis.*, 2001, **60**, 913.
3. J.R.J. Sorenson, *J. Med. Chem.*, 1976, **19**, 135.
4. D.H. Brown, W.E. Smith and J.W. Teape, *J. Med. Chem.*, 1980, **23**, 729.
5. R. Cini, G. Giorgi, A. Cinquantini, C. Rossi, M. Sabat, *Inorg. Chem.*, 1990, **29**, 5197.
6. V. Brumas, B. Brumas and G. Berthon, *J. Inorg. Biochem.*, 1995, **57**, 191.
7. H. Miche, B. Brumas and G. Berthon, *J. Inorg. Biochem.*, 1997, **59**, 27.
8. J.-L. Pierre, P. Chautemps, S. Refaif, C. Beguin, A. El Marzouki, G. Serratrice, E. Saint-Aman, P. Rey, *J. Am.Chem. Soc.*, 1995, **117**, 1965.
9. G. Tabbi, W.L. Driessen, J. Reedijk, R.P. Bonomo, N. Veldman and A.L. Spek, *Inorg. Chem.*, 1997, **36**, 1168.
10. Advances in Molecular and Cell biology, 1993, **6**, 36, Editors: E. Edward-Bittar and H.K. Kleiman, Jai Press Inc. Connecticut.
11. T.J. Lyons, A. Nersissian, J.J. Goto, H. Zhu, E.B. Gralla, J.S. Valentine, *JBIC*, 1998, **3**, 650.
12. J.A. Tainer, E.D. Getzoff, J.S. Richardson and D.C. Richardson, *J. Mol. Biol.*, 1982, **160**, 181.
13. J.A. Tainer, E.D. Getzoff, J.S. Richardson and D.C. Richardson, *Nature*, 1983, **306**, 284.
14. R.A. Edwards, M.M. Whittaker, J.W. Whittaker, G.B. Jameson, H.M. Baker and E.N. Baker, *JBIC*, 1998, **3**, 161.
15. M. Ferraroni, W.R. Rypniewski, B. Bruni, P. Orioli and S. Mangani, *JBIC*, 1998, **3**, 411.
16. R. Osman, H. Basch, *J. Am. Chem. Soc.*, 1984, **106**, 5710.

17. M. Rosi, A. Sgamelloti, F. Tarantelli, I. Bertini, C. Luchinat, *Inorg. Chem.*, 1986, **25**, 1005.

18. E.D. Getzoff, J.A. Tainer, P.K. Weiner, P.A. Kollman, J.S. Richardson and D.C. Richardson, *Nature*, 1983, **306**, 287.

19. J.A. Fee, C. Bull, *J. Biol. Chem.*, 1986, **261**, 13000.

20. J.J. Sines, S.A. Allison, J.A. McCammon, *Biochemistry*, 1990, **29**, 9403.

21. L. Banci, I. Bertini, C. Luchinat and R.A. Hallewell, *J. Am. Chem. Soc.*, 1988, **110**, 3629.

22. L. Banci, I. Bertini, C. Luchinat, M. Piccioli, *Coord. Chem. Rev.*, 1990, **100**, 67.

23. A. Petrovic, A. Comi, M.J. Ettinger, *J. Biol. Chem.*, 1996, **271**, 28331.

24. C. Steinkuhler, O. Sapora, M.T. Carri, W. Nagel, L. Marcocci, M.R. Ciriolo, U. Weser and G. Rotilio, *J. Biol. Chem.*, 1991, **266**, 24580.

25. D.P. Riley, *Chem. Rev.*, 1999, **99**, 2573.

26. J.G.L. Baquial and J.R.J. Sorenson, *J. Inorg. Biochem.*, 1995, **60**, 133.

27. G.E. Jackson, P.M. May and D.R. Williams, *J. Inorg. Nucl. Chem.*, 1978, **40**, 1227.

28. G.E. Jackson and M.J. Kelly, *Inorg. Chim. Acta*, 1988, **152**, 215.

29. G.E. Jackson and M.J. Kelly, *J. Chem. Soc., Dalton Trans.*, 1989, 2429.

30. G.E. Jackson and M.J. Kelly, *J. Chem. Soc., Dalton Trans.*, 1990, 1889.

31. A. Voye, PhD Thesis, University of Cape Town, 1993.

32. L. Mkhonta-Gama, PhD Thesis, University of Cape Town, 1999.

33. G.E. Jackson and B.S. Nakani, *J. Chem. Soc., Dalton Trans.*, 1996, 1373.

34. T.E. Nomkoko, MSc Thesis, University of Transkei, 2000.

35. P. Caravan, J.J. Ellison, T.J. McMurry, and R.B. Lauffer, *Chem. Rev.*, 1999, **99**, 2293.

36. V. Comblin, D. Gilsoul, M. Hermann, V. Humblet, V. Jacques, M. Mesbahi, C. Sauvage, J.F. Desreux, *Coord. Chem. Rev.*, 1999, **185**, 451.

37. D.E. Reichert, J.S. Lewis, C.J. Anderson, *Coord. Chem. Rev.*, 1999, **184**, 3-66.

38. S. Aime, M. Botta, L. Frullano, S.G. Crich, G.B. Giovenzana, R. Pagliarin, G. Palmisano and M. Sisti, *Chem. Eur. J.*, 1999, **5**, 1253.

39. E. Toth, D. Pubanz, S. Vauthey, L. Helm and A.E. Merbach, *Chem. Eur. J.*, 1996, **2**, 1607.

40. J.P. Andre, E. Toth, H. Fischer, A. Seeling, H.R. Macke and A.E. Merbach, *Chem. Eur. J.*, 1999, **5**, 2977.

41. J. Danielsson, J. Ulicny, and A. Laaksonen, *J. Am. Chem. Soc.*, 2001, 123, 9817.

42. A.M. Kligman and J.A. Leyden, *Safety and Efficacy of Topical Drugs and Cosmetics*, 1982, 99.

43. *Cosmetic Dermatology*, 1994, 1, [Editors: R. Baran and H. Maibach], Matin Dumitz Ltd London, UK.

44. P. Morganti, E. Ruocco, R. Wolf and V. Ruocco, *Clin. Dermatol.*, 2001, **19**, 489.

45. M.-H. Tan, M. Lebwohl, A.C. Esser, H. Wei, *J. Am. Acad. Dermatol.*, 2001, **45**, 392.

46. W. Stoeckenius, *J. Membrane Biol.*, 1994, **139**, 139.

47. A.S. Verkman, *J. Membrane Biol.*, 1995, **148**, 99.

48. T.X. Xiang and B.D. Anderson, *J. Membrane Biol.*, 1994, **140**, 111.

49. H.H. Ussing, *J. Membrane Biol.*, 1994 **137**, 91.

50. F.J. Sharom, *J. Membrane Biol.*, 1997, **160**, 161.

51. C.R. Leveille-Webster and I. M. Arias, *J. Membrane Biol.*, 1995, **143**, 89.

52. B.R. Cameron and I.R. Baird, *J. Inorg. Biochem.*, 2001, **83**, 233.

53. A. Lichtenstein and R. Margalit, *J. Inorg. Biochem.*, 1995, **60**, 187.

54. A. Leo, C. Hansch and D. Elkins, *Chem. Rev.*, 1971, **71**, 525.

55. H. Gao, J.A. Katzenellenbogen, R. Garg and C. Hansch, *Chem. Rev.*, 1999, **99**, 723.

56. R. Garg, S.P. Gupta, H. Gao, M.S. Babu, A.K. Debnath and C. Hansch, *Chem. Rev.*, 1999, **99**, 3525.

CHAPTER 3

A Theoretical Review of Literature

Glass Electrode Potentiometry, UV/Visible Spectrophotometry and Ancillary studies

3.1 Theoretical basis of solution chemistry

Solution co-ordination chemistry continues to provide the fundamental design properties of metal complexes in chemotherapy and as contrast agents in MRI. The chemical nature and concentration of each species present under equilibrium conditions in solutions are related to formation constants.[1] These are some of the basic design properties of utmost importance in biomedical analyses, and this study concerns itself primarily with these design principles.

3.1.1 Factors influencing complex stability and selectivity in aqueous solution

Stability constants measure the degree of interaction of metal ions and ligands at equilibrium under specific conditions.[1-5] Hancock and Martell[2] have given a comprehensive review of the factors that influence complex stability and the ligand design for selective complexation of metal ions in aqueous solution. These include among others the nature of donor atoms comprising the ligand, its denticity,[2,6] the extent of its preorganisation,[7,8] the nature of the rings formed due to complexation and the metal ion concerned.

In fact, it has been observed that subtle changes in the nature of the ligand backbone, its donor atoms and their arrangements can have a dramatic influence on the co-ordination behaviour of the ligand towards particular metal ions.[2,3] These changes together with some other functionalities not involved in metal ion coordination can also determine the bio-availability of the metal ion(s) concerned. Ligand design and the development of its efficient synthetic procedures, as a result underlie much of modern co-ordination chemistry.

It is well known that Cu^{2+} prefers ligands with nitrogen donor atoms, while Zn^{2+} on the other hand forms weaker complexes than Cu^{2+} with these ligands as predicted by the Irving-Williams series.[2,3] This is despite the borderline nature of both metal ions according to HSAB classification.[9]

In contrast, these nitrogen atoms are poor electron donors for hard metal ions such as Ca^{2+} and Gd^{3+}, but become better donors when hard negatively charged oxygen atoms are present. This is indicated by the high formation constants for

ligands of these metal ions with EDTA, DTPA, DOTA and related polyaminocarboxylates compared with en, diethylenetriamine and (12-14)aneN_4. These metal ions form weak or no complexes at all with these latter ligands.[2,3]

Although these formation constants can be predicted fairly accurately for polyamines using appropriate equations,[2,3] the predictions become less accurate for polyfunctional multidentate ligands. This is due to the uncertainty of the binding modes for these ligands and the nature of the species present in solution. These factors are influenced by the conformational aspects and preferences, hence their experimental determination becomes an obvious option.

Experimental methods[2-4] for their determination fall into two broad categories, namely: electrochemical and spectroscopic methods which are based on the observable that is proportional to the activity and number of molecules of a given type present, respectively. Glass electrode potentiometry (GEP) falls under the electrochemical methods and is usually supplemented by UV-visible spectrophotometry for structure elucidation.

3.1.2 Glass electrode potentiometry

GEP has been described[1-4] as 'by far the most accurate and widely applicable technique currently available for the study of ionic aqueous equilibria'. In fact, approximately eighty percent (80%)[3] of the reported stability constants in the literature[5] have been determined by this technique.

The ease of availability of the glass electrode, its linear Nernstian response, rapid reversibility and high sensitivity to aqueous hydrogen ions over a wide concentration range makes it an ideally suited technique for the study of these equilibria. Although a non-linear, non-Nernstian response could in theory be tolerated by using suitable calibration curves, such responses are often symptomatic of non-reversibility. Solvents have been observed to play an important role in this reversibility and, in reality, a glass electrode that is reversible in one solvent is not necessarily reversible in another solvent.[4,10,11]

GEP employs measurement of an electrode potential (eq. 3.10) across the membrane and its variation with changing H^+_{aq} concentration in the experimental solution.[1,4,10,11]

$$E = E^0 + s \log[H^+] \qquad ---3.10$$

where E^0 is the electrode response intercept and *s* the electrode response slope. The arrangement for such a cell may be represented as shown below.[10,11]

```
Ag|AgCl|KCl(3M)||test solution|glass-membrane |HCl(0.1M)|AgCl|Ag
External reference                             internal reference
```

The external reference electrode can be placed in the same package as the pH electrode - forming a combined micro-electrode, which has some advantages for routine analysis of small volume samples.

Its mode of functioning is very complex and an important stage probably involves the adsorption of H^+_{aq} ions into the glass lattice. This may thus explain the questionable reliability at pH values below 2 and above 12, where probably infiltration of Na^+ ions (if present) and anion surface adsorption, respectively, occurs.

3.1.3 Experimental technique and design

In order to obtain reliable values for the parameters of interest, e.g. formation constants, in an experiment, it must be well designed to 'define' the system as unequivocally as possible. This is because the agreement between the 'actual experiment' and the output data is influenced by the reliability of the input data.

As a fundamental requirement, a glass-electrode must be checked for reversibility to $H^+_{(aq)}$ ions before it can be used in any potentiometric work. Reversibility should always be checked by both increasing and decreasing the proton concentration and checking that both plots are superimposable within the experimental error. This constitutes an internal calibration of the electrode. In addition, it has been observed that E^0 varies on a day-to-day basis due to an asymmetry potential, E_a.[1,12-14] This potential may well originate in the different conditions of strain in the two surfaces separated by the glass-membrane.[1,12-14]

Standard buffers are normally used to ensure the constancy of E^0 over a selected range in what is known as external calibration.

Moreover, these acid-base calibration titrations are helpful in the evaluation of the electrode parameters such as the standard electrode potential, E^0, the electrode response slope (s) and the autoprotolysis constant of water (K_w). In fact, the determination of formation constants using iterative Newton-Raphson procedures requires that this set of initial estimates be very good.

On the other hand, the second set includes ligand concentration and protonation constants, and both sets depend upon the degree of certainty in the determination of the concentrations of acid and base. Acid and base concentrations are obtained by analysing acid-base titrations in the location of the volume-end point using specific techniques like the differential methods[15] and Gran plot procedure.[15,16]

Potentiometrically determined constants are affected by changes in ionic strength (I). To ensure constancy in this ionic strength, it is more proper to use a large excess of an inert background electrolyte which does not react with any of the metal, ligand, or metal-ligand species.[4] Alternatively, low concentrations of metal and ligand can be used so that any change in their concentrations, as a result of their reaction together has an insignificant effect on the overall ionic strength of the medium.

To correct for formation constants determined at various ionic strength conditions, the equation below which incorporates the extended Debye-Huckel formula is used,[17,18]

$$\log K^c = [(A \mid Z_+Z_- \mid (I)^{1/2})/1+Ba(I)^{1/2}] + cI + \log K^{I=0.0} \qquad \text{---3.11}$$

where Z_+ and Z_- are the charges of the ions constituting the dissolved electrolyte and for water at 25^0C where its density and relative permittivity are 0.997 $g.cm^{-3}$ and 78.54 respectively, the value of A is 0.509, a = 1/B, c =$0.3Az^2$ and I is as given below.[17,18]

$$I = 0.5 \sum c_i z_i^2 \qquad \text{---3.12}$$

However, formation constants are also affected by temperature as expressed by the van't Hoff equation 3.13.[18]

$$\partial \ln K/\partial T = \Delta H^0/RT^2 \qquad \text{---3.13}$$

The importance of this equation lies on the fact that it is easy to convert and compare formation constants determined at different temperatures if those temperatures and the value of ΔH^0 for the system are known.

Thus, when carrying out potentiometric studies (clearly this applies to any method of determination), it is extremely important to control the temperature to at least $\pm 0.05^0$C.

It has been shown that if the error in the temperature is $\pm 0.02^0$C, then the error in the activities will be 0.5z%, where z is the charge of the electro-active ion. Because of the close temperature control required it is advantageous, if temperatures far removed from room temperature are to be used, to use water-jacketed vessels and burettes.[4]

3.1.4 Formation constants determination

For a given ligand, all stability constant studies essentially involve competition between two metal ions (one of which may be H^+). Probably the most accurate and reliable method for their determination potentiometrically is to titrate one solution (acid or alkali) with another (of constant total metal and total ligand with alkali or acid), the potential being determined after each addition of titrant.[4]

The difficulty with this approach is for systems that form weak complexes. Here the change in potential consequent to dilution of the initial solution can be large relative to the change in potential due to complex formation. If a metal ion solution is being titrated with a ligand solution, then this difficulty can be obviated by making equal volume additions of ligand and metal solutions of exactly double the strength of the solution being titrated. This ensures that the total ion concentration remains constant.[4]

Although this method has been widely used to determine stability constants, there are a number of limitations.

- It cannot be used under conditions of extreme pH, where at high pH the concentration of free ligand is insensitive to pH change and at low pH the free ligand concentration becomes negligible owing to virtually complete protonation.
- At very low total metal concentrations ($T_M \approx 0$), the method is inapplicable because the complex formation function (Z-bar) cannot be determined reliably.
- The method is also inapplicable for very stable complexes because the protons are unable to compete effectively with such metal ions for such ligands. Such complexes may, however, be studied by replacing the proton with another metal ion that can compete effectively with the metal ion under test and be detected potentiometrically or by some other method.
- Since aqueous solutions always contain hydroxide ions and most metal ions form not only hydroxo-species but also polynuclear species,[4,17,18] care must be taken either to work in sufficiently acidic solutions that hydroxo-complex formation is negligible or to take these into account during data analysis.

To get reliable stability constant values in potentiometric titration calculations such as non-linear least-squares procedures, the following few points are perhaps pertinent.[4]

- The potentiometric equipment should be tested by a well documented system to see if it is functioning properly.
- Once that is done, the potentiometric titrations for the system of interest should be carried out at more than one total metal/ligand concentration.
- Ideally each titration ought to be followed with two or more electrodes of different types. The large volume of data generated is a positive advantage in defining the system.
- The residual sum of squares should be defined in terms of the observed dependent variable, emf, and not some function of it.
- Suspect values or trends manifested in the form of error must be carefully investigated.

In any solution of constant ionic strength, containing metal ions, M, ligands, L, and protons, H^+, a general equilibrium reaction can take place as described by equation 3.14 below, where p, q and r are the stoichiometries of the components in the complex.[19,20]

$$pM + qL + rH \rightleftharpoons M_p L_q H_r \qquad ---3.14$$

The equilibrium constant for this reaction is then designated by the symbol β_{pqr} given below.

$$\beta_{pqr} = [M_pL_qH_r]/[M]^p[L]^q[H]^r \qquad ---3.15$$

For convenience species $M_pL_qH_r$ is denoted by three stoichiometric coefficients given in the order M, L and H, i.e. 11-1 denotes the complex species MLH_{-1} with r = -1 referring to removal of a proton from either a coordinated ligand or a bound water molecule or an hydroxide ion addition to the complex.[19,20]

In an acidic solution many polydentate ligands give 'protonated complexes'. The name protonated complex denotes a complex in which some donor atoms of a polydentate ligand are co-ordinated to a metal ion while others are protonated, i.e. $M_pL_qH_r$ can be regarded as a protonated complex if $r \geq 1$.[4]

3.2 Theory of Data Analysis

Stability constants are not directly measurable but are calculated from an observed response function of a fixed, but experimentally adjustable, variable, the emf. These parameters of interest are then calculated from the experimental data and the assumed functional form relating the dependent to the independent variables.

It is this good mathematical model that is necessary in describing the data, otherwise the presence of further species in solution may be overlooked and inaccurate stability constants will be evaluated. The establishment and use of mass balance equations (m.b.e.'s) ensures that all possible complex species of a system in question are detected, and hence all their respective formation constants are

calculated.[4] Chemical knowledge and experience can then be applied as a final check that the calculated parameters are reasonable.

3.2.1 *Equilibrium Simulation for Titration Analysis* (ESTA) Program Library[21]

The program ESTA is a flexible computational tool for the determination of protonation and formation constants in aqueous chemical equilibria. In ESTA, a Gauss-Newton method is used to minimise the objective function, U_{obj}, while the m.b.e.'s are solved in an iterative Newton-Raphson manner.

This objective function is optimised by the task OBJE (optimisation with respect to the observed emf) within the ESTA2 module. Optimisation with respect to the emf is more appropriate because the dynamic range of the emf change is large. Total concentrations are sometimes used in the optimisation but these are not as sensitive to speciation as the emf.

To take full advantage of the large amount of data generated, ESTA calculates two other concentration variables (functions).[21] Depending on the chemical systems being investigated, like ligand, the binary and ternary systems, these functions are defined differently for all of them. They are the formation function (Z-bar) and deprotonation function (Q-bar) calculated by tasks ZBAR and QBAR respectively within the ESTA1 module.

A model is assumed to be correct if there is a satisfactory fit between the observed and calculated functions as well as reasonable low standard deviations in $\log\beta_{pqr}$'s and Hamiltonian R-factor.

This program library also incorporates the task SPEC within the same ESTA1 module. This calculates the distribution of species taking part in an equilibrium system as a function of pH of the solution.

3.2.1.1 The Objective Function (U_{obj})[21]

The objective function is described as the summation of all the squared residuals of the real parameter values from the calculated values.

This function is given by equation 3.16 below,

$$U_{obj} = (N - n_p)^{-1} \Sigma n_e^{-1} \Sigma w_{nq} (y_{nq}^{obs} - y_{nq}^{calc})^2 \quad ---3.16$$

where N is the total number of experimental points ≅ 70 for a single titration, n_p is the number of parameters being optimised, n_e is the total number of electrodes (equal to 1 in this study), and w_{nq} is the weight of the q^{th} residual while y_{nq} is the electrode emf of electrode q both at the n^{th} titration point.

In order to minimise U_{obj}, a Gauss-Newton approach is used. The objective function assumes that the function is quadratic with respect to all the parameters, hence U_{obj} can be expressed as:

$$U_{obj} = a + p^t b + (p^t H p)/2 \quad ---3.17$$

where H, the Hessian, is given by $H_{sr} = (\partial^2 U_{obj}/\delta p_s \delta p_r)$.

If a system is well defined, by using a good set of initial estimates including the hydrolysis constants, the system will converge. Once U_{obj} is minimised, the standard deviation, the Hamilton R-factor and its limit and the correlation coefficients are then calculated and reported together with the optimised values of the stability constants.[21]

3.2.1.2 Formation function (Z_M-bar)[21] and deprotonation function (Q_M-bar)[21]

The complex formation function, Z_M-bar, measures the average number of ligands bound per metal ion at each concentration of ligand. This function is usually plotted against pA, defined as -log[L][21] and is given by equation 3.18.

$$Z_M = (T_L - [L])/T_M \quad ---3.18$$

where T_L and T_M are the total ligand and metal concentrations respectively and [L] is the free-ligand concentration. T_L is given below by equations 3.19.

$$T_L = [L] + \Sigma q \, \beta_{pqr} [L]^q [H]^r \quad ---3.19$$

On the other hand, the deprotonation function, Q_M, is the average number of protons released from the ligand per metal ion, as a result of complexation.

$$Q_M = (T_H^* - T_H)T_M \qquad ---3.20$$

where T_H and T_M are the total proton and metal concentrations respectively; T_H^* is the calculated total concentration of protons that would be necessary to give rise to the observed pH if no complexation took place.

For the evaluation of T_H^*, one needs to solve for the free-ligand concentration using equation 3.19 as given above. This is followed by the total calculated proton concentration given below,

$$T_H^* = [H] - [OH] + \sum r\beta_{oqr}[L]^q[H]^r \qquad ---3.21$$

where $[OH] = K_w/[H]$. The summation is over all protonated ligand species.

In binary systems, a formation function representing the number of protons that would be bound on the ligand in the absence of the metal ion, is simultaneously defined as n_H. This function n_H is given by equation 3.22 below.

$$n_H = (T_H^* - [H] + [OH])/T_L \qquad ---3.22$$

The difference between n_H and Q_M gives the number of protons on the complex. This can be represented as:

$$r = (q \times n_H) - (Q_M \times p) \qquad ---3.23$$

where p and q are the stoichiometric co-efficients of the metal and the ligand respectively. If $p = q = 1$, and $n_H = Q_M$, then $r = 0$ and hence we talk of the ML species whose stability constant is given by β_{110}. It is possible that r may be less than 0 ($r<0$) in which case either the deprotonation of the complex formed or the formation of the hydroxo species is envisaged.

The degree of metal ion hydrolysis in aqueous solution depends on a number of factors, including the polarising power of the metal ion and the pH of the solution.

The contributing equilibria for hydroxide formation can be set out as follows for a divalent metal ion M^{2+}:[17,18]

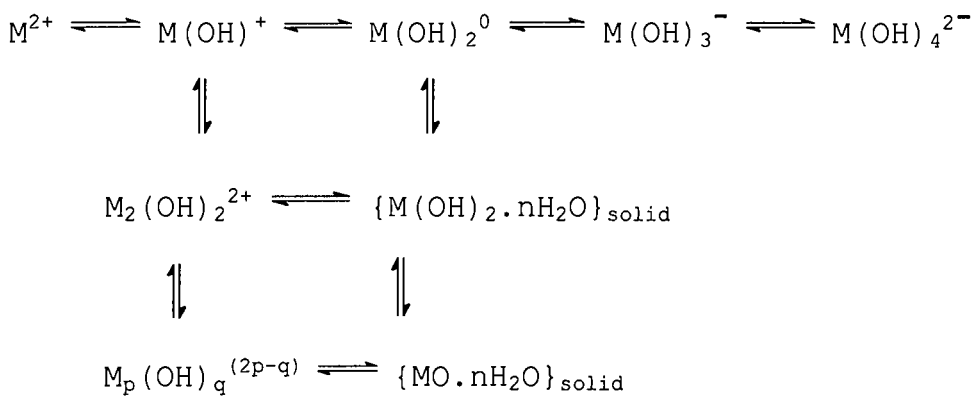

These equilibria have to be taken into account in the potentiometric determination of stability constants. Although most metal ions hydrolyse to form polynuclear species, in dilute solutions and in the presence of strong chelating agents, it is usually sufficient to consider the formation of mononuclear, monohydroxy complexes only.

For the reaction,

$$M + iH_2O \rightleftharpoons M(OH)_i + iH \qquad \text{---3.24}$$

the overall stability constant β_i^* is introduced in accordance with the IUPAC notation:

$$\beta_i^* = [M(OH)_i].[H]^i/[M] \qquad \text{---3.25}$$

Polynuclear complexes arise whenever there is a ligand capable of bonding to more than one metal ion. Such ligands include hydroxide, carboxylate etc., as well as multidentate ligands that may act in a bridging fashion. In general the presence or absence of polynuclear species can be confirmed by making a series of measurements at two or more widely different metal ion concentrations.

Analysis of these two or more sets of data should lead in the first instance to two or more identical sets of stability constants and then to two (or more) superimposable complex formation plots if polynuclear species are absent.[4] If this does not occur, i.e. if two or more distinct formation plots that only merge at very high

and very low ligand concentrations are observed, then polynuclear species are probably present.[4]

Such tests should always be carried out, even where polynuclear complexes are not suspected, to confirm their absence. Patterns in the residuals are also more easily seen if the calculated and observed curves formed by measurement of the dependent variable are plotted out. The residuals should always be examined and suspect values thoroughly investigated before a potentiometric model can be accepted.

3.2.1.3 Standard deviations[21]

When the estimates of the parameters being optimised are judged to be sufficiently close to the solution, the method of least-squares estimates the errors in the parameters of interest. The standard deviations are the errors of the parameters sought and may be calculated as shown below,

$$\sigma_r = [U \times G_{rr}/N - n_p]^{0.5} \qquad \text{---3.26}$$

where G is the reciprocal of the Hessian, i.e., $G = H^{-1}$.

3.2.1.4 Hamilton R-factor[4,21]

An important quantity which has been used in non-linear estimation situations is the Hamilton R-factor (R^H_f).

In this procedure the R^H_f is defined by:

$$R^H_f = [U/\Sigma n_e^{-1} \Sigma w_{nq}(y_{nq}^{obs})^2]^{1/2} \qquad \text{---3.27}$$

and is compared with R^H_{lim} calculated from:

$$R^H_{lim} = [N/\Sigma n_e^{-1} \Sigma w_{nq}(y_{nq}^{obs})^2]^{1/2} \qquad \text{---3.28}$$

The symbols have their usual meaning as outlined in section 3.2.1.1. R^H_{lim} is the best possible R value based on the error in the analytical data and the number of variables. The closer R^H_f is to R^H_{lim} the better is the fit between the experimental and

calculated data. Clearly the continued refinement of the model once $R^H_f < R^H_{lim}$ is meaningless.[4]

3.2.1.5 Correlation co-efficients[4,21]

The correlation co-efficient between two parameters can be quantified as,

$$r_{ij} = - G_{ij} /(G_{ii} G_{jj})^{0.5} \qquad ---3.29$$

where G is as indicated above. The correlation co-efficients have values between 0 and 1, and provide a measure of the linear dependence of one parameter on another while the remaining parameters are fixed.

Significant parameter correlation ($r_{ij} \geq 0.9$) has often been reported in the literature, particularly in potentiometric and spectrophotometric work.[4] Highly correlated parameters are not desirable because they are not separately defined by the data and only a linear combination of them can be estimated from the data. This means that it is possible to have a good fit to the data even with one parameter erroneously estimated, as the error in this parameter can be offset by an appropriate change in the other. Reduction of the correlation co-efficients always improves the conditioning.[4,21]

3.2.1.6 Species distribution curves

The real use of formation constants lies largely in the prediction of the feasibility of particular reactions to occur under specified experimental conditions. Linder et al.[1] put it in simple terms as: "Even if no practical reason can be put forward for the determination of formation constants and the calculation of the concentrations of the species present at equilibrium, there is always a strong, albeit non-utilitarian, case 'for knowing what is going on'". Recently, the formation constants have been extensively used in speciation calculations.[1]

After analysis of the potentiometric titration data, the equilibrium distribution of a well defined system would be easily found by use of task SPEC within the ESTA1 module.[21] The knowledge of concentration speciation based on solution

equilibria investigations gives a much deeper understanding of the principles underlying analytical techniques.

A distribution diagram represents a family of curves showing the relative proportions of the individual species taking part in an equilibrium system under different conditions.[18,21]

The distribution curves are defined by distribution co-efficient (δ) functions and when multiplied by 100 will give the % distribution of the metal, ligand or both as particular species.[21] The percentage distribution of these particular species is usually plotted against the pH of the solution. In the same way as the proton formation and complex formation functions as discussed above, the species distribution curves can be defined for proton-ligand equilibria and metal-ligand-proton equilibria.

For calculation of distribution co-efficients, the expression used for stepwise protonation is:[18]

$$\delta_{HnB(L)} = \beta_{Hn}[H^+]^n/(1+\sum\beta_{Hn}[H^+]^n) \qquad ---3.30$$

and for similar complexation equilibria,

$$\delta_n = [ML_n]/C_M = \beta_n[L]^n/(1+\sum\beta_n[L]^n) \qquad ---3.31$$

3.3 Theory on data error analysis

The optimisation of formation constants is affected by the magnitude of random and systematic errors, which are not always inherent to the system. Suspect values or trends manifested in the form of these errors must be carefully investigated.

Random errors usually cancel each other out as the number of titration points increases. Systematic errors do not, even when they are of equal and opposite magnitude. Because systematic errors cannot be quantified, it is through careful selection of parameters to be optimised that their ill-effects can be reduced (Monte Carlo technique) followed by proper weighting.

3.3.1 Weighting[22]

The purpose of weighting is to reduce as much as possible the adverse effects on optimised parameters that arise because errors in values held constant during the calculation tend to propagate differently at different points. Through proper weighting, reliable values of the formation constants can be obtained.

The appropriate weight of the q^{th} residual at the n^{th} titration point is:

$$w_{nq} = [\Sigma\, \delta(y_{nq}^{obs} - y_{nq}^{calc})/\delta p)^2 \sigma_p^2]^{-1} \qquad ---3.32$$

where σ_p is the standard deviation in the parameter p to be optimised. Starting with satisfactory estimates of optimized parameters, an excellent set of weights based on the particular model chosen can be calculated. These weights may then be applied as constants in a subsequent optimization.

3.3.2 The Monte Carlo Analysis of Error Propagation[23]

This technique examines the effects of errors applied in a Gaussian distribution manner to all the optimised parameters and through several optimisation cycles calculates minimised U_{obj}. It minimises the objective function with respect to the standard deviation of the optimised and fixed parameters. The Monte Carlo spread of optimised results obtained by repeated optimisation is likely to reflect the way the errors are propagated. If the spread is smaller, the errors associated with fixed parameters do not affect the optimisation of the parameters during the calculation.

Using this technique it is easy to identify which parameters are better fixed during the optimisation and how much a particular optimised parameter is affected by error in the fixed parameters. This inter-parameter effect is called correlation and has been discussed in section 3.2.1.5.

From this technique group parameters such as analytical errors in the titrant solutions, or the value of E^0 can be adjusted to fit the experimental data since they are common to a particular potentiometric titration. This is an important technique in chemical 'model building' because often a better fit to the data can be obtained by

adjusting these group parameters, than by assuming the presence of another species.[4,23] However, if these adjustments are much larger than the expected experimental error, or if they vary systematically in an implausible way, then it is likely that the model is incorrect and further species do exist.[4]

3.4 UV-Visible Spectroscopy

The interaction of electromagnetic radiation of wavelength 340-800 *nm* with Cu^{2+} and Ni^{2+} chelates in particular, gives rise to UV/Visible spectra of these complexes.[24,25] The interpretation of the spectra so produced can be used for chemical analysis, examining molecular energy levels and molecular structures. As a result, UV-Visible spectrophotometry is always regarded as a supplementary technique to glass-electrode potentiometry (GEP) when ionic equilibria are investigated.

Besides establishing the reliability of GEP, it also provides an additional method for comparing several possible chemical models not sensitive to the former technique.[4] In addition, the use of more than one method and, UV/Vis in particular, is essential in better defining the chemical model prior to a computer analysis of both the potentiometric and spectrophotometric data. This ensures that errors in the data are initially screened making the computer analysis of data less time consuming. These errors may be due to slow kinetics and/or the presence of invisible precipitates, as a result of the factors already discussed in sections 3.1.4 and 3.2.1.2.

UV/Vis spectrometry has also been widely used to determine formation constants in addition to structure elucidation. However, because UV/VIS spectra of most complexes contain broad overlapping absorption bands, parameter correlation arises, such that it is usually not possible to evaluate stability constants as precisely from spectrophotometric data as one would with potentiometric data.

There is therefore a dichotomy that potentiometric data may lead to a more precise analysis of the wrong model, whereas spectrophotometric data will indicate the correct model but give a less precise analysis of it. Clearly, the best approach is to combine spectrophotometric and potentiometric data, using the former for defining the chemical model and the latter for evaluation of the stability constants.

Spectrophotometric data, as well as producing qualitative inferences as to the chemical model, also involve intensive factors and these are molar absorptivities. The computer calculated molar absorptivities of the species in the model may be examined when a fit has been obtained to see if they are reasonable.

The molar absorptivities are characteristic of the molecular electronic spectra and by reasonable it is meant:[4] (i) they should all be positive; (ii) when plotted as a function of wavelength, smooth curves should result and no sharp discontinuities should be present and (iii) the prediction of any isosbetic points should be borne out by experiment.

In a typical M^{2+} chelate, the observed spectrum, in general, consists of a series of crystal field bands, which depend largely on the donor atoms of the ligand and on the metal ion itself.[24,25]

The Ni^{2+} ion with a d^8 configuration exhibits a variety of coordination geometries with different electronic spectra characteristic of these geometries. Hence, it is normally easy to postulate the structures of the different species in solution from these spectra.

Octahedral co-ordination is the most common geometry for this metal ion and is observed in a host of complexes with an extremely wide range of mono- and polydentate ligands. By far the majority of these six co-ordinate complexes have an approximately octahedral arrangement of donor atoms around the central metal ion. The absorption spectrum can often be assigned on the basis of the group O_h, but if the ligands are not all equivalent, as will often be the case, the actual symmetry is less than O_h.

The degeneracy of E and T terms will be partially or wholly lifted. This splitting may be small resulting in increased bandwidth, or may result in several absorption peaks. Ni^{2+} chelates are normally green and exhibit three spin-allowed crystal field bands corresponding to $\nu_1 = {}^3T_{2g}(F) \leftarrow {}^3A_{2g}(F)$, $\nu_2 = {}^3T_{1g}(F) \leftarrow {}^3A_{2g}(F)$ and $\nu_3 = {}^3T_{1g}(P) \leftarrow {}^3A_{2g}(F)$ as would be expected in an octahedral field.[24]

These absorption bands (ν_1 ,ν_2 and ν_3) generally fall within the ranges 7,000-13,000; 11,000-20,000 and 19,000-27,000 cm^{-1} respectively, with intensities less than 30 mol^{-1} dm^3 cm^{-1} in regular octahedral systems. The ν_1 transition corresponds to ligand-field splitting (10Dq).

In addition to the three spin-allowed absorption bands, two spin-forbidden bands are often prominent. The transition to the ^1E_g state occurs near the second spin-allowed transition, whereas the second, primarily, to the $^1T_{2g}$, occurs between the second and third spin-allowed bands. Many Ni^{2+} complexes show spin singlet bands at 18,000-24,000 cm^{-1}.[24] Tetragonally distorted octahedral and five co-ordinate square pyramidal Ni^{2+} complexes such as $Ni(TMC)(N_3)^+$ also show at least three d-d absorption bands.[24]

The configuration d^8 of Ni^{2+} is especially prone to form diamagnetic square planar complexes, especially with stronger field ligands or where steric hindrance impedes higher co-ordination numbers. Diamagnetism is a consequence of eight electrons being paired in the four lower lying d-orbitals. Such low symmetry complexes usually exhibit a single band at 18,000-25,000 cm^{-1}, of intensity between 50-500 dm^3 mol^{-1} cm^{-1}, and are often yellow, red, orange or brown in colour.[24]

The ground state for Ni-L (where L is a tetradentate ligand of N_4 type) systems of D_{4h} symmetry is $^1A_{1g}$. The two component bands constituting the broad band at 18,000-25,000 cm^{-1} may be tentatively assigned as ν_1 around 19,000 cm^{-1} ($^1B_{1g} \leftarrow {}^1A_{1g}$), and as ν_2 at about 24,000 cm^{-1} ($^1A_{2g} \leftarrow {}^1A_{1g}$). The $^1B_{1g} \leftarrow {}^1A_{1g}$ band corresponds to 10Dq. A second, more intense charge transfer band may be seen between 23,000-30,000 cm^{-1}. Square planar complexes differ from those discussed above in that absorption below 10,000 cm^{-1} is not seen because the ligand field strength in these complexes is very high.[24]

Even though Cu^{2+} can be dealt with as the equivalent of a one electron case, the detailed interpretations of its spectra and magnetic properties can be somewhat complicated. This is because of the relatively low symmetry (i.e., less that cubic) of

the environment in which Cu^{2+} is characteristically found. Unlike Ni^{2+}, the geometry of Cu^{2+} complexes cannot be easily predicted from the UV/Vis electronic spectra.

Cu^{2+} complexes are generally blue or green due to the broad absorption band (half-width $\approx 5000cm^{-1}$) in the 540-800 *nm* region of the spectrum. The envelope of this band is unsymmetrical, seeming to encompass several overlapping transitions, but definitive resolution into the proper number of sub-bands with correct locations is difficult due to the large half-width.[24,25]

In a tetragonally distorted octahedral system where Cu^{2+} is normally found, these sub-bands correspond to the three spin-allowed $^2A_{2g} \leftarrow {}^2B_{1g}$, $^2B_{2g} \leftarrow {}^2B_{1g}$ and $^2E_g \leftarrow {}^2B_{1g}$ transitions. These transitions can only be resolved unambiguously when polarised spectra of single crystals have been measured.[24]

However, in parallel with Ni^{2+}, Cu^{2+} systems with close to or square planar stereochemistry, will not have electronic absorption below 10,000 cm^{-1} due to the very high ligand field strength in these complexes.[24,25] The square planar copper(II) complexes are generally brown or reddish in colour. For other weak field systems these colours are due to the strong charge transfer bands in the ultra violet region tailing off into the blue end of the visible spectrum.[24,25]

While systems such as the macrocyclic and open forms of N_4 ligands readily form such square complexes, even ethylenediamine will form a square-planar $[M(en)_2]^{2+}$ species if a weakly co-ordinating counter-ion is used.[24] Thus, diamagnetic square-planar M^{2+} can often be converted to regular or tetragonal distorted octahedral species by strong donor solvents such as water or by addition of strongly binding counter-anions like $[AgI_2]^-$. Under these conditions, the equilibria:

$$[ML]^{2+} + H_2O \rightleftharpoons [ML(OH_2)]^{2+} + H_2O \rightleftharpoons [ML(OH_2)_2]^{2+}$$

between octahedral, square pyramidal and square planar M^{2+} complexes (and between square planar and tetrahedral) can be observed.[24,25] Care should be taken in that an observed spectrum might represent a mixture of species.

Tetrahedral coordination is relatively uncommon for Cu^{2+} and Ni^{2+} when compared to the square planar geometry. Good π-donor ligands (i.e. weak field ligands) such as halides tend to stabilise tetrahedral geometries, e.g., $[MCl_4]^{2-}$, while π-acceptor ligands (strong field ligands) such as PR_3 and CN^- afford square planar geometries, e.g., $[M(CN)_4]^{2-}$. Due to the low ligand fields exhibited by π-donor ligands, the corresponding complexes usually exhibit absorption bands below 10,000 cm^{-1}.

Tetrahedral Ni^{2+} complexes are generally highly coloured (blue or green) with three expected d-d transition, i.e., $\nu_1 = {}^3T_2(F) \leftarrow {}^3T_1(F)$, $\nu_2 = {}^3A_2(F) \leftarrow {}^3T_1$ and $\nu_3 = {}^3T_1(P) \leftarrow {}^3T_1(F)$. The observed spectra, however, tend to be complicated by spin-orbit coupling effects.[24] The presence of two or more nitrogen donor atoms around the metal ion usually enforces distortion toward square planar or octahedral geometries.

Billo[26] has proposed an equation for calculating the λ_{max} for tetragonally distorted octahedral complexes of the type N_XO_{6-X},

$$\nu_{max} = \Sigma\nu_i \qquad \text{---3.35}$$

where ν_i (10^3 cm^{-1}) is the contribution of each of the four equatorial donor atoms.

In many instances, the two axially sites are usually occupied by water molecules. According to Billo, the contributions of each peptide and amino nitrogens to the λ_{max} are $(4.85 \pm 0.04)\times10^3$ cm^{-1} and $(4.53 \pm 0.07)\times10^3$ cm^{-1} respectively, while that of carbonyl oxygen, H_2O and OH^- is $(3.01 \pm 0.03)\times10^3$ cm^{-1} each.

Jackson and Nakani[20] have recently proposed a value of 3.48×10^3 cm^{-1} for an oxime nitrogen. Although this equation can predict λ_{max} of several of these types of complexes with good accuracy, the equation cannot predict absorption maxima of mixtures which are likely to be present in solutions containing axially co-ordinating solvent molecules such as water.

3.4.1 Experimental design

Generally a solution of a metal ion and ligands will contain a number of different species at differing concentrations. The absorption spectrum will then be a weighted sum of all the species present. For this reason in labile systems it is difficult to obtain the spectrum of a single species. In this case spectral deconvolution techniques have to be used.

If a solute is dissolved in a transparent medium, then the absorbance of light, A, (given by the Beer-Lambert Law, $A=l\varepsilon c$), is proportional to the concentration of the solute. For a given concentration and path length, the actual absorbance depends on the molar absorption co-efficient of the species of interest.[4] For the electronic absorption spectra of solutions containing more than one absorbing species the Beer-Lambert Law can be expanded to give a linear combination of terms for each individual species.

If the path length l is given in *cm*, then the absorbance per *cm* at wavelength λ (A_{obs}^{λ}/l) is given by:

$$A_{obs}^{\lambda}/l = \varepsilon_1^{\lambda}c_1 + \varepsilon_2^{\lambda}c_2 + \varepsilon_3^{\lambda}c_3 + ...+ \varepsilon_n^{\lambda}c_n \qquad \text{---3.35}$$

where ε_1^{λ}, ε_2^{λ} and ε_n^{λ} are molar absorptivitites of species 1, 2 and n at the same wavelength λ, and c_1, c_2 and c_n are their respective concentrations.[4,19,20] If the concentration is given in $mol\ dm^{-3}$, then the molar absorptivity has the units $dm^3\ mol^{-1}\ cm^{-1}$. The important feature of the above equation is the linear dependence of A_{obs}^{λ} on the concentrations of the various species present. Obviously, if a species present has an ε^{λ} value of zero, that is, it does not absorb in the spectral region chosen, then it does not influence A_{obs}^{λ}.

If the UV/VIS spectra of a number of solutions of differing metal and ligand concentrations and pH are recorded at a number of wavelengths, then by solving the set of linear equations 3.35, the spectra of the individual species can be calculated. It is advisable to adjust the pH of the metal-ligand complex solutions with strong acids

and alkalis such as HCl and NaOH respectively, which do not absorb appreciably in the spectral region of interest.[4]

3.5 Theoretical calculations - Molecular mechanics and Molecular dynamics simulations

The UV/VIS spectrophotometric technique can fairly accurately predict the structures of the copper(II) and nickel(II) complex species present in solution. However, it is of no use for non-coloured chelates such as the majority of zinc(II) complexes. X-ray crystal structure determinations may give some valuable information on the geometry of the species in question.

However, it is sometimes difficult to grow crystals suitable for X-ray structure diffraction determinations. Furthermore, it is now recognised that the X-ray structure of a particular compound provides the average atomic positions, but the atoms exhibit fluid-like motions of sizeable amplitudes about these averages. Under these circumstances, molecular mechanics (MM) calculations and molecular dynamics (MD) simulations become the only choices.

The latter two techniques also offer possibilities of selecting the lowest energy conformations. Such a freedom is not offered by spectroscopic and X-ray structure diffraction techniques. In fact, the importance of MD simulations in particular lies with its ability to:

(i) determine or refine structures with data obtained from experiments such as X-ray diffraction and nuclear magnetic resonance (NMR),
(ii) determine thermodynamics of the system, and
(iii) examine its time development (i.e. its actual dynamics).

A crystal structure can serve as an initial model. However, in the absence of known crystal structures, model building of starting species of the ligands and corresponding complexes is necessary. This is usually accomplished by making use of fragments within the BUILDER module of Biosym/MSI's Insight II software package.[27]

The primary limitation of MD simulation methods is that they are approximate. This is because of the absence of perfect forcefield, (i.e., an empirical potential energy function) which also takes into account the effect of the solvent. Furthermore, the ESFF forcefield in particular, does not take into account the Jahn Teller distortion normally observed in octahedral copper(II) complexes. It is for these reasons that a true experiment is essential in validating the simulation method(s). The comparisons of simulated system with experimental data serve to test the accuracy of the calculated results and provide criteria for improving methodology.

3.6 The blood plasma model

It is difficult to get information from large chemical systems like biological fluids because of their complexity. On top of their complexity, the presently available analytical instruments cannot detect some of the species, which are present in these systems at very low concentrations. Even if they could, these instruments are likely to perturb the systems which are at equilibrium. Because of these two limitations computer models simulating these complex systems have been developed.

One of these models is the blood plasma model,[28,29] which simulates the complexing conditions occuring in biofluids. This model operates by determining a particular system under *in vitro* conditions at manageable concentrations and 'diluting' the effects to *in vivo* conditions by using appropriate mass balance equations.

Blood-plasma has a well defined composition and as a result the model contains all the species present in blood-plasma. The blood plasma model used in this study includes data for 10 metal ions and 42 ligand systems, giving rise to nearly 5,000 equilibria. This model also includes the important ternary complex equilibria.[28,29]

Like all computer models, the plasma model has a limitation in that it does not take into account the kinetics of the system and the system is assumed to be at equilibrium which is not the case in many instances. Deliberate omissions in the present model are protein equilibria, which are ill-defined.

To understand the effect of a ligand (or drug as in this study) on the equilibria present in this model, formation constants for the ligand and the species of interest determined *in vitro* are incorporated into a database. This database, on inclusion of the drug concentration, is efficiently and conveniently interrogated by the ECCLES computer program to yield results pertaining to the influence of this drug on these equilibria.

Because the protein equilibria are not included in this model, the concept of a plasma mobilising index (p.m.i.) is used. This is defined as the ratio of the total concentration of l.m.w. metal complex species in the presence of the drug to that in normal plasma. The p.m.i. is essentially a measure of an ability of the administered ligand to move metal ion from the protein bound fraction to the l.m.w. fraction.

In this calculation, the free metal ion is assumed to be constant and hence results are largely independent of the protein equilibria. This concept depends on the fact that while the absolute concentration of the metal ions is dependent on protein binding, the distribution amongst l.m.w. ligands does not, hence the percentage of metal appearing in a given species is constant, regardless of the exact free metal concentration.

This l.m.w. fraction of copper(II) is postulated to be involved in the transport of the ion across biomembranes to anti-inflammatory processes and can be manipulated in an attempt to increase the availability of the metal ion to the anti-inflammatory processes.[29]

3.7 Partition Co-efficients

Drugs' transport across the skin and bio-membranes, is in general, a process of limited diffusion. It is governed by the drugs' chemical and physical properties such as lipophilicity and protein binding. For percutaneous absorption, a drug's translocation depends on the disease state of the skin. Partitioning of the drugs in lipid bilayers of the skin's stratum corneum and biomembranes, is an initial step in this trans-location process.[30,31]

Presently, the reference parameter for the prediction of drug's passive diffusion through these biological barriers is the measure of its lipophilicity, expressed as the logarithm of the partition coefficient between 1-octanol and an aqueous phase.[30-33] For copper(II) complex as a drug, this is given as,

$$\text{Log } K_{oct/water} = \log([Cu^{2+}]_{org}/[Cu^{2+}]_{aq}) \qquad \text{---3.36}$$

The concentrations of Cu^{2+} in both phases can be determined by several techniques but in this study atomic absorption spectrophotometry was chosen because of its availability and reasonable sensitivity. A value of log $K_{oct/water}$ = 0.6 (or $K_{oct/water}$ = 3.98) indicates that the compound (drug) is reasonable lipophilic.

The technique has been widely used despite criticisms that this simple two-phase system seems to be an unrealistic model of bio-membranes. However, it has been observed that alcohol-water systems in general, and octanol-water system in particular, correlate well with the behaviour of biomembranes. This is not surprising since many NH and OH groups are present in membranes, enzymes and even biological transporters,[31] which are present in these membranes. Furthermore, its widespread use as a reference system stems from the fact that it has the largest number of measured values containing the widest selection of functional groups.[31]

Recent investigations[34] have shown that water/sodium dodecylsulfate micelle partition co-efficients correlate well with those obtained by the classical two phase system.

3.8 Superoxide Dismutase (SOD) Activity

A number of copper complexes have been observed to exhibit SOD-mimic like activity and have been suggested to be alternative human therapeutics to counteract the deleterious effects of $^{\cdot}O_2^-$ radicals. Measurement of this mimetic activity can indirectly reveal the amount of radicals generated and can be useful to predict the effect of these pharmacological agents on radical production *in vitro* and *in vivo*.[35,36]

Several methods are available for SOD activity determination and the UV/Vis spectrophotometric method is the most widely used technique. It is an indirect method based on two elements, a superoxide generator usually a xanthine-xanthine oxidase system and a detector, nitroblue tetrazolium (NBT).[37] In the absence of an SOD-mimetic agent (control experiment) the radicals react with the detector. If SOD mimetic is present (inhibition experiment), it competes with the detector for the superoxide anion. The systems are based on the following reactions.

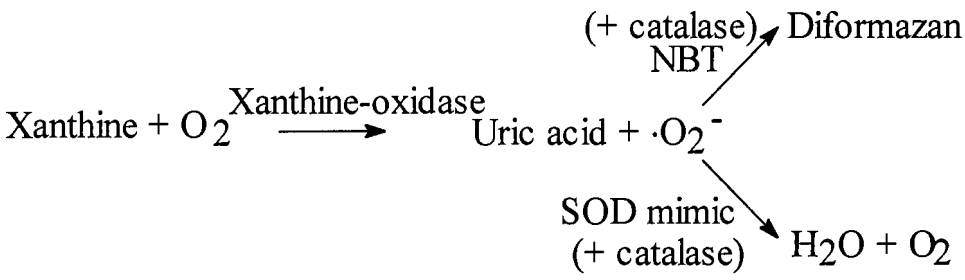

The SOD activity is then measured by the degree of inhibition of the intermediate (INT) and hence diformazan formation in the above sequence of reactions. The absorbance readings at 560 *nm* are obtained at several incremental time points (≈30 seconds) for a total period of 10-15 min for both the control and inhibition experimental solutions. For each set of readings corresponding to a control and particular concentrations of an SOD mimic (Cu^{2+}-L complex), the absorbance is usually plotted against time and the slope of the resulting plots computed. The %inhibition of the reduction of NBT to blue diformazan is calculated using the following equation:

$$\% \text{ Inhibition} = [(S_{cs} - S_{ies}) \times 100]/S_{cs} \qquad \text{---3.37}$$

where S_{ces} and S_{ies} are slopes of the control and inhibition experimental solutions respectively.

In particular, the inhibitory concentration (IC_{50}) defined as the concentration of the drug in the culture medium required to reduce the number of living cells (cell viability) by 50% is easily read from the plots.

In these experiments the disodium salt of EDTA is usually present in excess amounts compared to other components of the reaction mixture for two purpose:

(i) to simulate the competitive binding of endogenously available low molecular ligands,[36,37] and

(ii) to complex small amounts of metal ions such as Fe^{3+}, that may be present in NBT and/or xanthine, which are known to catalyse the dismutation of $^{\cdot}O_2^-$ as well.[37]

It should be noted that Cu^{2+}-EDTA complexes are inactive as SOD mimics.[36]

3.9 Animal biodistribution experiments

Since there are few absolute rules to correlate *in vitro* observations to the *in vivo* behaviour, it is always deemed necessary to perform biodistribution experiments on animal screens such as mice. Radionuclides of copper (^{60}Cu, ^{62}Cu, ^{64}Cu and ^{67}Cu) have several properties, which make them attractive for biomedical applications such as radioimaging, therapy and biodistribution studies. ^{64}Cu appears to be the only isotope for tracer studies as the others are short-lived or, in the case of ^{67}Cu, production is only possible from rather rare zinc or nickel targets or high energy ($\approx$ 60 MeV) proton flux.[38]

^{64}Cu has become a radionuclide of choice in these studies despite its short half-life. However, there is an advantage associated with its short half-life since the overloading of tissue with high activity over a long time is not possible. ^{64}Cu emits positrons which travel a short distance before annihilating to produce two 511 keV gamma rays. These rays travel in nearly opposite direction (180^0 apart) and are detected by detectors in positron emmiting (PET) scanners, which encircle the organ of interest or the animal as a whole. Since PET scanners are expensive and, hence unavailable in many laboratories, a gamma counter is sometimes used to detect this radiation.

Mice are animal screens of choice because they are less expensive and are easy to handle compared to rabbits and baboons. The animals are always injected under anaesthesia with the radio-labelled complex through the tail vein.[39] ^{64}Cu is used to

produce the most detailed distribution and clearance information for its complexes. These studies ultimately determine the clinical usefulness of the drug.

3.10 Conclusion

In order to obtain reliable results in any experiment, it must be well designed to 'define' the system as unequivocally as possible. This is of great importance among experimentalist in solution equilibria to determine meticulously the formation constants of metal-ligand systems.

All the relevant points discussed in this chapter have to be adhered to in order to achieve the task.

- Glass-electrode potentiometry has been selected for the determination of stability constants using the more convenient ESTA suite of computer programs for data analyses. It should be emphasised that any speciation conclusion based upon a computer model is only as good as the input data. Such good input data are needed and depend on a good experimental design (including good electrode calibration, proper model selection that adequately describes the data).

- UV/VIS spectrophotometry has also been selected as a supplementary technique to potentiometry to define the chemical model and to postulate the structures of the different copper(II) species in solution.

Ancillary studies

- The MM calculations and MD simulations were used to model the complexes in an attempt to get low energy conformations of these species.
- The computer blood plasma model was used to calculate p.m.i.'s.
- The lipophilicity and SOD mimetic activities of the copper complexes were determined using the shake-flask method and the NBT assay respectively.
- Biodistribution studies of ^{64}Cu-L complexes were carried out to produce the detailed distribution and clearance information for these complexes.

References

1. P.W. Linder, R.G. Torrington and D.R. Williams, Analysis using Glass Electrodes, 1984, 71, Open University Press.
2. R.D. Hancock and A.E. Martell, *Chem. Rev.*, 1989, **89,** 1875.
3. A.E. Martell and R.D. Hancock, *Metal Complexes in Aqueous Solutions,* Plenum Press, New York, 1996, 1, [Editor: J. P. Fackler, Jr].
4. F.R. Hartley, C. Burgess, and R. Alcock, *Solution Equilibria*, 1980, 33-144.
5. NIST STANDARD REFERENCE DATABASE 46, NIST CRITICALLY SELECTED STABILITY CONSTANTS OF METAL COMPLEXES DATABASE, VERSION 3.0, compiled by R.M. Smith and A.E. Martell, US Department of Commerce, NIST, USA.
6. K.R. Adam, M. Antolovich, D.S. Baldwin, L.G. Bridgen, P.A. Duckworth, L.F. Lindoy, A. Bashall, M. McPartlin and P.A. Tasker, *J. Chem. Soc., Dalton Trans.* 1992, 1869.
7. A.S. De Sousa, R.D. Hancock and J.H. Reibenspies, *J. Chem. Soc., Dalton Trans.*, 1997, 2831-2835.
8. P. Comba, A. Fath, A. Kuhner and B. Nuber, *J. Chem. Soc. Dalton Trans.* 1997, 1889.
9. R.G. Pearson, *J. Am. Chem. Soc.*, 1985, **107**, 6801.
10. *Electrochemistry, Past and Present, Am.Chem.Soc. Symposium Series* **390**, 1989, 287.
11. C.M.A. Brett and A.M.O. Brett, *Electrochemistry, Principles, Methods and Applications*, 1993, 142.
12. P.M. May, D.R. Williams, P.W. Linder and R.G. Torrington, *Talanta*, 1982, **29**, 249.
13. E. Leporati, J. Chem. Soc. Dalton Trans. 1989, 1299.
14. B.W. Tsang, J. Reibenspies and A.E. Martell, *Inorg. Chem.*, 1993, **32**, 988.
15. G. Gran, *Acta Chem. Scand.* 1952, 77, 661-671.
16. *Vogel's textbook of Quantitative Inorganic Analysis including Elementary Instrumental Analysis*, 4th Edition, 1978, 235, 319, [Editors: J. Bassett, R.C. Denney, G.H. Jeffrey and J. Mendham, Longman Ltd.

17. C.F. Baes, Jr., and R.E. Mesmer, "The Hydrolysis of Cations", Wiley-Interscience, NY, 1976, 439.

18. J. Kragten, *Atlas of Metal-Ligand Equilibria in Aqueous Solution*, 1978, 15, 104, 508, 742.

19. G.E. Jackson and M.J. Kelley, *J. Chem. Soc., Dalton Trans.*, 1989, 2429.

20. G.E. Jackson and B.S. Nakani, *J. Chem. Soc., Dalton Trans.*, 1996, 1373.

21. P.M. May, K. Murray and D.R. Williams, *Talanta*, 1985, **35**, 825.

22. P.M. May and K. Murray, *Talanta*, 1988, **35**, 927.

23. P.M. May, K. Murray and D.R. Williams, *Talanta*, 1988, **35**, 933.

24. A.B.P. Lever, *Studies in physical and theoretical Chemistry - Inorganic Electronic Spectroscopy*, 2nd Ed., 1984, 507-544.

25. B.R. Hathaway, In *Comprehensive Coordination Chemistry*, 1987, **5**, 652; [Eds: Sir G. Wilkinson, R.D. Gillard and J.A. McCleverty], Pergamon Press.

26. E.J. Billo, *J. Inorg. Nucl. Chem. Lett.* 1974, **10**, 613.

27. Insight II User Guide, October 1995.

28. P.M. May, D.R. Williams and P.W. Linder, *J. Chem Soc., Dalton Trans.*, 1977, 588.

29. G.E. Jackson, P.M. May and D.R. Williams, *J. Inorg. Nucl. Chem.*, 1978, **40**, 1227.

30. T.X. Xiang and B.D. Anderson, *J. Membrane Biol.*, 1994, **140**, 111.

31. A. Leo, C. Hansch and D. Elkins, *Chem. Rev.*, 1971, **71**, 525.

32. E. Cole, R.C.B. Copley, J.A.K. Howard, D. Parker, G. Ferguson, J.F. Gallagher, B. Kaitner, A. Harrison and L. Royle, *J. Chem Soc., Dalton Trans.*, 1994, 1619.

33. M. Polasek, D. Kohoutkova and K. Waisser, *Analytica Chimica Acta*, 1988, **212**, 279.

34. E. Pramauro, C. Minero, G. Saini, R. Graglia and E. Pellizzetti, *Analytica Chimica Acta*, 1988, **212**, 171.

35. N.A. Roberts and P.A. Robinson, *British Journal Rheumatology*, 1985, **24**, 128.

36. I. Fridovich, In *CRC Handbook of Molecular and Oxygen Radical Research;* Ed., R.A. Greenwald, CRC Press, 1985, 53.

37. C. Auclair and E. Voisin, In *CRC Handbook of Molecular and Oxygen Radical Research;* Ed., R.A. Greenwald, CRC Press, 1985, 125.

38. P.J. Blower, J.S. Lewis and J. Zweit, *Nucl. Med. Biol.*, 1996, **23**, 957.

39. L.J. Ackerman, D.X. West, C.J. Mathias and M.A. Green, *Nucl. Med. Biol.*, 1999, **26**, 551.

CHAPTER 4

Experimental and Analytical Methods

4.1 Physical measurements and analytical methods

Solvents such as dichloromethane, hexane, methanol, ethanol, ethylacetate, acetonitrile and triethylamine were dried and freshly distilled using the normal procedures[1] prior to use. All other reagents were commercially available and of analytical grade and were used without further purification unless noted otherwise.

Reactions and the progress of chromatographic separations were monitored by analytical thin layer chromatography (TLC). These were conducted on silica gel 60 F_{254} precoated TLC plates. The compounds were visualised on these plates by illumination with 254*nm* UV light. Alternative visualisation was accomplished by either staining with iodine vapour or by treatment with a solution of ceric ammonium sulphate in 10% H_2SO_4. Column chromatography was performed using silica gel 60, 230-400 mesh from Merck.

Melting points were measured using a Reichert Thermovar melting point apparatus and are uncorrected. Proton (^1H) and ^{13}C NMR proton decoupled spectra were obtained on a VXR-200 or MERCURY 300 or UNITY 400 MHz Varian spectrometers. ^{1}HNMR chemical shifts were referenced to TMS (0 ppm) as an internal standard using residual protio solvent peaks as external standards (singlets at δ_H of 2.50, 4.8 and 7.24 for CD_3SOCD_3, D_2O and $CDCl_3$ respectively).

Infra-red spectra were recorded on a Perkin-Elmer Paragon 1000 FT-IR spectrometer as KBr disks at room temperature. Mass spectra of the ligands were obtained either on a VG-Micro Mass 16 F spectrometer in EI mode or on a VG 70-SEQ mass spectrometer. Micro-analyses were done on an Elemental Analyser EA 1108 CHNS-O (Fisons Instruments) and are reported as an average of two combustions.

4.2 Organic Synthesis - Preparation of ligands

4.2.1 3,3,9,9-tetramethyl-6,7-diazaundecane-2,10-dione dioxime (PrAO)

The ligand was synthesised according to the method of Vassian and Murmann[2-4]. Nitrosyl chloride was prepared from 52.0*g* of sodium nitrite (0.754 *mol*)

added to 300 cm^3 conc. HCl (3.00 *mol*) and was obtained in 12.16% yield (0.092 moles). Since nitrosyl chloride is a gas, which decomposes above -5.0^{0}C, the temperature was maintained at -20.0^{0}C using an ice slurry (a mixture of 4 parts of crushed ice to 5 parts of solid $CaCl_2.6H_20$) instead of the methanol baths used in previous studies.[2-4] 2-Chloro-2-methyl-3-nitrosobutane was prepared by the reaction of nitrosyl chloride (6g, 0.092 *mole*) added to an excess of anhydrous 2-methyl-2-butene (7.014g, 0.10 *mole*, 10.60 cm^{-3}). A rearrangement within 2-Chloro-2-methyl-3-nitrosobutane resulted in the formation of 4.84g (0.0349 *mol*) of 2-Chloro-2-methyl-3-butanone oxime in 38.1% yield, m.p. 67.5-69.0^0, lit. 68-69^0.

0.01745 *mole* (1.29g, 1.45 cm^{-3}) of 1,3-diaminopropane was added to a 10% excess (0.0349 *mole*, 4.84g) of 2-Chloro-2-methyl-3-butanone oxime in 100 cm^3 of ice-cold absolute methanol. The resulting solution was maintained between 0.0^{0}C-5.0^{0}C for 2 hr and at room temperature for another 2 hr; before refluxing it for 15 hr. After removal of solvent under vacuum, the solid was extracted with water and neutralised with an excess of saturated solution of Na_2CO_3 followed by several cm^3 of 10 *mol* dm^{-3} NaOH until a pH of 10-11 was reached. The solid was collected, washed with cold water and recrystallized from boiling methanol.

The ligand crystallised as a white solid, yield 1.25*g* (0.00459 *mole*, 26.24%) which gave melting point 181-182^{0}C, lit. 180-181^{0}C; ^{1}H-NMR, δ_H (D_2O), 1.44 (12 H, s, 3,3,9,9-CH_3), 1.88 (2 H, m, 6-CH_2), 1.98 (6 H, s, CH_3) and 2.82 (4 H, t, 5,7-CH_2) and micro analysis - Observed (Calc. for $C_{13}H_{28}O_2N_4$): C, 57.21 (57.32); H, 10.23 (10.36); N, 20.38 (20.57).

4.2.2 N, N'-bis(2-hydroxyiminopropionyl) propane-1,3-diamine (H_2pap)

The ligand N,N'-bis(2-hydroxyiminopropionyl) propane-1,3-diamine was synthesised analogously to the methods reported by Gutche et al.[5] and Kozlowski and coworkers[6] for its ethane-1,2-diamine analogue except that ethyl pyruvate instead of pyruvic acid was used as the starting material. This resulted in the elimination of the alkylation step using methanol[5] or ethanol[6] in the presence of sulphonyl chloride ($SOCl_2$) as reported by these authors.

To a solution of 20*g* of ethyl pyruvate (0.1722 *mol*) in 8.61 cm^3 of water was added 12.022*g* of hydroxylamine hydrochloride (0.173 *mol*) in 17.1 cm^3 of water. The mixture was shaken at room temperature for 4 hours, and the white precipitate was collected, washed with water and filtered at the pump. This gave 16.453*g* (0.1525 *mol*, 88.56% yield) of ethyl pyruvate oxime as a white powder in pure form, m.p. 94.5-96.0^{0}C, ^{1}H-NMR, δ_H ($CDCl_3$) 1.35 (3H, t), 2.10 (3H, s) and 4.30 (2H, q).

Ethyl pyruvate oxime, (16.453*g*, 0.1525 *mol*) was dissolved in methanol (63 cm^3), then 4.40 cm^3 (3.91g, 0.053 *mol*) of 1,3-diaminopropane was added. The reaction mixture was set aside for 24 hours at room temperature, then the solvent was removed on a rotary evaporator. The addition of water (15 cm^3) to the obtained oil and cooling of the mixture at 0.0^{0}C overnight resulted in the precipitation of the crude product. This crude product was filtered at the pump under vaccum washed several times with water and had m.p. 193-196^{0}C.

Recrystallisation from water gave the pure oxime in the form of colourless single crystals, yield 8.5g (66%), m.p. 195-196^{0}C, ^{1}H-NMR (300 MHz, [$^2H_6$]dmso), δ_H: 1.564 (qnt, 2H, β-CH_2), 1.859, (s, 6H, CH_3), 3.142 (q, 4H, α-CH_2), 7.930 (t, 2H, NH) 11.632(s, br, 2H, OH). FT-IR (ν in cm^{-1}) 3328 ν(N-H str., s); 3215 ν(O-H str., br); 2981, 2965 2943, 2872 ν(C-H, s); 1670 ν(C=N str., m,); 1655 ν(C=O str., amide I, s); 1542 (N-H bend, amide II, m), 1304 ν(C-N str., m), and 1024 ν(N-O, str., w). Anal. Found (Calc. for $C_9H_{16}N_4O_4$): C, 44.51 (44.25); H, 6.88 (6.62); and N, 22.93 (22.94). EI-MS, molecular ion peak (M^+) situated at m/z = 244 agrees with the calculated molecular mass of the compound, which is 244.2448 *g/mol*.

4.2.3 (1,15)-bis(N,N-dimethyl-5,11-dioxo-8-(N-benzyl)-1,4,8,12,15-pentaazapentadecane (BIDPAP)

The ligand was prepared by a procedure similar to those reported before for similar ligands.[7,8]

4.2.3.1 Bis (N,N-ethyl propionate)benzylamine

2.4 cm^{-3} (3.38g, 0.019 *mol*) of ethyl bromopropionate was added dropwise with continuous stirring to 1.02 cm^{-3} (1.00g, 0.0087 *mol*) of benzylamine in acetonitrile and the Huenigs base (diisopropyl ethylamine) for 30min in a cycloaddition tube. The mixture was heated under reflux at 120^0C, while monitoring the reaction progress by TLC.

After a 24hr period of continuous heating under reflux, the TLC confirmed the absence of starting materials. It also revealed the presence of the mono- and bis(N,N-ethylpropionate) benzylamine, with R_f values of 0.5 and 0.8 respectively in 4:1 (v/v) hexane-ethyl acetate eluent mixture. The reaction mixture was concentrated on a rotary evaporator. The hydrobromide salt of diisopropyl ethylamine was dissolved in a saturated solution of Na_2CO_3 and the organic components of the mixture were extracted three times with ethyl acetate. The combined organic layers were dried over anhydrous magnesium sulphate, filtered and concentrated on a rotary evaporator.

Column chromatography using the same eluent as for TLC yielded the oily mono- and bis(N,N-ethylpropionate) benzylamine in pure forms. Monoalkylated form, yield 0.3055g, 20.4%; ^{1}HNMR (200 MHz) δ_H ($CDCl_3$) 1.25 (3H, t, R-CH_3), 1.85 (1H, s, R_1NHR_2), 2.45 (2H, t, $ROOCCH_2$-R_1), 2.85 (2H, t, RCH_2-NR_1R_2), 3,79 (2H, s, NR_1R_2-CH_2-Ar) 4.25 (2H, q, -COO-CH_2-R), 7.30 (5H, m, Ar-H); dialkylated form, yield 2.464g, 79.2%, δ_H ($CDCl_3$) 1.22 (6H, t, RCH_3), 2.5 (4H, $ROOCCH_2$-R_1), 2.85 (4H, t, RCH_2-NR_1R_2), 3.53 (2H, s, $N(R_2)_2$-CH_2-Ar), 4.14 (4H, q, R_1-COO-CH_2-R), 7.30 (5H, m, Ar-H). ^{13}C NMR (75,45 MHz), δ_H ($CDCl_3$), 14.077 (CH_3RNRCH_3), 32.714 ($ArCH_2N(R_1)_2$), 49.173 (ROC=O$\underline{C}H_2R_1$), 58.230 ($R_1R_2NCH_2R_3$), 60.177 (R$\underline{C}H_2$OC=OR_1), 128.085 (C-Ar), 139.050 ($ArCH_2N(R_1)_2$), 172.382 (R_1C=OR_2).

4.2.3.2 1,15-bis(N,N-dimethyl-5,9-dioxo-7-(N-benzyl)-1,4,8,12,15-pentaazapentadecane

To 2.221g (0.0072 *mol*) of bis(N,N-ethylpropionate) benzylamine was added 1.60g (2 cm^{-3}, 0.0181 *mol*) of N,N-dimethylethylenediamine in a cycloaddition tube. The reaction mixture was heated under reflux at 80^0C for 24 hours while

simultaneously monitoring the reaction progress using TLC. After this 24hr period, the TLC in dichloromethane-methanol-triethylamine, 9:5:1 ratio (v/v) revealed the absence of bis(N,N-ethylpropionate) benzylamine, one of the starting materials. The excess N,N-dimethylethylenediamine was then removed on a vaccum pump. The resulting residue was then dissolved in a minimum amount of dichloromethane. On column chromatography with the same eluent as for TLC, 2.464g (0.0063 *mol*, 87% yield) of the product BIDPAP was obtained.

In contrast to the earlier syntheses of related ligands,[7,8] the compound BIDPAP was obtained in a form suitable for analysis and potentiometric titrations. This resulted in the elimination of the hydrochloridation step involving the bubbling of dried HCl gas over the BIDPAP solution. The higher molecular weight of BIDPAP compared to its previously synthesised analogues is probably the reason for the compound to be obtained in the solid form.

The compound was dissolved several times in dichloromethane followed by filtration to remove impurities. The excess solvent was removed initially on a rotary evaporator and by drying the compound on a vaccum pump. After these purification steps, BIDPAP was recovered in 90% yield, m.p. 198-200^{0}C. ^{1}HNMR (300 MHz), δ_H ($CDCl_3$), 2.22 (12H, s, $(CH_3)_2NRN(CH_3)_2$), 2.40 (4H, m, R-$NHCH_2$-CH_2-$N(R_1)_2$), 2.76 (4H, m, ($R_2HNOC{=}OCH_2R_1$)), 2.88 (4H, m, $R_1CH_2N(Ar)CH_2R_1$, 3.25 ($(R_1)_2NCH_2CH_2RCH_2CH_2N(R_1)_2$), 3.80 ($ArCH_2N(R_1)_2$), 7.30 (7H, m). ^{13}C NMR (75,45 MHz), δ_H ($CDCl_3$), 33.87 ($ArCH_2N(R_1)_2$), 45.07 ($R_1(CH_2)N(CH_2)R_1$), 49.91 ($ROC{=}O\underline{C}H_2R_1$), 58.23 ($R_1R_2NCH_2R_3$), 60.18 ($R\underline{C}H_2OC{=}OR_1$), 128.30 (C-Ar), 139.47 ($ArCH_2N(R_1)_2$), 172.11 ($R_1C{=}OR_2$).

It should be mentioned that some carbon signals were observed to exist in pairs, indicating the presence of the cis and trans forms or a mixture thereof. The higher than expected number of carbon signals is expected for compounds containing the amide moiety.[9] However, this behaviour was not observed for H_2pap and related compounds, which were studied before.[8] The presence of the extra methylene groups in this compound may have enhanced this cis/trans isomerism.

FAB-MS gave m/z values, Found (Calcd.), M^+ = 391.5426 (391.5546 for $C_{21}H_{37}N_5O_2$), $M+H^+$ = 392.54259 (392.5541 for $C_{21}H_{38}N_5O_2$) and $M+Na^+$ = 414.55 (414.5453 for $NaC_{21}H_{38}N_5O_2$). Anal. Found (Calc. for $C_{21}H_{37}N_5O_2$): C, 63.20 (64.42); H, 8.68 (9.52); and N,15.81 (17.89). The discrepancy between the observed and calculated values is probably due the hygroscopic nature of this compound.

The purity of these three ligand systems was also confirmed by acid-base glass electrode potentiometric titrations at 25^{0}C and I = 0.15 *mol dm*$^{-3}$ and were found to be greater than 95% pure. This was reflected by an excellent fit, which was obtained between the calculated and experimental observed protonation function (Z_H).

4.3 Preparation of Solutions

All solutions were prepared in glass-distilled, or deionised water which had been passed through a Milli-Q water purification system (Millipore Corp.). The distilled and/or purified water was then boiled to remove dissolved CO_2 and cooled in a container protected by a "Carbosorb" (BDH) carbon dioxide trap.[10-12]

These solutions were made up to an ionic strength of 0.15 *mol dm*$^{-3}$ with sodium chloride in order to ensure isotonicity with blood-plasma. All other reagents such as $CuCl_2.2H_20$, $NiCl_2.6H_20$, $ZnCl_2$, $CaCl_2.2H_20$, $GdCl_3.9H_20$, NaCl, HCl, NaOH and EDTA (Merck) were commercially available and of analytical grade. These were also used without further purification.

Solutions of 0.100 *mol dm*$^{-3}$ NaOH and 0.100 *mol dm*$^{-3}$ HCl were prepared from Merck Titrisol ampoules and were stored in polyethylene plastic bottles in Metrohm exchange units. Solutions of hydrochloric acid were then standardised by titration with sodium tetraborate using the standard methods of Vogel.[13] Carbonate free-sodium hydroxide solutions were also standardised by titration with potassium hydrogen-phthalate.

The 0.100 *mol dm*$^{-3}$ NaOH solutions prepared were further standardised against standard 0.100 *mol dm*$^{-3}$ HCl solutions. These acid-base titrations were also used to check the carbonate content of the sodium hydroxide titrant solution using the Gran method.[14] Otherwise these standardised solutions were used within a short

period of preparation and were discarded whenever there were signs of carbonate contamination.

4.4 Standardisation of Cu^{2+}, Ni^{2+}, Zn^{2+}, Ca^{2+} and Gd^{3+} solutions: Direct titrations using EDTA

The accurate concentrations of standard metal ion solutions are necessary for the initial estimates in data analysis. These initial estimates were determined by direct titrations using EDTA.

The 0.02 *mol* dm^{-3} solutions of the divalent cations were prepared from $CuCl_2.2H_20$, $NiCl_2.6H_20$, $ZnCl_2$, $CaCl_2.2H_20$ and $GdCl_3.9H_20$ salts at the indicated ionic strength. 5 cm^3 portions of the 0.02 *mol* dm^{-3} solutions of the divalent metal ions were titrated against a 0.01 *mol* dm^{-3} standard solution of the disodium salt of ethylenediamine - tetraacetic acid using the standard methods of Vogel.[13] The concentrations of these metal ions ranged between 0.0195 and 0.021 *mol* dm^{-3}.

4.5 Potentiometric titrations

4.5.1 Conditions and Equipment

The final adjustments were made to an ionic strength of 0.15 *mol* dm^{-3} with Cl^- (Na^+) in all solutions for the potentiometric and UV/VIS measurements.

The potentiometric titrations were performed using a Radiometer PHM 84 research pH meter and Metrohm Dosimat 665 piston burette, which were linked and controlled by a computer. The pH meter was equipped with a Metrohm 6.0130.100 separate glass electrode and 6.0726.100 Ag/AgCl reference electrode with a renewable liquid junction of 0.15 *mol* dm^{-3} NaCl.[10,11] In some instances, with UV/Visible titrations in particular, a Metrohm 6.0204.100 combined micro glass-electrode was used.

The electrode(s) were immersed in the solution **S** contained in a double-walled titration vessel thermostated at 25.0 ± 0.1^{0}C by circulating water from a constant temperature Haake thermostat bath. The titrant **T** was delivered to the titrated solution

S through an immersed capillary tip from a Metrohm Dosimat 665 piston burette using a Pascal program developed in this laboratory to monitor the electromotive force (emf) and the volume of **T** added for each titration point. These titrations were carried out at least in duplicate.

During the titration, stirring was effected with a Teflon magnetic stirrer bar. Throughout the titration, the magnetically stirred solution was protected from the intrusion of atmospheric oxygen and carbon dioxide by passing a continuous flow of high purity nitrogen stream over it. The double-walled vessel was sealed apart from a small exit for this nitrogen stream. The gas was first bubbled through a series of solutions;

- 50% w/w potassium hydroxide to remove carbon dioxide impurities,
- Fieser's solution to remove traces of O_2,
- excess glass wool in empty container,
- distilled water and
- background electrolyte of ionic strength 0.15 $mol\ dm^{-3}$ (Cl^-) to humidify the gas.

The last three traps were thermostated at 25^0C in accordance with titration conditions.

The glass electrode was calibrated as an H^+ probe using three standard buffer solutions. The Nernstian slope of the glass electrode was checked against these buffers over the pH range 2-11, and was found to vary between 59.14 and 58.75. After calibration using buffers, precision calibration of the instrument was carried out by titration of 0.100 $mol\ dm^{-3}$ NaOH (2 cm^3) from the autoburette against 0.100 $mol\ dm^{-3}$ HCl (1 cm^3) in the vessel and vice versa in the same pH range 2.0-11.0.

The value of the response intercept, E^0, was found to vary from 415-418 mV while an average pK_w value of 13.73 was evaluated from these acid-base titrations before each protonation and complexation titration. The measurement of these constants at the beginning of each experiment was also used to verify the correct functioning of the electrode, the reliability of the potentiometric measurements as well

as to ensure the reproducibility and reversibility of equilibria. These parameters were fixed in the computation and refinement of log β_{pqr}'s.

It should be emphasised that many workers[15-19] have previously reported autodissociation constants of the solvent which vary from 13.78 to 13.69 for titrations performed under exactly the same experimental conditions as employed in this study. At 0.1 $moldm^{-3}$ (Cl^-) ionic strength, pK_w values of 13.76-78 have also been reported. It is believed that a value of 13.73 should be appropriate for pK_w at 25^0C and I = 0.15 $mol\ dm^{-3}$.

4.5.2 Protonation and complexation titrations with 0.02 *mol dm*$^{-3}$ solutions of the divalent cations

About 0.015g of ligand L (L=L^1, L^2 or L^3) was dissolved in a calculated volume of 0.100 $mol\ dm^{-3}$ ($\approx$ 1-1.5 cm^3) HCl or NaOH (L^2 was observed to be insoluble in hydrochloric acid). The minimum initial volume required to cover the electrode(s) was made with 0.15 $mol\ dm^{-3}$ NaCl in a double-walled titration vessel. The solution was titrated against 3.0 cm^3 of 0.100 $mol\ dm^{-3}$ NaOH (HCl). 1.0-2.0 cm^3 of 0.100 $mol\ dm^{-3}$ HCl was added to bring the pH down to about 2.5 before addition of V cm^3 of metal ion solution. This was done to prevent the hydrolysis of metal ions under strongly alkaline conditions.

The resulting solution was titrated with 3.0 cm^3 of 0.100 $mol\ dm^{-3}$ NaOH. This constituted an in situ calibration of the electrode system. The procedure was repeated with varying initial concentrations of solutions of the metal ions.[10,11] The titrations were terminated at the first visual sign of precipitation.

The following hydrolysis constants obtained from the data of Baes and Mesmer[20] and Kragten[21] at 25^0C were corrected for ionic strength I = 0.15 $mol\ dm^{-3}$ where necessary. They were used in the computation and refinement of the formation constants. All the species given below are solvated in aqueous solution.

For copper(II),

$$Cu^{2+} + H_2O \rightleftharpoons Cu(OH)^+ + H^+;\ \log K_{10\text{-}1} = -7.87$$

$Cu^{2+} + 2H_2O \rightleftharpoons Cu(OH)_2 + 2H^+$; $\log K_{10\text{-}2} = -14.33$

$Cu^{2+} + 3H_2O \rightleftharpoons Cu(OH)_3^- + 3H^+$; $\log K_{10\text{-}3} = -27.80$

$Cu^{2+} + 4H_2O \rightleftharpoons Cu(OH)_4^{2-} + 4H^+$; $\log K_{10\text{-}4} = -39.03$

$2Cu^{2+} + 2H_2O \rightleftharpoons Cu_2(OH)_2^{2+} + 2H^+$; $\log K_{20\text{-}2} = -10.65$

For nickel(II),

$Ni^{2+} + H_2O \rightleftharpoons Ni(OH)^+ + H^+$; $\log K_{10\text{-}1} = -10.20$

$Ni^{2+} + 2H_2O \rightleftharpoons Ni(OH)_2 + 2H^+$; $\log K_{10\text{-}2} = -19.20$

$Ni^{2+} + 3H_2O \rightleftharpoons Ni(OH)_3^- + 3H^+$; $\log K_{10\text{-}3} = -30.00$

$Ni^{2+} + 4H_2O \rightleftharpoons Ni(OH)_4^{2-} + 4H^+$; $\log K_{10\text{-}4} = -44.00$

$2Ni^{2+} + H_2O \rightleftharpoons Ni_2(OH)^{3+} + H^+$; $\log K_{20\text{-}1} = -10.5$

$4Ni^{2+} + 4H_2O \rightleftharpoons Ni_4(OH)_4^{4+} + 4H^+$; $\log K_{40\text{-}4} = -27.30$

For zinc(II) hydrolysis,

$Zn^{2+} + H_2O \rightleftharpoons Zn(OH)^+ + H^+$; $\log K_{10\text{-}1} = -9.17$

$Zn^{2+} + 2H_2O \rightleftharpoons Zn(OH)_2 + 2H^+$; $\log K_{10\text{-}2} = -17.1$

$Zn^{2+} + 3H_2O \rightleftharpoons Zn(OH)_3^- + 3H^+$; $\log K_{10\text{-}3} = -28.4$

$Zn^{2+} + 4H_2O \rightleftharpoons Zn(OH)_4^{2-} + 4H^+$; $\log K_{10\text{-}4} = -40.7$

$2Zn^{2+} + H_2O \rightleftharpoons Zn_2(OH)^{3+} + H^+$; $\log K_{20\text{-}1} = -8.9$

$2Zn^{2+} + 6H_2O \rightleftharpoons Zn_2(OH)_6^{2-} + 6H^+$; $\log K_{20\text{-}6} = -57.6$

Ca^{2+} has a slight tendency to hydrolyse and its only hydrolysis constant is,

$Ca^{2+} + H_2O \rightleftharpoons Ca(OH)^+ + H^+$; $\log K_{10\text{-}1} = -12.7$

Just like Cu^{2+} and Zn^{2+}, gadolinium(III) also undergoes extensive hydrolysis in aqueous solution and the contributing equilibria are,

$Gd^{3+} + H_20 \rightleftharpoons Gd(OH)^{2+} + H^+$; $\log K_{10\text{-}1} = -8.0$

$Gd^{3+} + 2H_20 \rightleftharpoons Gd(OH)_2^+ + 2H^+$; $\log K_{10\text{-}2} = -16.4$

$Gd^{3+} + 3H_20 \rightleftharpoons Gd(OH)_3 + 3H^+$; $\log K_{10\text{-}3} = -25.3$

$Gd^{3+} + 4H_20 \rightleftharpoons Gd(OH)_4^- + 4H^+$; $\log K_{10\text{-}4} = -34.4$

4.5.3 Data Analysis

All the data collected from each titration were imported into a preformatted data file for the calculation of electrode parameters, protonation and formation constants, log β_{pqr}. These parameters of interest were calculated using the task OBJE within the ESTA2A module of the ESTA library of computer speciation modelling programs.

The analysis was performed by fitting these constants to the titration data, based upon minimisation of the objective function, U_{obj}, with respect to emf. No other variables such as E^0, $[H]^+_{vessl}$, $[L]_{vessl}$ and $[M]_{vessl}$ were refined in addition to $\log\beta_{pqr}$'s sought. The results are presented in Table 5.1 and 5.2.

To take full advantage of the large amount of data generated, complex formation and deprotonation functions were calculated from the determined log β_{pqr} values using the tasks ZBAR and QBAR respectively within the ESTA1 module of ESTA. These functions were then used as criteria for testing the validity of the potentiometric model proposed in the analysis of data.

Finally, the task SPEC within the same ESTA1 module, was used to determine the distribution, as a function of pH, of all the $M_pL_qH_r$ species present in solution over the pH range 2 to 11.

4.6 UV-Visible electronic spectra of Cu^{2+}/Ni^{2+} complexes

UV-visible electronic spectra of a 3.0 cm^3 aqueous solution containing a ratio of Cu(II)/Ni(II): L^2 or L^3 = 1:3, in a cuvette, were taken over the pH range 2.00-11.00. Small amounts of 0.100 $mol\ dm^{-3}$ HCl and NaOH were used to adjust the pH during the titration. The temperature of the solutions was kept at 25.0 ± 0.1^{0}C.[10-12]

Spectrophotometric measurements were taken manually at 10 *nm* intervals in the range 340-800 *nm* using a Unicam SP 1700 Ultraviolet Spectrophotometer with slit and band widths set at 0.4 *mm* and 1.2 *nm* respectively.

4.7 Crystal structure determination, MM calculations and MD simulations

4.7.1 Synthesis and crystallisation of $[NiL^1H_{-1}]^+ClO_4^-$

0.1 g (0.367 *mmol*) of L^1 was dissolved initially in 5.00 cm^{-3} of 0.1M HCl and 10.00 cm^{-3} of absolute methanol was added. To this ligand solution was added 18.3 cm^{-3} of 0.02 $moldm^{-3}$ $NiCl_2.6H20$ followed by 5.00 cm^{-3} of 0.1M NaOH to adjust the pH to 7.15.

The mixture was stirred at room temperature for two hours during which time a yellow complex was formed. Addition of an excess of $NaClO_4$ solution to this yellow mixture resulted in the formation of a colloidal precipitate. After five (5) days the desired orange-yellow complex crystallised out of solution. The crystals were filtered off, washed with small amounts of acetone and dried over anhydrous $CaCl_2$. Yield 0.08g (51%).

4.7.2 Crystal-structure determination

An orange-yellow crystal (≈ 0.25 x 0.23 x 0.20 *mm*) of $[NiL^1H_{-1}]^+ClO_4^-$ was mounted on an Enraf-Nonius Kappa diffractometer equipped with a graphite-crystal monochromator situated in the incident beam for data collection. Unit cell determinations and data collections were performed with Mo-Kα radiation (λ = 0.71073 A) at 197(2) K. A Lorentz-polarisation correction was applied to the data, as well as an empirical absorption correction[22] following the DIFABS procedure (minimum and maximum absorption transmission were 0.7445 and 0.7875 respectively).

The structure was solved by direct methods (SHELXS-90, 1990)[23] and refined using full-matrix least-squares on F^2 (SHELXL-97, 1997).[24] Non-hydrogen atoms were treated anisotropically while hydrogen atoms were placed in geometrically calculated positions and linked to common thermal parameters. Pertinent crystal and structure refinement data are discussed in chapter 5.

4.7.3 MM calculations and MD simulations

Model building of ligands and the corresponding starting complexes in particular, was based on known or related crystal structures of these species or from UV/Vis spectrophotometric data. This was accomplished by making use of fragments within the BUILDER module of the *Biosym/MSI's II* software package.[25] Structures were then optimised prior to dynamics runs to remove the strain using the SHAKE algorithm with the default ESFF force fields. The optimisation procedure in essence constrained all the bond lengths to their equilibrium value while a constant temperature algorithm was used to keep the temperature at 298 K.

MD simulations of the complex species were performed by the *DISCOVER_3* module (98 Version) which is run as an application in the *INSIGHT II* package.[25] Hydrogen bonds were not restrained during the simulation since molecular dynamics is a more natural and ideal way of simulation. These MM calculations and simulations were performed on a Silicon Graphics Indigo computer.

4.8 Octan-1-ol/water partition coefficients

Partition coefficients were measured using the shake flask method.[26,27] The organic solvent was purified by double distillation after reflux for 5 hrs using standard methods.[1] 25.0 cm^3 of 0.007 $mol\ dm^{-3}$ Cu^{2+}-L^2/L^3 solutions were prepared. Because of the low solubility of the ligand L^2 in HCl, it was initially dissolved in an appropriate amount of 0.1 $mol\ dm^{-3}$ NaOH followed by an addition of a calculated amount of 0.1 $mol\ dm^{-3}$ HCl before the addition of the metal ion. Into eighteen, 10.0 cm^3 glass vials, 1.0 cm^3 portions of the metal-ligand solution were pipetted. The first vial was left at pH 2.5 and the rest of the vials were adjusted to 0.5 pH increments apart using a highly concentrated solution of NaOH.[26,27]

Into each vial, 1.0 cm^3 portion of water presaturated octan-1-ol was added. Each vial was then stoppered, shaken by hand for about a minute, swirled gently to collect droplets from the sides of the vial and set aside to allow the two phases to separate. The temperature was maintained at 25.0 ± 0.1^{0}C using a temperature controlled water bath. The organic phase was then removed, by Pasteur pipette, into

10.0 cm^3 of 0.100 $mol\ dm^{-3}$ HCl for extraction of the partitioned solute back into the aqueous phase while the aqueous solution was diluted 100 fold with the same concentration of the acid.

These solutions were then analysed for copper(II) ion content using a Spectr AA-5 atomic absorption spectrophotometry (AAS). The air-acetylene flame was used for atomization while the wavelength and slight width were set at 324.7 *nm* and 0.2 *nm* respectively.

4.9 Determination of Cu^{2+}-L SOD Mimetic Activity

The superoxide dismutase mimetic activity of Cu^{2+}-L (L = L^1, L^2 and L^3 complexes were determined using the NBT assay as described by Fridovich[28] and Auclair and Voisin[29] to assay tissue homogenates.

Standard solutions of i) 0.0004 M xanthine, ii) 0.0001M EDTA, iii) 0.0001 g/cm^3 of catalase, iv) 0.018 units/cm^3 xanthine oxidase and (v) 0.0001M solutions of Cu^{2+}-L in a 0.05M phosphate buffer pH 7.80 were prepared.

In a four (4) cm^3 cuvette, 0.6 cm^3 of xanthine, 0.2 cm^3 EDTA, 0.2 cm^3 NBT, 0.1 cm^3 catalase and 2.9 cm^3 of a 0.05M phosphate buffer were added and this constituted a blank solution. In a control experiment, in addition to these components, 0.4 cm^3 xanthine oxidase and 2.4 cm^3 instead of 2.9 cm^3 buffer were added, while in a test solution varying amounts of Cu^{2+}-L complexes were added prior to the addition of xanthine oxidase.

The absorbance readings at 560 *nm* were obtained at 30 seconds intervals for a total period of 15 min for both the control and experimental solutions. For each set of readings corresponding to a control and particular concentrations of an SOD mimic (Cu^{2+}-L complex), the absorbance was plotted against time and the slope of the resulting plots were computed. The %inhibition of the reduction of NBT to blue formazan was calculated using equation 3.37 and IC_{50} values[28,29] similarly determined from a plot of %inhibition vs the concentration of the Cu^{2+}-L complex.

4.10 Biodistribution experiments of ^{64}Cu-L on mice

The biodistribution studies on mice were approved by the Research Animals Ethics Committee of the University of Cape Town (permission number 01/060). The authority to possess and use the radioactive nuclide ^{64}Cu was granted by the university's radiation protection and health safety committee in conjunction with Department of Health (authority number 33/3/01/0327).

^{64}Cu-labeled [$CuLH_1$] complexes were prepared by spiking 14.8 cm^3 of Cu^{2+} (0.001 *mol* dm^{-3}) - L (0.003 *mol* dm^{-3}) solutions with 7.5 mCi of $^{64}CuCl_2$. The copper complexes of these ligands were found to be kinetically and thermodymamically quite stable *in vitro* once given enough equilibration time because slow kinetics have been observed in these systems. No assumptions were made on the lability of the copper complexes *in vivo*. Radio-TLC indicated that the copper(II) species of L^1, L^2 and L^3 were 93%, 97% and 90% radio-labeled respectively.

A total of 48 female Balb/c mice of age 6-8 weeks weighing between 19-22g were used in these experiments. The mice were housed in groups of four (4) mice per Macrolon cage and were given food and water *ad libitum* during the investigation period, with sawdust provided as bedding prior to injection.

Three (3) groups of 4 halothane-anaesthetised mice (12 in total) were injected intravenously via the tail vein with 0.2 cm^3 of 5 μCi of ^{64}Cu-L (L = L^1, L^2 or L^3).[30-34] Another group of mice was injected with $^{64}CuCl_{2(aq)}$ to serve as a control experiment. The mice were individually placed in Macrolon cages containing paper towelling for urine absorption.

After 1, 6 and 24 hours post-injection, these groups of mice (3 per time point) were deeply anaesthetised by halothane inhalation. Blood samples were immediately collected by puncture of the inferior vena cava.[30-34] This resulted in the death of the animals.

The mice were dissected and the liver, muscle, tail, heart, lung, kidney, intestines, spleen, brain, head and carcass were excised, rinsed with NaCl-0.9%,[30] blotted dry and weighed. The radio-activity in these tissue samples was counted in a

Minaxi Auto-Gamma Counter (5000 Series-Packard) using a window set at 350-550 keV.[30-34] The urine impregnated towelling was extracted with 100 cm^3 of 10% v/v HCl. Diluted aliquots of the injectates served as standards for calculation of the total injected dose. Radio-activities of the 10 cm^3 standard diluted aliquots of the injectates, the urine extract and samples of the droppings were also counted.

The percentages of radio-activity dose per gram (g) tissue and/or per organ were computed from the corresponding mean wet organ weights after correction for radio-activity decay.[30-34]

4.10.1 Radiation protection

Although much less activity of ^{64}Cu was used in these experiments, the high tissue penetrating abilities of high energy positrons and gamma radiation resulting from their annihilation necessitated adherence to the following precautionary measures.

- During these experiments, disposable gowns, face masks, gloves and radiation badges were worn.
- Preparation of ^{64}Cu-L complexes as well as the injection of mice with the radio-labeled species were performed behind lead bricks inside a fume-cupboard.[34]
- Aqueous stock solutions of these ^{64}Cu-L complexes (or $^{64}CuCl_2$) were kept in closed containers in the refrigerator.
- Since the half-life of ^{64}Cu is reasonably short, the syringes and needles which were used during injection, the disposables, the sacrificed animals together with the organs excised were initially kept in a refrigerator for two weeks to allow the radioactivity to decay before being incinerated.

References

1. *Vogel's Textbook of Practical Organic Chemistry including Qualitative Organic Analysis*, 1978, 4th Ed., 270 [Revised by: B.S. Furniss et al.].
2. J.R. Morton and H.W. Wilcox: "*Inorganic Synthesis*", 1953, **4**, 48-52.
3. R.K. Murmann, *J. Am. Chem. Soc.*, 1957, **79**, 521.
4. E.G. Vassian and R.K. Murmann, *Inorg. Chem.* 1967, **6**, 2043.
5. H.-P. Lau and C.D. Gutsche, *J. Am. Chem. Soc.* 1978, **100**, 1857.
6. A.M. Duda, A. Karaczyn, H. Kozlowski, I.O. Fritsky, T. Glowiak, E.V. Prisyazhnaya, T. Y.-Sliva and J. S.-Koslowska, *J. Chem. Soc. Dalton Trans.* 1997, 3853.
7. J.F. Elsworth, L.N. Msimang and G.E. Jackson, *S. Afr. J. Chem.* 1996, **49**, 1,2, 31-39.
8. L. Mkhonta-Gama, PhD Thesis, University of Cape Town, 1999.
9. C. Schiene-Fischer and G. Fischer, *J. Am. Chem. Soc.* 2001, **123**, 6227.
10. G.E. Jackson and M.J. Kelley, *J. Chem. Soc., Dalton Trans.* 1989, 2429.
11. G.E. Jackson and B.S. Nakani, *J. Chem Soc. Dalton Trans.* 1996, 1373.
12. F.R. Hartley, C. Burgess and R. Alcock, *Solution Equilibria*, 1980, 180.
13. *Vogel's textbook of Quantitative Inorganic Analysis including Elementary Instrumental Analysis*, 4th Edition, 1978, 235, 319, [Editors: J. Bassett, R.C. Denney, G.H. Jeffrey and J. Mendham, Longman Ltd.
14. G. Gran, *Acta Chem. Scand.* 1952, **77**, 661.
15. R.J. Motekaitis, Y. Sun, A.E. Martell and M.J. Welch, *Can. J. Chem.*, 1999, **77**, 614.
16. R. Cini, A. Sabatini, A. Vacca and F. Zanobini, *Can. J. Chem.*, 1997, **75**, 212.
17. B. Song, P. Mehrkhodavandi, P. Buglyo, Y. Mikata, Y. Shinohara, K. Yoneda, S. Yano and C. Orvig, *J. Chem. Soc. Dalton Trans.*, 2000, 1325.
18. B. Song, J. Reuber, C. Ochs, F. E.-Hahn, T. Lugger and C. Orvig, Inorg. *Chem.*, 2001, 1527.
19. A. Bianchi, L. Calabi, M. Foresti, P. Losi, L. Paleari, A. Rodriguez and B. Valtancoli, *Inorg. Chim. Acta.* 1999, 288, 244.
20. C.F. Baes, Jr., and R.E. Mesmer, "The Hydrolysis of Cations", Wiley-Interscience, NY, 1976, 439.

21. J. Kragten, "*Atlas of Metal-Ligand Equilibria in Aqueous Solution*", 1978, 15, [Editor: M. Masson].

22. A. T. C. North, D. C. Phillips and F. S. Mathews, *Acta Crystallogr., Sect. A*, 1968, **24**, 351.

23. G. M. Sheldrick, *Acta Crystallogr., Sect. A*, 1990, **46**, 467.

24. G. M. Sheldrick, *SHELXL 97, Suite of programs for crystal structure determinations* 1997.

25. Insight II User Guide, October 1995.

26. A. Leo, C. Hansch and D. Elkins, *Chem. Rev.*, 1971, **71**, 525.

27. T.X. Xiang and B.D. Anderson, *J. Membrane Biol.*, 1994, **140**, 111.

28. I. Fridovich, In *CRC Handbook of Molecular and Oxygen Radical Research;* Ed., R.A. Greenwald, CRC Press, 1985, 53.

29. C. Auclair and E. Voisin, In *CRC Handbook of Molecular and Oxygen Radical Research;* Ed., R.A. Greenwald, CRC Press, 1985, 125.

30. L.J. Ackerman, D.X. West, C.J. Mathias and M.A. Green, *Nucl. Med. Biol.* 1999, **26**, 551.

31. J.S. Lewis, A. Srinivasan, M.A. Schmidt and C.J. Anderson, *Nucl. Med. Biol.* 1999, **26**, 267.

32. M. Yu, H. Qing, H. Guojian, Z. Shu, H. You-Feng and T. Kuikka, *Nucl. Med. Biol.*, 1998, **25**, 111.

33. T.M. Jones-Wilson, K.A. Deal, C.J. Anderson, D.W. McCarthy, Z. Kovacs, R.J. Motekaitis, A. Dean-Sherry, A.E. Martell and M.J. Welch, *Nucl. Med. Biol.* 1998, **25**, 523.

34. L.M. Guerdoud, R. Ouellet and J.E. Van Lier, *Nucl. Med. Biol.* 1994, **21**, 437.

CHAPTER 5

Results and Discussion

5.1 Glass electrode potentiometry

5.1.1 Protonation constants

The protonation constants for H^+-L equilibria were evaluated in the pH range 2-11 where the ligands were found to take up two or three protons. Reversibility of the reactions was confirmed by complete overlap of titration curves obtained by titrating the experimental solution in both directions with hydrochloric acid and sodium hydroxide solution. The $\log\beta_{0qr}$ values of the ligands L^1, L^2 and L^3 are given in Table 5.1, together with literature values.

Table 5.1: $\log\beta_{0qr}$'s of L^1, L^2 and L^3 determined at 25°C and I = 0.15 *mol dm*$^{-3}$ $(Cl^-)Na^+$. σ_{pqr} denotes the standard deviation in $\log\beta_{0qr}$; R_H is the Hamiltonian R-factor and R_H^{lim} is its limit, n_T and n_p are the number of titrations and points respectively. The general formula of a complex is $M_pL_qH_r$ denoted by the stoichiometric coefficients pqr where p=0.

L	p q r	log β_{pqr}	σ_{pqr}	R_H	R_H^{lim}	$n_T(n_p)$	Lit.
L^1	0 1 1	8.968	0.002	0.001	0.001	5(703)	8.97[1]
	0 1 2	16.175	0.004				16.18
L^2	0 1 1	10.408	0.001	0.004	0.003	9(975)	10.38[4]
	0 1 2	20.072	0.001				19.99
L^3	0 1 1	8.823	0.010	0.012	0.010	8(943)	
	0 1 2	17.254	0.008				
	0 1 3	24.152	0.012				

5.1.1.1 H^+-L^1 system

Figure 5.1(a) shows the proton formation function, Z_H-bar for L^1 plotted against the pH. This function rises to two for this system indicating simple stepwise protonation of two basic sites. An excellent agreement between the experimental and theoretical curves at different total ligand concentrations illustrates the reproducibility of the experimental protonation procedure.

The secondary amino groups of L^1 are protonated in this pH range of 2-11, with pK_{a1} = 7.207 and pK_{a2} = 8.968. A difference of 1.761 between the two pK_a's

indicates that proton addition to the second amine of an already protonated ligand is difficult compared to the protonation of the neutral ligand. This is because of electrostatic repulsion between two charged sites and the close proximity of these amino groups to each other. Furthermore, this difference can be explained in terms of the decreased number of available sites for proton addition to occur once a first proton has been attached to one of the amino groups. These amino groups are observed to be less basic compared to the nitrogen donor atoms of 1,3-diaminopropane. This decrease in basicity is expected as one moves from primary to secondary amines due to steric hindrance and solvation effects that override the positive inductive effect of the carbon chain.

Figure 5.1: (a) Experimental ($[L^1]_T=3\times10^{-3}$(♦), 5×10^{-3}(*) and 8×10^{-3}(x) *mol dm*$^{-3}$) and theoretical (line) Z_H-bar (b) calculated L^1H^{n+} species ($[L^1]_T=3\times10^{-3}$ *mol dm*$^{-3}$) distribution both plotted against pH.

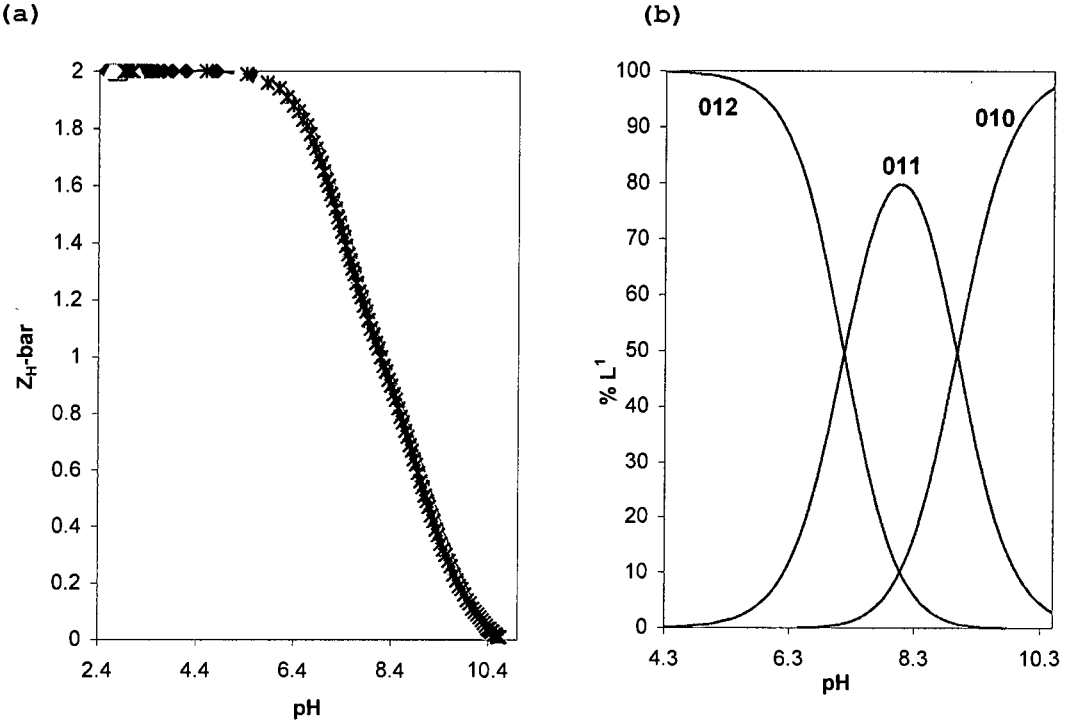

For L^1, this base weakening has also been attributed to the electron-withdrawing properties of the oxime group with a possible contribution from intramolecular hydrogen-bonding interactions originating from the same oxime group.[1-3] The pK_a values of this ligand agree quite well with those that have been determined in previous studies.[1,2] The oxime groups in L^1 have been observed to exhibit pK_a values in the range 12-13, hence cannot be evaluated under the conditions

of the present study. However, co-ordination of these groups to metal ions such as copper and nickel facilitates their ionisation process. The degree of the deprotonation of the oxime groups of L^1 has been observed to be metal ion dependent.[2] Figure 5.1(b) shows that in the pH range 4.0-8.0 the protonated forms of this ligand predominate while above this pH range the neutral deprotonated ligand exists.

5.1.1.2 H^+-L^2 system

The Z_H-bar function given in Figure 5.2(a) levels off at 2 indicating that just like L^1, L^2 also exhibits two measurable acid dissociation constants. The superimposability of the experimental and calculated Z_H-bars at different $[L^2]_T$ confirms the validity of the proposed protonation model.

Figure 5.2: (a) Experimental ($[L^2]_T=3\times10^{-3}$(♦), 5×10^{-3}(▲) and 8×10^{-3}(•) *mol dm*$^{-3}$) and theoretical (line) Z_H-bar (b) calculated L^2H^{n+} species ($[L^2]_T=3\times10^{-3}$ *mol dm*$^{-3}$) distribution both plotted against pH.

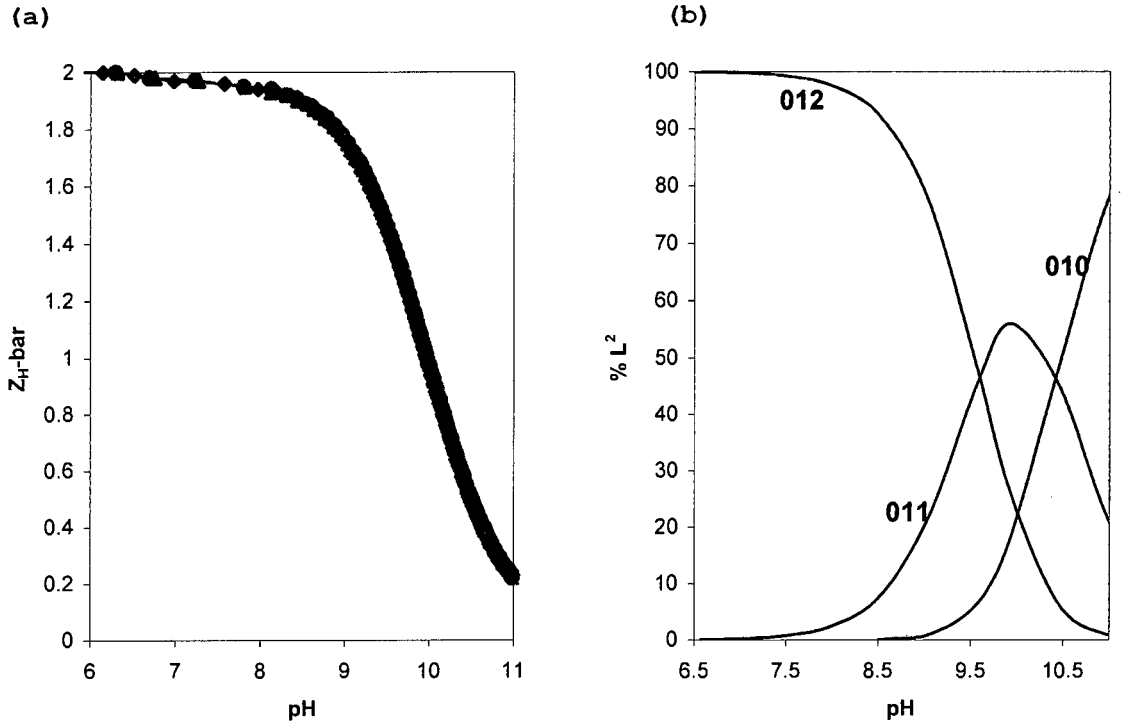

Unlike with L^1, the two acidity constants correspond to stepwise deprotonation of the terminal oximes with $pK_{a1}=9.664\pm0.001$ and $pK_{a2}=10.408\pm0.001$. The observed pK_a's are 0.02-0.03 log units higher than those determined previously by Kozlowski et al.,[4] at 0.10 *mol dm*$^{-3}$ (KCl). However, there is an excellent agreement in these

constants when corrected for ionic strength using the extended Debye-Huckel equation.

A difference of about 0.744 between pK_{a1} and pK_{a2} indicates that the deprotonation steps of these two oxime groups are almost independent of each other. The linear nature of the ligand reduces the repulsion between these negatively charged deprotonated oxime groups.

These values are three orders of magnitude lower than those of normal oximes, a point which may be explained in terms of the electron withdrawing effects of the amide groups at the alpha(α)-positions. For oximes such as L^1, the loss of these protons is usually metal ion assisted.[1-3,5,6] Figure 5.2(b) reveals that deprotonation of the ligand begins above pH 6.5 while the dinegative deprotonated form predominates in highly basic conditions.

5.1.1.3 H^+-L^3 system

Figure 5.3(a) indicates that L^3 contains three protonation sites as revealed by the levelling off of the Z_H-bar function at 3.

Figure 5.3: (a) Experimental ($[L^3]_T$=3×10^{-3}(♦), 5×10^{-3}(*) and 8×10^{-3}(•) *mol dm*$^{-3}$) and theoretical (line) Z_H-bar (b) calculated L^3H^{n+} species ($[L^3]_T$=3×10^{-3} *mol dm*$^{-3}$) distribution both plotted against pH.

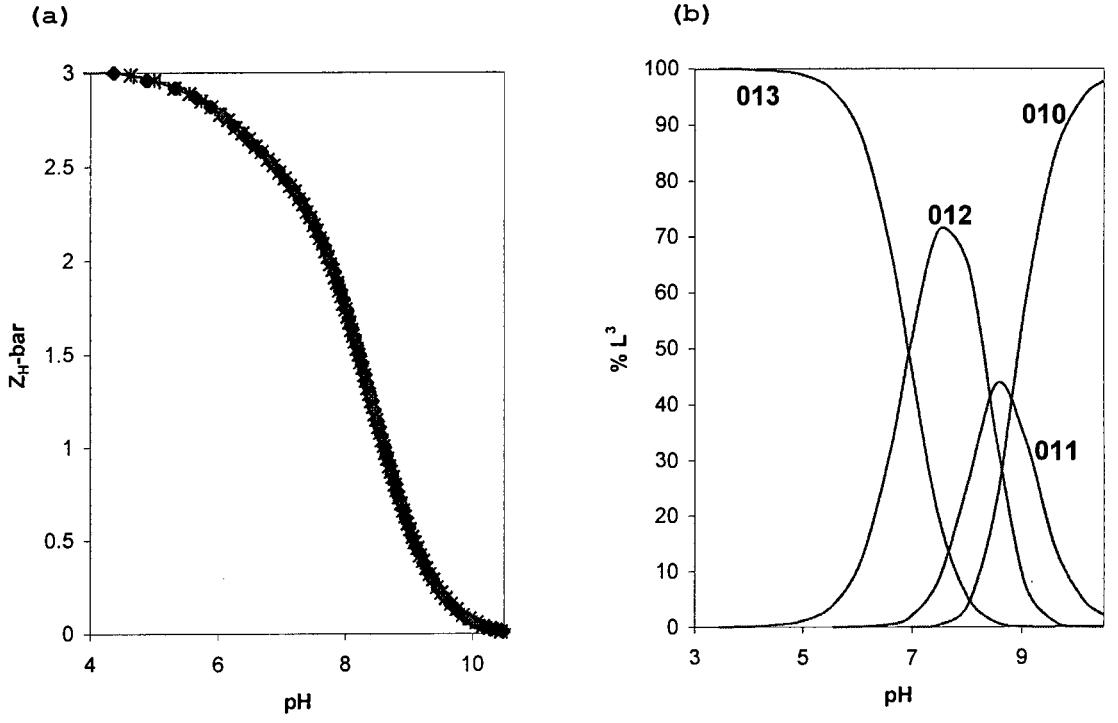

An excellent agreement between the experimental and theoretical functions supports the L^3 protonation model. The three protonation constants correspond to proton additions to the tertiary amines with $\log K_1=8.823\pm0.007$, $\log K_2=8.431\pm0.007$ and $\log K_3=6.898\pm0.010$.

The difference between the first and second protonation constants is 0.39 log units. These constants are close to each other and refer to proton additions to the two terminal tertiary amines. The difference in the protonation constants of these similar sites is due to the difficulty of proton addition to a molecule already containing a protonated site. The third protonation constant is 1.92 and 1.53 log units smaller than $\log K_1$ and $\log K_2$ respectively. This indicates the protonation of the less basic benzylamine. Proton addition to this central amine is also difficult due to the already protonated terminal nitrogen donor atoms as a result of electrostatic repulsion. Furthermore, on statistical grounds, there are few available basic sites for proton addition to occur.

The terminal amino groups of L^3 have $pK_{a2}=8.431$ and $pK_{a3}=8.823$, which are both one order of magnitude lower than those of N,N,N',N'-(tetramethylethylenediamine) and other tertiary amines. This is due to the electron withdrawing effect of the amide groups at the beta(β)-positions, which equally affects the basicity of these amines. Steenland et al.[6] have recently observed a similar electron withdrawing property of an amide group in the dioxomacrocylic analogues (L^i and L^j) of L^3.

The central benzylamine of L^3 is 1.93 and 1.53 log units less basic than the terminal amino groups due to an extra electron withdrawing property of the benzene ring. This amine is also 2.36 to 3.70 orders of magnitude more basic than similar sites of recently studied L^{d1}, L^{d2}, L^{d3} and L^{d4} ligands[8] where $\log K_3$'s are 4.54, 3.2, 3.63 and 3.44 respectively. L^3 contains an extra methylene group on each side of the amine, which due to their inductive effect increase the basicity of this central amino group.

Figure 5.3(b) indicates that deprotonation of the triple protonated L^3 ligand begins around pH 4.0 while in more basic conditions the neutral form of the ligand predominates. Due to the strong overlap between the deprotonation of the acidic

groups of the ligands, the real acidity of the individual groups can be obtained only through the complete evaluation of the microscopic scheme of the ligands. It should be mentioned that the amide nitrogens in both L^2 and L^3 are too acidic to be protonated under the conditions of this study. Jubert et al.[9] and Martell and coworkers[10-12] have also observed that protonation of the amide moiety is not possible in the pH range 2-11 nor is its deprotonation. In fact, the deprotonation of the amide protons can only be facilitated by the presence of a metal ion such as copper(II).[9-18]

5.1.2 Complex formation and Deprotonation functions

The reliability of the evaluated $\log\beta_{pqr}$ values was confirmed by two functions, which are derived from the experimental data and quantitatively related to the $\log\beta_{pqr}$'s. The complex formation function, Z_M-bar, measures the average number of ligands bound per metal ion due to complexation. This function is plotted against the negative logarithm of the ligand concentration (pL).

The deprotonation function, Q-bar, which indicates the average number of protons released on complexation is plotted against the pH of the solution. The Q-bar is compared with the n-bar function, which measures the average number of protons that would be bound to the ligand in the absence of complexation.

Based on the results reported here, and by analogy with related ligands, structures for the various metal complex species are postulated here. However, these structures will be discussed later in relation to spectroscopic evidence and computational evidence.

5.1.2.1 Cu-L systems

Figure 5.4(a) shows the Z_M-bar function for the Cu-L^2 system plotted against pL. The levelling off of the Z_M-bars at a value of one indicates the existence of mononuclear complexes of 1:1 M:L ratio. The fanning back of this complex formation function at pL values less than five suggests the formation of hydroxo- or mixed hydroxo complex species of 11-1 and 11-2 stoichiometry.

Figure 5.4: Experimental (with $Cu^{2+}:L^2$ ratios of 1:3(•), 1:4(▲) and 1:5(♦) and theoretical (line) (a) Z_M-bar and (b) Q-bar and n-bar (line) both plotted against pH.

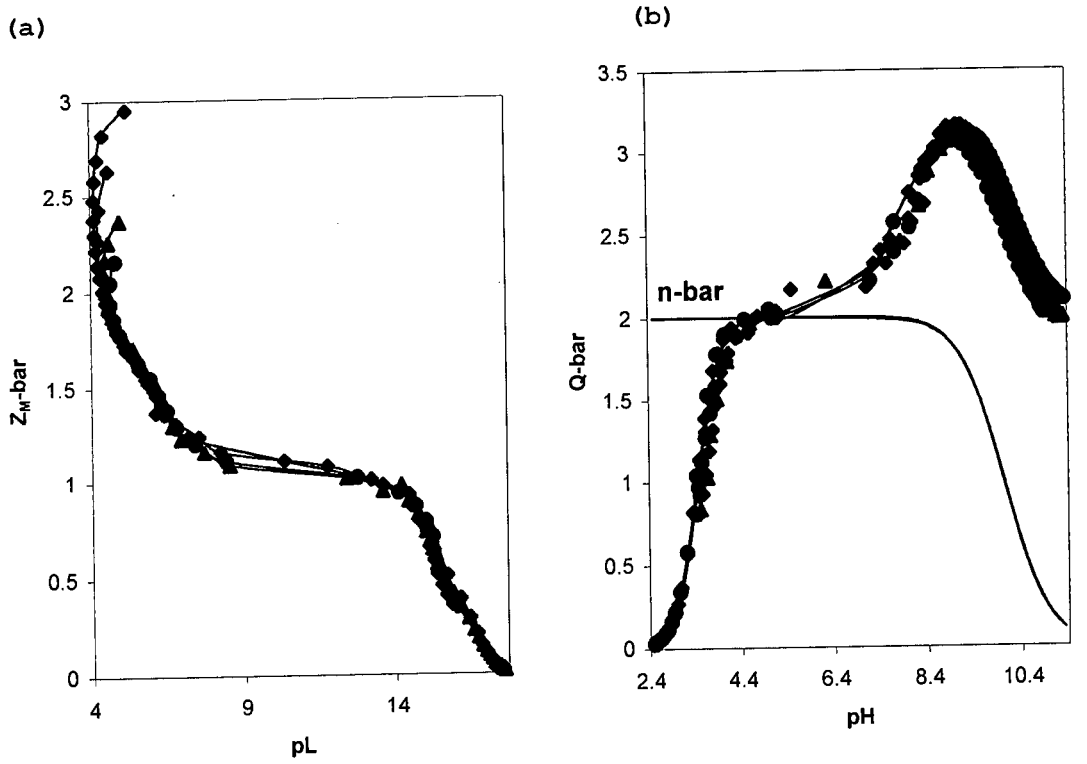

The Q-bar function given in Figure 5.4(b) increases from zero to two in the pH range 2.4-4.4 indicating that 2 protons have been released into solution due to complexation. The slight levelling off of the Q-bars in this pH range is due to accumulation of the 110 species. Above pH 4.4, this function rises again to three indicating an extra proton loss, which is ascribed to the formation of the 11-1 complex.

As seen from Figure 5.4(b), this function rises above the n-bar value of 2 confirming the presence of these hydroxo complex species. Above pH 9.00, the Q-bar decreases signifying that complexation is complete. Instead, in this pH range the 11-1 species undergoes a further loss of a proton, which is believed to be metal ion assisted to a little extent to yield the 11-2 complex. This is because the ligand has been observed to ionise by releasing both oxime protons in solution above pH 6.5.

It should be mentioned that a number of researchers have reported similar observations before.[1,2,19,20] The excellent agreement between the observed and calculated complex formation and deprotonation functions supports the potentiometric

model used in data analysis. ESTA analysis of the data yielded the results given in Table 2. The previously determined formation constants of L^1 with copper(II), nickel(II) and zinc(II) are included for comparison. Calcium(II) was found not to form complexes with the ligand, L^1.

Copper(II) forms relatively stable complexes with L^2. The enhanced stability of Cu^{2+}-L^2 complexes is reflected by $\log\beta_{110}$, $\log\beta_{11-1}$ and $\log\beta_{11-2}$ equal to 14.076, 9.903 and 1.625 for the 110, 11-1 and 11-2 species respectively. Kozlowski et al.[4] have recently reported $\log\beta$ values of 9.95 and 2.08 for the aforementioned 11-1 and 11-2 complexes. The formation constants of copper with L^2 determined in this study decrease with increasing ionic strength of the medium in accordance with the Debye-Huckel equation. However, a good agreement is observed when these formation constants are corrected for ionic strength despite the different background electrolytes used in these investigations.

In addition, these authors[4] reported the presence of the 111 complex. In contrast, no 111 species has been observed in this study, instead a 110 complex was detected. Furthermore, although the reported 111 species is chemically possible and its formation constant ($\log\beta_{111}$=19.61) equally reasonable, the reported structure is incorrect. These authors proposed that the non-coordinated oxime nitrogen is protonated. In fact, protonation of the oxime nitrogens is not possible under the investigated conditions. The proposed 111 species can only result from the co-ordination of one amide and one oxime nitrogen donor atom.

The 110 complex reported in this study is postulated to result from the loss of one of the oxime protons. It has been postulated that the high acidic nature of both dione dioxime groups in this ligand is enhanced by the amido groups at the alpha-positions. However, the co-ordination of the metal ion to the amide and oxime nitrogens should further enhance their acidity. The formation of the presently reported 110 species is as a result of this acid enhancement. In fact, the co-ordinated oxime nitrogen is believed to release its proton into solution.

Table 5.2: Logβ_{pqr}'s of L^1, L^2 and L^3 with the metal ions at 25^{0}C and I = 0.15 *mol dm^{-3}* (Cl^-) Na^+. The other symbols have their usual meaning as explained in Table 5.1.

L	Metal ion	p	q	r	Log β_{pqr}	σ_{pqr}	R_H	R_H^{lim}	$n_T(n_p)$	Lit.
L^1	Cu^{2+}	1	1	0	14.223	0.010	0.002	0.001	3(176)	
		1	1	-1	11.345	0.008				
		1	1	-2	0.221	0.024				
	Ni^{2+}	1	1	0	11.531	0.060	0.008	0.006	4(60)	
		1	1	-1	7.623	0.032				
		1	1	-2	-2.201	0.030				
	Zn^{2+}	1	1	0	5.011	0.070	0.003	0.003	3(160)	
		1	1	-1	0.261	0.002				
		1	1	-2	-8.790	0.006				
	Gd^{3+}	1	1	0	15.530	0.030	0.008	0.007	4(984)	
		1	1	-1	7.640	0.033				
		1	1	-2	0.270	0.006				
L^2	Cu^{2+}	1	1	0	14.076	0.030	0.008	0.001	6(656)	
		1	1	-1	9.903	0.030				9.95[4]
		1	1	-2	1.625	0.053				2.08
	Ni^{2+}	1	1	1	15.460	0.035	0.017	0.015	6(656)	
		1	1	-1	2.842	0.010				1.14[4]
		1	1	-2	-8.368	0.035				-7.05
	Zn^{2+}	1	1	0	6.736	0.020	0.007	0.006	4(444)	
		1	1	-1	-3.360	0.008				
		1	1	-2	-14.498	0.052				
	Ca^{2+}	-			-	-	-	-	-	-
	Gd^{3+}	1	1	-1	-0.836	0.050	0.021	0.011	4(509)	
		1	1	-2	-7.833	0.010				
		1	1	-4	-22.876	0.034				
L^3	Cu^{2+}	1	1	1	15.020	0.022	0.034	0.013	6(389)	
		1	1	0	8.911	0.018				
		1	1	-1	-0.896	0.039				
		1	1	-2	-8.677	0.042				
	Ni^{2+}	1	1	2	23.280	0.072	0.032	0.015	5(465)	
		1	1	1	16.100	0.103				
		1	1	0	7.570	0.014				
		1	1	-2	-9.640	0.117				
	Zn^{2+}	1	1	2	19.920	0.045	0.030	0.013	6(697)	
		1	1	0	3.462	0.147				
		2	1	-2	-9.018	0.044				
		1	1	-2	-13.20	0.027				
	Ca^{2+}	1	1	2	19.636	0.034	0.022	0.012	6(674)	
		1	1	1	10.808	0.116				
		1	1	0	2.424	0.046				
		1	1	-1	-8.857	0.052				
	Gd^{3+}	1	1	2	21.333	0.037	0.065	0.022	4(509)	
		2	2	-2	0.305	0.045				
		1	1	-2	-9.695	0.030				
		1	1	-3	-19.343	0.036				
		1	1	-4	-30.924	0.074				

Furthermore, the deprotonation of the free ligand begins to occur at pH 6.5 while the formation of the 110 occurs throughout the pH range 3.5-7.0. This is revealed by the Cu-L^2 speciation plots in Figure 5.5(a). The calculated Cu^{2+} assisted deprotonation constant ($pK_{ML\text{-}OH}$) associated with the formation of the $[CuL^2H_{-1}]$ is defined as the difference between $\log\beta_{110}$ and $\log\beta_{11\text{-}1}$. The calculated $pK_{ML\text{-}OH}$=4.173 is approximately four and five log units lower than the first hydrolysis constant of copper(II) and the first pK_a of the ligand, which are 7.87[21] and 9.66 respectively. This value is in the range expected for the deprotonation of the amide proton.[10-13]

Figure 5.5: Calculated speciation of Cu^{2+}(0.001M)-L(0.003M) (L=L^2(a) and L^3 (b) systems as a function of pH.

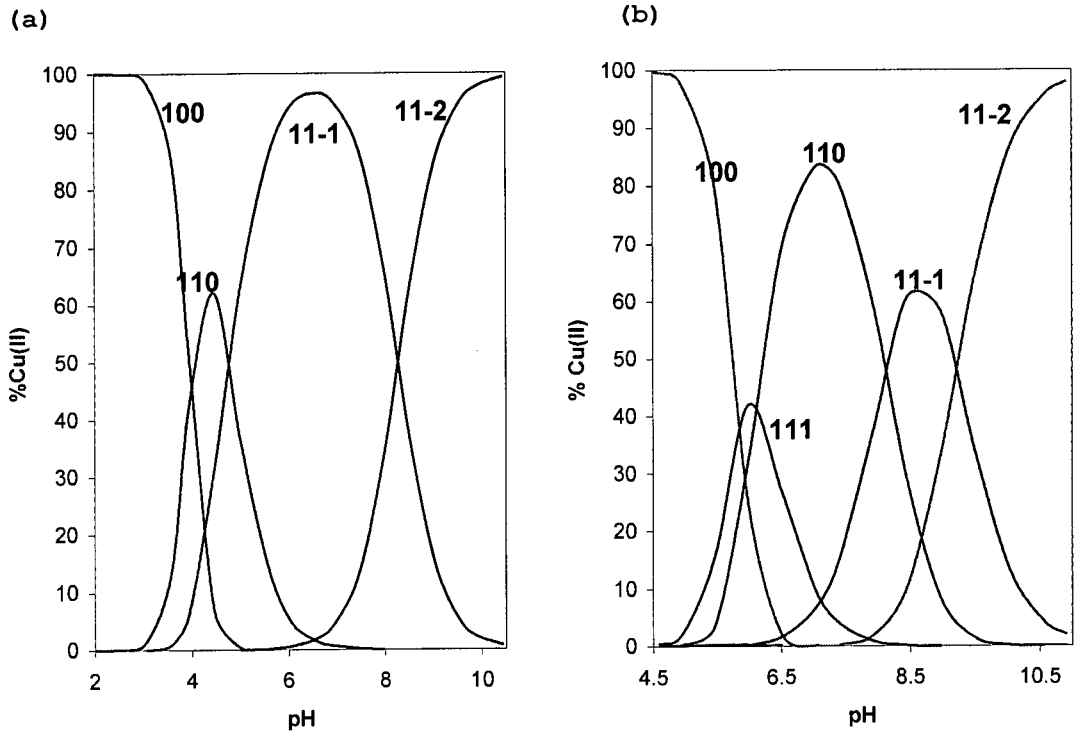

However, the formation of the 11-2 from the 11-1 species would be expected to be metal ion assisted to a small extent since the ligand's oxime protons dissociate above pH 6.5. The calculated $pK_{ML\text{-}OH}$=8.278 is 2.13 log units lower than the dissociation constant of the free ligand but higher than the first hydrolysis constant of Cu^{2+}. The latter point excludes the ionisation of an axially coordinated water molecule.[21] Furthermore, considering the fact that this proton is believed to be involved in a hydrogen bond, this value is low enough to propose a Cu^{2+} assisted deprotonation of this pseudomacrocycle.

Figure 5.6: Proposed structures for MHL, ML, MLH_{-1} and MLH_{-2} complexes of Cu^{2+} and Ni^{2+} ions. The axially co-ordinated water molecules are omitted in these representations for clarity.

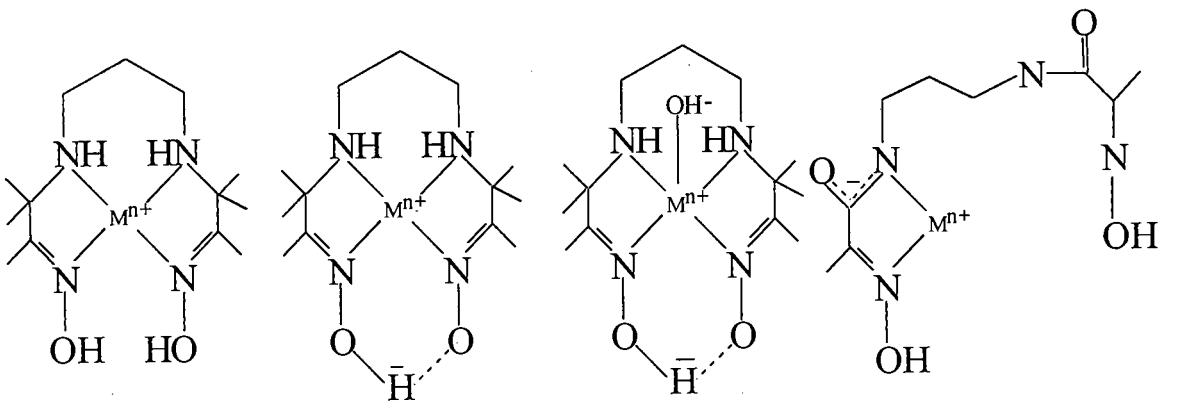

(a) 110 (L^1) (b) 11-1 (L^1) (c) 11-2 (L^1) (d) 111 (L^2)

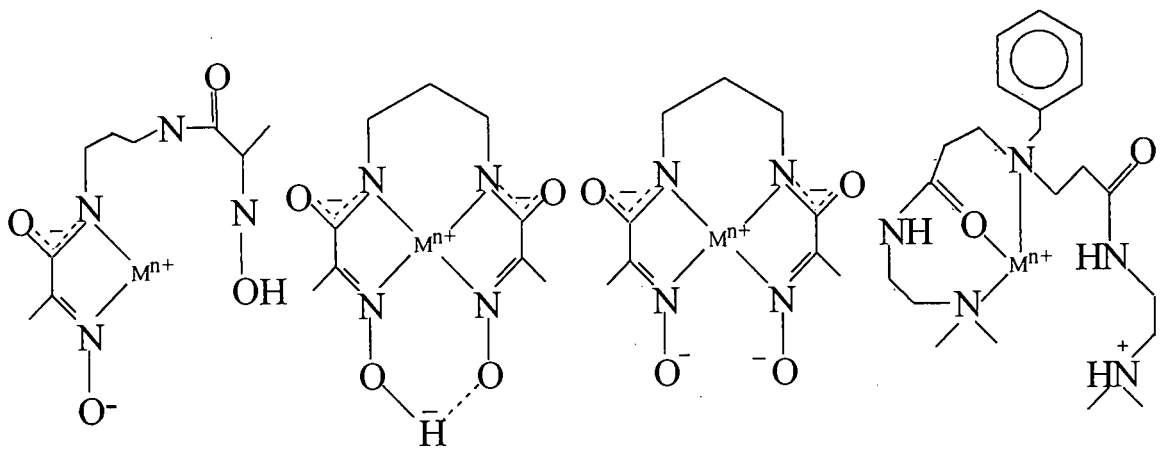

(e) 110 (L^2) (f) 11-1 (L^2) (g) 11-2 (L^2) (h) 111 (L^3)

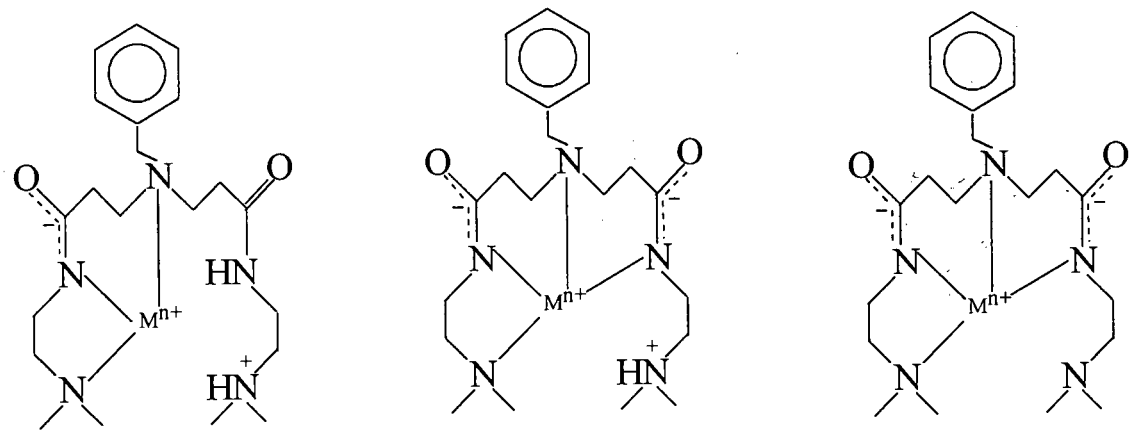

(i) 110 (L^3) (j) 11-1 (L^3) (k) 11-2 (L^3)

Although the stability constant of the 110 complex of Cu^{2+} with L^1 ($\log\beta_{110}$ = 14.22) is close to that of the corresponding L^2 species, the value of the $[CuL^1H_{-1}]$ ($\log\beta_{11\text{-}1}$ = 11.35) is 1.5 log units higher than that of the $[CuL^2H_{-1}]$ complex. This may be due to the strong hydrogen bond responsible for the pseudomacrocycle in the L^1 complex. In contrast, the 11-2 L^1 complex is 1.5 log units lower that of corresponding L^2 complex. This reversal in stability of the 11-2 complexes may be due to the stronger donating ability of two deprotonated oxime groups in the L^2 complex. The weak hydrogen bond bridging the oximato oxygens in the 11-1 L^2 species is believed to break while the formation of the 11-2 species in an L^1 system is postulated to be as a result of the ionisation of an axially coordinated water molecule. Hence, the pseudomacrocyle in the L^1 system remains intact (Figure 5.6(c)).

The complexation chemistry of the Cu^{2+}-L^3 system is characterised by exclusive formation of mononuclear species of 1:1 M:L stoichiometry. This is indicated by the levelling off of the Z_M-bars at a value of 1 (Figure 5.7(a)). The formation of either hydroxo and/or mixed-hydroxo complexes also characterises this system as evident from the fanning back of the Z_M-bars at pL values less than 4.

Figure 5.7: Experimental (with Cu^{2+}:L^3 ratios of 1:3(♦),1:4(•) and 1:5(▲) and theoretical (line) (a) Z_M-bar and (b) Q-bar and n-bar (line) both plotted against pH.

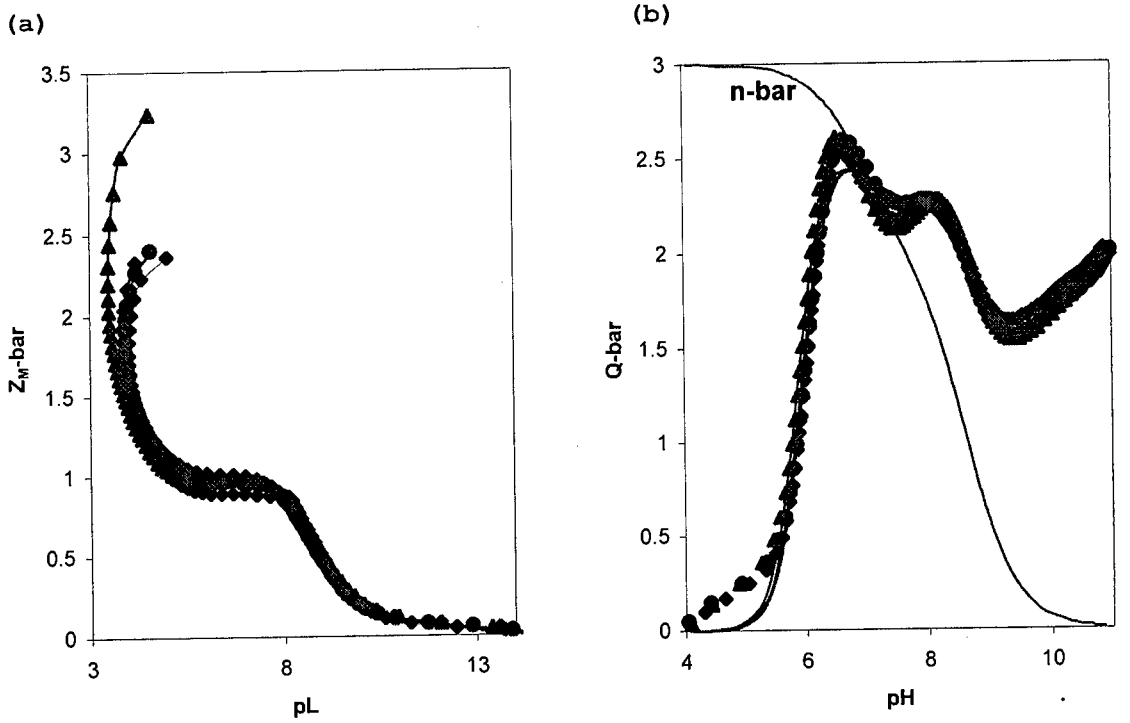

The Q-bar function, on the other hand, rises to an average value of 2.7 in the small pH range of 5.5-6.5. This is an indication that approximately three protons have been released due to complexation. Ideally, 2 and 3 protons are supposed to be released due to the exclusive formation of 111 and 110 complexes respectively. The obtained average Q-bar=2.7 is due to the simultaneous formation of these two species as seen from the speciation plots given in Figure 5.5(b).

Another feature, which is worth noting from Figure 5.7(b), is the fact that the Q-bar never rises above the n-bar plot below pH 8.0. This is because of the presence of protonated nitrogen donor atoms on the ligand in the acidic to weakly basic conditions. An excellent agreement between the observed and calculated Z_M-bars and Q-bars gives confidence to the proposed complexation model.

The four proposed 111, 110, 11-1 and 11-2 complexes (Figure 5.6 (h), (i), (j) and (k) in their respective order) comprising the Cu^{2+}-L^3 system have logβ values equal to 15.020, 8.911, 0.896 and -8.677 respectively. The 111 species is formed by deprotonation and co-ordination of both the benzylamine and one of the terminal tertiary amines. It should be mentioned that there is little or no stabilisation of this species due to the binding of the neutral carbonyl oxygen(s) to Cu^{2+}.[22] Hence, despite the presence of the fused six and seven membered rings in the 111 complex species, the chelate effect is not observed due to the low basicity of the carbonyl oxygen.

The deprotonation of one of the amide nitrogens with $pK_{ML\text{-}OH} = 6.11$ results in the 110 species, which is subsequently converted to the 11-1 complex by deprotonation of the second amide group ($pK_{ML\text{-}OH} = 8.02$). The loss of a proton from the first amide group is approximately 2 log units much easier than the deprotonation of the second amide moiety or the hydrolysis of an axially coordinated water molecule. The 110 species is stabilised by the formation of 5- and 6-membered rings. The formation of the 11-1 results in two contiguous six-membered rings which destabilise the complex compared to 5,6,5-chelate rings.

For the formation of the neutral 11-2 species, several co-ordination possibilities exist. Two key contributions to the thermodynamic stability of two likely 11-2 complexes deserve further comment. The co-ordination of the central

benzylamine, one terminal amine and both amide nitrogens would result in the formation of two contiguous less stable six-membered rings. The formation of these six-membered rings will destabilise the 11-2 complex. Moreover, the decreased basicity of the central anchoring amine should further lower the thermodynamic stability of $[CuL^3H_{-2}]$.

In contrast, the co-ordination of the more basic terminal amine should yield a more stable $[CuL^3H_{-2}]$ complex. However, this increased stability is offset by the formation of a ten-membered ring, which destabilises the complex.

Because of these two factors, there should be little or no difference in terms of stability between these two proposed $[CuL^3H_{-2}]$ species. In fact, the presence of varying amounts of these two species in the same solution cannot be ruled out.

A third possibility is that of co-ordination of the three tertiary amino and the two amide nitrogens. This will result in a five co-ordinate species where either the central amine or one of the terminal amines occupies an axial position. However, it is known that Cu^{2+} prefers six co-ordinate tetragonally distorted species where two weak ligands such as the water molecules occupy the axial positions. In these species the equatorial plane is defined by the four nitrogen donor atoms of the ligand. The third possibility is unlikely for this 11-2 complex.

The calculated Cu^{2+} assisted deprotonation constant ($pK_{ML\text{-}OH}$) associated with the formation of the $[CuL^3H_{-2}]$ is defined as the difference between $\log\beta_{11\text{-}1}$ and $\log\beta_{11\text{-}2}$. The calculated $pK_{ML\text{-}OH}$=7.78 is 0.65 log units smaller than the second deprotonation constant (pK_{NH}) of the tertiary amine and quite close to the ionisation constant of an axially co-ordinated water, which are 8.431 and 7.87 respectively. The $pK_{ML\text{-}OH}$ value is compared to the second deprotonation constant of the free ligand because of the decreased basicity of this amino group due to the presence of the metal ion. In fact, the actual pK_{a2} value of the ligand should be less than 8.431 because of the dipositive nature of the metal ion compared to the proton. From the potentiometric data it is difficult to propose with certainty the origin of this proton loss, but in both cases, the involvement of the metal ion is suggested together with the parallel formation of the two proposed isomers. Consequently, the deprotonation function

never rises above the n-bar plot in this L^3 system as was observed in the corresponding L^2 system discussed above.

Since Cu^{2+} is not known to form stable complexes when bigger membered rings are involved, it is more likely that the second terminal tertiary amine remains uncoordinated in this species. Steenland et al.[7] have postulated a similar kind of co-ordination for the macrocyclic analogues (L^i and L^j) of L^3 towards Cu^{2+}. This kind of coordination should be more feasible for L^3 compared to L^i and L^j because of the close proximity of protonated site to the coordinated metal ion as a result of electrostatic repulsion in the latter ligands.

Steric requirements also rule out the co-ordination of both terminal tertiary amino groups to the same metal ion. This is because of the sp^2 hybridised nature of the deprotonated amide nitrogens which co-ordinate in the square-planar fashion in addition to the coordinated central anchoring amine and a terminal amino group.

Although copper forms stable complex species with L^3, the reported constants are 1-1.5 log units lower than those of the previously investigated systems.[8] Furthermore, the increased basicity of the central amine in L^3 is not reflected in the formation constants of Cu^{2+} with the ligand. This may be due to the formation of two less stable contiguous six-membered rings on deprotonation and co-ordination of the two amide groups.

Steenland et al.[7] have reported $\log\beta_{110}$'s of 8.5 and 10.1 for Cu^{2+} with the dioxomacrocycles they investigated. A $\log\beta_{110}$ of 8.5 is close to the one reported in this study for the same species. The presently reported constants for 11-1 and 11-2 are 4-5 log units lower than those reported by these authors[7] ($\log\beta_{11\text{-}1}$ = 4.6 and 3.3, $\log\beta_{11\text{-}2}$ of -4.3 and -5.9). This is due to the strain introduced by having two contiguous six membered rings instead of five- and six-membered rings. In fact, these systems are believed to be stabilised by having alternating five and six membered rings.

He Bu et al.[13] have recently reported Cu^{2+} and Zn^{2+} complexation equilibria with two mono- and dioxo-cyclam ligands containing 2-pyridylmethyl groups. Quite

contrary to expectations, copper(II) does not seem to facilitate the deprotonation of the amide groups. In fact, the crystal structure of the 110 complex of Cu^{2+} with one of these ligands indicates that the ligand is co-ordinated to the metal ion through the appended pyridylmethyl nitrogens and the backbone amino and carbonyl oxygen atoms. This is because the pyridyl nitrogens are more basic compared to hard nitrogen donor atoms of the amide moiety.

Santos and coworkers[14] have also revealed the binding of the oxygen donor atoms of the appended hydroxamate moiety towards Cu^{2+} at neutral pH. The pH driven translocation of Cu^{2+} from one ligand compartment (containing predominantly nitrogen donor atoms) to another (which contains amide groups)[16] is also evidence of the difficulty associated with the deprotonation of the hard amide moiety. It should be mentioned that in basic conditions the metal assisted ionisation of the amide groups occurs with ease. Another notable feature about these dioxo-macrocycles is the presence of the 11-1 as a minor species. This may mean that this complex is rather a mathematical than a physical form. It may also be an intermediate species, which is converted to the thermodynamically stable 11-2 by the deprotonation of the second amide group.

5.2.2.2 Ni-L systems

Figure 5.8(a) below shows the complex formation function of the Ni^{2+}-L^2 system, which levels off at a Z_M-bar value of 1.5. This is because the ML^2 species is not the predominant or only species in this system as observed by Witt et al.[23]. In fact, hydroxo species predominate in its equilibria. The fanning back of the Z_M-bar at low pL values of 4 is indicative of these hydroxo species. These plots, however, do confirm the presence of mononuclear species of 1:1 M:L ratio.

The Q-bar function given in Figure 5.8(b) increases to a maximum value of 3 in the pH range 6.0-7.5 indicating the simultaneous dissociation of three protons due to metal ion co-ordination. This function rises above the n-bar plot to suggest that the complex releases an extra proton compared to the number of protons postulated to be attached on the ligand. Above pH 8.5, the Q-bar decreases and runs parallel to the n-bar to indicate that complexation is complete at these basic conditions.

Figure 5.8: Experimental (with Ni^{2+}:L^2 ratios of 1:3(♦), 1:4(▲) and 1:5(•) and theoretical (line) (a) Z_M-bar and (b) Q-bar and n-bar (line) both plotted against pH.

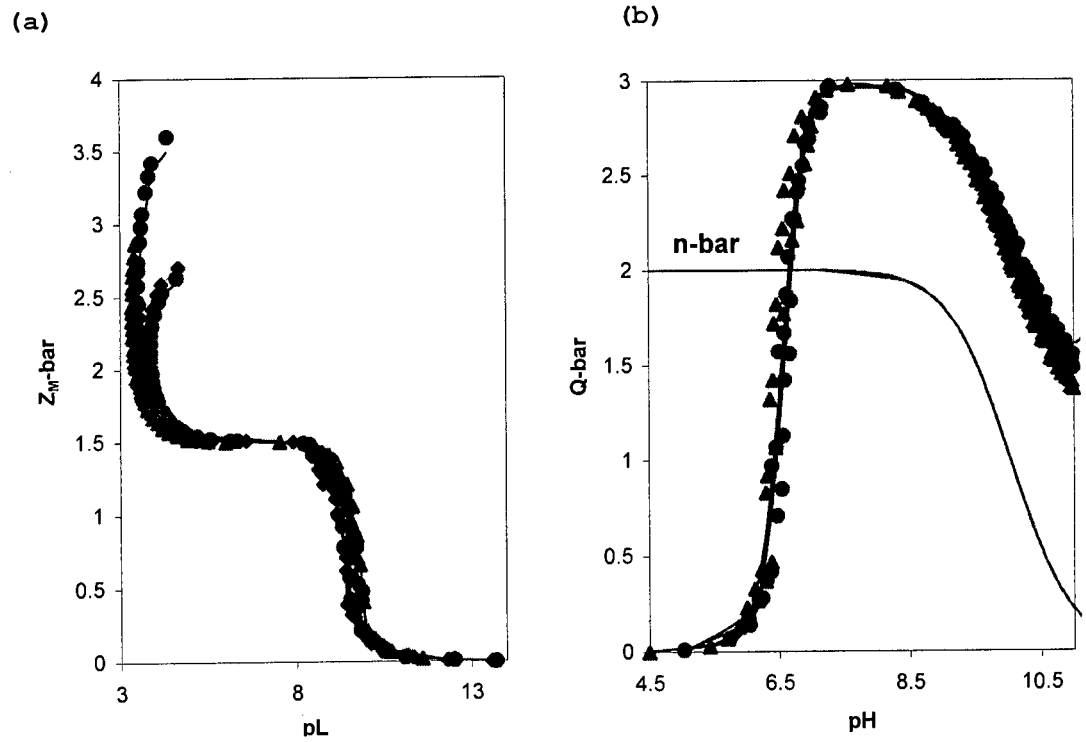

It should be emphasised that slow kinetics was observed in this Ni^{2+}-L^2 system. Despite the known limitations associated with slow kinetics, there is an excellent agreement between the observed and calculated functions. This validates the potentiometric model used in the data analysis.

The ligand L^2 seems to co-ordinate strongly to the Ni^{2+} ion as indicated by $\log\beta_{111}$=15.460, $\log\beta_{11\text{-}1}$=2.842 and $\log\beta_{11\text{-}2}$=-8.368 for 111, 11-1 and 11-2 species respectively. In order to make these formation constants more explicit, the distribution curves of the three species are plotted in Figure 5.9(a). The speciation plots indicate that the metal ion does not exceed 5% as the 111 species indicating its minority in these equilibria. The 11-1 complex predominates in the pH range 7-10 while above pH 10.00, the 11-2 becomes the dominant species.

The ligand is believed to be co-ordinated to the metal ion through one amide and one oxime nitrogen atoms in the 111 complex. The proposed structure of this species is depicted in Figure 6(d). Ni^{2+} appears to sit in a square-planar arrangement of the ligand donor atoms in the 11-1 and 11-2 species (Figure 6(f) and (g)

respectively), hence the observed reasonably high formation constants. The metal ion also appears to have a high affinity for oxime containing ligand systems as it has been observed with L^1 and similar, previously studied, ligands.[2,6]

Figure 5.9: Calculated speciation of (a) Ni^{2+}(0.00023)-L^2(0.0008M) and (b) Ni^{2+}(0.001)-L^3(0.0035) solutions as a function of pH.

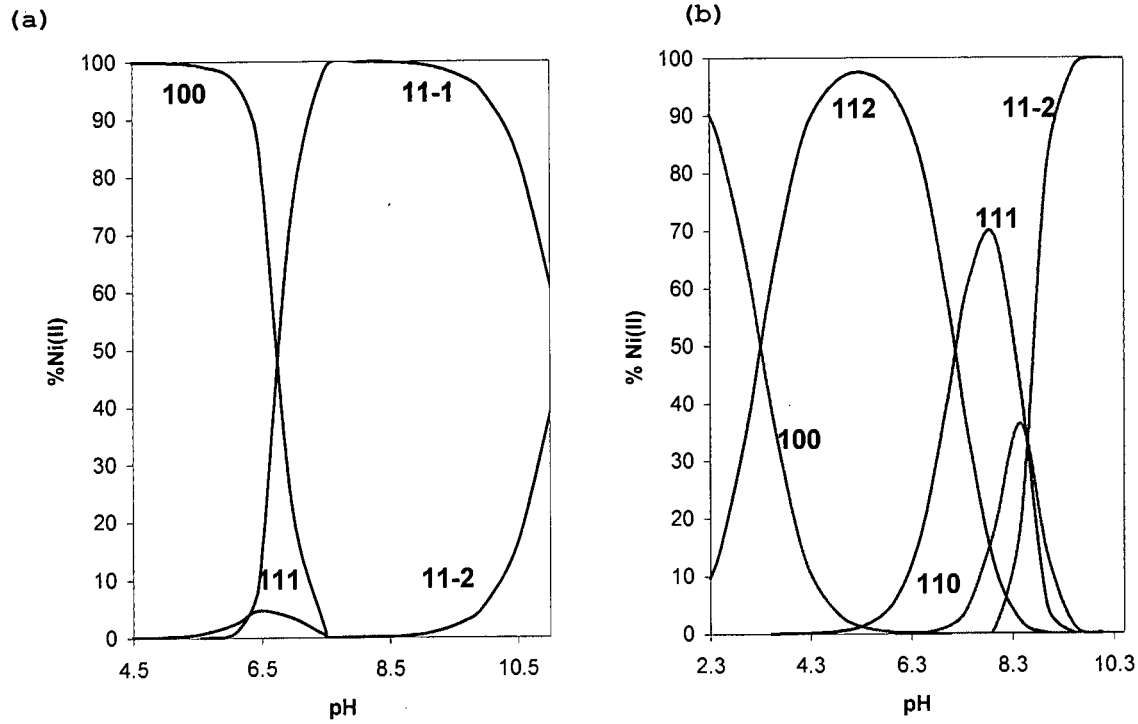

The presently evaluated Ni-L^2 constants are two log units higher than those reported by Koslowski et al.[4]. These authors reported that the equilibria are reached instantaneously in this system. This is in sharp contrast to the slow kinetics observed in the present investigations, where long delays were required between titration points in order to allow the system to come to equilibrium.

The previously reported formation constants of the 11-1 ($\log\beta_{11\text{-}1}$=7.68) and 11-2 ($\log\beta_{11\text{-}2}$=-2.43) Ni^{2+}-L^1 complexes are 5 log units higher than those observed for the corresponding L^2 species. This is due to the stronger hydrogen bond in [NiL^1H_{-1}] compared to the L^2 complex. Since the formation of the 11-2 complex for both L^1 and L^2 is due to the breaking of the hydrogen bond, the stability of the L^1 complex should reside on the three 5,6,5-chelate rings.

In contrast to the Ni^{2+}-L^2 system mentioned above, the metal ion appears to co-ordinate weakly to the L^3 ligand. This is revealed by the Z_M-bars (Figure 5.10(a)) which remain close to 0.5 throughout the ligand concentration range investigated. The fanning back of the Z_M-bars at low pL values is indicative of hydroxy and/or mixed-hydroxy species formation.

Figure 5.10: Experimental (with Ni^{2+}:L^3 ratios of 1:4(♦),1:3(▲) and 1:2(•) and theoretical (line) (a) Z_M-bar and (b) Q-bar and n-bar (line) both plotted against pH.

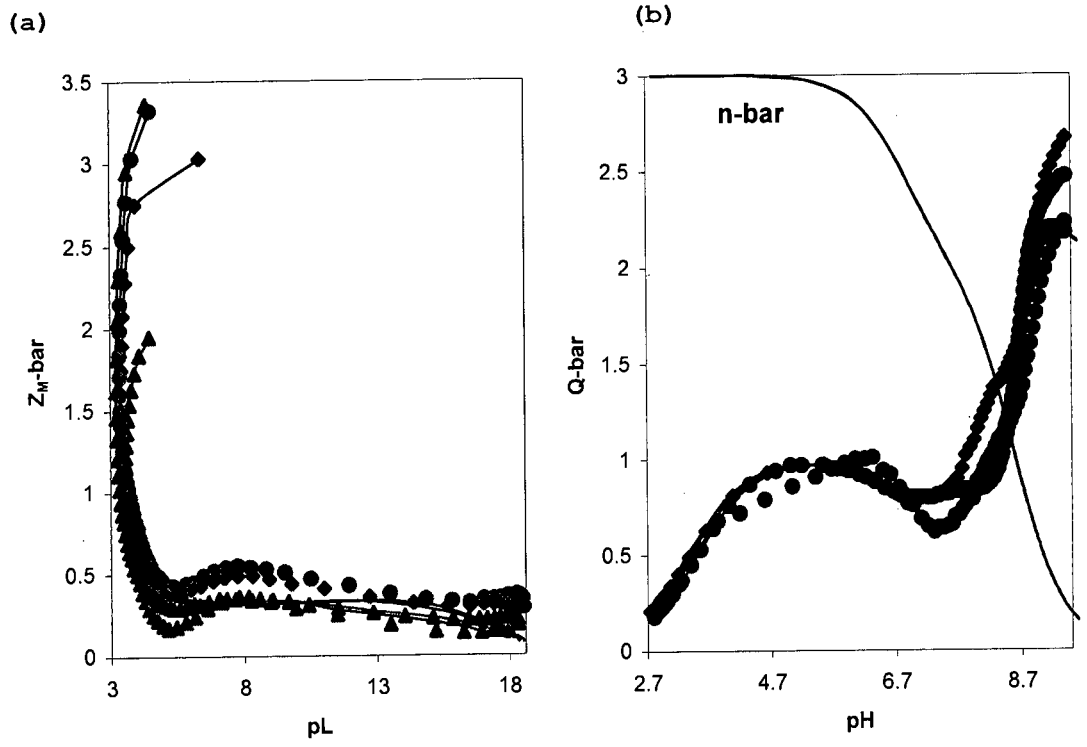

The Q-bars plotted in Figure 5.10(b) increases from to 0.2 to 1.00 in the pH range 2.7-5.0 indicating the loss of one proton due to complexation. Above pH 6.0, the function decreases probably due to an onset of hydrolysis. In the pH range 7.5-9.0, this function rises to two indicating another proton loss.

The titration procedure was terminated or the data above pH 9.00 discarded at the visual sign of precipitation. The Z_M-bars and Q-bars remain lower than the expected values of 1 and 3 respectively in support of this weak binding ability of L^3 towards Ni^{2+}. There is, however, a good agreement between the observed and calculated Z_M-bars and Q-bars in support of the evaluated constants.

One of the reasons for this weak binding is related to the difficulty associated with the deprotonation of the amide nitrogens. As indicated by the speciation plots (Figure 5.9(b)), the protonated 112 ($\log\beta_{112}$=23.28) and 111 ($\log\beta_{111}$=16.10) species dominate in the pH range 2.5-8.3. The deprotonation of either a co-ordinated water molecule or an amide nitrogen occurs above pH 7.0 leading to the formation of the 110 species with $\log\beta_{110}$=7.57. The 110 species can also be formed by the coordination of the three tertiary amines. The calculated $pK_{ML\text{-}OH}$=8.53 is close to the second deprotonation constant of the ligand (pK_{a2}=8.43) and 1.5 log units lower than the hydrolysis constant of the metal ion ($pK_{M\text{-}OH}$=10.20)[21]. This indicates that the proton is more likely to have been released from the amide group. The deprotonation of the amide moiety of the ligand by Cu^{2+} has been observed to be 2 log units much easier than the hydrolysis of a coordinated water molecule.

Another noticeable feature about the complexation behaviour of this system is the absence of the 11-1 species. Instead, above pH 8.5 the 11-2 complex species with $\log\beta_{11\text{-}2}$=-9.64 predominates. This can be explained in terms of the pH delayed co-ordination of either the second amide nitrogen or both amide groups if the terminal nitrogens are coordinated in the 110. If the latter assumption is true, this behaviour is reminiscent of complexation solution chemistry of macrocyclic dioxo tetraamine ligands.[10-13] In cases where there is a 11-1 species formed in these macrocycles, it is normally present as the minor complex.[10-13]

If the neutral $[NiL^3H_{-2}]$ is formed by deprotonation of the amide groups, it is believed to be further stabilised by the co-ordination of the fifth terminal nitrogen in an axial position. However, this increased stability is further offset by the formation of contiguous six-membered rings due to the co-ordination of the second amide nitrogen. It should be mentioned that the pH range of investigation was limited to pH 9.0 due to precipitation of probably the neutral $[NiL^3H_{-2}]$ species.

Amendola et al.[15] have recently designed and studied the solution chemistry of a two compartmental ligand capable of binding Ni^{2+} in a pH dependent manner. In weakly acidic or basic conditions, the metal ion resides in a compartment containing two quinoline nitrogens and two amino nitrogen donor atoms. Above pH 8.0, Ni^{2+} translocates into amide and amino groups containing compartment after deprotonation

of the amide moieties. The development of these ditopic ligands is important in keeping the metal ion in solution until a high pH is reached for the ionisation of the amide groups to occur. These observations support the solution behaviour observed for Ni^{2+} with L^3. The neutral $[NiL^3H_{-2}]$ which precipitates above pH 9.0 may also be a mixture of the above proposed species or a mixed-hydroxo complex.

5.1.2.3 Zn-L systems

Figure 5.11(a) shows the Z_M-bars of the Zn-L^2 system. The function levels off at a Z_M-bar value of 1 indicating the presence of mononuclear species of 1:1 Zn^{2+}:L^2 ratio. The fanning back of the complex formation function is indicative of hydroxo and/or mixed-hydroxo species.

Figure 5.11: Experimental (with Zn^{2+}:L^2 ratios of 1:3(♦),1:4(•) and 1:5(▲) and theoretical (line) (a) Z_M-bar and (b) Q-bar and n-bar (line) both plotted against pH.

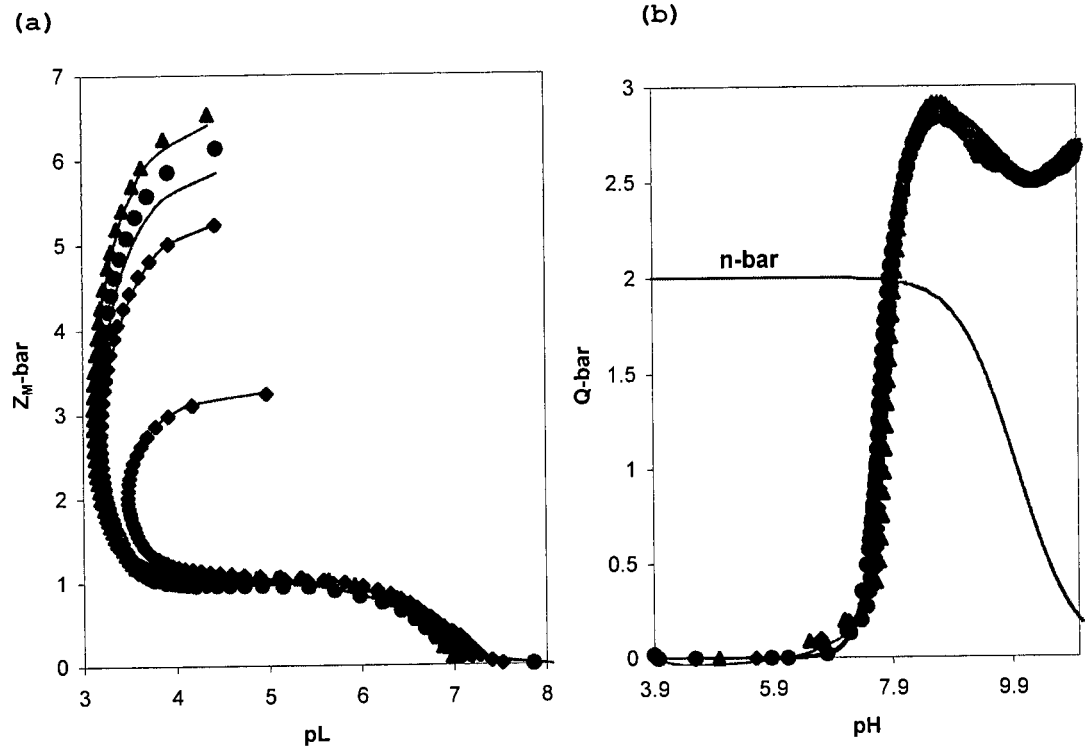

The Q-bar function (Figure 5.11(b)), on the other hand, increases to an average of three in the pH range 6-8. This is attributed to the simultaneous release of three protons into solution in this weakly acidic to basic region. The Q-bar function rises above the n-bar plot further confirming an additional proton loss compared to the neutral ligand. Between pH 8.5 and 10, the Q-bar and n-bar curves are parallel

indicating that no further complexation takes place in this pH range. Above a pH of 10, the Q-bar function continues to increase indicating an extra proton loss due to the formation of the 11-2 species. The complete superimposability of the experimental and theoretical complex formation and deprotonation functions for various M:L ratios lends support to the potentiometric model used in data analysis.

A $\log\beta_{110}$ value of 6.736 for the 110 complex indicates a reasonably strong co-ordinating ability of the ligand towards Zn^{2+}. The ligand is postulated to be co-ordinated to the metal ion in this species through the two oxime nitrogens, the hydroxide ion and the water molecule(s) or the carbonyl oxygen. One of the oxime oxygens is deprotonated in the 110 complex. The arrangement of the ligand's donor atoms is such that a tetrahedral or an octahedral environment around Zn^{2+} is preserved. Figure 5.12(a) indicate that the 110 species is present in small amounts in the pH range studied.

Figure 5.12: Calculated speciation of the Zn^{2+}(0.001M-L(0.003M) [$L=L^2$(a) and $L=L^3$ (b)] system as a function of pH.

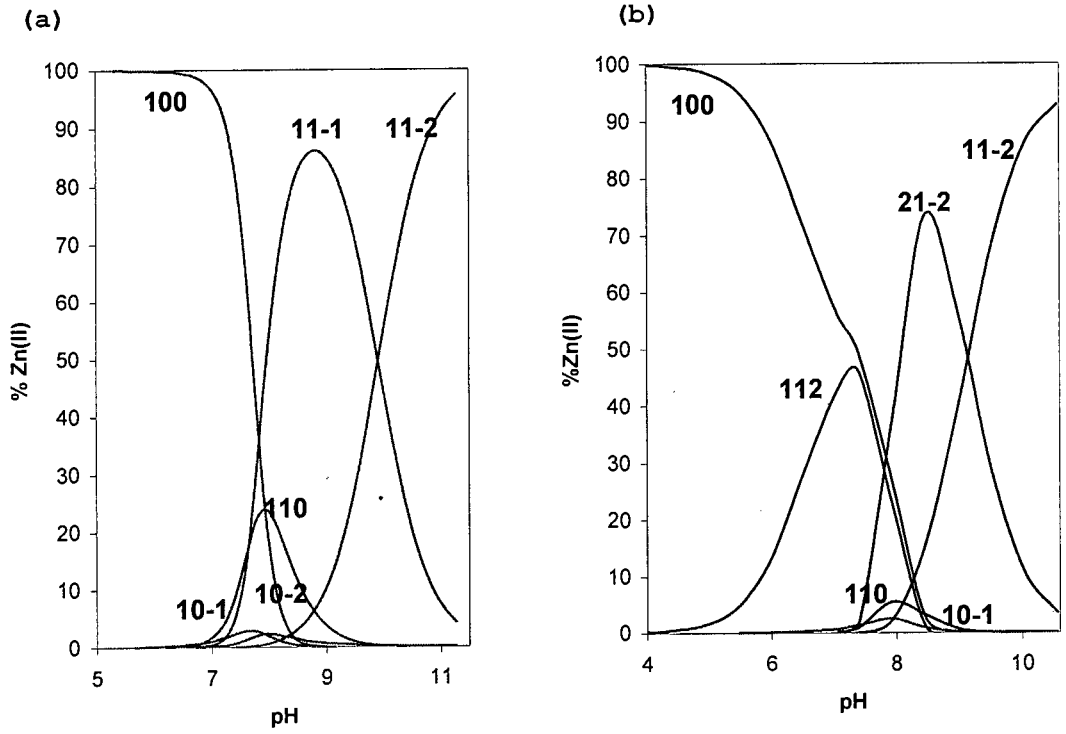

Since Zn^{2+} is not known to deprotonate amide nitrogens,[13] the formation of the 11-1 complex ($\log\beta_{11\text{-}1}$=-3.360) may be due to ionisation of the co-ordinated water molecule. At pH values above 9.5 dissociation of the second oxime proton occurs to

yield the 11-2 ($\log\beta_{11\text{-}2}$ = -14.498) species and both the 11-1 and 11-2 complexes predominated in the basic pH range (Figure 5.12(a)).

The calculated first and second $pK_{ML\text{-}OH}$'s are 10.12 and 11.0 respectively. The first $pK_{ML\text{-}OH}$=10.12 is quite close to the first hydrolysis constant of the metal ion and the ionisation constants of the ligand. The second $pK_{M\text{-}OH}$=11.0 is approximately 1.5 log units higher than the first pK_a of the ligand indicating that the proton loss may originate from the hydrogen bond of the pseudomacrocycle. These $pK_{M\text{-}OH}$'s support the assumption of the inability of the Zn^{2+} ion to deprotonate the amide moiety.

The complex formation behaviour of the Zn^{2+}-L^3 system is shown in Figure 5.13(a). The Z_M-bar remains close to zero throughout the investigated pH range. This system seems to be characterised by the formation of hydroxo species as revealed by the fanning back of the complex formation function at high ligand concentrations. The Q-bar curve (Figure 5.13(b)) rises to two at pH 8.0 indicating the release of two protons.

Figure 5.13: Experimental (with Zn^{2+}:L^3 ratios of 1:3(♦),1:4(▲) and 1:5(•) and theoretical (line) (a) Z_M-bar and (b) Q-bar and n-bar (line) both plotted against pH.

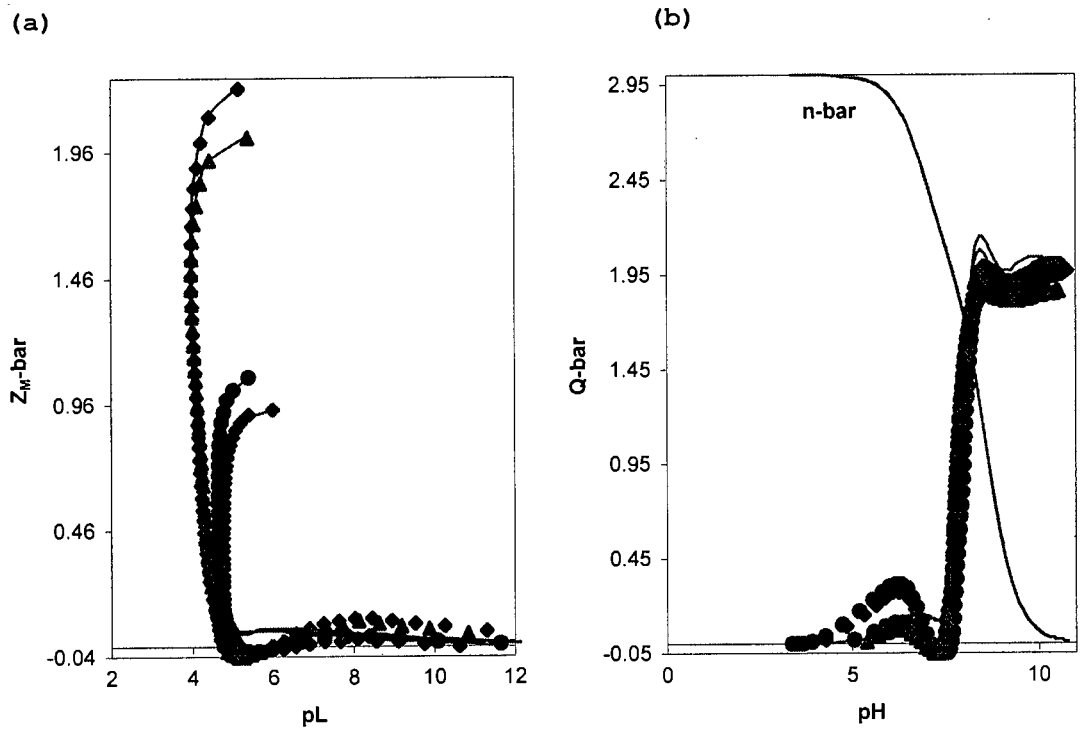

The Q-bar function never rises above the n-bar plot indicating that there is a proton still attached on one of the ligand's donor atoms. A notable feature about these curves is an excellent agreement between the calculated and observed Z_M-bars and Q-bars, which is in support of the validity of the proposed Zn^{2+} complexation model.

The presence of protonated 112 with $\log\beta_{112}$=19.920 (Figure 5.11(b)) in the pH range 5.0-8.0 is an indication of the lower binding strength of this ligand towards Zn^{2+}. A 110 complex with a $\log\beta_{110}$=3.462 occurs to a small extent and is subsequently converted to the 21-2 ($\log\beta_{21\text{-}2}$=-9.02) and 11-2 ($\log\beta_{11\text{-}2}$=-13.20) species by the hydrolysis of co-ordinated water molecules.

The 110 species is formed by co-ordination of the central amine, one terminal amine, the hydroxide ion and one or both oxo groups (or binding of water molecules). In the 21-2 complex, the ligand is postulated to be co-ordinated to the two zinc(II) ions through the terminal amines and oxo groups in a bidentate and bridging fashion. Two hydroxide ions, one on each metal ion and the water molecules complete the tetrahedral and/or octahedral co-ordination environment. Elimination of this species in the speciation model yields greater standard deviations in $\log\beta$'s of the other detectable species as well as a higher $R_H{}^f$ indicating its importance in the model.

Unlike divalent copper and nickel, zinc(II) appears to deprotonate the amide nitrogens of these ligands with difficulty.[13,14] The low stability constants of Zn^{2+} with L^2 and L^3 are partly due to the afore-mentioned phenomenon. Furthermore, it is known that Zn^{2+} prefers more or less a tetrahedral geometry. This has been observed in a majority of simple ligand systems, for example, 1,5,9-triazacyclododecane.[24] The metal ion seems to adopt the same co-ordination geometry in biological metallo-enzymes. These include enzymes such as carbonic anhydrase,[24] carboxypeptidase A,[25] copper-zinc SOD[26] and phosphate esterases.[27,28]

In fact, complexes of zinc(II) with 1,5,9-triazacyclododecane have been used as models for the active site of carbonic anhydrase.[24] While the biological functions of zinc in these proteins varies considerably, their active zinc sites exhibit a common pseudotetrahedral structural motif. These zinc centers contain nitrogen and oxygen donors, the latter mostly being derived from solvent (water) molecules. Hence, the

low stability constant values of Zn^{2+}-L^2 complexes may also be due to the postulated square-planar arrangement of nitrogen donor atoms forced on the metal ion by the ligand. The subsequent bonding of two axial water molecules results in octahedral zinc(II) species. This leads to a further decrease in thermodynamic stability. A similar behaviour has been observed for the previously investigated Zn^{2+}-L^1 system.[2]

5.1.2.4 Ca-L systems

Unlike the metal ions discussed above, calcium(II) does not form complexes with L^2. This was observed previously with L^1.[2] In contrast, Ca^{2+} seems to have a low but measurable affinity for the donor atoms of L^3. This is confirmed by the complex formation function (Figure 5.14(a)) for the Ca^{2+}-L^3 system, which does not increase to significant levels in the pH range investigated.

Figure 5.14: Experimental (with Ca^{2+}:L^3 ratios of 1:3(▲),1:4(●) and 1:5(♦) and theoretical (line) (a) Z_M-bar and (b) Q-bar and n-bar (line) both plotted against pH.

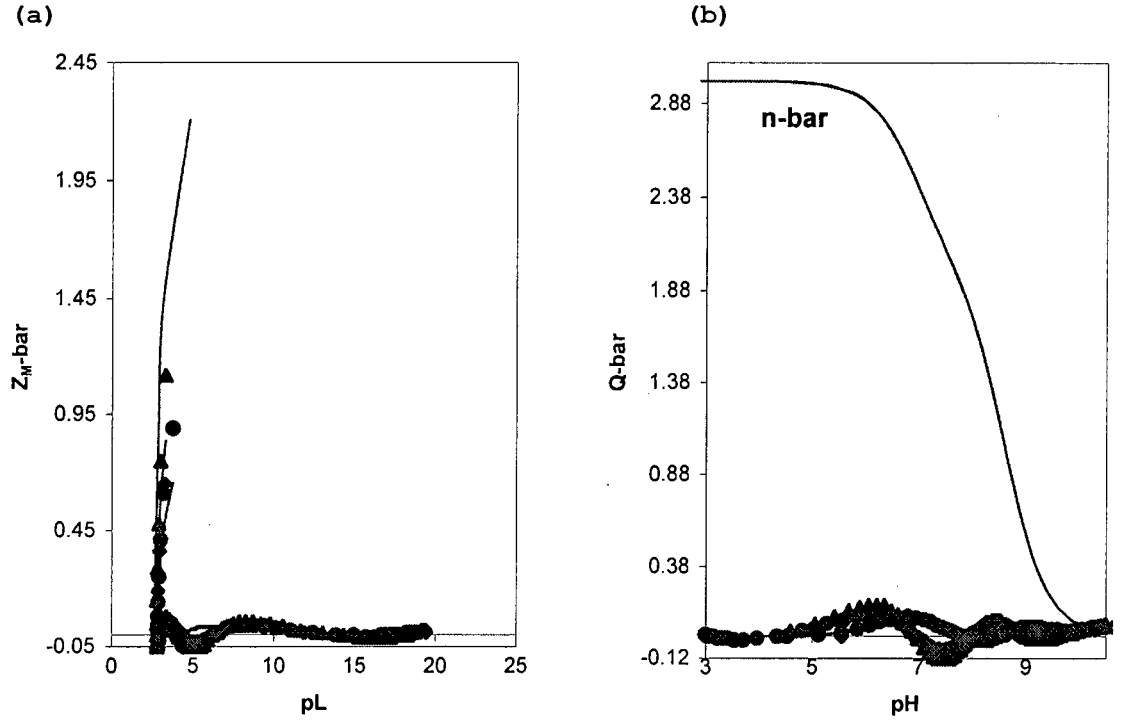

Furthermore, the Q-bar function (Figure 5.14(b)) remains almost constant at a value close to zero. This indicates the absence of significant complexation in this system. Consequently, both these functions never rise to the expected Z_M-bar and Q-bar values of 1 and 3 respectively. Despite this insignificant complexation, there is,

however, a good agreement between the observed and the theoretical Z_M-bar and Q-bar functions to validate the proposed model.

In fact, as seen from Figure 5.15(a), the Ca^{2+}-L^3 system is characterised by the formation of protonated complexes. Because this metal ion has a slight tendency to hydrolyse, such a behaviour is expected. There appears to be a little difference between the calculated speciation of the L^3 ligand (Figure 5.3(b)) and that of its Ca^{2+} system.

Figure 5.15: Calculated speciation of (0.001M) (a) Ca^{2+}- (b) Gd^{3+}-L^3 (0.003M) solutions as a function of pH.

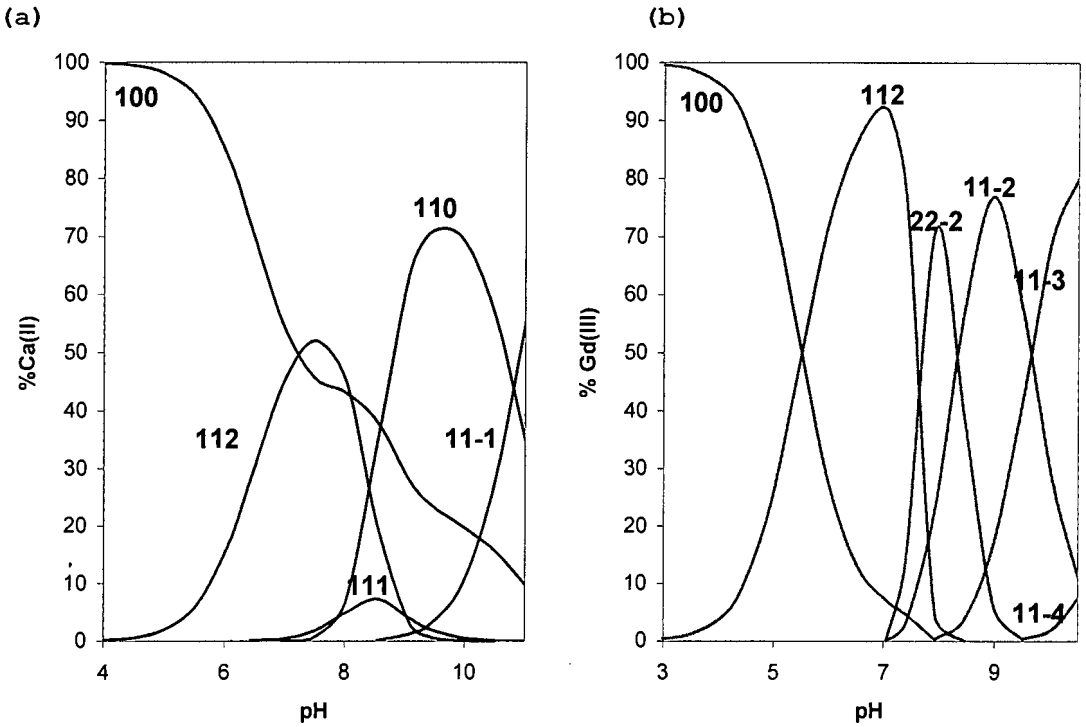

The evaluated constants with $\log\beta_{112}$=19.636, $\log\beta_{111}$=10.808, $\log\beta_{110}$=2.424 and $\log\beta_{11\text{-}1}$=-8.857 for the 112, 111, 110, 11-1 complexes respectively is an indication of this weak co-ordinating ability of L^3 towards Ca^{2+}. The formation of 111 from 112 and 110 from 111 are due to an insignificant metal ion assisted deprotonation of the terminal amino groups with $pK_{ML\text{-}OH}$ of 8.83 and 8.39 respectively. On the other hand, the third calculated $pK_{ML\text{-}OH}$ of 11.28 resulting in the formation of 11-1 from 110 is one log unit less than the metal ion's only hydrolysis constant, which is 12.45. The weak complexes formed by this system may have been facilitated by the presence of two carbonyl oxygens and the hard nitrogen donor atoms.

It should be emphasised that there are no reported constants of this metal ion with the majority of ligands containing nitrogen donor atoms, such as 1,3-diaminopropane, triazanonane and other linear and macrocyclic polyamine ligands.[29]

This behaviour for calcium, which is classified as a hard Lewis acid (HSAB theory),[30] is expected as this metal ion prefers ligands with hard negatively charged donor atoms such as oxygen in EDTA and DTPA. The amide nitrogens in L^2 and L^3 are known to be strong σ-donors in a deprotonated state. However, this metal ion is not known to be capable of deprotonating the amide nitrogens. The calculated pK_{ML-OH}'s attest to the aforementioned phenomenon. Hence, the absence of any reported formation constants of this metal with L^2 and the formation of weak complexes with L^3 is as a result of this behaviour.

5.1.2.5 Gd-L systems

Figure 5.16 (a) shows the complex formation function of the Gd^{3+}:L^1 system plotted against pL. The function rises and levels off at one indicating the formation of mononuclear species of 1:1 M:L ratio.

Figure 5.16: Experimental (with Gd^{3+}:L^1 ratios of 1:2(♦),1:3(▲) and 1:4(•) and theoretical (line) (a) Z_M-bar and (b) Q-bar and n-bar (line) both plotted against pH.

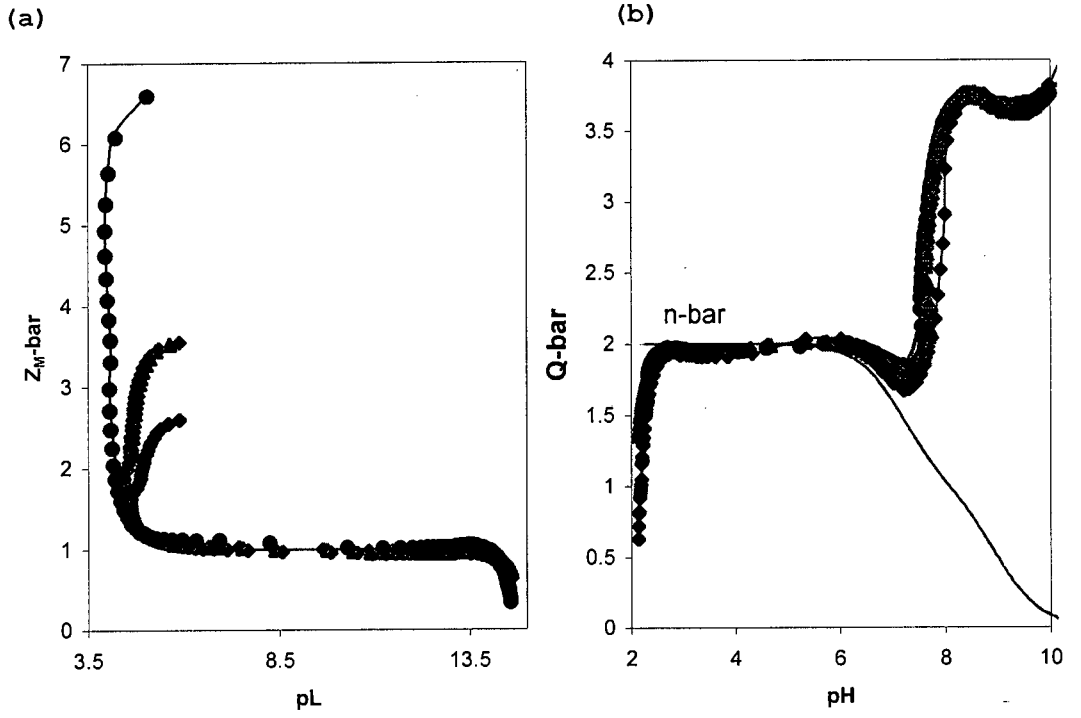

As expected for a metal ion which undergoes hydrolysis with ease, the Z_M-bar curves fan back to indicate the formation of either hydroxo and/or mixed-hydroxo species. The Q-bar curves given in Figure 5.16(b) increases to 2 in the pH range 2.0-3.0 suggesting the loss of two protons due to the formation of the 110 species. In the pH range 3-6, the Q-bar and n-bar curves are parallel indicating that no change in complexation takes place.

The Q-bar function rises above the n-bar plot to an average of 4 between pH 7.0-8.5 before the onset of precipitation. This is due to the loss of two extra protons as a result of the simultaneous formation of the 11-1 and 11-2 species (Figure 5.17(a)). An excellent agreement between the observed and calculated complex formation and deprotonation functions supports the validity of Gd^{3+}-L^1 complexation model.

Figure 5.17: Calculated speciation of (a) $Gd^{3+}(0.00062)$-$L^1(0.0022M)$ and (b) $Gd^{3+}(0.001)$-$L^2(0.0035)$ solutions as a function of pH.

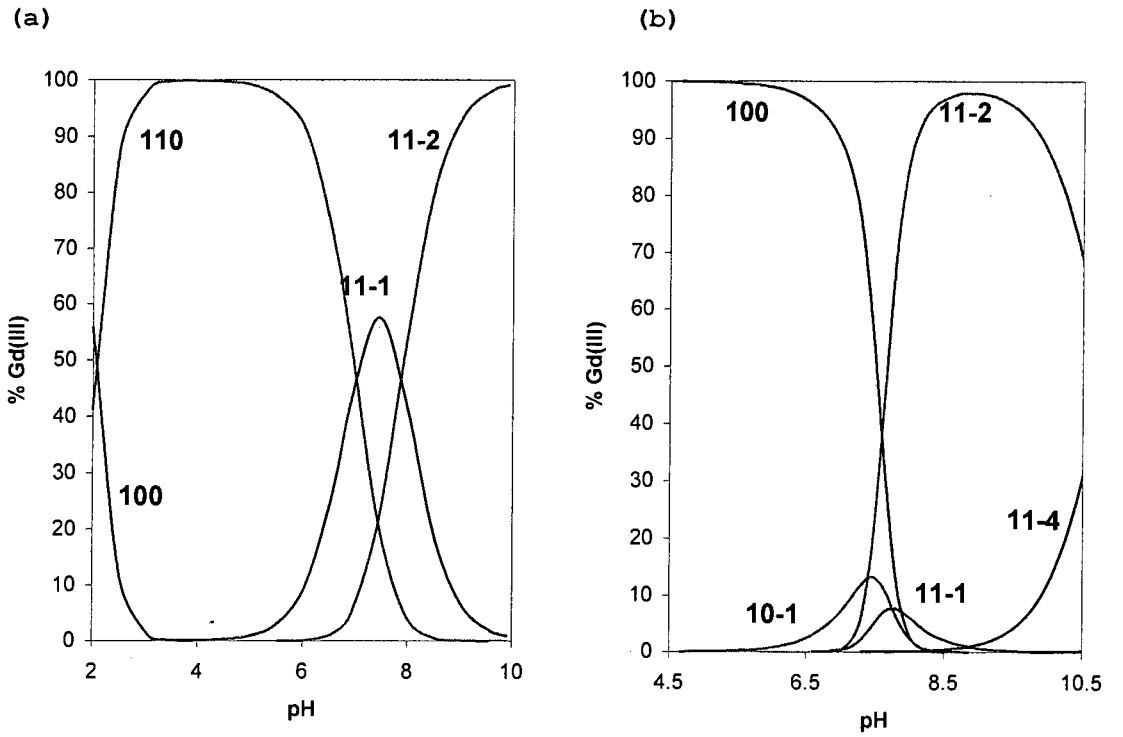

The three complex species formed by Gd^{3+} with L^1 have logβ's of 15.530, 7.640 and 0.240 for the 110, 11-1 and 11-2 complex species respectively. The first $pK_{GdL\text{-}OH}$ of 7.89 associated with the formation of 11-1 from 110 is close to the first hydrolysis constant of Gd^{3+} which is 8.10. The second $pK_{GdL\text{-}OH}$ = 7.37 leading to the formation of 11-2 is 5 log units slightly less than the acid dissociation constant of an

oxime group of a free ligand. The 11-1 and 11-2 complexes may originate from metal assisted stepwise dissociation of protons from a co-ordinated water molecule and an oxime nitrogen respectively.

In the three species mentioned above, it is postulated that the metal ion is co-ordinated to the four nitrogen donor atoms. Since the metal ion prefers co-ordination numbers 8 and 9, it would seem therefore that Gd^{3+} in these complexes is co-ordinatively unsaturated. The remaining co-ordination sites are believed to be occupied by water molecules.

The formation of a whitish colloidal precipitate above pH 10.00 may well originate in the dissociation of either a proton involved in the terminal oxime hydrogen bond or a co-ordinated water molecule. This gives a neutral mixed-hydroxo 11-3 species. The extent of this hydrolysis has been observed to depend on the metal ion concentration.[21] A 0.001 *mol dm*$^{-3}$ Gd^{3+} ion solution will begin to precipitate as $Gd(OH)_3$ ($\log K_{sp}$ is -15.6 at 25^{0}C)[21] around pH 7.6, while a higher concentration of the metal ion will precipitate at a lower pH. The above-mentioned concentration of the metal ion is the highest used in these studies. Although, no attempts were made to filter and characterise the precipitate, the ability of the species to precipitate at pH values above 10.0 is evidence of an existence of a neutral mixed-hydroxo complex rather than a $Gd(OH)_3$.

In contrast to the above-mentioned Gd^{3+}-L^1 system, the complex formation function in the Gd^{3+}-L^2 system (Figure 5.18(a)) levels off at a Z_M-bar value of 2. This is because the ML species is not the predominant or only species in this system.[23] In fact, mixed-hydroxo species predominate in the equilibria of this system as indicated by the fanning back of the Z_M-bars at pL values below 4.

Attempts were made to include mononuclear species of M:L ratio of 1:2 but the model did not converge indicating the absence of such complexes in the system. Futhermore, since gadolinium(III) prefers negatively charged oxygen donor atoms, the possibility of co-ordination of two or more ligands to the same metal ion was considered but no evidence of such species could be obtained from the complex formation function.

Figure 5.18: Experimental (with Gd^{2+}:L^2 ratios of 1:3(▲), 1:4(•) and 1:5(♦) and theoretical (line) (a) Z_M-bar and (b) Q-bar and n-bar (line) both plotted against pH.

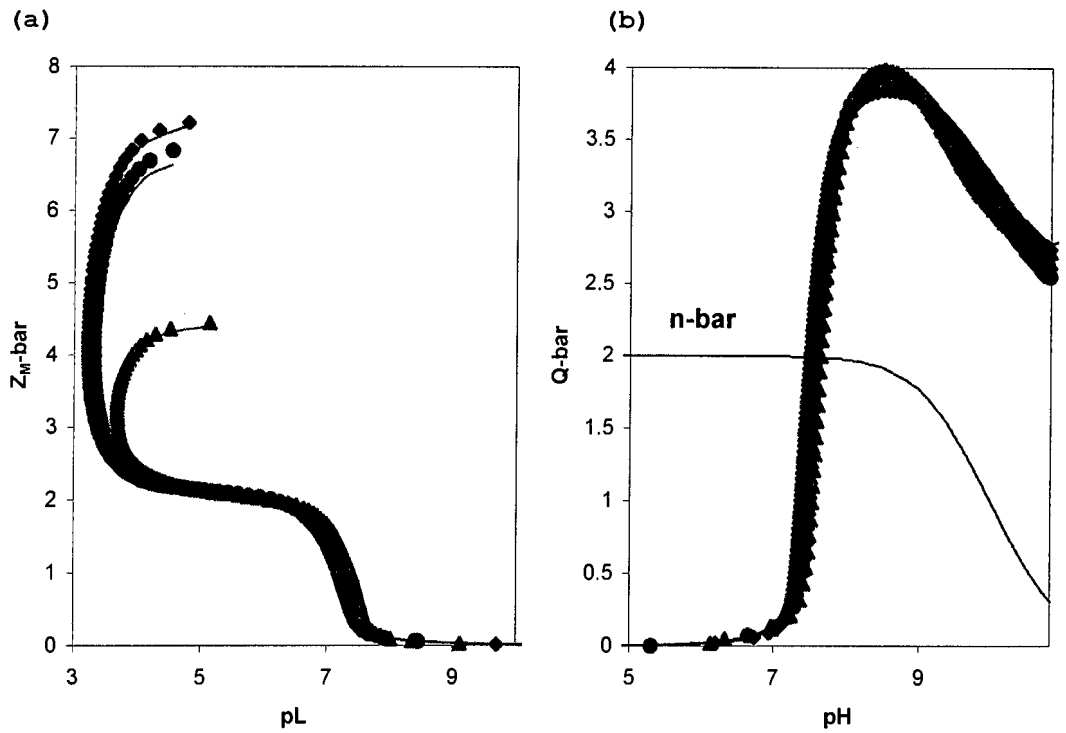

There seems to be a correlation between the extent of metal ion hydrolysis and the levelling off of the Z_M-bars above the expected value of 1. The out-of-plane co-ordination with respect to the four amino/amido nitrogens of two ligand molecules toward Gd^{3+} is possible. However, the resulting complex would be too strained to remain stable in aqueous solution. This is due to the high concentration of co-ordinating water and hydroxide-ion ligands containing hard oxygen donor atoms.

The deprotonation function (Figure 5.18(b)) increases sharply between pH 7.0 and 8.5 from zero to four indicating simultaneous dissociation of 4 protons. Above pH 8.5 the Q-bar decreases indicating that complexation is complete in this pH range. Despite the levelling off of the Z_M-bars at 2, these plots, however, do confirm the presence of only mononuclear species. An excellent agreement between the Z_M-bars and Q-bars gives validity to the proposed Gd^{3+}-L^2 complexation model.

Figure 5.17(b) indicates that complexation in this system begins above pH 7.00 and hydroxo and mixed-hydroxo complexes are the predominant species in this system. The $\log\beta_{11\text{-}1}$, $\log\beta_{11\text{-}2}$ and $\log\beta_{11\text{-}4}$ of -0.836, -7.833 and -22.876 for the 11-1, 11-2 and 11-4 complex species respectively have been determined. These values

indicate a low binding affinity of the ligand towards Gd^{3+}. The ligand is postulated to be co-ordinated to the metal ion through the carbonyl oxygens and the oxime nitrogens.

Deprotonation of one oxime oxygen, and at least two water molecules results in the formation of 11-1, 11-2 and 11-4. Furthermore, the weak complexes formed by Gd^{3+} and its extensive hydrolysis around pH 7.0 may contribute significantly to the levelling off of the Z_M-bar value at 2.0.

The Z_M-bars given in Figure 5.19(a) for the Gd^{3+}-L^3 system do not reach appreciable levels indicating the low binding ability of the ligand towards the metal ion. The fanning back of the complex formation function at low pL values is indicative of either loss of a proton from the ligand due to complexation or co-ordination of hydroxide ion.

Figure 5.19: Experimental (with Gd^{3+}:L^3 ratios of 1:3(▲),1:4(♦) and 1:5(•) and theoretical (line) (a) Z_M-bar and (b) Q-bar and n-bar (line) both plotted against pH.

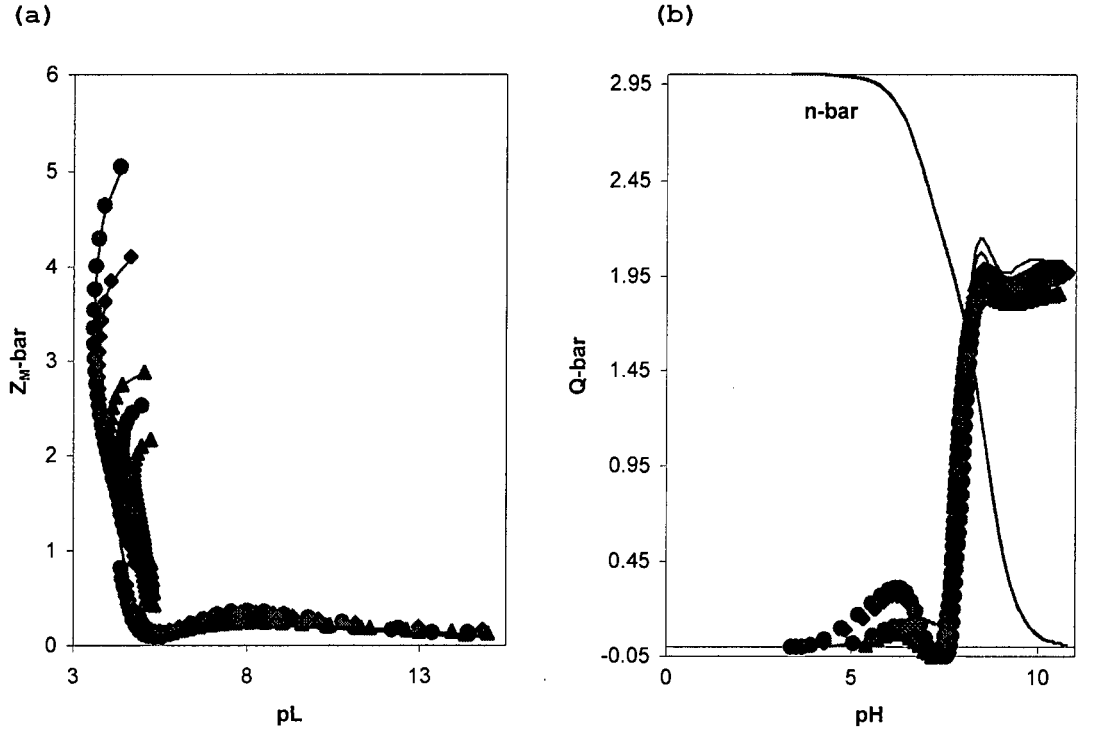

This assumption is verified by the Q-bar (Figure 5.19(b)), which reaches a maximum value of 2 indicating the loss of two protons due to complexation. A good agreement between the observed and calculated complex formation and deprotonation

functions supports the validity of the evaluated constants. The speciation plots given in Figure 5.15(b) confirm that protonated 112, mixed-hydroxo 22-2, 11-2 and 11-3 and 11-4 complexes predominate in the aqueous solution of Gd^{3+} with L^3. In fact, logβ's of 21.333, 0.305, -9.695, 19.343 and -30.924 for the 112, 22-2, 11-2, 11-3 and 11-4 complexes respectively have been obtained.

The mixed hydroxo species are formed by the hydrolysis of the coordinated water molecules. In the 22-2 complex, one Gd^{3+} ion is believed to bridge the two ligand molecules by coordinating through the carbonyl oxygens and terminal amines. In all these species the ligand is believed to be coordinated to the metal ion in an "exo" nature.

Gd^{3+} forms weak complexes with both L^2 and L^3. This is due to the inability of the metal ion to deprotonate the amide nitrogens. In fact, in gadodiamide, a contrast agent used in MRI scans,[31] the ligand is co-ordinated to the metal ion by the carbonyl oxygens rather than the nitrogen atoms of the amide moieties.

This is an extra-destabilisation of the complexes since both the carbonyl oxygen and the amino nitrogen are known to be poor donors for lanthanides.[31] The negatively charged oxygen donors as in carboxylates, are used as anchors thereby enhancing the thermodynamic stability of these contrast agents.

It should be noted that the aqueous chemistry of Gd^{3+} parallels in many ways that of Ca^{2+}. This is not surprising in view of the fact that both metal ions have nearly the same ionic radii.[32] They are also "hard" in terms of the HSAB theory[30] and hence prefer hard negatively charged oxygen donor atoms. In fact, the Gd^{3+} ion has been used to probe the structural and functional behaviour of Ca^{2+} in *in vivo* systems.

5.1.3 Discussion - Formation constants

On the basis of the complex formation and deprotonation curves, the formation constants reported in Table 5.2 were selected as the best possible to describe the equilibria observed in this study. Furthermore, the reasonably low standard deviations in the constants and Hamiltonian R_H-factors support the complexation model used in data analysis.

The possibility of formation of polynuclear $M_pL_qH_r$, $p \geq 2$ species, was checked but only the 21-2 and 22-2 complexes reported for the Zn^{2+}- and Gd^{3+}-L^3 systems respectively were found under the conditions of this study. This is in spite of both the 'endo' and 'exo' nature of the co-ordination modes, which can be exhibited by these dioxo L^2 and L^3 ligands. In fact, the formation of these binuclear species is possibly due to the inability of the two metal ions to deprotonate the amide groups, hence 'exo' binding of the ligand in a bridging fashion becomes the only possibility. Furthermore, metal to ligand (M:L) ratios of 1:2-5 were used because at 1:1 and 2:1 M:L ratios, these investigations were hampered by precipitation in all systems.

In general, the presence of polynuclear species is confirmed by making a series of measurements at two or more widely different metal ion concentrations. Analysis of these two or more sets of data should lead, in the first instance, to two or more different sets of stability constants. Secondly, two (or more) distinct complex formation plots that only merge at very high and very low ligand concentrations will be observed if polynuclear species are present.

Kozlowski et al.[4] have observed that at Cu^{2+}/Ni^{2+}:L^2 ratios greater than 1:5 these complex species precipitate out of solution. In contrast, it has been observed in this study that precipitation is a transient process leading to the formation of the neutral 110 species. However, this species is not stable enough and is immediately converted to the 11-1 species. Furthermore, at 1:1 M:L ratios the dissolution of the precipitate has been observed to occur on further equilibration of the system. However, under these conditions care must be taken to ensure that the system is at equilibrium.

It should also be mentioned that the loss of the first amide proton in these M^{n+}-L^2/L^3 systems is kinetically slow compared to the deprotonation of the second amide moiety. This process has been noticed as a potential drift in the pH range 3.5-7.0.[33] This phenomenon can be attributed to the required orientation of the nitrogen lone pair of electrons towards the metal ion. This is followed by simultaneous bond-formation and proton release. The proximity of the remaining amide nitrogen makes it statistically favourable to complete the reaction resulting in the formation of higher species such as the MLH_{-2}.

In contrast to these linear diamide ligands, the deprotonation of amide groups in macrocyclic analogues has been observed to occur cooperatively.[10-13] This is due to the close proximity of the amide moieties in these macrocycles.

In light of the foregoing discussion, it is proposed that the slow kinetics of both Cu^{2+} and Ni^{2+} with L^2 and L^3 observed in this study is a consequence of both steric hindrance to complexation and the conformational changes demanded by the metal ion. It is, therefore, the presence of the metal ion, which reorganises the ligand to adopt a conformation that will promote complexation.[34] This ability is a property of a particular metal ion and will differ from one metal to another.

Furthermore, the drastically decreased binding of these less pre-organised ligand systems can in part be attributed to the differences in their solvation. A significant entropic cost has to be paid to organize the ligand binding sites of the flexible ligand to a conformation involved in metal ion complexation.[34]

It should be emphasised that in H_2L^2 ligand, the donor atoms bearing the two ionisable protons are not involved in metal ion co-ordination. This, as a result posed another problem in the calculation of accurate formation constants in these M^{n+}-H_2L^2 systems. This is in contrast with the analogous L^1 and L^3 solution equilibria where complexation is a direct replacement of the proton by the metal ion.

The data in Table 5.2 can be summarised in terms of selectivity factors given in Table 5.3.

Table 5.3: Selectivity factors of the studied ligands towards Cu^{2+} compared with the other investigated metal ions.

Ligand	Zn^{2+}	Ca^{2+}	Ni^{2+}	Gd^{3+}
L^1	11.08	≥ 11.35	3.53	3.732
L^2	10.30	≥ 11.1	6.00	11.31
L^3	> 4.48	> 8.60	7.04	≥ 11.35

Selectivity for Cu^{2+} is defined[35] as the difference in the formation constant of $[CuLH_{-1}]$ with that of the corresponding species for a particular M^{n+}-L system.

Although the formation constants[2] of Cu^{2+}, Ni^{2+}, Zn^{2+} and Ca^{2+} with L^1 were not determined in the present study, they are however reported in Table 5.2 and are discussed extensively in section 5.2.1 and hence a comparison will made because of the similarity of this ligand to L^2 and L^3. These factors give an insight about the overall contribution of several factors that might have a bearing on the determined constants.

The studied ligands are highly selective for copper compared to Ni^{2+}, Zn^{2+}, Ca^{2+} and Gd^{3+}. This is borne out by the calculated selectivity factors, which are in the range of 6-9 orders of magnitude in favour of Cu^{2+}. In fact, the stability order is $Gd^{3+} \approx Ca^{2+} < Ni^{2+} < Cu^{2+} > Zn^{2+}$. This is the Irving-Williams stability order normally observed for the first row of the transition elements.

The higher formation constants of Cu^{2+} with these ligands are due to ease with which the metal ion deprotonates the amide groups. Furthermore, the increased stability of these complexes is as a result of the square-planar ligand field created by both L^1 and L^2. Although L^3 is postulated to form tetragonally distorted octahedral species, the donor atoms of the ligand continue to define the close to or equatorial metal co-ordination. This leaves two axial sites occupied by water molecules, which constitutes a tetragonal co-ordination environment. Both geometries are preferred by Cu^{2+}.

It is possible that Cu^{2+} in both the tetragonally distorted octahedral (0.87Å) and square-planar (0.71Å) environments[32] may have the optimum size to fit better into the ligand's 'bite' cavity than the other studied metal ions. However, it is believed that the L^3 cavity may be too big for Cu^{2+} and Ni^{2+}, hence the observed low equilibrium constants. The ability of Gd^{3+} and Ca^{2+} to form complexes with the L^3 ligand may be related to their large ionic radii.[32]

As discussed in section 5.2.1, no significant metal assisted ionisation of the oxime groups has been observed in the M^{n+}-L^2 systems. Instead, metal promoted deprotonation of the amide groups ($pK_{M\text{-}CONH}$) given by the differences between $\log\beta_{110}$ and $\log\beta_{11\text{-}1}$ have been predicted from the evaluated constants. The following $pK_{M\text{-}CONH}$ values of 4.01, 5.03, 9,6 and 8.0 for Cu^{2+}, Ni^{2+}, Zn^{2+} and Gd^{3+} systems

respectively clearly indicate that the protons are released from the amide moiety in the copper(II) and nickel(II) species. For Zn^{2+} and Gd^{3+}, these values correspond to the deprotonation of the co-ordinated water molecules. This should be expected in view of the inability of the latter two metal ions to deprotonate the amide groups.

In contrast, significant metal promoted deprotonation of the dione dioxime groups ($pK_{M\text{-}NOH}$) has been observed in L^1 systems. This is indicated by the calculated first $pK_{M\text{-}NOH}$ values for L^1 with Cu^{2+}, Ni^{2+}, Zn^{2+} and Gd^{3+} which are 2.897, 3.92, 4.747, 7.30 respectively. This signifies that the $[CuL^1(OH_2)_2]^{2+}$ complex is more acidic than the analogous Ni^{2+}, Zn^{2+} and Gd^{3+} species. These $pK_{M\text{-}NOH}$ values further indicate that the proton is indeed lost from a terminal oxime group rather than from an axially bound water molecule.

Similar trends have been observed with H_2tmdddo,[5] (L^h, Figure 1.1) an analogue of L^1. Co-ordination of H_2tmdddo to copper(II) was also observed to increase the acidity of the oxime proton by nine orders of magnitude. For H_2tmdddo, $pK_{N\text{-}OH}$=12.3, while for its complex with copper(II) the value is 3.24.

In L^2 systems, the formation of the $[MLH_{-2}]$ complex species from $[MLH_{-1}]$, is due to proton loss as a result of the breaking of the hydrogen bond. The formation of this species in the previously studied Ni^{2+}-L^1 system[2] is due to the metal ion promoted dissociation of the oxime proton involved in the hydrogen bond. However, the formation of the same $[MLH_{-2}]$ is associated with the ionisation of the axially bound water molecule for Cu^{2+}-, Zn^{2+}- and Gd^{3+}-L^1 systems.

The $pK_{ML\text{-}OH}$ values associated with the deprotonation of the amide groups in L^3 systems are 6.10 and 8.53 for Cu^{2+} and Ni^{2+} respectively. These values are 1.5 and 2.0 log units lower than the hydrolysis constants of the metal ions. This indicates that the deprotonation of the first amide group is easier than losing a proton from a coordinated water molecule probably due to the higher donating ability of a deprotonated amide group. For Zn^{2+}, Ca^{2+} and Gd^{3+} these $pK_{ML\text{-}OH}$'s correspond to deprotonation of axially coordinated water molecules confirming the inability of these metal ions to facilitate proton loss from the amide moieties.[13,14]

5.2 UV/VIS spectroscopy

During solution studies of the Cu^{2+}/Ni^{2+}-L^2/L^3 systems, distinct colour changes were noted as the titrations progressed. This is because the speciation of the solution changes with pH, and the different complex species have differing absorption spectra. To gain more insight about the co-ordination geometries of these species, individual species spectra were calculated. This was achieved by analysis of the UV/Vis data using a Local BASIC program to solve for the expanded Beer-Lambert Law equation.

5.2.1 Cu-L systems

Figure 5.20 (a) shows the UV/Vis spectra of the Cu^{2+}-L^2 system as a function of pH. A band at 690 *nm* is seen to initially increase with pH and then decrease in intensity. Above pH 5.8 a band at 470 *nm* develops in intensity while at pH values above 9.45 the intensity of this band decreases.

Figure 5.20: (a) Electronic and (b) calculated species absorption spectra of solutions containing 0.0008 *mol dm*$^{-3}$ Cu^{2+} and 0.003 *mol dm*$^{-3}$ L^2 as a function of wavelength.

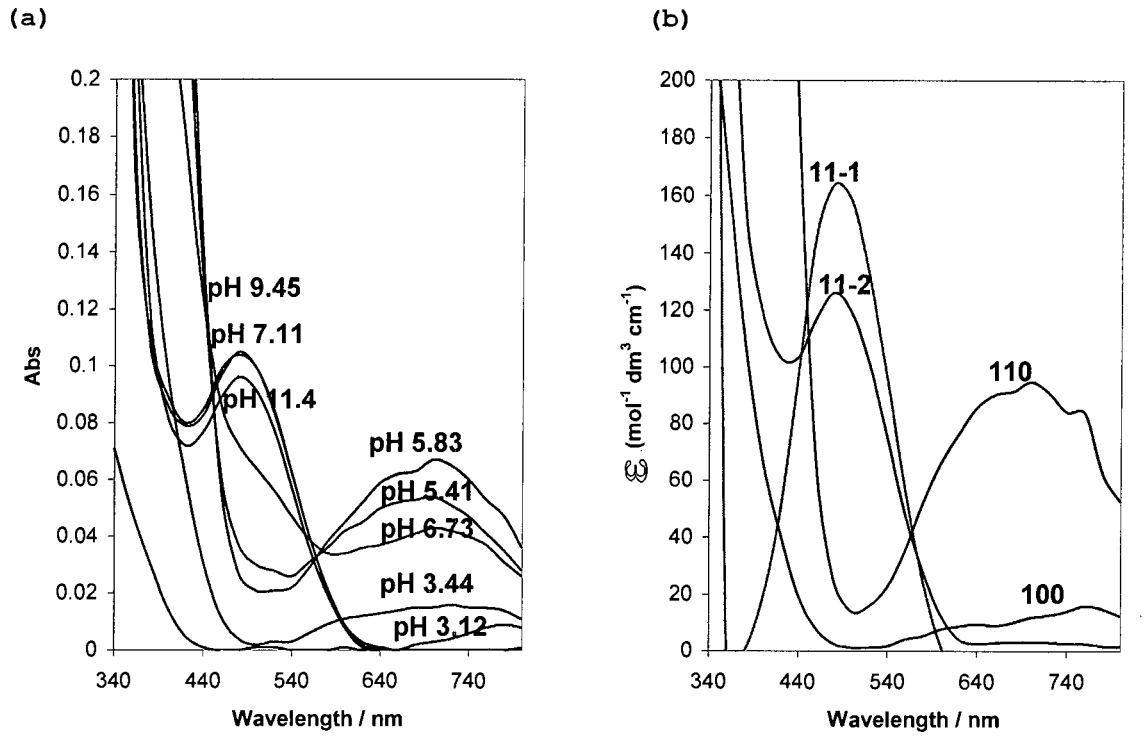

The wavelength absorption maximum (λ_{max}) at 780 *nm* with low molar extinction coefficients at the acidic pH range of 2.5-3.0 is easily seen in this Cu^{2+}

system (Figure 5.20(b)). This absorption is due to the uncomplexed octahedral $[Cu(OH_2)_6]^{2+}$ (100) complex species with the molar extinction coefficient (ε) of 15 $mol^{-1} dm^3 cm^{-1}$.[36,37]

Between pH 3.5 and 6.0, copper(II) exists as a 110 species with a λ_{max} of 690 *nm*. The ligand in this species is postulated to be co-ordinated to the metal ion in a bidentate fashion through one of the nitrogen donor atoms of the hydroxyimino groups and the amide moieties. The other four co-ordination sites are believed to be occupied by water molecules. The molar extinction coefficient of this 110 complex is 90 $mol^{-1} dm^3 cm^{-1}$ (Figure 5.20(b)), which is typical of Cu^{2+} in an octahedral environment.

In the pH range 6.0-8.0, λ_{max} shifts to 470 *nm* due to the predominance of the 11-1 complex species of MN_4 co-ordination. A blue shift of about 210 *nm* is due to the binding of the extra two nitrogens and the change of the metal ion co-ordination sphere from an octahedral to a square-planar geometry. An increase of ε_{max} from 90 to 165 $mol^{-1} dm^3 cm^{-1}$ is in support of this change in co-ordination.

There is an observed 10 *nm* increase in λ_{max} above pH 8.0, which is due to the accumulation of the $[CuL^2H_{-2}]^{2-}$ complex with $\varepsilon = 125\ mol^{-1} dm^3 cm^{-1}$. Despite the red shift in the absorption maximum and a decrease in ε, there are no significant changes in the spectra of this system above pH 8.0. It has been observed that the loss of a proton from a co-ordinated water molecule results in an red shift of λ_{max} by approximately 50-90 *nm*.[1] The 10 *nm* increase in λ_{max} is believed to be associated with the loss of a proton involved in the hydrogen bond in the $[CuL^2H_{-1}]^-$ complex. This is an indication that the proton loss from 11-1 species to form a 11-2 complex does not lead to a significant destabilisation of the latter complex and above this pH complexation is complete. It is also a confirmation of an earlier hypothesis that the pseudomacrocylic $[CuL^2H_{-1}]^-$ complex is not stabilised by the hydrogen bond as it has been observed in other oximes.[1,2,5,6]

It has been observed that an incorrect potentiometric model yields to disjointed species spectra. The continuous calculated electronic spectra of the individual species are in further support of the potentiometric model used in the analysis of the data. The broad band observable between pH 7.11 and 11.4 for Cu^{2+} is characteristic of purely

square-planar d^9 $[ML^2H_{-1}]^-$ and $[ML^2H_{-2}]^{2-}$ complexes. This absorption band is made up of three spin-allowed transitions namely: $^2A_{1g} \leftarrow {}^2B_{1g}$, $^2B_{2g} \leftarrow {}^2B_{1g}$ and $^2E_g \leftarrow {}^2B_{1g}$. Two of these transitions are indicated by humps in the absorption spectra at pH values below 7.00 (Figure 5.20(a)) and in the species spectra of 100 and 110 (Figure 5.20(b)).

Unlike L^2, electronic spectra of copper complexes with both PrAO[1] and H_2tmdddo[3] indicate that dissociation of an oxime proton causes a small increase in the donor strength of the oxime nitrogen atom. This is observed as the blue shift in λ_{max} on formation of the pseudomacrocyclic species. This should be expected in view of the fact that L^2 behaves as a weak diprotic acid in neutral to strongly basic pH range 7.0-10.5. In fact, the ligand loses both protons in the afore-mentioned pH range whereas the loss of this (these) proton(s) in PrAO, H_2tmdddo and dimethylglyoxime is (are) usually metal ion assisted.[2,6]

Billo[38] predicts a ν_{max} (λ_{max}) of 18760 cm^{-1} (526 *nm*) for $[CuL^2H_{-1}]^-$ and $[CuL^2H_{-2}]^{2-}$ complex species of N_4 co-ordination type involving two amido and two amino nitrogens. This ν_{max} value is 2073 cm^{-1} less than the ν_{max} observed in this study. The discrepancy is possibly due to the higher than predicted donating ability of the hydroxyimino groups. The $\nu_{N\text{-}OH} = 4.41\times10^3$ cm^{-1} of an oxime nitrogen predicted by Jackson and Nakani[1] is still too low to account for the observed ν_{max} of these species.

Furthermore, it has been observed that the presence of the alpha-amide groups in L^2 increases the acidity of the hydroxyimino (oxime) nitrogen by nine orders of magnitude compared to other related oximes as discussed in section 5.1.1.2. It is more likely that the basicity of the oxime nitrogen is enhanced due to the electron withdrawing effect of this amide, hence the increased value of ν_{max}. The NH-COCHN-OH moieties in this ligand can be viewed as electron sinks for metal ions such as Cu^{2+}, which are capable of deprotonating the hard amide groups.

Figure 5.21(a) is a plot of the Cu^{2+}-L^3 solution UV/Vis spectra as a function of pH. At pH values below and up to 3.54, an absorption band at 780 *nm* predominates. The absorption spectrum at pH 5.55 seems to encompass at least two λ_{max}, one at 780 *nm* and the others as humps between 640-700 *nm*. In the pH range 6.09-9.05, there is

an evolution of a single band which increasing intensity as the pH increases while above this pH range the intensity of this band decreases.

Figure 5.21: (a) Electronic and (b) individual species absorption spectra of solutions containing 0.001 *mol dm*$^{-3}$ Cu^{2+} and 0.003 *mol dm*$^{-3}$ L^3 both plotted against the wavelength.

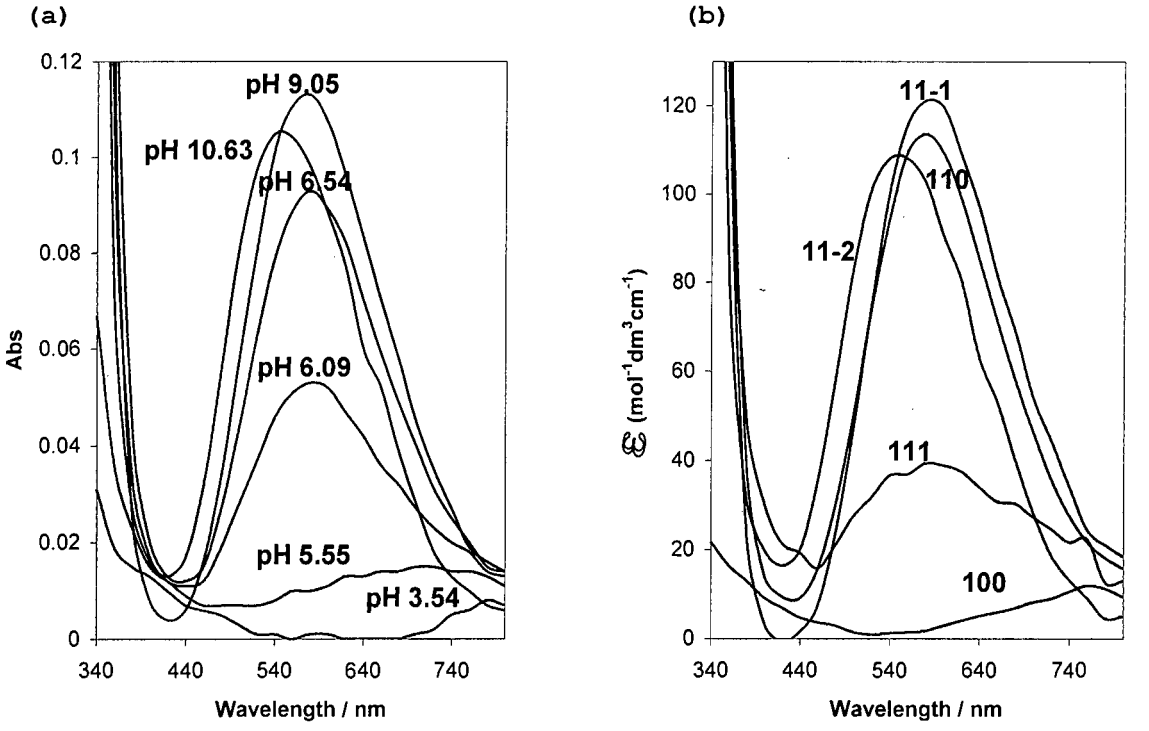

Complexation in this system begins above pH 3.54 since the hydrated Cu^{2+} species predominates below this pH. The λ_{max} at 780 *nm* with low ε values (<20 *mol*$^{-1}$ *dm*^{3} *cm*$^{-1}$) is due to this complex. The 111 species (λ_{max} = 620 *nm*, ε=40 *mol*$^{-1}$*dm*^{3}*cm*$^{-1}$) seems to predominate in the pH range 3.54-5.55. The 160 *nm* blue shift in the absorption maximum is due to the co-ordination of the central amine, one terminal amino group and probably one carbonyl oxygen (Figure 5.6(h)). Co-ordination of one amide nitrogen leads to the 110 with λ_{max} at 580 *nm* and ε=115 *mol*$^{-1}$*dm*^{3}*cm*$^{-1}$. The 40 *nm* blue shift in λ_{max} and the three fold increase in the molar extinction coefficient of the 110 species is ascribed to the strong donating ability of the deprotonated amido nitrogen.

The 11-1 and 11-2 complexes exhibit λ_{max} values of 560 *nm* and 540 *nm* with ε values of 120 and 110 *mol*$^{-1}$*dm*^{3}*cm*$^{-1}$ respectively. The former species is formed by binding of the second amide nitrogen to Cu^{2+}, while the latter is due to the deprotonation of the terminal amine. The molar absorption coefficients of the two

species are typical of Cu^{2+} in a distorted tetragonal environment. The continuous individual spectra given in Figure 5.21(b) are in support of the potentiometric model used in data analysis.

The broad absorption band observed for the 111, 110, 11-1 and 11-2 complexes envelopes the expected $^2A_{1g} \leftarrow {}^2B_{1g}$, $^2B_{2g} \leftarrow {}^2B_{1g}$ and $^2E_g \leftarrow {}^2B_{1g}$ transitions which are spin-allowed. Two of these transitions are prominent in the calculated spectrum of the protonated 111 complex (Figure 5.21(b)).

The 11-1 and 11-2 species are observed to have absorption maxima which are 20-40 *nm* less than the values predicted by Billo's equation.[38] This is probably due to the destabilisation of the complexes by the formation of the two contiguous six membered-rings (Figure 5.6 (j) and (k)). In fact, the 20-60 *nm* increase as one moves from 111 to 11-2 is due to the destabilisation of the 11-1 and 11-2 on the formation of these contiguous rings. The stability of these species is further decreased by the low basicity of the coordinated central anchoring amino group, which leads to the formation of six-membered rings. Co-ordination of both terminal amines will also reduce the thermodynamic stability of these species due to the formation of a bigger ten-membered ring.[39]

Square-pyramidal and trigonal bipyramidal Cu^{2+} complexes of N_5 co-ordination usually exhibit two bands at 728 and 900 *nm*.[18,37,39] Jubert et al.[9] have observed a broad band around 700 *nm* which they attributed to six co-ordinate CuN_6 species. The axial co-ordination of amino groups in these Cu^{2+} complexes causes a red shift of the λ_{max} of approximately 100 *nm* compared to the absorption maxima observed in this study. This is an indication of the absence of axially co-ordination of amino groups in the $[CuL^3H_{-1}]$ and $[CuL^3H_{-2}]$ species.

Instead, UV/Vis data reveal an insignificant blue shift in λ_{max} ($\Delta\lambda_{max}$=20*nm*) and a decrease in the molar absorptivity due to the formation of the $[CuL^3H_{-2}]$ from $[CuL^3H_{-1}]$. This blue shift is probably due to the slight stabilisation of the contiguous six-membered rings of the 11-2 following the deprotonation of the second terminal amine.

Cu^{2+} prefers six co-ordinate tetragonally distorted species where two weak ligands such as water molecules occupy the axial positions. In these species the equatorial plane is defined by the four nitrogen donor atoms of the ligand. It is predicted therefore that both amide nitrogens, the central amine and one of the terminal tertiary amines are co-ordinated. The second terminal amine is protonated in the $[CuL^3H_{-1}]^+$ species while the formation of the $[CuL^3H_{-2}]$ may be due to its deprotonation. There is no evidence from UV/Vis data of co-ordination of this amine.

On the basis of the above observations and taking into account the ligand structure, the co-ordination of the fifth nitrogen is unlikely. A similar structure was suggested by Steenland et al.[7] for the macrocyclic diamide analogues (L^i and L^j) of L^3.

5.2.2 Ni-L systems

The absorption spectra of a Ni^{2+}-L^2 solution at various pH values are given in Figure 5.22(a). In the pH range 3.5-10.73, there is only one band centred at 350-370 *nm*. At pH values below 3.00 (Figure 5.22 (a)-Insert), a band at 580-740 *nm* is easily seen in addition to the band tailing off in the visible region.

Figure 5.22: (a) Electronic and (b) calculated species absorption spectra of solutions containing 0.00023 *mol* dm^{-3} Ni^{2+} and 0.0008 *mol* dm^{-3} L^2.

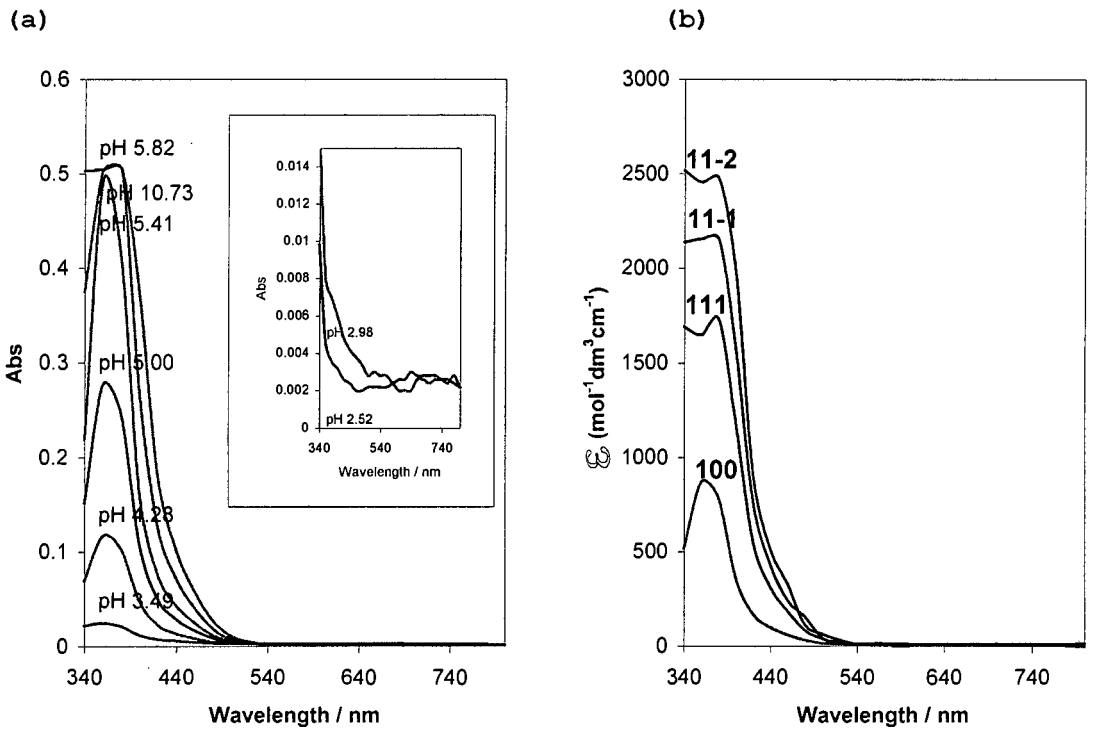

At pH values below 3.00 the solution is composed of the hydrated $[Ni(OH_2)_6]^{2+}$ species with ε less than 10 $mol^{-1}dm^3cm^{-1}$. The $^3T_{1g}(P)\leftarrow{}^3A_{2g}$ and $^3T_{1g}(F)\leftarrow{}^3A_{2g}$ transitions at 360 and 680 *nm* respectively can been seen from these spectra (Figure 5.22(a)-Insert) although the former is obscured by a ligand to metal charge transfer (LMCT) band. These two transitions at 360 and 680 *nm* with low molar extinction coefficients are typical of Ni^{2+} in an octahedral environment. It appears that at this acidic pH range the metal ion is unable to bind to the ligand's donor atoms.

Above pH 3.49, a single band centred at 350 *nm* is observed. This is an LMCT transition originating either from the carbonyl oxygen, deprotonated amide nitrogen or the oxime nitrogen to the vacant $^1A_{2g}$ orbital of the metal ion. The molar extinction coefficient of this band for 111, 11-1 and 11-2 species (Figure. 5.22(b)) is in the range of 1785.7 to 2500 $mol^{-1}dm^3cm^{-1}$ in support of its CT character.

Bojczuk et al.[40] have proposed three O^-, N^- and $NH_2\rightarrow Cu^{2+}$ CT transitions which lie at 385, 327 and 277 *nm* respectively. The intra-ligand $\pi\rightarrow\pi^*$ transition, on the other hand, occurs around 250 *nm*.[37] Such a transition has not been observed in the Cu^{2+}- and Ni^{2+}-L^1 systems[1,2] which contain both the co-ordinated amino and deprotonated oxime groups. This suggests that this band is neither due to $O^-\rightarrow Ni^{2+}$ nor $NH_2\rightarrow Ni^{2+}$ electronic transition.

Ni^{2+} has been found to be capable of deprotonating the amide groups of L^2 (section 5.1.2.2) which are absent in L^1. It is more likely that this LMCT band is due to an electron transition from the deprotonated amide nitrogen (N^-) to the vacant $^1A_{2g}$ orbital of the metal ion.

A two component band at 470 *nm* and 430 *nm* (Figure 5.21 (b)) is seen for the 11-1 and 11-2 complexes respectively as a shoulder on this LMCT transition. The band constitutes the $^1A_{2g}\leftarrow{}^1A_{1g}$ and $^1B_{1g}\leftarrow{}^1A_{1g}$ transitions typical of square planar Ni^{2+} species. This band is also obscured by the LMCT absorption. The d-d transitions fall in the predicted 420-450 *nm* range with ε=120-500 $mol^{-1}\ dm^3\ cm^{-1}$ as was observed for Ni-L^1 system[2] and recently by Enyedy et al.[39] for similar ligands. It should be mentioned that increasing the nickel and ligand concentratios does not lead

to the better elucidation of the d-d transitions due to the high molar extinction of the LMCT band. Hence, this charge transfer band dominates the electronic spectrum of this system.

The absence of absorption above 500 *nm* is indicative of square-planar $[NiL^2H_{-1}]^-$ and $[NiL^2H_{-2}]^{2-}$ complex species. There is no observable absorption by the octahedral hydrated Ni^{2+} and 111 species above pH 3.49 in support of the calculated speciation plots given in Figure 5.9(a). The continuous calculated species electronic spectra give confidence to the results for the potentiometric model used in the analysis of the data.

In contrast to the above observations, nickel does not seem to deprotonate the amide nitrogens of L^3 with ease. The hydrated Ni^{2+} and the protonated 112, 111, 110 complexes predominate the whole acidic to neutral pH region before the onset of precipitation. It seems the potentiometrically determined 112, 111 and 110 complexes are too weak to absorb appreciably in the wavelength range studied. As a result, no information could be obtained from the absorption spectra of these potentiometrically detectable species. Moreover, Ni^{2+} does not seem to form the positively charged 11-1 species with L^3, which has been detected in the corresponding Cu^{2+} system.

5.2.3 Discussion - UV/Vis spectroscopy

At low pH values, the calculated individual spectra of the M^{2+}-L^2/L^3 systems are characterised by hydrated $[M(OH_2)_6]^{2+}$ species. The presence of these hydrated complexes partly indicates the lower affinity of the donor atoms of these ligands towards these metal ions when compared with L^1. This may be viewed as the necessary orientation of the ligands' nitrogen lone pair electrons towards the metal ion to enhance complexation.

The $[ML^2H_{-1}]^-$ and $[ML^2H_{-2}]^{2-}$ species of Cu^{2+} and Ni^{2+} exhibit a single band in the 430-480 *nm* region. This band indicates the presence of MN_4 complexes similar to those of the corresponding L^1 systems. The noticeable blue shift observed in the M^{2+}-L^2 systems is due to the stronger ligand field contributions of two deprotonated amide nitrogens. The ligand field created by L^2 is assisted by the sp^2 hybridised nature

of the deprotonated amido nitrogens which results in the loss of the axially co-ordinated water molecules. The ligand forms 5,6,5,6 (11-1) and 5,6,5 (11-2) chelate rings around the Cu^{2+} and Ni^{2+} metal ions. There is little movement of the d-d transition (Δv=150 cm^{-1}) upon formation of $[ML^2H_{-2}]$ from $[MLH_{-1}]$. This suggests that, in these complexes the stabilisation of the square-planar geometry is determined mostly by the presence of three 5,6,5 chelate rings.

From the relative position of the λ_{max} values of $[M\text{-}L^2]$ complex species, it appears that the systems undergo a change in co-ordination from octahedral 110 and 111 to square-planar 11-1 and 11-2 species of D_{4h} symmetry. The increase in the molar extinction coefficients is consistent with this hypothesis. There is no evidence of further absorption below 10,000 cm^{-1}, which is also typical of square-planar Cu^{2+} and Ni^{2+} complexes.[2,37]

The ability of less sterically hindered L^2 to form square-planar $[CuL^2H_{-1}]^{1-}$ and $[CuL^2H_{-2}]^{2-}$ complexes may be as a result of the sp^2 hybridised nature of the deprotonated amide nitrogens. This is in sharp contrast with L^1, which forms tetragonally distorted octahedral complexes with the metal ion. The axial $H_2O\text{-}Cu^{2+}$ bonds are believed to be able to stretch to great extents leading to an increase in the stability of complexes despite the steric barrier caused by the methyl groups of the ligand. In such a situation the tetragonally distorted $[Cu\text{-}L^1H_{-1}(OH_2)_2]^{n+}$ species could justifiably be viewed as square-planar complexes.

The $[CuL^3H_{-1}]^+$ and $[CuL^3H_{-2}]$ complexes have λ_{max} values in the range of 540-560 *nm*. The values indicate a weak co-ordinating ability of the ligand donor atoms towards the metal ion. An interesting feature about the two trans-dioxopentaazamacrocycle-Cu^{2+} systems studied by Steenland et al.[7] lies with their UV/VIS spectra. The 11-2 complexes of the macrocycles exhibit a single transition at 430 *nm* and 490 *nm*.[7] The corresponding $Cu^{2+}\text{-}L^3$ species has a λ_{max} which is 50 and 110 *nm* higher than those of the dioxo-macrocycles. These differences can be explained in terms of the weak-ligand field contributions of amine (amide) nitrogen donor atoms in the linear L^3 compared to the high-ligand field afforded by its macrocylic analogues.

The values obtained for Cu^{2+}-L^2 species also fall within this range of square-planar MN_4 type of co-ordination for two deprotonated amide and two amino groups in these Cu^{2+}-dioxopentaazamacrocycles. Due to precipitation of the probably neutral $[NiL^3H_{-2}]$, it was not possible to get descent spectra for this system.

From the relative positions of the d-d band maxima it is clear that the tetragonal distortion towards square-planar increases in the order $Cu(N_{amine})_2(N_{amide})_2$ < $Cu(N_{amine})_2(N_{oxime})_2$ < $Cu(N_{amide})_2(N_{oxime})_2$. In fact, in the latter system it has been observed that the shift is due to the formation of purely square planar species.

5.3 X-ray diffraction studies

UV/Vis spectroscopy predicted the geometries of the studied Cu^{2+}/Ni^{2+}-L^2/L^3 systems fairly accurately. However, the nature and number of the donor atoms of L^3 involved in the co-ordination with these metal ions cannot be ascertained unambiguously. Furthermore, the proposed structures given in Figure 6 do not give any information about the lowest possible energy conformations. Moreover, the relative orientation of the alkyl substituents relative to the molecular plane defined by the ligand's donor atoms is unknown.

In order to assess fully the co-ordination nature of L^1, L^2 and L^3 towards these metal ions, attempts were made to isolate crystals of the $[MLH_{-1}]$ species. However, these investigations were unsuccessful and only the $[NiL^1H_{-1}]^+$ species was isolated. This cationic species (Figure 5.23) crystallised as a perchlorate salt with a molecular formula $C_{13}H_{27}ClN_4NiO_6$, M_r=429.55 *g/mol*. The crystal system is orthorhombic with space group-Pbca (#61) and unit cell dimensions a=13.3960(10), b=12.3490(10), c=21.9330(10), Z=8, F(000)=1808. The calculated volume (U) and density of the crystal (D_c) are 3628.3(4) $Å^3$ and 1.573 $Mg.m^{-3}$ respectively.

This structure resembles the chloride mono hydrate of $[NiL^1H_{-1}]^+$ which has been reported before by Hussain and Schlemper.[41] The only significant difference lies with the space group, which they reported as $P2_12_12_1$. It is believed that this space group is applicable to chiral molecules. There is no carbon atom in the ligand backbone which can endow the overall molecule with chirality. It is therefore

suggested that the presently reported space group is the correct one for this crystal system.

Figure 5.23: Ortep presentation of the crystal structure of cationic $[NiL^1H_{-1}]^+$ species and the perclorate (ClO_4^-) anion showing 50% probability ellipsoids and the atom labelling scheme. Hydrogen atoms are represented as open circles.

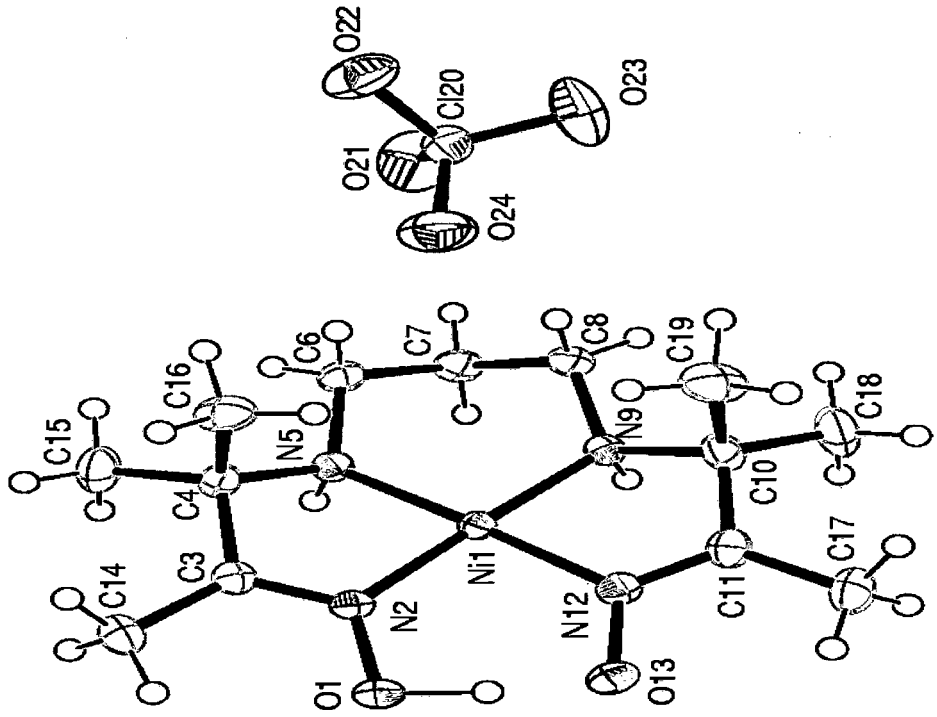

The aza (N5 and N9) and oxime (N2 and N12) nitrogen atoms are involved in an equatorial co-ordination to the metal ion with Ni-N_{aza} and Ni-N_{oxi} bonds of length 1.8720(14)-1.8731(15) and 1.9238(14)-1.9332(14) Å respectively. These Ni-N bond lengths compare quite well with those of the crystal structure of $[Ni(L^1)H_{-1}]Cl\ 1.5H_2O$ observed by Hussain et al.[41]

There are no water molecules of crystallisation in the presently reported structure due to complete evaporation of the solution. The absence of co-ordinated water molecules in the crystal structure reported by these authors[41] in spite of the water of crystallisation observed is firm evidence of the square-planar nature of the coordinated ligand nitrogen donor atoms towards the metal ion. Both these studies give full credibility to the square-planar geometry inferred previously from the

UV/Vis data.[2,42] The other observed differences such as the calculated density and unit cell dimensions are expected in view of the different counter-ions involved. The appendix gives a full listing of bond-lengths, angles and crystal refinement data of the $[Ni(L^1)H_{-1}]^+ClO_4^-$.

As expected, the methyl groups at C-4 and C-10 are staggered due electrostatic repulsion of the hydrogens. Another noticeable feature about the crystal structure of the $[Ni(L^1)H_{-1}]^+ClO_4^-$ is the displacement of the central methylene group of the propylene bridge by 0.05 Å from the square-planar plane defined by the metal ion and the ligand's donor atoms. This may be due to the hydrogen bond which is displaced by the same margin in the opposite direction.

Kozlowski et al.[4] recently reported a crystal structure of $[Ni(L^2)H_{-1}]^+$ complex, whose Ni-N bond lengths vary between 1.96 and 1.97Å. In fact, in the $[Ni(L^2)H_{-1}]^+$ crystal system the $Ni\text{-}N_{am}$ and $Ni\text{-}N_{ox}$ bond lengths are equal to within 0.005 Å. This is an indication of an equal electron donating ability of these nitrogens towards the metal ion. Of particular interest is the observation that the $Ni\text{-}N_{aza}$ and $Ni\text{-}N_{ox}$ bond distances of the $[Ni(L^1)H_{-1}]^+$ crystal system are approximately 0.1 and 0.7 Å respectively longer than the $Ni\text{-}N_{am}$ and $Ni\text{-}N_{ox}$ bond lengths of $[Ni(L^2)H_{-1}]^+$ observed by these researchers.[4] The shorter Ni-N bonds in L^2 species compared to L^1 complexes further indicate the high basicity of these nitrogens, hence the blue-shift in the spectra of the corresponding Cu^{2+} and Ni^{2+} 11-1 and 11-2 species.

Unfortunately, it has not been possible to prepare single crystals of either $[CuL^3H_{-1}]$ and/or $[CuL^3H_{-2}]$ suitable for X-ray structure analysis. A precise structural elucidation of the co-ordinated donor atoms of this ligand towards copper must await more X-ray structural information.

5.4 MM calculations and MD simulations of $[M(L^1)H_{-1}]^+$ systems

In the absence of suitable crystals for X-ray structure analysis, MM calculations and MD simulations may give some insight about the coordination behaviour of a particular ligand's donor atoms towards a given metal ion. In these calculations care is taken of the preferred coordination geometry of the metal ion. The

structures of $[M(L^1)H_{-1}]^+$ systems were built and their potential energies minimised using the ESFF forcefield. Molecular dynamics (MD) simulations of these species were run in order to assess the relative orientation of the methyl groups in the energy minimised $[M(L^1)H_{-1}]^+$ complexes.

5.4.1 $Ni(L^1)H_{-1}]^+$ species

Figure 5.24(a) and (b) shows the crystal structure of $[Ni(L^1)H_{-1}]^+$ superimposed onto the simulated species. As seen from the figure, there is a very good agreement between the experimental determined structure and the simulated species. The only difference between the two lies with the relative orientation of the propylene bridge separating the aza nitrogens.

Figure 5.24: Superimposed crystal (top) and simulated species (bottom) of $[NiL^1H_{-1}]^+$ in (a) ball and stick model and (b) stick representation (atoms at the crossing points), Color code: Ni^{2+}-pink, nitrogen-blue, oxygen-red, carbon-green and hydrogen-gray).

(a) (b)

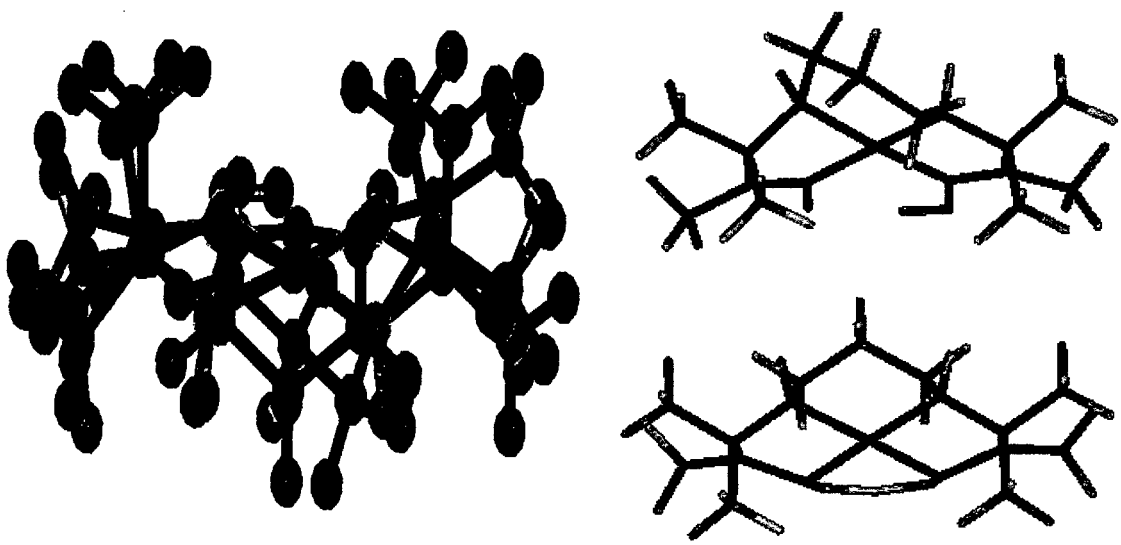

In the crystal structure this bridge is projecting away form molecular plane define by the metal ion and the nitrogen donor atoms of the ligand. The simulated structure, in contrast, has the propylene bridge in the same plane as the metal ion and the co-ordinated donor atoms. These studies indicated very little conformational

differences between the observed crystal and energy minimised simulated structures. This is a very important result in the development of force-fields for modelling of transition metal complexes. The force-fields can be modified to account for the Jahn Teller distortion normally observed for copper complexes. Furthermore, a structure of a particular complex can be inferred with confidence from these MM calculations and MD simulations in the absence of single crystals suitable for X-ray diffraction studies.

5.4.2 $[Zn(L^1)H_{-1}]^+$ and $[Cu(L^1)H_{-1}]^+$ species

The excellent agreement between the simulated and observed $[Ni(L^1)H_{-1}]^+$ crystal structures led to the extension of these simulations to the corresponding Zn^{2+} and Cu^{2+} species. The simulations of the former system was important due the relatively few techniques available for its investigation. The zinc(II) ion due to its d^{10} electronic configuration is spectroscopically silent. In fact, the geometries of the Zn^{2+} complexes are normally inferred from the corresponding Cu^{2+} and Ni^{2+} species. Although during the energy minimisation and simulations of the $[ZnL^1H_{-1}]^+$ species a tetrahedral Zn^{2+} ion was assumed, the square-planar zinc(II) complex (Figure 5.25 (a)) was observed.

This result is unexpected as Zn^{2+} prefers a tetrahedral arrangement of the donor atoms around itself. However, this observation is in agreement with the postulation made previously that the ligand's donor atoms are co-ordinated to Zn^{2+} in a square-planar fashion.[2] It also confirms that the low stability constant observed for this system is due to the square-planar arrangement of the ligand's donor atoms forced on the metal ion.[2] Just like the simulated $[NiL^1H_{-1}]^+$ species, the methylene groups of the propylene bridge are within experimental error on the same plane as the co-ordinated metal and the nitrogen donor atoms of L^1.

MD simulations of $[CuL^1H_{-1}]^+$ species (Figure 5.25(b)) indicated also a square-planar co-ordination of the ligand's nitrogen donor atoms towards the metal ion as was predicted from UV/Vis data.[1,2] Furthermore, the relative orientation of the propylene bridge in the simulated Cu^{2+} complex resemble that observed in the crystal structure of the corresponding Ni^{2+} species.

Figure 5.25: Simulated species of (a) $[ZnL^1H_{-1}]^+$ and (b) $[CuL^1H_{-1}]^+$, Zn^{2+}-brown, Cu^{2+}-pink, nitrogen-blue, oxygen-red, carbon-green and hydrogen-gray). The atoms are at the crossing points.

(a) (b)

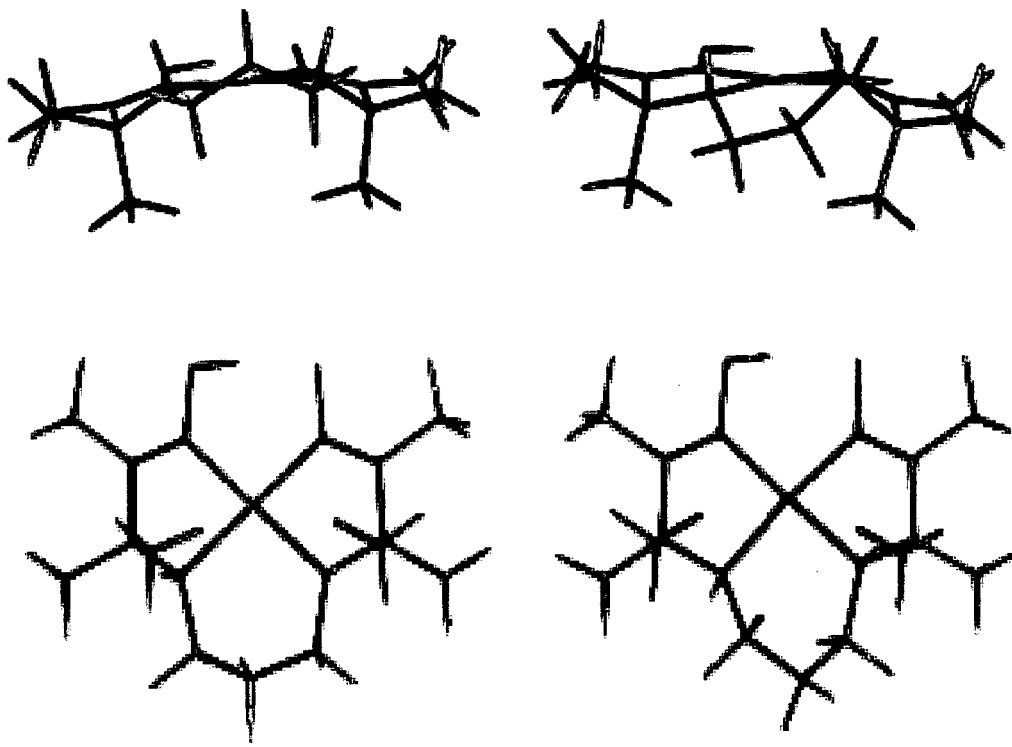

Overall, these simulations indicate that the conformation in the crystal structure is probably the stable one in solution. The design of therapeutics, in general, and the envisaged copper-based anti-arthritic agents in particular, will probably require detailed knowledge of their conformational requirements. Such conformational properties may be important for diffusion across the biological barriers as an initial step and into entering the cytosol. Biological activity of these complexes may also rely on their conformational requirements. These MD simulations serve as a first step in this direction.

5.5 Blood-plasma simulation studies

A justifiably conclusion that the ligands are more selective towards copper(II) can be drawn on the basis of the selectivity factors obtained in this study. However, the "high" concentrations of zinc(II) in blood plasma relative to copper(II),[43] put such

conclusions to the test. Hence, it is always predicted that the zinc(II) complexes predominate in blood-plasma.

True selectivity of the ligand towards copper(II) is investigated using the blood-plasma mobilising index (p.m.i.) defined as the ratio of low molecular weight copper complex species in the presence of a drug and on its absence. P.m.i.'s for Cu^{2+}, Ni^{2+}, Zn^{2+}, Ca^{2+} and Gd^{3+} were calculated by incorporating the formation constants for the ligands into the plasma model. In the calculation, the total ligand L concentration was varied over the range 10^{-3}-10^{-9} *mol* dm^{-3}. The results are shown in Figure 5.26 (a) and (b).

Figure 5.26: P.m.i. curves for (a) Cu^{2+} with L^1 and L^2 and (b) those of Cu^{2+}, Ni^{2+} and Gd^{3+} with L^1 plotted against log[L].

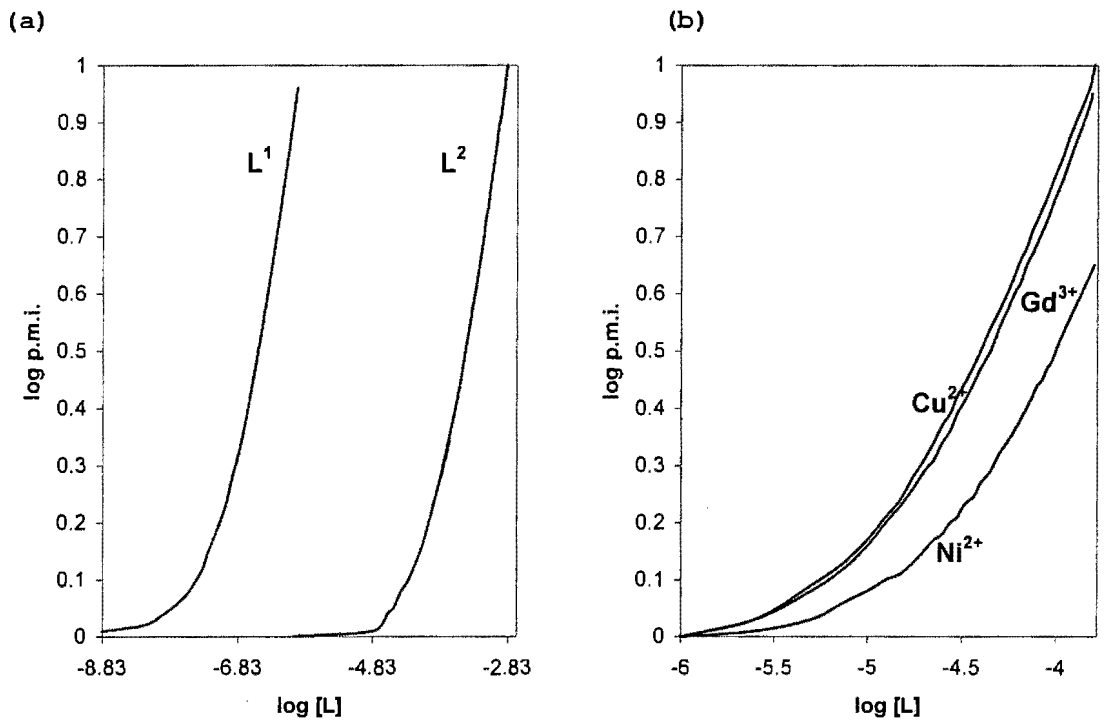

One important observation from Figure 5.26(a) is the absence of copper(II) mobilising curve induced by L^3. The figure indicates that L^3 is devoid of any copper(II) mobilising ability. In fact, at a total L^3 concentration of 1M, the Cu^{2+} p.m.i. is less than 0.01. This is due to the weak complexes formed by the metal ion with this ligand. In addition, the ligand has been found to form complexes with zinc(II) and calcium(II). Due to the high concentration of these metal ions and the presence of better co-ordinating ligands *in vivo*, L^3 is unable to increase the l.m.w. copper(II) fraction.

In contrast, the copper(II) mobilising abilities of L^1 and L^2 are 6 and 3 orders of magnitude respectively greater than that of L^3. This is indicated by the distinct separation of the copper mobilising curves when plotted as a function of the ligand concentration. The remarkably high mobilising ability of L^1 is related to the stable complexes it forms with Cu^{2+}. In addition, the predominant $[CuL^1H_{-1}]$ species present under physiological pH is further stabilised by hydrogen bonding. The hydrogen bond in the corresponding L^2 species is very weak as discussed in section 5.1.2.1.

At a total ligand concentration of 10^{-6} *mol dm*$^{-3}$ and 10^{-3} *mol dm*$^{-3}$ for L^1 and L^2 respectively, Zn^{2+} and Ca^{2+} p.m.i.'s are also less than 0.01. In spite of the higher Zn^{2+} and Ca^{2+} concentrations in blood plasma and predominance of the 11-1 species of the former ion under physiological condition, their weak binding strength with the ligands make them less important as competitors of copper(II) *in vivo*.

These p.m.i. calculations (Figure. 5.26(b)) reveal that the injected $[GdL^1H_{-1}]^{2+}$ species is also capable of surviving *in vivo*. However, copper is more likely to induce trans-metallation because of its high affinity for the nitrogen donor atoms of this ligand. These studies further indicate that the ligands, in their present form, will be of little use as contrast agents in MRI. However, modified analogues of these ligands, and L^1 in particular, incorporating pendant methylenecarboxylate and methylenephosphonate groups will be worthy of investigation as contrast agents in MRI.

In conclusion, it is predicted that the $[CuL^1H_{-1}]^+$ and $[CuL^2H_{-1}]^-$ complexes are unlikely to release their copper to proteins and/or to other l.m.w. chelating agents in biological systems. This is indicated by the ability of L^1 and L^2 ligands to bind copper(II) at very low concentrations.

5.6 Octan-1-ol/water partition co-efficient studies

Although copper(II) complexes when administered orally and intravenously do increase available copper, it is difficult to move this co-ordinated metal ion through a series of body compartments without protein binding.[43] Of the various classical ways of drug administration such as orally, by injection intravenously, intraperitoneally etc.,

percutaneous absorption offers one obvious advantage of being less painful and hence tolerable to the patient. However, the usefulness of percutaneous drug administration relies on the lipophilicity and molecular weight of the drug.[44]

For this reason, this study also investigated the octanol/water partition coefficients of copper complexes with a view to establishing whether these species can be administered transdermally. The two component octan-1-ol/water mixture was used as a biophase analogue. Figure 5.27 shows the logarithms of the partition coefficients ($logP_{oct/aq}$) of (a) Cu^{2+}-L^2 and (b) Cu^{2+}-L^3 complexes plotted as a function of pH.

Figure 5.27: $LogP_{oct/aq}$ of (a) Cu^{2+}-L^2 (•) and (b) Cu^{2+}-L^3 (♦) complexes plotted against pH. Each dot or square is a mean of three independent observations. The errors in the mean are not included because they are too small.

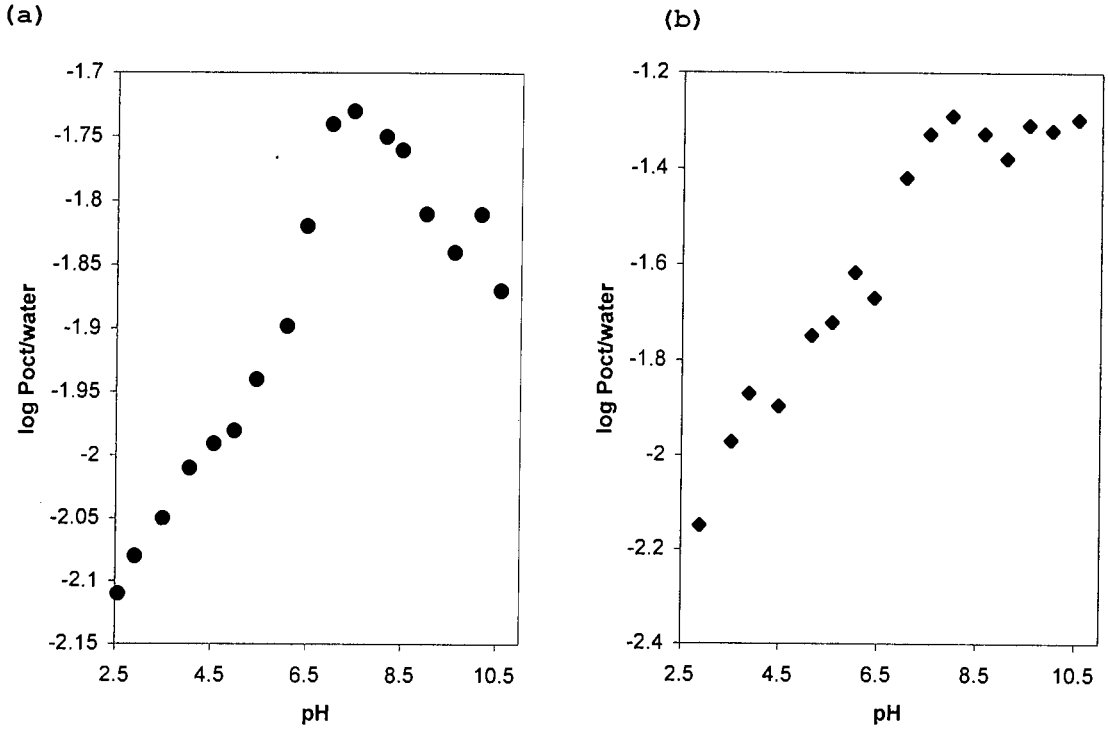

These $logP_{oct/aq}$ values were determined at 25^0C and an ionic strength of 0.15 *mol* dm^{-3} (Cl^-). $LogP_{oct/aq}$ is often used as a measure of the lipophilicity of a drug (complex),[44-49] and for a drug to be reasonably lipophilic, the $logP_{oct/aq}$ value must be at least 0.6.

5.6.1 Cu-L^2 system

One of the noticeable features about figure 5.27 (a) is the fact that all $logP_{oct/aq}$ values are negative. The negative values of the lipophilicity measure indicate that these complexes are largely hydrophilic. The low $logP_{oct/aq}$ values in the acidic pH range of 2.5-4.0 is expected in view of the high concentration of hydrated $[Cu(OH_2)_6]^{2+}$ in this pH range. At pH values above 4.0, complexation begins to occur through the deprotonation and co-ordination of the amide and oxime groups. This leads to the formation of the neutral 110 species. A $logP_{oct/aq}$= -1.97 is assigned to this species on the basis of the speciation calculations of the Cu-L^2 system.

The $logP_{oct/aq}$ at the physiological pH 7.4 is -1.73, which can be approximated as the value for $[CuL^2H_{-1}]^-$. The speciation calculations indicate that Cu^{2+} is 95% present as the mononegatively charged $[CuL^2H_{-1}]^-$ at this pH. There is a decrease in $logP_{oct/aq}$ as the pH increases above pH 8.0 and reaches a value of -1.88 at pH 10.5. This is due to the predominance of the dinegatively charged $[CuL^2H_{-2}]^{2-}$ complex in this pH range (see Figure 5.5(a) speciation curves).

In the pH range of 2.5-10.5 studied, the $logP_{oct/aq}$ values of the Cu^{2+}-L^2 system vary between -2.11 and -1.73. A difference of 0.38 ($\Delta logP_{oct/aq}$ = 0.38) between the maximum and minimum $logP_{oct/aq}$ values is an indication that all three complexes of copper(II) with the ligand are equally lipophilic. This comes as no surprise if one realises that these complexes differ from each other by two protons at most.

Hydrogen bonding between the carbonyl oxygens and the water molecules is the main contributor to the decreased lipophilicity of these complexes. Although the 110 species is electrically neutral, the presence of four co-ordinated water molecules also increases its hydrophilicity. It is postulated that the deprotonated oxime oxygen may hydrogen bond to the water molecules, thus decreasing its partitioning into the organic phase. The decreased lipophilicity of the 11-2 complex can be ascribed to the presence of negatively charged oxime oxygens which are capable of hydrogen-bonding to water molecules. The 11-1 species is the least hydrophilic of these complexes probably due the absence of co-ordinated solvent molecules. Furthermore, the presence of the hydrogen bond in this 11-1 species leading to the formation of the

pseudo-macrocycle reduces the number of available oxygen sites for hydrogen bonding.

A $logP_{oct/aq}$ = -1.73 for the $[CuL^2H_{-1}]$ complex which predominates in the pH 6.5-8.0 means 1.86 % of the species goes into octanol phase. Since this pH range encompasses the pH of the skin and the blood-plasma, it is more likely that a similar percentage is likely to penetrate the skin when applied transdermally.

Packard et al.[46] have recently studied the partition coefficients of monocationic copper(II) complexes of diimine dioxime ligands L^k, L^l and L^m. The $logP_{oct/aq}$ values of their systems varied between -2.05 and -1.60. These diimine dioxime complexes are as lipophilic as the Cu^{2+}-L^2 complexes investigated in this study. However, they are less lipophilic than the 110, 11-1 and 11-2 species of the Cu^{2+}-L^1 system, whose $logP_{oct/aq}$ values are -1.78, -1,22 and -1.20 respectively. This is because L^1 has more alkyl substituents than L^2, L^k, L^l and L^m.

5.6.2 Cu^{2+}-L^3 system

The copper(II) complexes formed by this metal ion with L^3 are equally hydrophilic. This is revealed by the negative $logP_{oct/aq}$ values (Figure 5.27(b)) obtained throughout the pH range studied. Low $logP_{oct/aq}$ values at the acidic pH range of 2.5-4.0 are due to the coexistence of the hydrated Cu^{2+} and the protonated 111 complexes. In fact, a $logP_{oct/aq}$=-2.0 can be assigned to this 111 species. The assignment is based on the assumption that the contribution of $[Cu(OH_2)_6]^{2+}$ to the observed $logP_{oct/aq}$ is much smaller than -2.0. This is a justifiable assumption because of the presence of at least two hydration shells around Cu^{2+} in the 100 species.

In the protonated 111 complex, the ligand is postulated to be co-ordinated to the metal ion through one carbonyl oxygen, the central anchoring amine and one terminal amino group. This leaves three to four co-ordination sites on the metal ion to be occupied by the water molecules, hence its observed low lipophilicity.

The dipositively charged 110 is slightly more lipophilic than the 111 complex. This is observed as an increase in $logP_{oct/aq}$ as the pH is raised to 6.5 where the former complex predominates. A lipophilicity measure of -1.79 is assigned to the 110

complex where the coordination of the first amide group is believed to decrease hydrogen bonding with water molecules. A further slight increase in $logP_{oct/aq}$ above pH 6.5 to a maximum value of -1.25 is a consequence of the steady accumulation of the 11-1 species where the second amide group is postulated to be coordinated to the metal ion. In fact, a $logP_{oct/aq}$=-1.25 at pH 8.0 can be assigned to the monopositively charged 11-1 complex.

Above pH 8.0 there is no change observed in $logP_{oct/aq}$ where the dominant species is the 11-2. Thus, a $logP_{oct/a}$=-1.25 can also be assigned to this neutral complex. Co-ordination of the second terminal amine should increase the lipophilicity of the 11-2 complex by decreasing the number of available nucleophilic sites capable of hydrogen bonding. This is in support of the assumption that there is no evidence of co-ordination of the five nitrogen donor atoms to the metal ion. A $\Delta logP_{oct/aq}$=0.93 between the maximum and minimum $logP_{oct/aq}$ values is indicative of differing lipophilicities of the various Cu^{2+}-L^3 complexes formed. The $logP_{oct/aq}$=-1.25 for the 11-1 complex indicates that 5.62% of the drug is likely to penetrate the skin despite its low thermodynamic stability

Unlike the results which have been reported before for L^{d2},[8] the copper complexes of L^3 have been found to be reasonably lipophilic. In fact, L^3 and L^{d2} can be viewed as members of a homologous series differing by two methylene groups. L^3 contains two methylene groups, one on each side of the benzylamine. Leo et al.[45] have observed that incorporation of two methylene groups to a ligand backbone adds approximately one log unit ($\Delta logP_{oct/aq}$=1.0) to the observed $logP_{oct/aq}$. A $logP_{oct/aq}$ value of -3.4 is predicted for the $[CuL^3H_{-1}]$ complex. This species, however, has been observed to be two log units more lipophilic than predicted using Leo et al.[45] additive rule. This difference is not easy to rationalise.

In general, the presence of alkyl groups as part of the backbone structure of a ligand or as substituents to it do increase its lipophilicity. The presence of benzyl and methyl groups on L^3 should render the molecule lipophilic enough for a reasonable amount of its copper complexes to enter the octanol phase. A closer look at the ligand structure reveals that only the uncoordinated carbonyl oxygen can hydrogen bond to the solvent molecules. However, such interactions should be weak due to the low

basicity of the carbonyl oxygen. Even after deprotonation of the amide groups due to metal ion complexation, the negative charge is delocalised over the amide moiety (Figure 5.6 (i), (j) and (k)) and the proximity of the metal ion makes hydrogen bonding with bulk water molecules impossible. Hence, the reasonably high lipophilicity of Cu^{2+}-L^3 complexes should be expected in view of these considerations.

5.6.3 Discussion - Partition coefficients

The presently investigated Cu-L complexes have been observed to be largely hydrophilic. Four key contributions to the overall hydrophilicity of these complexes are:

- the presence of co-ordinated water molecules,
- hydrogen bonding interactions between the carbonyl oxygen atoms and the bulk water molecules,
- hydrogen bonding between charged groups in these species and the solvent molecules, and
- the overall charge of the 111, 110, 11-1 and 11-2 complex species.

The low lipophilicity observed for Cu^{2+}-L^2 compared to Cu^{2+}-L^1 and Cu^{2+}-L^3 systems is expected in view of the fact that L^1 and L^3 have more alkyl substituents than L^2. Moreover, the negatively charged oxygen(s) of the hydroxyimino groups, not involved in bonding with the metal ion, probably decrease its partitioning into the organic phase.

To demonstrate the effect of the above-mentioned factors and the role played by alkyl substituents on the lipophilicity of these complexes, Table 5.4 summarises the $\log P_{oct/aq}$ values of the $[CuLH_{-1}]$ species for the presently investigated ligands and those of similar ligand systems (Figure 1.1).

Martell et al.[10-12] have recently investigated several copper(II) complexes of monooxo and dioxotetraazamacrocyles which are based on the cyclam backbone as myocardial perfusion agents. These macrocyclic ligands resemble L^1 and L^2 except the absence alkyl subsituents on the macrocycles' backbone. Although Cu^{2+} forms stable

11-2 species with these cyclic ligands as expected from the macrocyclic effect, they are, however, largely hydrophilic to enter into the octanol phase. They concluded that although these systems are reasonably stable, they are not lipophilic as required for myocardial perfusion agents.[10-12]

Table 5.4: $LogP_{oct/aq}$ of $[CuLH_{-1}]$ species for L^1, L^2 and L^3 and those of similar ligands (PuPy=N,N'-bis(2-pyridyl)methylene-1,4-butanediamine)[50] with Cu^{2+}.

Ligand	Log P	Ligand	Log P	Ligand	Log P
L^1	-1.22	L^l	-1.60[46]	L^p	3.27[48]
L^2	-1.73	L^m	-2.05[46]	L^q	3.42[48]
L^3	-1.25	L^n	1.97[47]	L^r	3.61[48]
L^k	-1.96[46]	L^o	2.42[48]	PuPy	-0.85[50]

In fact, it has been postulated that copper complexes with $logP_{oct/aq}$ values greater than 0.6 are lipophilic enough to be regarded as promising myocardial perfusion agents and could possible penetrate the blood-brain barrier.[44-49] The ^{67}Cu- and ^{64}Cu-labeled [N(2-pyridylmethyl-N1-(salicylaldimino)-1,3-propanediamine], (L^n) and pyruvaldehyde bis(N^4-methylthiosemicarbazone) derivatives (L^o, L^p, L^q and L^r) recently studied by Green and coworkers[47,48] have $logP_{oct/aq}$ in the range of 1.97 to 3.61 (Table 5.4). These ligands are lipophilic enough to penetrate blood-brain barrier and indeed, they showed a high uptake in the brain and other fatty tissues such as the heart and liver.

The monocationic and anionic copper complexes of the dione/diamide/diimine/ dioxime ligands L^k, L^l, and L^m, on the other hand, are approximately three to four orders of magnitude less lipophilic when compared to salicylaldimino and methylthiosemicarbazone ligands.[46] The former ligands were not found to penetrate the blood-brain barrier.[46] This means that the presently investigated copper(II)-dione dioxime ligands could be of little use as brain and/or myocardial perfusion agents.

Through control of the co-ordination geometry of the metal ion of interest such as changing the steric environment of the co-ordination axis using suitable

substituents, lipophilicity increases of several orders of magnitude can be achieved. Alkyl groups as substituents do control the accessibility of the axial ligands to the co-ordinated metal ion due to their steric effect.

The barrier to partitioning of drugs in skin and bio-membranes is always associated with the ordered chain region of the lipid bilayers.[43] It is anticipated that the partitioning of these complexes in this biophase analogue must compare favourably with partitioning in these biological barriers. The results indicate that, overall, approximately 2-6% of the 11-1 species dominant at physiological pH is likely to permeate the skin and membrane when administered percutaneously and in the absence of proper vehicles.

5.7 Superoxide dismutase mimetic activities of Cu^{2+}-L complexes

It has been observed that l.m.w. copper(II) complexes are capable of catalysing the dismutation of the super oxide anion radical to molecular oxygen, water and/or hydrogen peroxide.[51-56] These complexes could be used as $Cu^{2+}{}_2Zn^{2+}{}_2$ SOD mimics. Because of this property, the superoxide dismutase mimic activities of the copper(II) complexes were investigated using the NBT assay. Figure 5.28 shows the percentage inhibition plotted against the concentration of the copper complex. From these curves the concentration of the drug required to reduce diformazan formation by 50% (also termed an IC_{50} value) is easily read.

IC_{50} values equal to 58, 110 and 11.7 $\mu mol\ dm^{-3}$ for the $[CuL^1H_{-1}]^+$, $[CuL^2H_{-1}]^-$ and $[CuL^3H_{-1}]^+$ complexes respectively have been obtained. The IC_{50} value of the native CuZn SOD is IC_{50}=0.011 $\mu mol\ dm^{-3}$.[51] The high IC_{50} values exhibited by these Cu^{2+} complexes are indicative of their low SOD mimetic activities when compared to the native enzyme.

The dismutation of the $O_2^{-\cdot}$ has been proposed to occur via the reversible binding of the superoxide anion to the metal ion. During this reaction, Cu^{2+} is reduced to Cu^+ while the $O_2^{-\cdot}$ anion is oxidised to molecular oxygen.[51]

Figure 5.28: %Inhibition as a function of the concentration of the copper complex.

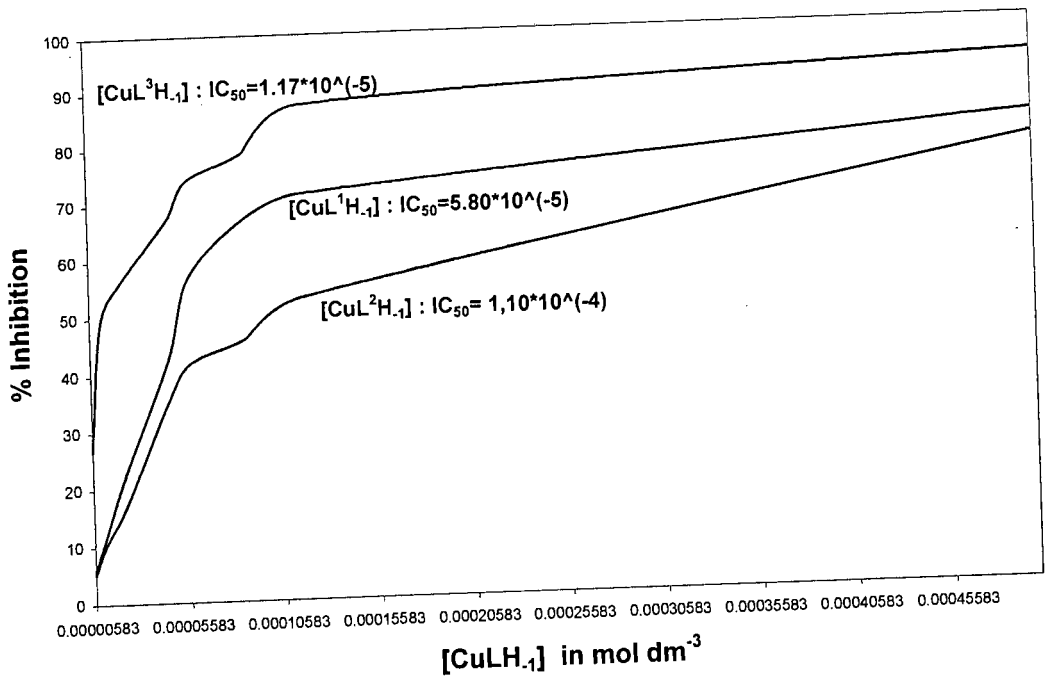

The $[CuL^2H_{-1}]^-$ species exhibits an IC_{50} value which is 10000 times greater than that of the native enzyme. This can be rationalised in terms of the square-planar arrangement of the ligand donor atoms around Cu^{2+} in this species. There are, in fact, no available binding sites for the superoxide anion radical ($O_2^{-\cdot}$) to co-ordinate to the metal ion due to the high ligand field afforded by L^2.

On the other hand, the higher SOD mimic activity exhibited by the $[CuL^1H_{-1}]^+$ complex can be ascribed to the available axially co-ordination sites usually occupied by water molecules. In fact, the dismutation of the superoxide ion is thought to proceed through the replacement of one of the axially co-ordinated water molecules by $O_2^{-\cdot}$.

The low IC_{50} value exhibited by $[CuL^3H_{-1}]^+$ can be interpreted in terms of the possible replacement of co-ordinated water molecules by the $O_2^{-\cdot}$. Furthermore, the presence of protonated ligand's sites should also contribute to the dismutation of $O_2^{-\cdot}$ through hydrogen bonding. The insignificant SOD mimetic behaviour displayed by these $[CuLH_{-1}]$ species is further exacerbated by competition with EDTA, which has been used to simulate the endogenous ligands. The Cu^{2+}-EDTA complex is a poor

mimic of the enzyme[50-56] probably due its co-ordinatively saturated nature and hence the high ligand field provided by EDTA.

No correlation has been found between the SOD mimetic activity of these complexes and their lipophilicity. This is despite the assertion that good SOD mimics tend to display the lowest lipophilicities.[51] Instead, the dismutation of $O_2^{\cdot-}$ seems to be favoured by weak complexes containing axially co-ordinated water molecules.

Many researchers[50-56] have reported IC_{50} values in the range of 0.09 to more than 20.0 *μmol dm*$^{-3}$ for a number of Cu^{2+} complexes, some of which are given in Table 5.5. The majority of the complexes of the anti-inflammatory drugs have IC_{50} values that are approximately a 1000 times higher than the value exhibited by the native enzyme indicating that they are poor mimics of Cu-Zn SOD. Some of these complexes such as those of cryptand (Crpd)[53] and hexaazamacrocyclic (Bpzp-Bpzbiap) ligands[54], however, show promising characteristics of being models of the enzyme. These are also worthy of further investigation as human therapeutics in models of rheumatoid arthritis such as collagen induced arthritis (CIA).

Table 5.5: IC_{50} *(μmol dm*$^{-3}$**)** of $[CuLH_{-1}]$ species for L^1, L^2 and L^3 and those of similar ligands ([D-Pen-D-penicillamine, Asp-Aspirin, **Ind**-Indomethacin, Car-Carprofen, Azat-Azathioprine, Chlrq-Chloroquine, Sulph-Sulphasalazine, Crpd-Cryptand, Bpzp-Bpzbiap, PuPy-N,N'-bis(2-pyridyl)methylene-1,4-butanediamine and the other ligands are based are PuPy])[50] with Cu^{2+}.

Ligand	IC_{50}	Ligand	IC_{50}	Ligand	IC_{50}
L^1	58	Car.	19[51]	PuPhePy	0.27[50]
L^2	110	Azat.	>20[51]	Pu-MePy	2.25[50]
L^3	11.7	Chlrq.	>19.5[51]	Apz-Pn	0.09[50]
CuZnSOD	0.01[51]	Sulph.	20[51]	Pyal-en	0.45[50]
D-Pen	8.0[51]	Crpd	0.50[53]	Depy	0.45[50]
Asp.	20[51]	Bpzp	0.26[54]	Dpbi	0.62[50]
Ind.	19[51]	PuPy	0.60[50]	Dmbi	1.58[50]

It should be emphasised that no model compounds can ideally mimic the native copper-zinc enzyme and the IC_{50} values exhibited by these complexes are within the range expected for model compounds. In particular, the values exhibited by the imidazolate-bridged dinuclear copper(II) complexes of a cryptand[53] and hexaazamacrocyclic ligands[54] represent upper limits which can be observed for these mimics (Table 5.5).

This is probably due the entatic (or "strained") nature of the enzymes, in general, and metallo-enzymes, in particular.[57] It is believed that the active site in an enzyme is constrained by the surrounding protein matrix to adopt a geometry similar to that of the transition state than would exist in a similar unconstrained systems, thereby reducing the re-organisational energy.[57]

The reactivity of this active site is also fine tuned not only by the ligands co-ordinated to the metal ion but also by the environment provided by the folded protein. These differences between the native enzyme and the model systems should always be taken into account whenever comparisons are made.

More recently, it has been observed by Roe et al.[58] that the reduced $Cu^{+}_{2}Zn^{2+}_{2}$ SOD is more stable than its oxidised analogue. Thus, in the presence of paramagnetic $O_2^{-\cdot}$ the formation of the reduced form of the enzyme is favoured over that of the oxidised species. This may also explain why there is a high concentration of an inactive form of the enzyme in the synovial joints of arthritic patients. Under, these conditions the rate of $O_2^{-\cdot}$ production exceeds that of synthesis and/or activation of the enzyme. It may be viewed that the enzyme in both the reduced and oxidised states is co-ordinatively unsaturated. This is in sharp contrast to the high field provided by L^1 and L^2 ligands.

In conclusion, the $[CuLH_{-1}]$ complexes of L^1, L^2 and L^3 are poor mimics of the native enzyme because of the high IC_{50} values obtained. However, the low SOD mimic activities exhibited by these complexes *in vitro* can be enhanced in the synovial cavity due to the low complexing conditions in the latter compared to the former medium.

5.8 Biodistribution experiments on mice

On the basis of the aforementioned encouraging *in vitro* results, it was deemed necessary to perform biodistribution experiments. Radio-labelled ^{64}Cu-L complexes were injected intravenously through the tail vein on mice as animal screens. Activity of these complexes were measured in various excised organs after 1, 6 and 24 hours postinjection. Since the interest initially was the investigation of the amount of activity excreted through the urine, only the activity in the liver, blood, tail and muscle were investigated after 1 hour postinjection. Table 5.6 shows the %ID/organ and per gram for all complexes including the control for this 1 hour time point calculated on the basis of wet organ weight.

Table 5.6: %ID/organ and per gram(g) tissue of the injected complexes including $CuCl_2$ 1 hour postinjection.

Organ	Complex			
(%ID/org and/g	CuL^1H_{-1}	CuL^2H_{-1}	CuL^3H_{-1}	$CuCl_2$
Liver	48.91 ± 1.34	52.73 ± 0.93	51.98 ± 2.58	65.66 ± 0.60
	53.01 ± 4.85	50.99 ± 0.71	38.89 ± 0.99	63.1 ± 0.03
Blood	0.50 ± 0.06	0.50 ± 0.11	0.61 ± 0.13	0.81 ± 0.18
	1.36 ± 0.27	1.07 ± 0.19	1.31 ± 0.21	1.72 ± 0.38
Carcass	47.24 ± 0.48	42.84 ± 7.69	40.82 ± 0.37	30.24 ± 2.10
	2.78 ± 0.05	1.72 ± 0.13	1.73 ± 0.01	1.76 ± 0.21
Tail	1.60 ± 0.10	1.91 ± 0.23	1.68 ± 0.12	1.86 ± 0.05
	3.46 ± 0.6	14.78 ± 4.01	40.09 ± 7.82	3.66 ± 0.29
Urine	0.59 ± 0.043	1.75 ± 0.83	4.76 ± 0.30	0.09 ± 0.007

The high activity in the carcass necessitated the excission of other organs in order to investigate the localisation of this activity. These results are reported in Table 5.7, 5.8, 5.9 and 5.10 for $[CuL^1H_{-1}]$, $[CuL^2H_{-1}]$, $[CuL^3H_{-1}]$ and $[CuCl_2]$ where Int. is an abbreviation for intestines. One of the noticeable features about these complexes is their rapid clearance from the blood circulatory system. Furthermore, of importance in these systems is their initial rapid and high uptake by the liver. In fact, the activity increases from 50% after 1 hour and reaches a maximum of approximately 70% at 6 hours. After a 24 hour period there is approximately 30% of activity in this organ. The

exception is the [CuL^2H_{-1}] complex where there is about 11% of the activity still remaining.

Table 5.7: %ID/organ and per gram tissue for [CuL^1H_{-1}] species.

Organ	6hr(%ID/org)	6hr (%ID/g)	24hr(%ID/org)	24hr(%ID/g)
Liver	66.89 ± 1.77	53.45 ± 4.31	32.81± 2.47	24.69± 1.95
Blood	0.48 ± 0.13	1.71 ± 0.04	0.96 ± 0.70	4.43 ± 1.00
Carcass	6.63 ± 0.41	0.69 ± 0.09	21.27± 1.71	2.04 ± 0.19
Tail	1.11 ± 0.03	2.11 ± 0.07	1.78 ± 0.46	3.73 ± 1.18
Muscle	0.07 ± 0.01	0.78 ± 0.13	0.14 ± 0.01	2.09 ± 0.74
Heart	0.62 ± 0.09	3.83 ± 0.33	1.45 ± 0.60	14.45± 6.56
Lung	1.27 ± 0.06	8.07 ± 0.66	1.73 ± 0.80	9.53 ± 3.06
Kidney	1.59 ± 0.04	5.16 ± 0.46	4.39 ± 1.32	13.07± 4.93
Head	1.61 ± 0.04	0.63 ± 0.01	6.65 ± 0.55	2.85 ± 0.28
Int.	10.65 ± 0.69	4.31 ± 0.57	22.08± 0.56	6.77 ± 0.01
Spleen	0.27 ± 0.05	1.97 ± 0.25	0.77 ± 0.27	6.26 ± 1.35
Brain	0.08 ± 0.01	0.33 ± 0.03	0.47 ± 0.01	1.25 ± 0.16
Urine	1.89 ± 0.70		4.47 ± 0.16	

Table 5.8: %ID/organ and per gram tissue for [CuL^2H_{-1}] species.

Organ	6hr(%ID/org)	6hr (%ID/g)	24hr(%ID/org)	24hr(%ID/g)
Liver	41.72 ± 2.98	29.14± 1.81	9.48 ± 0.49	7.19 ± 0.80
Blood	0.29 ± 0.01	1.25 ± 0.03	0.39 ± 0.16	1.OO ± 0.09
Carcass	4.66 ± 0.18	0.48 ± 0.06	6.12 ± 0.28	0.52 ± 0.04
Tail	0.82 ± 0.01	1.67 ± 0.23	0.54 ± 0.15	1.05 ± 0.27
Muscle	0.08 ± 0.02	0.51 ± 0.14	0.05 ± 0.003	0.68 ± 0.08
Heart	0.33 ± 0.07	2.62 ± 0.60	0.25 ± 0.023	1.84 ± 0.10
Lung	0.67 ± 0.09	4.71 ± 0.55	0.57 ± 0.024	3.11 ± 0.37
Kidney	3.60 ± 0.93	11.03± 1.50	1.52 ± 0.17	3.84 ± 0.17
Head	1.16 ± 0.15	0.27 ± 0.05	1.43 ± 0.58	0.55 ± 0.23
Int.	7.76 ± 0.09	3.00 ± 0.39	2.54 ± 0.08	0.76 ± 0.03
Spleen	0.23 ± 0.02	1.49 ± 0.32	0.17 ± 0.01	1.22 ± 0.02
Brain	0.07 ± 0.01	0.23 ± 0.03	0.09 ± 0.01	0.26 ± 0.01
Urine	37.34 ± 4.05		76.02± 1.54	

Table 5.9: %ID/organ and per gram tissue for [CuL^3H_{-1}] species.

Organ	6hr(%ID/org)	6hr (%ID/g)	24hr(%ID/org)	24hr(%ID/org)
Liver	64.93 ± 0.10	46.43± 3.97	28.21± 4.24	22.44± 3.19
Blood	0.31 ± 0.003	1.96 ± 0.02	0.22 ± 0.14	3.45 ± 0.86
Carcass	7.98 ± 0.46	0.82 ± 0.15	19.87± 4.30	1.94 ± 0.27
Tail	1.26 ± 0.05	3.48 ± 0.76	1.41 ± 0.29	3.30 ± 0.70
Muscle	0.11 ± 0.01	0.7 ± 0.10	0.14 ± 0.05	1.64 ± 0.32
Heart	0.50 ± 0.001	3.96 ± 0.46	0.83 ± 0.13	7.82 ± 1.30
Lung	1.36 ± 0.07	9.34 ± 0.31	2.04 ± 0.35	13.75± 2.60
Kidney	1.91 ± 0.02	6.19 ± 0.39	3.14 ± 0.79	11.06± 2.30
Head	1.74 ± 0.06	0.72 ± 0.01	6.38 ± 1.39	2.64 ± 0.60
Int.	14.77± 0.72	4.85 ± 0.45	26.18± 1.58	9.41 ± 2.15
Spleen	0.25 ± 0.01	2.32 ± 0.34	0.52 ± 0.19	5.57 ± 2.08
Brain	0.08 ± 0.001	0.36 ± 0.08	0.37 ± 0.22	1.05 ± 0.17
Urine	7.67 ± 2.48		25.16± 2.11	

Table 5.10: %ID/organ and per gram tissue for $CuCl_2$.

Organ	6hr(%ID/org)	6hr (%ID/g)	24hr(%ID/org)	24hr(%ID/org)
Liver	73.50± 1.89	57.75± 5.14	37.14 ± 9.20	29.66± 5.42
Blood	0.21 ± 0.07	2.19 ± 0.18	0.70 ± 0.47	4.61 ± 1.55
Carcass	6.86 ± 1.40	0.61 ± 0.06	21.87± 3.88	2.00 ± 0.44
Tail	1.28 ± 0.06	2.85 ± 0.67	1.79 ± 0.53	3.60 ± 1.22
Muscle	0.08 ± 0.02	0.83 ± 0.16	0.15 ± 0.05	1.94 ± 0.80
Heart	0.42 ± 0.06	2.73 ± 0.24	1.07 ± 0.43	10.49± 4.40
Lung	0.85 ± 0.02	5.59 ± 0.67	1.51 ± 0.83	10.50± 5.70
Kidney	1.47 ± 0.04	4.27 ± 0.08	3.57 ± 0.59	11.44± 2.38
Head	1.21 ± 0.11	0.56 ± 0.01	6.16 ± 0.64	2.63 ± 0.60
Int.	12.10± 0.52	4.11 ± 0.51	27.84± 4.0	8.05 ± 1.50
Spleen	0.23 ± 0.02	2.33 ± 0.26	0.65 ± 0.17	5.89 ± 1.76
Brain	0.07 ± 0.005	0.21 ± 0.02	0.43 ± 0.12	1.03 ± 0.2
Urine	5.16 ± 1.41		11.16 ± 0.92	

This high activity in the liver should be expected in view of the fact that the copper storing proteins and its metabolism occur in this organ. Moreover, it is well known that lipophilic complexes generally have more uptake in the liver or in fatty

tissues. The high uptake of ^{64}Cu-labeled complexes by liver has also been reported by many researchers.[46-49] Since the muscle constitutes about 40% of the total body weight,[46-49] the high activity in the carcass should reside in the muscle. Furthermore, neither the injected copper complexes nor their metabolites are bone seeking, hence the activity in the carcass cannot be due to accumulation of these species in the bone.

In addition, there has been a significant uptake of these complexes by the heart, lung and spleen. The high uptake of these complexes by the aforementioned organs could be explained in part by their reasonably high lipophilicity ($logP_{oct/aq}$ varies between -1.73 and -1.22). In addition, the high perfusion of these organs might have enhanced this uptake. In general, positively charged species tend to accumulate in the heart. The significant uptake of the mono-positively charged $[^{64}CuL^{1}H_{-1}]^{+}$ and $[^{64}CuL^{3}H_{-1}]^{+}$ species by the mycocardium in particular should be expected. In contrast, no significant activity was recorded in the brain. It seems these complexes are unable to cross the blood-brain barrier in accordance with the observed lipophilicities.

Since the liver is the centre of copper metabolism, the mode of removal of these complexes is by the hepatobilliary route. This accounts for the high activity which has been observed in the intestines (abbreviated - Int.). The activity in the droppings is not reported in the Tables above because of the variations in the samples counted due to the difficulty of correcting for activity in the droppings excreted at different time points.

In contrast to earlier observations,[59] the presently investigated $[^{64}CuLH_{-1}]$ complexes have been found to be retained significantly by most of these organs. One of the reasons for this increased accumulation of these complexes in these organs is their high lipophilicity. This *in vivo* behaviour is not surprising for the monopositively charged $[CuL^{1}H_{-1}]$ species since speciation calculations using the blood-plasma model suggest that this complex, which predominates at physiological pH is likely to survive in plasma.

It has been suggested that the high uptake of ^{64}Cu by the liver is due to transchelation of the radioisotope by albumin and histidine.[60] This is because these *in*

vivo proteins and l.m.w. ligands bind strongly to Cu^{2+}. The thermodynamically and kinetically stable ^{64}Cu-labeled cyclam, et-cyclam, teta and DOTA derivatives recently investigated by Anderson et al.[60] showed a biodistribution similar to that observed for the complexes investigated in this study. These results suggest that there is little correlation between the thermodynamic stability and the high liver uptake. However, the dissociation of the weak $[CuL^3H_{-1}]$ complex, which showed the biodistribution similar to that of $CuCl_2$ cannot be ruled out. In fact, the rapid accumulation of the control in the liver attests to this possibility. For $[CuL^3H_{-1}]$, the transchelation process is preceded by the complex dissociation. The observed biodistribution of $[CuL^3H_{-1}]$ should be expected since speciation calculations indicate that the complex does not exceed 20% at physiological pH while blood-plasma simulation studies predict that L^3 is a poor mobiliser of copper(II) *in vivo*.

Although no attempts have been made so far to characterise the metabolites or the form of activity excreted in the urine or droppings, such studies can give a better insight on the true *in vivo* stability of these injected ^{64}Cu-labeled species. Blower[61] and Sarkar[62] have recently discussed the various forms in which Cu^{2+} exists *in vivo* and suggested that the metal ion may be excreted as a bile acid complex.

Unlike $[CuL^3H_{-1}]$, species distribution and speciation calculations using the blood-plasma model suggest that the $[CuL^2H_{-1}]$ complex should predominate under *in vivo* conditions. Biodistribution experiments confirmed the afore-mentioned prediction in that the $[^{64}CuL^2H_{-1}]$ species seems to be excreted predominantly by the renal route as expected for negatively charged species. This is because of the high activity observed in both the kidney and urine after 6 and 24 hours postinjection. However, this excreted activity is still less than the 90% urine recovered activity from previously reported ^{67}Cu-labelled ligands.[59] Packard et al.[46] and Anderson and coworkers[60] have reported a similar renal elimination of the copper labelled complexes.

Anderson et al.[60] noted that the clearance of negatively charged ^{64}Cu-TETA species by the renal route can be of profound importance in the imaging of the renal excretory system. This led to the investigation of the biodistribution behaviour of ^{64}Cu-TETA-Tyr^3-Octreotate, where octreotate is a somatostatin analogue conjugated

to TETA (L^e).[49] This compound was observed to exhibit a high uptake in somatostatin-rich organs such as the pancreas. Similar conjugation of $[^{64}CuL^2H_{-1}]$ to octreotate may enable the imaging of pancreas and related glands and organs.

Since these complexes, and $[^{64}CuL^1H_{-1}]$ in particular, have been observed to have a reasonably long biological half-life, they merit further evaluation in collagen induced arthritis. They can be administered orally, by injection and transdermally. The latter form of administration may require the development of appropriate vehicles to enhance percutaneous absorption.

A water/dimethyl sulphoxide mixture as an initial vehicle model will be worth trying. Encapsulation of these complexes in liposomes might offer some advantages over the two phase water/DMSO mixture.

It has been reported that copper complexes with $logP_{oct/aq}$ values greater than 0.6 are lipophilic enough to be regarded as promising myocardial perfusion agents and could possibly penetrate the blood-brain barrier. Since these complexes are reasonably lipophilic, the corresponding ligands can be alkylated further to achieve these high lipophilicities. Extra-functionalisation and bioconjugation may be necessary for local targeting. This can be achieved by using appropriate biological indicators such as an octreotide for targeting somastotatin rich-organs.[49]

References

1. G.E. Jackson and B.S. Nakani, *J. Chem. Soc., Dalton Trans.*, 1996, 1373.
2. T.E. Nomkoko, MSc Thesis, University of Transkei, 2000.
3. H. Kipton, J. Powell and J.M. Russell, *Aust. J. Chem.*, 1977, **30**, 1467-1473.
4. A.M. Duda, A. Karaczyn, H. Kozlowski, I.O. Fritsky, T. Glowiak, E.V. Prisyazhnaya, T. Y.-Sliva and J. S.-Koslowska, *J. Chem. Soc., Dalton Trans.* 1997, 3853.
5. J.W. Fraser, G.R. Hedwig, H.K.J. Powell and W.T. Robinson, *Aust. J. Chem.*, 1972, **25**, 747.
6. R.K. Murmann, *J. Am. Chem. Soc.*, **79**, 521, 1957.
7. M.W.A. Steenland, I. Dierck, G.G. Herman, B. Devreese, W. Lippens, J. Van Beeumen and A.M. Goeminne, *J. Chem. Soc., Dalton Trans.* 1997, 3879.
8. L. Mkhonta-Gama, PhD Thesis, University of Cape Town, 1999.
9. C. Jubert, A. Mohamadou, C. Gerard, S. Brandes, A. Tabard and J.-P. Barbier, J. *Chem. Soc. Dalton Trans.*, 2002, 2660.
10. R.J. Motekaitis, Y. Sun, A.E. Martell and M.J. Welch, *Can. J. Chem.*, 1999, **77**, 614.
11. R.J. Motekaitis, Y. Sun, A.E. Martell and M.J. Welch, *Can. J. Chem.*, 1999, **77**, 614.
12. D. Chen, Y. Sun, A. E. Martell, M. J. Welch, *Inorg. Chim. Acta*, 2002, **335**, 119.
13. X.H. Bu, D.L. An, X.C. Cao, R.H. Zhang, T. Clifford and E. Kimura, *J. Chem. Soc., Dalton Trans.* 1998, 2247.
14. M.-A. Santos, M. Gaspar and M.T. Amorim, *Inorg. Chim. Acta*, 1999, **284**, 20.
15. V. Amendola, L. Fabbrizzi, C. Mangano, P. Pallavicini, A. Perotti and A. Taglietti, *J. Chem. Soc., Dalton Trans.* 2000, 185.
16. V. Amendola, C. Brusoni, L. Fabbrizzi, C. Mangano, H. Miller, P. Pallavicini, A. Perotti and A. Taglietti, *J. Chem. Soc., Dalton Trans.* 2001, 3528.
17. X.-C. Su, Z.-F. Zhou, H.-K. Lin, S.-R. Zhu, H.-W. Sun, G.-H. Zhao and Y.-T. Chen, *Can. J. Chem.* 2001, **79**, 221.

18. A. Jancso, I. Torok, L. Korecz, A. Rockenbauer and T. Gadja, *J. Chem. Soc. Dalton Trans.*, 2002, 2601.

19. G.E. Jackson and M.J. Kelley, *J. Chem. Soc., Dalton Trans.*, 1989, 2429.

20. G.E. Jackson and J.G. Du Toit, *J. Chem., Dalton Trans.*, 1991, 1463.

21. C.F. Baes, Jr. and R.E. Mesmer, The Hydrolysis of Cations, A Wiley-Interscience Publication, 1976, 137,

22. S. Kholeif and G. Anderegg, *Inorg. Chim. Acta.* 1997, **257**, 225.

23. G.C. de Witt, P.M. May, J. Webb and G.Hefter, *Inorg. Chim. Acta.* 1998, **275-276**, 37.

24. E. Kimura, T. Shiota, T. Koike, M. Shiro and M. Kodama, *J. Am. Chem. Soc.*, 1990, **112**, 5805-5811.

25. M. Krauss and D.R. Garmer, *J. Am. Chem. Soc.* 1991, **113**, 6426.

26. E.D. Getzoff, J.A. Tainer, P.K. Weiner, P.A. Kollman, J.S. Richardson and D.C. Richardson, *Nature*, 1983, **306**, 287.

27. T. Koike and E. Kimura, *J. Am. Chem. Soc.* 1991, **113**, 8935.

28. T. Koike, T. Abe, M. Takashi, K. Ohtami, E. Kimura and M. Shiro, *J. Chem. Soc. Dalton Trans.*, 2002, 1764.

29. NIST STANDARD REFERENCE DATABASE 46, NIST CRITICALLY SELECTED STABILITY CONSTANTS OF METAL COMPLEXES DATABASE, VERSION 3.0, compiled by R.M. Smith and A.E. Martell, US Department of Commerce, NIST, USA.

30. R.G. Pearson, *J. Am. Chem. Soc.*, 1985, **107**, 6801.

31. A.E. Martell and R.D. Hancock, Metal Complexes in Aqueous Solutions, 1996, Plenum Press, New York.

32. R.D. Shannon, *Acta Crystallogr. Sect. A.*, 1976, **32**, 751.

33. M. Micheloni, P. Paoletti and A. Sabatini, *J. Chem. Soc., Dalton Trans.* 1983, 1189.

34. P. Comba, A. Fath, A. Kuhner and B. Nuber, *J. Chem. Soc., Dalton Trans.* 1997, 1889.

35. K.V. Damu, M.S. Shaikjee, J.P. Michael, A.S. Howard and R.D. Hancock, *Inorg. Chem.* 1986, **25**, 3879.

36. C. Kallay, K. Varnagy, I. Sovago, D. Sanna and G. Micera, *J. Chem. Soc., Dalton Trans.* 1998, 92.

37. A.B.P. Lever, *Studies in physical and theoretical chemistry - Inorganic Electronic Spectroscopy*, 2nd Ed., 1984, 507.

38. E.J. Billo, *J. Inorg. Nucl. Chem. Lett.* 1974, **10**, 613.

39. E.A. Enyedy, H. Csoka, I. Lazar, G. Micera, E. Garriba and E. Farks, *J. Chem. Soc., Dalton Trans.*, 2002, 2632.

40. M. J.-Bojczuk, W. Lesniak, W. Szczepanik, K. Gatner, A. Jezierski, M. Smoluch and W. Bal, *J. Inorg. Biochem.* 2001, **84**, 189.

41. M.S. Hussain and E.O. Schlemper, *Inorg. Chem.* 1979, **18**, 2275.

42. E.G. Vassian and R.K. Murmann, *J. Am. Chem. Soc.*, 1967, **6**, 2043.

43. G.E. Jackson, P.M. May and D.R. Williams, *J. Inorg. Nucl. Chem.* 1978, **40**, 1227.

44. T.X. Xiang and B.D. Anderson, *J. Membrane Biol.* 1994, **140**, 111.

45. A. Leo, C. Hansch and D. Elkins, *Chem. Rev.*, 1971, **71**, 525.

46. A.B. Packard, J.F. Kronauge, P.J. Day and S.T. Treves, *Nucl. Med. Biol.* 1998, **25**, 531.

47. M.A. Green, *Nucl. Med. Biol.* 1987, **14**, 59.

48. M. Sri-Aran, C.J. Mathias, J.K. Lim and M.A. Green, *Nucl. Med. Biol.* 1998, **25**, 107.

49. J.S. Lewis, A. Srinivasan, M.A. Schmidt and C.J. Anderson, *Nucl. Med. Biol.* 1999, **26**, 267.

50. M.L.P. Santos, I.A. Bagatin, E.M. Pereira and A.M. Da Costa Ferreira, *J. Chem. Soc. Dalton Trans.*, 2001, 838.

51. N.A. Roberts and P.A. Robinson, *Br. J. Rheumatol.*, 1985, **24**, 128.

52. M. Yu, H. Qing, H. Guojian, Z. Shu, W. Wenqing, H. Youfeng and J.T. Kuikka, *Nucl. Med. Biol.*, 1998, **25**, 111.

53. J.-L. Pierre, P. Chautempts, S. Refaif, C. Beguin, A. El Marzouki, G. Serratrice, E. S.-Aman and P. Rey, *J. Am. Chem. Soc.*, 1995, **117**, 1905.

54. H.-L. Zhu, L.-M. Zheng, D.-G. Fu, X.-Y. Huang, M.-F. Wu and W.-X. Tang, *J. Inorg. Biochem.*, 1998, **70**, 211.

55. C.-J. Feng, Q.-H. Luo, Z.-L. Wang, M.-C. Shen, H.-W. Wang and M.-H. Zhao, *J. Inorg. Biochem.*, 1999, **75**, 1.

56. G. Tabbi, W.L. Driessen, J. Reedijk, R.P. Bonomo, N. Veldman and A.L. Spek, *Inorg. Chem.* 1997, **36**, 1168.

57. Q. Yu, C.A. Salhi, E.A. Ambudo, M.A. Heeg, L.A. Ochrymowyez and D.B Rorabacher, *J. Am. Chem. Soc.*, 2001, **123**, 5720.

58. J.A. Roe, A. Butler, D.M. Scholler, J.S. Valentine, L. Marky and K.J. Breslauer, *Biochemistry*, 1988, **27**, 950.

59. A. Voye, PhD Thesis, University of Cape Town, 1993.

60. T.M. J.-Wilson, K.A. Deal, C.J. Anderson, D.W. McCarthy, Z. Kovacs, R.J. Motekaitis, A. D.-Sherry, A.E. Martell and M.J. Welch, *Nucl. Med. Biol.* 1998, **25**, 523.

61. P.J. Blower, J.S. Lewis and J. Zweit, *Nucl. Med. Biol.* 1996, **23**, 957.

62. B. Sarkar, *J. Inorg. Biochem*, 2000, **79**, 187.

CHAPTER 6

Overall discussion and Conclusion

6.11 Introduction

The past two decades or so have seen a considerable surge of interest in the co-ordination chemistry of copper(II) and gadolinium(III) in biomedical analyses.[1] In fact, some Cu^{2+} and Gd^{3+} complexes are currently used while others are under further development as diagnostic and/or therapeutic agents. This resurgence of interest in metal-ion therapeutics and diagnostic agents stems from an advanced understanding of biological structure and function.[1]

Recently, effort has been directed at the design and synthesis of gadolinium(III)-based contrast agents in MRI.[1] Gd^{3+} is ideally suited to this because of its high magnetic moment and hence high relaxivity resulting from its seven unpaired electrons. The majority of these contrast agents contain multi-chelating poly(aminocarboxylate) ligands to increase the thermodynamic stability of the complexes. Preorganised macrocyclic ligands containing pendant carboxylates are becoming preferred systems for this purpose.[1]

The role of copper(II) in several biological systems and processes is well known.[1,2] Copper(II) is normally present in low molecular weight species and in the active sites of metallo-enzymes such as copper-zinc SOD.[2] The elevation of copper(II) complex species in the plasma and synovial fluids of rheumatoid arthritic (RA) patients is also well documented.[2] This indicates some involvement of copper in this disease. In addition, a number of Cu^{2+} chelates have been shown to exhibit anti-inflammatory activity.[1,2]

A further review of literature has shown that the metal ion is unable to reach ribosomes and therefore, fails to be incorporated into the relevant enzyme systems.[2] For RA sufferers, this is indicative of a defective Cu^{2+} 'carrier' being present only within the plasma resulting in the metal ion being unable to partition across the plasma membrane barrier as an initial step into entering the cytosol.[2]

Several studies have pursued the goal of designing chemically stable copper complexes for their end use as anti-arthritic human pharmaceutical agents.[3-5] It appears that a `carrier ligand, L, which can complex copper and enhance its

transportation across a membrane is required. The initial goal has been to maximize the number of nitrogen donor atoms in the ligand, thereby increasing the stability of the resulting complex to *in vivo* dissociation.[3] This ligand should be reasonably lipophilic and must possess one or two dissociable protons to give neutral copper(II) species. These neutral and lipophilic species are known to be capable of permeating membrane.

However, for this ligand to be of potential application in the treatment of RA, it must be able to either compete with histidine for copper in plasma or form ternary complexes of the type Cu-Histidine-L.[2] Such a ligand must also bind copper selectively from calcium(II) and zinc(II), as these are potential competitors *in vivo*.[3-5] It is a well known fact that none of the first transition metal ions, including calcium(II) matches copper(II) in its ability to form stable chelates with ligands containing predominantly nitrogen donor atoms. Ligands of choice should resemble 3,3,9,9-tetramethyl-4,8-diazaundecane-2,10-dione dioxime (L^1) which appears to be promising in this regard.[4,5]

The real challenge pertaining to the design of functional metal-containing agents is the need for a precise control of the metal-ion inner coordination sphere. Such control is necessary to enhance the chemical stability of the species sought *in vivo*.[1] Metal complexes that will ultimately prove successful in chemotherapy and as contrast agents in MRI must meet numerous criteria. These include high efficacy and an overall image enhancement, low toxicity *in vivo*, tissue and organ specificity and rapid clearance by the biological system.

Despite these challenges, researchers are striving to develop new ligand systems that simultaneously offer biomimicry, biostability, biocompatibility and bioactivity. Successful research in this area will be able to produce therapeutic agents and biomimetic agents that will be useful and safe for *in vivo* applications.[1]

This study investigated the solution equilibria of H^+, Cu^{2+}, Ni^{2+}, Zn^{2+}, and Gd^{3+} with L^2 and L^3 as well as those of Gd^{3+} with L^1 at 25^0C and at 0.15 *mol* dm^{-3} Cl^- (Na^+) using glass-electrode potentiometry. The interest is centered on the possible use

of the copper and gadolinium complexes in chemotherapy and as contrast agents in MRI respectively.

The interest in L^2 and L^3 stems from the fact that these two ligands resemble oligopeptides. It has been observed that a variety of receptors expressed on cell surfaces are able to bind small peptides with high affinity.[6] However, the widespread use of oligopeptides is limited by their short biological half-life resulting from their enzymatic hydrolysis.

Furthermore, complex formation of these ligands with copper, in particular, is relatively instantaneous. These ligands can also be attached to biologically important molecules directly or indirectly using a linker for local targeting.

6.12 Protonation and formation constants

L^1, L^2 and L^3 have been found to take up two or three protons in the pH range 2-11. In L^1 and L^3 these correspond to proton additions to the secondary and tertiary amino groups respectively. In contrast, for L^2, these correspond to protonation of the negatively charged oxime oxygens. The observed protonation constants agree with those which had been published previously for these ligands or their analogues.

On the basis of the complex formation and deprotonation functions, the constants reported in Table 5.2 where chosen as the best possible to describe the solution thermodynamics of these systems. Moreover, the reasonably low standard deviations in $\log\beta_{pqr}$'s and Hamilton R-factors further confirm the validity of the potentiometric model used in data analysis.

Substantial variations in the determined formation constants are reflected in the $\log\beta_{pqr}$ values, which vary according to the sequence $Ca^{2+} \approx Gd^{3+} < Ni^{2+} < Cu^{2+} > Zn^{2+}$. This is the predicted Irving-Williams stability order normally observed for divalent first row transition elements.

Copper and nickel form reasonably stable mononuclear complexes of 1:1 ratio with both L^2 and L^3 ligands. In fact, MLH_{-1} and MLH_{-2} are the predominant species at pH values above 6.5. In L^2 systems, these species are formed by stepwise dissociation

of the oxime protons following the initial deprotonation of the amide nitrogens. The indication from the formation constants is that Ni^{2+} and Cu^{2+} sit in a more or less square-planar environment of nitrogen donor atoms in $[ML^2H_{-1}]$ and $[ML^2H_{-2}]$.

On the other hand, the formation of these species in L^3 complexes is as a result of metal ion assisted stepwise dissociation of the amide protons. For copper, however, the calculated second $pK_{ML\text{-}OH}$ value defined as the difference between $\log\beta_{11\text{-}1}$ and $\log\beta_{11\text{-}2}$ is 7.78. This value is close to the hydrolysis constant of Cu^{2+} which is 7.87 and 0.56 log units lower than the second deprotonation constant (pK_{NH}) of the tertiary amine, which is equal to 8.43. For this reason it is difficult to propose with certainty the origin of this proton loss from potentiometric data alone. Copper(II) complexes are known to be destabilised by bigger membered rings such as those that can be formed by coordination of both terminal amines in L^3. It is postulated therefore that the two amide nitrogens, the tertiary central amine and one of the terminal amino groups are all coordinated to copper in the $[CuL^3H_{-1}]^+$ species. In this complex, the second terminal amine is protonated and the formation of the neutral $[CuL^3H_{-2}]^0$ is due to the deprotonation of this group. There is no evidence of coordination of this last amino group as expected for Cu^{2+} in a tetragonal distorted octahedral environment.

Ni^{2+} forms a stable 110 complex ($\log\beta_{110}$=7.57) and the $pK_{ML\text{-}OH}$ associated with its formation is 8.53. This $pK_{ML\text{-}OH}$ is 1.5 log units lower than its first hydrolysis constant indicating a possibility of a metal ion promoted dissociation of the amide proton. It has been observed that the metal ion deprotonates these amide groups with difficulty indicating another possibility of an ionisation of a coordinated water molecule to form a 110, although unlikely from the calculated $pK_{ML\text{-}OH}$. Ni^{2+} does not seem to form the 11-1 species. Instead, the neutral 11-2 complex is formed by deprotonation of the second amide group. If the 11-2 species is formed by simultaneous deprotonation of the two amide groups, this complexation behaviour is reminiscent of macrocylic diamide systems. This species is believed to be stabilised by the coordination of all five nitrogen donor atoms. Full investigation of the Ni^{2+}-L^3 system was limited to pH 9.0 due to precipitation of the neutral 11-2 species.

L^3 is believed to form distorted octahedral species with these metal ions. It appears that L^3 is unable to enforce a square planar type of coordination observed with

L^1 and L^2. A more likely explanation for this behaviour is the presence of the two contiguous six-membered rings involving the central anchoring tertiary amine. The folding of these less stable six-membered rings may distort the trans-equatorial coordination of the two amide nitrogens as shown in figure 6 (i), (j) and (k).

With the exception of Gd^{3+} and L^1, the other metal ions form very weak complex species with the studied ligands. Their equilibria as a result are characterised by protonated MLH_x^{n+} (x=1,2) and mixed-hydroxo species. One possible reason for this weak coordinating ability of these metal ions is their inability to deprotonate the amide nitrogens. In fact, Co^{2+}, Cu^{2+} and Ni^{2+} are the only first row transition elements which are capable of deprotonating these amide moieties. Although Gd^{3+} forms stable 110, 11-1 and 11-2 complexes with L^1, above pH 10, this system precipitates out of solution, probably as the neutral 11-3 species.

Ligand selectivities for Cu^{2+} over Zn^{2+} and Ca^{2+} are 9-11 orders of magnitude higher. Overall, the potentiometric results confirmed the high affinity of the ligands donor atoms towards copper as was indicated in the introductory remarks.

6.13 Blood-plasma simulation studies

Zinc(II) and calcium(II) ions being present in blood-plasma in large concentrations are regarded as potential competitors of copper(II) *in vivo*. The fact that calcium(II) does not form or only form very weak complexes with L^1, L^2 and L^3, precludes this ion from being a competitor of copper(II).

It has long been postulated that Zn^{2+} species are likely to predominate at physiological pH because of its high concentration and the ability to form complex species at this pH. Figure 5.26 reveals that, at L^1 and L^2 concentration of 10^{-6} *mol dm*$^{-3}$ and 10^{-3} *mol dm*$^{-3}$ respectively, both the Zn^{2+} and Ca^{2+} p.m.i.'s are less than 0.01. In contrast, the calculated Cu^{2+} p.m.i.'s are an order of magnitude greater. L^3 on the other hand, has no mobilising ability at these concentrations. In fact, the selectivity and mobilising ability order is $L^1 > L^2 > L^3$. These calculations indicated that the dipositively charged $[GdL^1H_{-1}]^{2+}$ is capable of surviving *in vivo* although Cu^{2+} is likely to induce trans-metallation because of its high affinity for L^1 nitrogen donor

atoms. Overall the Gd^{3+} complexes of these ligands in their present form would be of no use as contrast agents in MRI.

On the basis of these calculations, it is therefore predicted that exogenously administered L^1 and L^2 ligands can compete and successfully mobilise copper(II) *in vivo* without altering the equilibria of this metal's competitors. This is an important result in the development of copper anti-inflammatory drugs for rheumatoid arthritis.

6.14 UV-VIS spectroscopy

Because copper(II) and nickel(II) form coloured chelates with these ligands, the co-ordination geometries of the complex species present in solution have been confirmed by UV/VIS spectrophotometry. The spectroscopic measurements indicate that both Cu^{2+} and Ni^{2+} sit in a square-planar environment of nitrogen donor atoms of the L^2 ligand for 11-1 and 11-2 complex species. L^3, on the other hand, is believed to form tetragonally distorted octahedral 11-1 and 11-2 species with Cu^{2+}. As suggested from potentiometric data, there is no spectroscopic evidence of coordination of five L^3 nitrogen donor atoms towards Cu^{2+} nor the loss of a proton from an axially coordinated water molecule. The geometries of potentiometrically detected Ni^{2+}-L^3 species could not be predicted because of the low binding ability of this ligand towards the metal ion and precipitation above pH 9.0.

The smooth convoluted calculated individual spectra of the complex species further support the correctness of the potentiometric model used in data analysis.

6.15 Crystal structure, MM calculations and MD simulations

The $[NiL^1H_{-1}]^+$ was precipitated as a perchlorate, with a molecular formula (M_r) of 429.55 *g/mol*. This crystal system is orthorhombic with a space group-Pbca(#61). However, Hussain and Schlemper reported the $P2_12_12_1$ space group for the $NiL^1H_{-1}]^+Cl.H_2O$ system. Since, there is no chiral carbon in this molecule, it is thus believed that the presently reported space group is the correct one. Despite this discrepancy, the other differences are expected in view of the different counter-ions used and the presence of the water of crystallisation.

This crystal structure further attests to the square-planar N_4 coordination postulated previously from potentiometric and UV/VIS data.[5] MD simulations of $[NiL^1H_{-1}]^+$ species indicate very little conformational changes compared to the observed crystal structure. The exceptions are the relative orientations of the central propylene carbons. These simulations indicate that the conformation in the crystal structure is probably the stable one in solution.

Because of this excellent agreement between the simulated and crystal structures of the $[NiL^1H_{-1}]^+$ species, these simulations were extended to the corresponding Cu^{2+} and Zn^{2+} complexes. The simulated $[CuL^1H_{-1}]^+$ further confirms the square-planar structure predicted from UV/Vis data.[4] There are relatively few available techniques to study Zn^{2+} systems in aqueous solution. Because it was not easy to prepare $[ZnL^1H_{-1}]^+$ crystals suitable for X-ray diffraction studies, these MD simulations were of great value in understanding the geometry of this species. In fact, the simulated $ZnL^1H_{-1}]^+$ species indicates that the metal ion sits in a square-planar environment of the ligand's donor atoms. These results confirm an earlier postulation[5] that the low formation constants observed for the zinc(II) complexes are due to square-planar arrangement of donor atoms of the ligands around the metal ion.

6.16 Partition coefficients

The ligands L^2 and L^3 were designed with the hope that the dominant copper(II) complex at pH 7.4 would be the neutral $[CuLH_{-2}]^0$ species. However, the species distribution diagrams in Figure 5.5(a) and (b) show that this metal ion is approximately 80% and 20% present as the single negatively and positively charged $[MHL_{-1}]$ at physiological pH for L^2 and L^3 respectively. This is in sharp contrast to the previously studied L^1 ligand,[4] which was observed to be approximately 100% present as the $[CuL^1H_{-1}]^+$ in the pH range 4.0-9.0.

In general, methyl and aryl groups are known to increase the lipophilicity of molecules, hence the ligands were designed with this fact in mind. Octanol/water partition coefficients, in the form of $logP_{oct/water}$, were determined as a measure the lipophilicity of the copper complexes. These studies indicated that the copper(II) complexes of these ligands are largely hydrophilic. In fact, the observed log $P_{oct/water}$

values varied between -2.10 and -1.25. These values are closer to the previously reported values for copper(II) complexes of L^1 and other diamide dioximes ligand systems.

The hydrophilic nature of these complexes stems from: (i) hydrogen bonding between the non-coordinated neutral carbonyl oxygens and negatively charged oxygens and the water molecules, and (ii) the presence of coordinated water molecules. Hydrogen bonding to solvent water molecules is possible in complexed L^2 and L^3 ligands due to the presence of deprotonated oxime group(s) and protonated nitrogen sites respectively.

Although these [$CuLH_{-1}$] complexes are largely hydrophilic, at least 2-6% of these species is extracted into the octan-1-o1 phase. This result suggests that a similar amount of these complexes is likely to permeate the skin and cell membranes when applied transdermally.

6.17 Superoxide Dismutase Mimic Activities

Accumulating evidence indicates that reactive oxygen free radicals such as the superoxide ($O_2^{\cdot-}$) are involved in the pathogenesis of rheumatoid arthritis. It has, however, been observed that copper(II) complexes are able to dismute this $O_2^{\cdot-}$ radical to water and hydrogen peroxide. This study investigated whether the presently studied copper complexes are capable of catalysing the superoxide dismutation by making use of the classical NBT assay.

The results indicate that the copper(II) complexes of these ligands exhibit IC_{50} values in the range of 8.0-110 $\mu mol\ dm^{-3}$. These values are 2-4 orders of magnitude higher than those of the corresponding complexes of cryptand and the native Cu_2Zn_2-SOD enzyme. These studies reveal that the investigated copper complexes are poor mimetics of the native SOD enzyme. This result should be expected since potentiometric studies suggest that all three ligands are reasonably stronger chelators of copper(II). Furthermore, the competitive binding of EDTA (used to simulate *in vivo* ligands) to Cu^{2+} to yield copper-EDTA complexes which are poor mimics of the enzyme cannot be ruled out.

Moreover, it is known that the enzyme is capable of accommodating both the Cu^{2+} and Cu^{+} in its 'entactic' state. Accumulating evidence also indicates that the enzyme is much more stable in its reduced state than in its oxidised form. It appears that Cu^{2+} in the enzyme is coordinatively unsaturated in contrast to the high donor field exhibited by the present ligands. In addition, it has been observed that the presence of positively charged groups at the active site increase the rate of approach of the $O_2^{\cdot-}$ ion towards the metal ion.

6.18 Biodistribution studies on mice

On the basis of the above observations it was demeed necessary to perform biolocalization experiments on mice as animal screens. This was accomplished by intravenous injection of these animals with a dilute solution of ^{64}Cu-labeled [$CuLH_{-1}$].

The biodistribution studies revealed a rapid clearance of these complexes from the blood. Significant uptake of these complexes by the liver was observed. In fact, more than half of the total activity was recorded in this organ six hours postinjection. The high uptake of these complexes by this organ is expected since copper metabolism occurs here. This copper is excreted by the hepatobiliary route, hence the observed high activity in the intestines. In addition, there was a noticeable uptake by the muscle, lung and heart partly due to the reasonably high lipophilicity of these species and the high perfused nature of these organs.

As expected for negatively charged species, the $^{64}Cu[CuL^2H_{-1}]^-$ was observed to be excreted exclusively by the renal route. This observation indicates that this complex or its derivatives thereof could be investigated for imaging the renal system. These studies further confirmed that the Cu-L^1/L^2 complexes are able to survive *in vivo* as reflected by their long biological half-life. In fact, these copper complexes merit further evaluation and development as anti-arthritic agents.

6.19 Future studies

The strategy of designing copper chemotherapies for RA to improve their therapeutic effectiveness should be re-evaluated in light of these findings. For copper chemotherapy various possibilities exist which include the replacement of the amide

moieties by amino groups. The nitrogen atoms of amide groups are poor donors for metal ions in general, and copper(II) in particular. The reduction of these amide groups and subsequent replacement by amino groups would confer an enhanced chemical stability to the resulting complexes.

In fact, an increase of about two log units is expected for such modification from H_2pap (L^2) and BIDPAP (L^3) to Hpap (L^5) and BIMPAP (L^6) respectively. These modifications are demonstrated in Figure 6.1. The 11-1 Hpap complex species would be further stabilised by the hydrogen bond between the hydroxyimino groups compared to the corresponding H_2pap complex.

Furthermore, the close proximity of this amino group to one of the nitrogens of the oxime moiety (L^5) and to the anchoring tertiary benzylamine (L^6) would enhance a stronger complexation behaviour of these ligands towards copper(II). In addition, the two contiguous six-membered rings observed in the $[CuL^3H_{-1}]$ and $[CuL^3H_{-2}]$ complexes have been observed to decrease the thermodynamic stability of these species. An increase of about 1 to 1.5 log units in the stability of the $[CuL^6H_{-1}]$ complex is predicted if one of the six-membered rings is converted to a five-membered chelate ring.

L^1 and L^2 (as well as its afore-mentioned derivative) can be further functionalised by incorporating one or more methyl groups in the propylene bridge connecting the diaza and/or diamide groups. The modifications are also demonstrated in L^4 and L^5. These methyl groups would increase the lipophilicity of the resulting complexes without destabilising them. $LogP_{oct/aq}$ values in the range of -1.0 to 0.0 are expected for these methylated derivatives.

The octanol/water partition coefficients of L^1, L^2 and L^3 copper complexes are lower than the value ($logP_{oct/aq}$=0.6) believed to be optimal for brain and/or myocardial uptake.[7] However, it is hoped, that the above-mentioned derivatives will have lipophilicities meriting them for further investigation for use in myocardial imaging with copper radio-isotopes. The resulting complexes may also serve as suitable candidates for copper chemoradiotherapy.

Figure 6.1: Structures of ligands of future interest

(a)

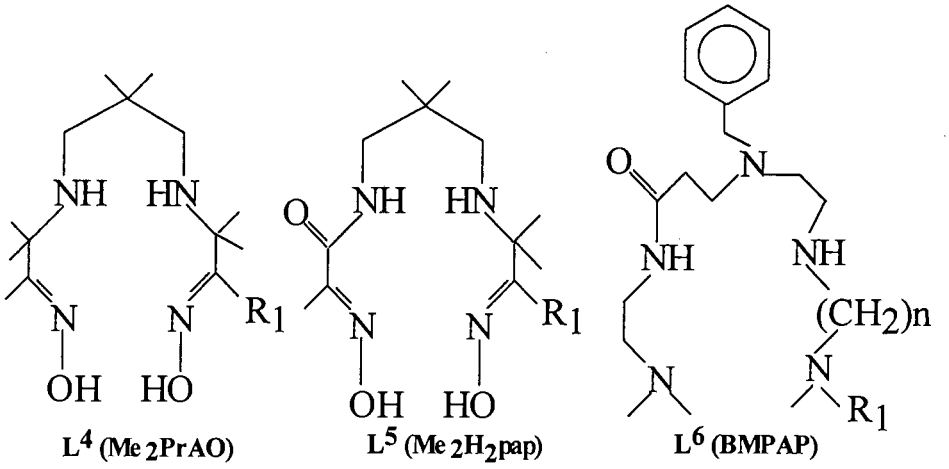

L^4 (Me_2PrAO) L^5 (Me_2H_2pap) L^6 (BMPAP)

R = -H_2N-Ala-Gly-Cys-Lys-Asn-Phe -**Phe-Trp**Somatostatin
HO-Cys-Ser-Thr-Phe-**Thr-Lys**

R_1=-H_2N-(D)Phen-Cys-**Phen-(D)Trp** Octreotide
(ol)-Thr-Cys-**Thr-Lys**

n=2,3

(b)

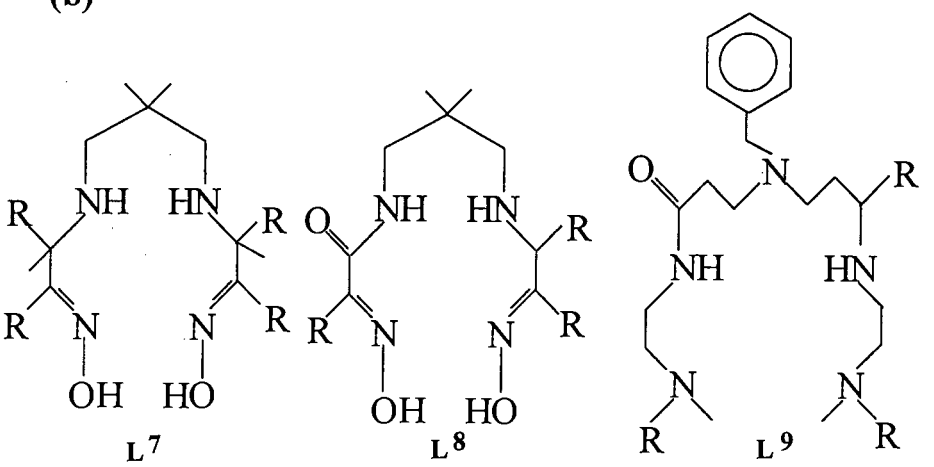

L^7 L^8 L^9

R = -CH_2COOH, $CH_2PO_2H_2$ or -$CH_2PO_2H(OC_2H_5)$

The design of Gd^{3+}-based contrast agents would require the incorporation of pendant carboxylate and phosphonate groups in these ligands' backbone. The former should be used as extracellular agents while the latter could be directed towards bone-like matrices. However, since the aqueous chemistry of Gd^{3+} parallels that of Ca^{2+} in many ways, these ligands are likely to co-ordinate to the latter metal ion. The high coordination numbers (8-9) exhibited by these ligands compatible with those of Gd^{3+} should exclude effective competition with Ca^{2+}. This is due to the fact that Ca^{2+} is restricted to coordination numbers 4-6. Although eight (8) is a very common coordination number for calcium(II), the two extra binding sites are normally occupied by solvent (water) molecules rather than the nitrogen donor atoms of the ligand whereas gadolinium(III) coordinates strongly to these nitrogens.

The results of the present study are encouraging enough to merit progression to the next stages of drug development. These might include the design of proper vehicles for enhancing copper permeation across the skin. The species can be incorporated into liposomes or attached to biologically relevant molecules such as the somatostatin analogues (octreotide or octreotate) for local targeting. The use of the somatostatin analogues is important for imaging of pancreatic receptors. It should be emphasised that the four amino acids shown in bold-face in Figure 6.1 (a) constitute the bioactive receptor-binding β-turn portion of the hormone.

The synthetic methods presented in Chapter 4.2 should be suitable for preparing some of these derivatives if proper starting materials are used.

References

1. D.E. Reichert, J.S. Lewis and C.J. Anderson, *Coord. Chem. Rev.*, 1999, **184**, 3.
2. S.H. Laurie and E.S. Mohammed, *J. Chem. Soc., Dalton Trans.*, 1995, 129.
3. G.E. Jackson and M.J. Kelly, *J. Chem. Soc., Dalton Trans.*, 1989, 2429.
4. G.E. Jackson and B.S. Nakani, *J. Chem. Soc., Dalton Trans.*, 1996, 1373.
5. T.E. Nomkoko, MSc Thesis, University of Transkei, Umtata, South-Africa, 1999.
6. A. Signore, A. Annovazzi, M. Chianelli, F. Corsetti, C. Van de Wiele, R.N. Watherhouse, F. Scopinaro, *Eur. J. Nucl. Med.*, 2001, **28**, 1555.
7. J.S. Lewis, A. Srinivasan, M.A. Schmidt and C.J. Anderson, *Nucl. Med. Biol.* 1999, **26**, 267.
8. M. Sri-Aran, C.J. Mathias, J.K. Lim and M.A. Green, *Nucl. Med. Biol.* 1998, **25**, 107.
9. M. Yu, H. Qing, H. Guojian, Z. Shu, W. Wenqing, H. Youfeng and J.T. Kuikka, *Nucl. Med. Biol.*, 1998, **25**, 111.
10. T.M. J.-Wilson, K.A. Deal, C.J. Anderson, D.W. McCarthy, Z. Kovacs, R.J. Motekaitis, A. D.-Sherry, A.E. Martell and M.J. Welch, *Nucl. Med. Biol.* 1998, **25**, 523.
11. L.M. Guerdoud, R. Ouellet, J.E. Van Lier, *Nucl. Med. Biol.*, 1994, **21**, 437.

Appendix

Table 1. Crystal data and structure refinement for TN1_NI.

Identification code	tn1_ni
Empirical formula	C13 H27 Cl N4 Ni O6
Formula weight	429.55
Temperature	197(2) K
Wavelength	0.71073 A
Crystal system, space group	Orthorhombic, Pbca (#61)
Unit cell dimensions	a = 13.3960(10) A alpha = 90 deg. b = 12.3490(10) A beta = 90 deg. c = 21.9330(10) A gamma = 90 deg.
Volume	3628.3(4) A^3
Z, Calculated density	8, 1.573 Mg/m^3
Absorption coefficient	1.254 mm^-1
F(000)	1808
Crystal size	0.25 x 0.23 x 0.20 mm
Theta range for data collection	1.86 to 27.51 deg.
Limiting indices	-17<=h<=12, -16<=k<=12, -28<=l<=28
Reflections collected / unique	18035 / 4146 [R(int) = 0.0397]
Completeness to theta = 27.51	99.3 %
Absorption correction	Empirical (Scalepack)
Max. and min. transmission	0.7875 and 0.7445
Refinement method	Full-matrix least-squares on F^2
Data / restraints / parameters	4146 / 0 / 236
Goodness-of-fit on F^2	1.030
Final R indices [I>2sigma(I)]	R1 = 0.0294, wR2 = 0.0664
R indices (all data)	R1 = 0.0417, wR2 = 0.0708
Largest diff. peak and hole	0.370 and -0.318 e.A^-3

Table 2. Atomic coordinates (x 10^4) and equivalent isotropic displacement parameters (A^2 x 10^3) for TN1_NI.
U(eq) is defined as one third of the trace of the orthogonalized Uij tensor.

---

	x	y	z	U(eq)
Ni(1)	392(1)	5271(1)	4179(1)	18(1)
O(1)	599(1)	6706(1)	5191(1)	27(1)
N(2)	131(1)	6505(1)	4649(1)	20(1)
C(3)	-514(1)	7195(1)	4456(1)	22(1)
C(4)	-968(1)	6891(1)	3848(1)	23(1)
N(5)	-871(1)	5669(1)	3816(1)	21(1)
C(6)	-1197(2)	5197(2)	3224(1)	29(1)
C(7)	-949(1)	3998(1)	3190(1)	28(1)
C(8)	161(1)	3799(2)	3131(1)	27(1)
N(9)	678(1)	3979(1)	3722(1)	21(1)
C(10)	1793(1)	3805(2)	3696(1)	28(1)
C(11)	2183(1)	4228(2)	4298(1)	27(1)
N(12)	1599(1)	4911(1)	4560(1)	22(1)
O(13)	1899(1)	5364(1)	5097(1)	28(1)
C(14)	-765(2)	8221(2)	4774(1)	33(1)
C(15)	-2055(2)	7247(2)	3802(1)	39(1)
C(16)	-340(2)	7412(2)	3343(1)	35(1)
C(17)	3193(2)	3950(2)	4536(1)	41(1)
C(18)	2040(2)	2599(2)	3608(1)	45(1)
C(19)	2246(2)	4489(2)	3181(1)	42(1)
Cl(20)	580(1)	5745(1)	1619(1)	29(1)
O(21)	-322(1)	5159(2)	1731(1)	61(1)
O(22)	429(1)	6569(1)	1172(1)	53(1)
O(23)	1332(1)	5009(1)	1414(1)	61(1)
O(24)	914(1)	6242(1)	2172(1)	56(1)

Table 3. Bond lengths [A] and angles [deg] for TN1_NI.

Ni(1)-N(2)	1.8720(14)
Ni(1)-N(12)	1.8731(15)
Ni(1)-N(9)	1.9238(14)
Ni(1)-N(5)	1.9332(14)
O(1)-N(2)	1.3654(18)
N(2)-C(3)	1.287(2)
C(3)-C(14)	1.485(2)
C(3)-C(4)	1.513(2)
C(4)-N(5)	1.516(2)
C(4)-C(15)	1.524(3)
C(4)-C(16)	1.532(3)
N(5)-C(6)	1.490(2)
C(6)-C(7)	1.519(3)
C(7)-C(8)	1.513(3)
C(8)-N(9)	1.487(2)
N(9)-C(10)	1.511(2)
C(10)-C(11)	1.513(3)
C(10)-C(19)	1.535(3)
C(10)-C(18)	1.537(3)
C(11)-N(12)	1.287(2)
C(11)-C(17)	1.490(3)
N(12)-O(13)	1.3640(19)
Cl(20)-O(22)	1.4266(16)
Cl(20)-O(23)	1.4290(17)
Cl(20)-O(21)	1.4302(16)
Cl(20)-O(24)	1.4320(16)

N(2)-Ni(1)-N(12)	96.23(6)
N(2)-Ni(1)-N(9)	178.01(6)
N(12)-Ni(1)-N(9)	82.22(6)
N(2)-Ni(1)-N(5)	81.75(6)
N(12)-Ni(1)-N(5)	177.70(6)
N(9)-Ni(1)-N(5)	99.78(6)
C(3)-N(2)-O(1)	118.32(14)
C(3)-N(2)-Ni(1)	118.91(12)
O(1)-N(2)-Ni(1)	122.77(10)
N(2)-C(3)-C(14)	124.22(16)
N(2)-C(3)-C(4)	113.33(15)
C(14)-C(3)-C(4)	122.39(15)
C(3)-C(4)-N(5)	104.63(13)
C(3)-C(4)-C(15)	111.74(15)
N(5)-C(4)-C(15)	111.50(14)
C(3)-C(4)-C(16)	108.15(15)
N(5)-C(4)-C(16)	109.77(14)
C(15)-C(4)-C(16)	110.83(16)
C(6)-N(5)-C(4)	113.78(13)
C(6)-N(5)-Ni(1)	121.14(11)
C(4)-N(5)-Ni(1)	108.04(10)
N(5)-C(6)-C(7)	111.06(14)
C(8)-C(7)-C(6)	112.20(15)
N(9)-C(8)-C(7)	111.05(14)
C(8)-N(9)-C(10)	113.99(14)
C(8)-N(9)-Ni(1)	119.08(11)
C(10)-N(9)-Ni(1)	109.53(11)
N(9)-C(10)-C(11)	105.01(14)
N(9)-C(10)-C(19)	109.95(16)
C(11)-C(10)-C(19)	108.39(16)
N(9)-C(10)-C(18)	110.78(16)
C(11)-C(10)-C(18)	111.68(17)
C(19)-C(10)-C(18)	110.85(18)
N(12)-C(11)-C(17)	123.09(18)
N(12)-C(11)-C(10)	114.06(16)
C(17)-C(11)-C(10)	122.65(17)
C(11)-N(12)-O(13)	118.41(15)
C(11)-N(12)-Ni(1)	118.69(13)
O(13)-N(12)-Ni(1)	122.87(11)
O(22)-Cl(20)-O(23)	109.73(12)
O(22)-Cl(20)-O(21)	111.02(11)
O(23)-Cl(20)-O(21)	109.15(11)
O(22)-Cl(20)-O(24)	108.74(10)
O(23)-Cl(20)-O(24)	108.61(12)
O(21)-Cl(20)-O(24)	109.55(12)

Table 4. Anisotropic displacement parameters (A^2 x 10^3) for TN1_NI. The anisotropic displacement factor exponent takes the form: -2 pi^2 [h^2 a*^2 U11 + ... + 2 h k a* b* U12]

	U11	U22	U33	U23	U13	U12
Ni(1)	16(1)	19(1)	18(1)	0(1)	-1(1)	0(1)
O(1)	30(1)	32(1)	20(1)	-4(1)	-5(1)	1(1)
N(2)	20(1)	23(1)	18(1)	0(1)	0(1)	-2(1)
C(3)	20(1)	23(1)	24(1)	1(1)	3(1)	-1(1)

C(4)	23(1)	21(1)	26(1)	1(1)	-3(1)	2(1)
N(5)	19(1)	22(1)	21(1)	0(1)	-1(1)	-1(1)
C(6)	29(1)	32(1)	25(1)	-4(1)	-9(1)	2(1)
C(7)	27(1)	29(1)	27(1)	-4(1)	-4(1)	-5(1)
C(8)	31(1)	27(1)	22(1)	-4(1)	-1(1)	1(1)
N(9)	20(1)	20(1)	22(1)	0(1)	2(1)	-1(1)
C(10)	20(1)	32(1)	32(1)	-4(1)	4(1)	3(1)
C(11)	21(1)	28(1)	33(1)	2(1)	1(1)	1(1)
N(12)	20(1)	25(1)	23(1)	1(1)	-1(1)	-2(1)
O(13)	25(1)	35(1)	24(1)	-3(1)	-9(1)	0(1)
C(14)	36(1)	27(1)	35(1)	-6(1)	0(1)	7(1)
C(15)	27(1)	34(1)	55(1)	-6(1)	-11(1)	8(1)
C(16)	48(1)	28(1)	27(1)	6(1)	0(1)	-6(1)
C(17)	25(1)	50(1)	48(1)	-4(1)	-6(1)	13(1)
C(18)	35(1)	38(1)	64(2)	-17(1)	-2(1)	13(1)
C(19)	28(1)	63(2)	34(1)	0(1)	9(1)	-7(1)
Cl(20)	32(1)	24(1)	32(1)	2(1)	1(1)	-1(1)
O(21)	40(1)	61(1)	84(1)	14(1)	8(1)	-17(1)
O(22)	72(1)	46(1)	41(1)	16(1)	-10(1)	-3(1)
O(23)	46(1)	40(1)	98(2)	-23(1)	10(1)	6(1)
O(24)	82(1)	50(1)	35(1)	-4(1)	-10(1)	-2(1)

Table 5. Hydrogen coordinates (x 10^4) and isotropic displacement parameters (A^2 x 10^3) for TN1_NI.

	x	y	z	U(eq)
H(1)	1240(20)	6120(20)	5178(13)	75(9)
H(5)	-1343	5419	4094	25
H(6A)	-861	5582	2885	34
H(6B)	-1926	5297	3176	34
H(7A)	-1199	3634	3562	33
H(7B)	-1296	3675	2835	33
H(2)	276	3045	2994	32
H(8B)	442	4293	2819	32
H(9)	448	3420	3969	25
H(14A)	-1447	8179	4934	49
H(14B)	-715	8827	4487	49
H(14C)	-298	8335	5112	49
H(15A)	-2443	6901	4127	58
H(15B)	-2325	7033	3404	58
H(15C)	-2096	8035	3845	58
H(16A)	-272	8189	3423	52
H(16B)	-669	7304	2949	52
H(16C)	323	7077	3335	52
H(17A)	3368	4446	4867	62
H(17B)	3685	4014	4207	62
H(17C)	3189	3205	4690	62
H(18A)	1745	2178	3941	68
H(18B)	2766	2500	3609	68
H(18C)	1767	2349	3218	68
H(19A)	2066	4173	2786	63
H(19B)	2975	4500	3222	63
H(19C)	1988	5230	3206	63

Table 6. Torsion angles [deg] for TN1_NI.

(right-hand rule, Klyne & Prelog.(1960). Experientia,16,521)
(s.u. following Stanford & Waser, Acta Cryst.(1972).A28,213)

				Angle	s.u.
N5	-Ni1	-N2	-O1	161.79	0.00
N5	-Ni1	-N2	-C3	-18.38	0.00
N9	-Ni1	-N2	-O1	26.97	0.07
N9	-Ni1	-N2	-C3	-153.20	0.07
N12	-Ni1	-N2	-O1	-16.88	0.00
N12	-Ni1	-N2	-C3	162.95	0.00
N2	-Ni1	-N5	-C4	31.30	0.00
N2	-Ni1	-N5	-C6	164.40	0.00
N9	-Ni1	-N5	-C4	-150.26	0.00
N9	-Ni1	-N5	-C6	-17.16	0.00
N12	-Ni1	-N5	-C4	63.79	0.06
N12	-Ni1	-N5	-C6	-163.12	0.06
N2	-Ni1	-N9	-C8	154.68	0.07
N2	-Ni1	-N9	-C10	-72.30	0.07
N5	-Ni1	-N9	-C8	20.11	0.00
N5	-Ni1	-N9	-C10	153.12	0.00
N12	-Ni1	-N9	-C8	-161.28	0.00
N12	-Ni1	-N9	-C10	-28.27	0.00
N2	-Ni1	-N12	-C11	-164.86	0.00
N2	-Ni1	-N12	-O13	13.32	0.00
N5	-Ni1	-N12	-C11	162.82	0.06
N5	-Ni1	-N12	-O13	-19.00	0.07
N9	-Ni1	-N12	-C11	16.65	0.00
N9	-Ni1	-N12	-O13	-165.17	0.00
N2	-O1	-H1	-O13	-41.53	0.02
H1	-O1	-N2	-Ni1	18.32	0.00
H1	-O1	-N2	-C3	-161.51	0.00
O1	-H1	-O13	-N12	37.80	0.02
Ni1	-N2	-C3	-C4	-0.81	0.00
Ni1	-N2	-C3	-C14	-177.77	0.00
O1	-N2	-C3	-C4	179.03	0.00
O1	-N2	-C3	-C14	2.06	0.01
N2	-C3	-C4	-N5	25.66	0.00
N2	-C3	-C4	-C15	146.26	0.00
N2	-C3	-C4	-C16	-91.48	0.00
C14	-C3	-C4	-N5	-157.30	0.00
C14	-C3	-C4	-C15	-36.70	0.00
C14	-C3	-C4	-C16	85.56	0.00
N2	-C3	-C14	-H14A	-110.93	0.00
N2	-C3	-C14	-H14B	129.07	0.00
N2	-C3	-C14	-H14C	9.08	0.01
C4	-C3	-C14	-H14A	72.36	0.01
C4	-C3	-C14	-H14B	-47.63	0.01
C4	-C3	-C14	-H14C	-167.63	0.00
C3	-C4	-N5	-Ni1	-37.88	0.00
C3	-C4	-N5	-C6	-174.76	0.00
C15	-C4	-N5	-Ni1	-158.73	0.00
C15	-C4	-N5	-C6	64.38	0.00
C16	-C4	-N5	-Ni1	78.00	0.00
C16	-C4	-N5	-C6	-58.89	0.00
C3	-C4	-C15	-H15A	-59.86	0.00
C3	-C4	-C15	-H15B	-179.86	0.00
C3	-C4	-C15	-H15C	60.14	0.00
N5	-C4	-C15	-H15A	56.69	0.00
N5	-C4	-C15	-H15B	-63.31	0.00
N5	-C4	-C15	-H15C	176.69	0.00

C16	-C4	-C15	-H15A	179.45	0.00
C16	-C4	-C15	-H15B	59.45	0.00
C16	-C4	-C15	-H15C	-60.55	0.00
C3	-C4	-C16	-H16A	-53.17	0.00
C3	-C4	-C16	-H16B	-173.17	0.00
C3	-C4	-C16	-H16C	66.82	0.00
N5	-C4	-C16	-H16A	-166.78	0.00
N5	-C4	-C16	-H16B	73.22	0.00
N5	-C4	-C16	-H16C	-46.79	0.00
C15	-C4	-C16	-H16A	69.64	0.00
C15	-C4	-C16	-H16B	-50.36	0.00
C15	-C4	-C16	-H16C	-170.37	0.00
Ni1	-N5	-C6	-H6A	-79.66	0.00
Ni1	-N5	-C6	-H6B	162.10	0.00
Ni1	-N5	-C6	-C7	41.22	0.00
C4	-N5	-C6	-H6A	51.00	0.00
C4	-N5	-C6	-H6B	-67.24	0.00
C4	-N5	-C6	-C7	171.88	0.00
N5	-C6	-C7	-H7A	50.15	0.00
N5	-C6	-C7	-H7B	167.78	0.00
N5	-C6	-C7	-C8	-71.04	0.00
H6A	-C6	-C7	-H7A	171.03	0.00
H6A	-C6	-C7	-H7B	-71.34	0.01
H6A	-C6	-C7	-C8	49.84	0.00
H6B	-C6	-C7	-H7A	-70.74	0.01
H6B	-C6	-C7	-H7B	46.89	0.01
H6B	-C6	-C7	-C8	168.08	0.00
C6	-C7	-C8	-H2	-163.72	0.00
C6	-C7	-C8	-H8B	-45.45	0.00
C6	-C7	-C8	-N9	75.41	0.00
H7A	-C7	-C8	-H2	75.10	0.01
H7A	-C7	-C8	-H8B	-166.63	0.00
H7A	-C7	-C8	-N9	-45.77	0.00
H7B	-C7	-C8	-H2	-42.54	0.01
H7B	-C7	-C8	-H8B	75.73	0.01
H7B	-C7	-C8	-N9	-163.41	0.00
C7	-C8	-N9	-Ni1	-47.96	0.00
C7	-C8	-N9	-C10	-179.11	0.00
H2	-C8	-N9	-Ni1	-168.82	0.00
H2	-C8	-N9	-C10	60.03	0.00
H8B	-C8	-N9	-Ni1	72.90	0.00
H8B	-C8	-N9	-C10	-58.25	0.00
Ni1	-N9	-C10	-C11	33.77	0.00
Ni1	-N9	-C10	-C18	154.57	0.00
Ni1	-N9	-C10	-C19	-82.52	0.00
C8	-N9	-C10	-C11	169.39	0.00
C8	-N9	-C10	-C18	-69.81	0.00
C8	-N9	-C10	-C19	53.10	0.00
N9	-C10	-C11	-N12	-22.39	0.00
N9	-C10	-C11	-C17	162.69	0.00
C18	-C10	-C11	-N12	-142.39	0.00
C18	-C10	-C11	-C17	42.69	0.00
C19	-C10	-C11	-N12	95.21	0.00
C19	-C10	-C11	-C17	-79.71	0.00
N9	-C10	-C18	-H18A	-57.65	0.00
N9	-C10	-C18	-H18B	-177.64	0.00
N9	-C10	-C18	-H18C	62.36	0.00
C11	-C10	-C18	-H18A	58.87	0.00
C11	-C10	-C18	-H18B	-61.13	0.00
C11	-C10	-C18	-H18C	178.87	0.00
C19	-C10	-C18	-H18A	179.80	0.00
C19	-C10	-C18	-H18B	59.81	0.00

C19	-C10	-C18	-H18C	-60.19	0.00
N9	-C10	-C19	-H19A	-72.19	0.00
N9	-C10	-C19	-H19B	167.80	0.00
N9	-C10	-C19	-H19C	47.81	0.00
C11	-C10	-C19	-H19A	173.70	0.00
C11	-C10	-C19	-H19B	53.69	0.00
C11	-C10	-C19	-H19C	-66.30	0.00
C18	-C10	-C19	-H19A	50.65	0.00
C18	-C10	-C19	-H19B	-69.35	0.00
C18	-C10	-C19	-H19C	170.65	0.00
C10	-C11	-N12	-Ni1	0.26	0.00
C10	-C11	-N12	-O13	-178.01	0.00
C17	-C11	-N12	-Ni1	175.13	0.00
C17	-C11	-N12	-O13	-3.13	0.01
C10	-C11	-C17	-H17A	164.39	0.00
C10	-C11	-C17	-H17B	44.39	0.01
C10	-C11	-C17	-H17C	-75.61	0.01
N12	-C11	-C17	-H17A	-10.07	0.01
N12	-C11	-C17	-H17B	-130.07	0.00
N12	-C11	-C17	-H17C	109.93	0.00
Ni1	-N12	-O13	-H1	-11.24	0.00
C11	-N12	-O13	-H1	166.94	0.00

Hydrogen bond details

O1 - H1 ... O13		
O1 - H1	1.135(3)	A
H1 ... O13	1.282(3)	A
O1 ... O13	2.415(3)	A
O1 - H1 ... O13	175(3)(	